Technical Report: Economic & Clean Energy Benefits of Establishing a Competitive Wholesale Electricity Market in the Southeast United States

Prepared By:

Vibrant Clean Energy, LLC
Christopher T M Clack
Aditya Choukulkar
Brianna Coté
Sarah A McKee

Prepared For:

Energy Innovation: Policy & Technology, LLC

Table of Contents

1. Executive Summary

The present study uses the WIS:dom®-P optimization model to investigate the individual Integrated Resource Plans (IRP) released by the southeastern states and compare them to optimal capacity expansion scenarios. The goal of this modeling was to investigate whether optimal capacity expansion and economic dispatch combined with setting up a Regional Transmission Organization (RTO) for the southeast states would provide any economic benefits as well as emission reductions.

In addition, scenarios were also performed to investigate the impact of optimal capacity expansion without setting up an RTO and the effect of not retiring the nuclear fleet even if uneconomic. Table 1.1 summarizes the scenarios performed in this study.

Table 1.1. Description of the scenarios performed in this study.

Scenario	Description	Transmission Expansion	DER Coordination	Wheeling Charges
SE IRP	The individual IRPs released by utilities in the southeast states are combined and run through optimal dispatch.	Not allowed	Off	Across state lines
SE Economic IRP	Optimal capacity expansion for the southeast states without creating an RTO	Not allowed	Off	Across state lines
SE RTO	Optimal capacity expansion with an RTO setup in 2025 over the southeast region	Allowed	On	None from 2025 onwards
SE RTO with Nuclear	Optimal capacity expansion with an RTO setup in 2025 over the southeast region. Nuclear is not retired even if uneconomic.	Allowed	On	None from 2025 onwards

Results from this study show that the "SE IRP" prescribed capacity buildout resulted in the highest total resource costs and as a consequence the highest retail rates to consumers. This study found that setting up an RTO was the most economic option for the southeast with cumulative savings in the electric sector of $383.7 billion by 2040 compared to the IRP scenario. In the scenario "SE Economic IRP", where only economic capacity expansion was modeled without creating an RTO, the total system costs were still found to be lower than the "SE IRP" scenario resulting in cumulative savings of $298.14 billion in the electric sector by 2040. In the "SE RTO with Nuclear" scenario, it was found that the additional cost of not retiring uneconomic nuclear generation was about $9 billion more than the "SE RTO" scenario. Therefore, the "SE RTO with Nuclear" scenario still saved $374.66 billion cumulatively by 2040 compared to the "SE IRP" scenario, while reaping the benefits of cleaner generation over a longer period resulting in the lowest emissions of all scenarios.

In addition, it is found that the "SE IRP" results in lowest amount of job creation while creating the highest emissions of all species of pollutants. The "SE RTO" scenario resulted in the highest job creation (407,631 additional jobs by 2040 in the electric sector) and the "SE RTO with Nuclear" scenario resulted in the lowest emissions across all species of pollutants with a cumulative reduction of 2.47 billion tonnes of CO_2 compared to the "SE IRP" scenario.

The impact of DER co-optimization on distribution costs was also investigated in this study. Turning on DER co-optimization (done for the "SE RTO" and "SE RTO with Nuclear" scenarios) results in cumulative savings of $38.49 billion in the "SE RTO" scenario and $37.8 billion in the "SE RTO with Nuclear" scenario by 2040. Savings were larger in the "SE RTO" scenario due to slightly higher utilization of DER technologies.

The "SE RTO with Nuclear" scenario demonstrated that it is possible to get substantial greenhouse gas emission savings at a minimal additional cost ($1.10/MWh) by not retiring the nuclear generators. It was found that the generation from unretired nuclear in the "SE RTO with Nuclear" scenario displaced almost one-to-one generation from natural gas in the "SE RTO" scenario with minimal impact on generation from variable renewable energy (VRE) sources.

A complementary policy report can be found here:
https://energyinnovation.org/wp-content/uploads/2020/08/Policies-To-Support-A-Competitive-Wholesale-Electricity-Market-In-The-Southeast-US.pdf

A companion summary report by Energy Innovations can be found here:
https://energyinnovation.org/wp-content/uploads/2020/08/Economic-And-Clean-Energy-Benefits-Of-Establishing-A-Southeast-U.S.-Competitive-Wholesale-Electricity-Market_FINAL.pdf

The summary WIS:dom®-P model output spreadsheets can be found here:
Summary: https://vibrantcleanenergy.com/wp-content/uploads/2020/08/WISdomP_Outputs.zip

The complete WIS:dom®-P model input and output data can be found here:
Inputs: https://drive.google.com/drive/folders/1rI0nMpgX9HJFc472WTBO936PnK-yLw7T?usp=sharing
Outputs: https://drive.google.com/drive/folders/1NPpDMFooumxsU73qPjTd7Pxs_WtBoeg3?usp=sharing

2. Results

2.1 Incorporating IRP Data into WIS:dom®-P

The latest available Integrated Resource Plan (IRP) information for several major utilities in the Southeast states were incorporated as inputs into this study. The inputs incorporated from the IRP data included capacity changes (generator resource buildouts or specific generator retirements), load growth expectations and forecasts, DSM and energy efficiency programs and reserve requirements.

Utility	State
Alabama Power Company	Alabama
Tennesse Valley Authority	Alabama, Tennessee, Mississippi, North Carolina (very small amount), Georgia (negligible amount)
Georgia Power	Georgia
Duke Energy Florida	Florida
Tampa Electric Company	Florida
Gulf Power Company	Florida
Florida Power and Light	Florida
Entergy Mississippi	Mississippi
Mississippi Power Company	Mississippi
South Carolina Electric and Gas Company	South Carolina
South Carolina Public Service Authority	South Carolina
Duke Energy Progress	North Carolina, South Carolina
Duke Energy Carolinas	North Carolina, South Carolina

Table 2.1: The list of utilities in the Southeast where IRP information was utilized. The list of states these utilities have some influence over in the Southeast is also provided.

The IRP data was stitched together to form a state-level granularity input dataset across the Southeast. As an example, the state of Alabama has generation owned by Alabama Power and Tennessee Valley Authority (TVA). The entire generator fleet of Alabama Power is in Alabama, therefore 100% of the data from the Alabama Power IRP was included in the Alabama state totals. However, TVA also has a presence of generation in Alabama. The percentage of generation from TVA within Alabama was calculated using the ratio of existing TVA generation in Alabama versus total generation owned by TVA. That calculated percentage was applied to the data from the TVA IRP and added to the Alabama State totals.

The process also relied on EIA 860 and 923 data which, together, attaches both capacity and generation to states and utilities. These calculated percentage of utility generation within a state was applied to all data pulled from the IRPs. Georgia was a simple scenario that just had one utility available to incorporate for the entire state. Florida had several utilities within the state from which to amalgamate data. North Carolina and South Carolina both shared large portions of Duke Energy Carolinas and Duke Energy Progress. Mississippi was a special case where part of the state resides within MISO. The MISO portion of this state was matched to available EIA860 data. The remainder of the state was set to match the IRP data.

For the generation capacity changes and retirements, VCE® grouped these changes by generator technology. The additions and retirements were grouped into investment periods modeled for this study. For thermal generator, if details of the additions and retirements were unavailable, WIS:dom® determined

the optimal location for the addition or the most uneconomic plant to retire. For all VRE generation added by the IRP, WIS:dom® determined optimal siting within each state.

In the "SE IRP" scenario, WIS:dom® dispatched the thermal generation using the state-wide average capacity factors for each generation type to simulate the uneconomic dispatch of thermal generation. It was assumed that the individual states will continue their current practice of self-dispatching the thermal generation even as more thermal generation is added over the investment periods.

It is important to note that in a few cases, the 2018 technology capacities for each state were updated with the IRP data. The Input Generator datasets described in detail below come from the 2018 EIA 860 data and usually set the base of what is installed across the US. In this study, there were a few instances that were updated with the IRP information. Usually, this was retirements that had occurred and were not yet portrayed in the 2018 EIA numbers. All other scenarios were initialized using the IRP proposed installed capacities for 2018. However, from the next investment period optimal capacity expansion was modeled.

2.2 Impact of Optimal Capacity Expansion

In all scenarios (except the "SE IRP" scenario) optimal capacity expansion was modeled to meet demand in the southeast. When modeling optimal capacity expansion, WIS:dom® has to ensure reliability through keeping a 7% load following reserve at all times and never allowing a loss of load event to occur. To meet resource adequacy requirements, the model has to ensure that there is enough installed capacity to meet unforced capacity (UCAP) planning reserve margins (PRM) for the balancing region using Eq. (3.14.1). UCAP represents the capacity available at a given time taking into account the generator's forced outrage rate. The modeled forced outage rates for thermal generators are given in Table 2.2. The UCAP for VREs are not prescribed, but rather determined based on the most difficult period in terms of demand and available VRE generation.

Generator	Coal	NGCC	NGCT	Nuclear	Hydro	Geo	CCS	SMR	MSR
UCAP	87.7%	86%	85.3%	90.3%	89.5%	89.1%	86%	95%	95%

Table 2.2: Unforced capacity fractions for thermal generators

All scenarios start from the same initialization, based on the projected installed capacities by the IRP for 2018. By 2020, the "SE IRP" scenario installed generation vastly in excess of what is required to meet load in the southeast region with the required North American Electric Reliability Corporation (NERC) PRM. It was found that the "SE IRP" scenario resulted in UCAP PRM of 49% (see Figure 2.1). The excessively high PRM is one of the reasons for high total system costs as well as high retail rates for customers.

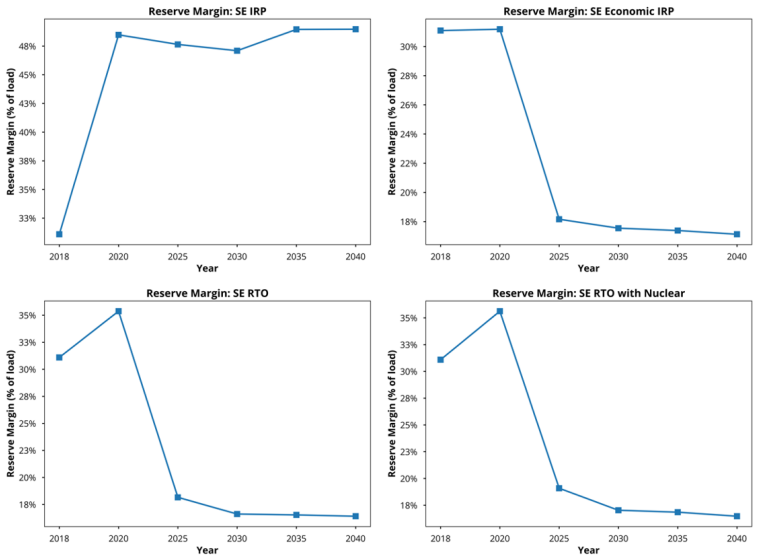

Figure 2.1: Unforced capacity planning reserve margins for the scenarios modeled for the southeast region.

In addition to the excessively high PRM, the "SE IRP" scenario models the current operation of thermal generators in the southeast where these generators are "self-dispatched". As a result of the self-dispatching of the thermal generation, operation costs are higher, while resulting in higher emissions from the electric sector. The self-dispatch of the thermal generators in the southeast is modeled by calculating the state-level average annual capacity factor for each generator type. It is assumed that each state will continue to operate its thermal assets in the same uneconomic manner that as it is done currently. Therefore, in the "SE IRP" scenario, WIS:dom® is required to meet this minimum state-level capacity factor constraint for each generator type throughout the investment periods.

Figure 2.2 shows the state-level annual average capacity factors for coal and gas for each southeast state modeled in 2018. Comparing these prescribed capacity factors to capacity factors from economic dispatch, it is seen that coal is over-dispatched while gas is under-dispatched. As a result of this uneconomic dispatch decisions, the "SE IRP" scenario has excessive carbon-dioxide and Sulphur-dioxide emissions.

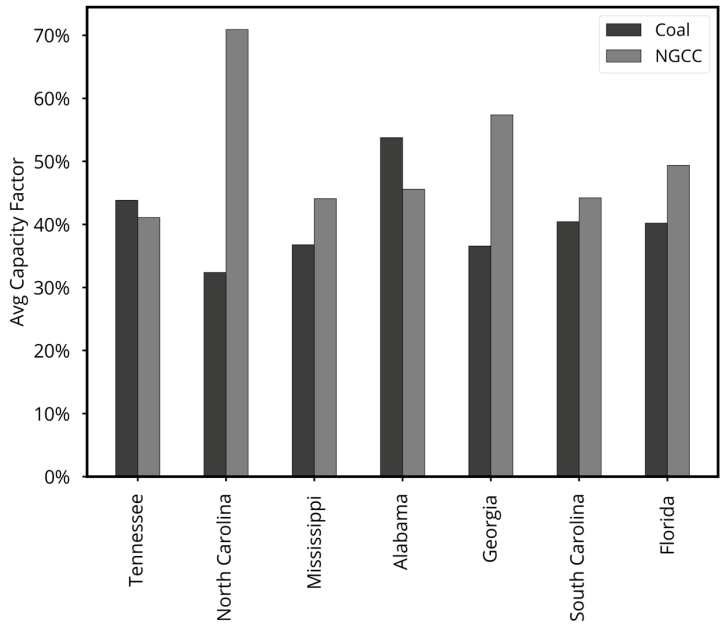

Figure 2.2: Average capacity factors of generation over the investment periods for the scenarios modeled for the southeast.

2.3 Economics of Optimal Capacity Expansion

In order to evaluate the economic benefits of the various scenarios modeled in this study, the total resource cost, distribution costs, retail rates and job creation in each scenario are compared against the "SE IRP" scenario values (see Figure 2.3). It is found that the "SE IRP" scenario has the highest total resource costs (driven partly by the excess capacity as shown in Figure 2.1). The "SE RTO" scenario is found to have the lowest total resource costs with cumulative savings of $383.7 billion by 2040 compared with the "SE IRP" scenario. The "SE RTO with Nuclear" came in second with cumulative savings of $374.66 billion by 2040 compared to the "SE IRP" scenario, followed by the "SE Economic IRP" scenario with cumulative savings of $298.14 billion by 2040. The magnitude of uneconomic capacity buildout in "SE IRP" scenario can be seen from the fact that just choosing economic capacity expansion results in 75% of the savings resulting from setting up an RTO in the southeast.

The "SE RTO" and "SE RTO with Nuclear" scenarios, which co-optimized distribution scale generation along with utility scale generation included cumulative savings in distribution costs of $37.8 billion for the "SE RTO with Nuclear" and $38.49 billion for "SE RTO" compared to the "SE IRP" scenario. The "SE Economic IRP" did not co-optimize utility and distribution scale generation and, hence, did not show any benefits compared to the "SE IRP" scenario.

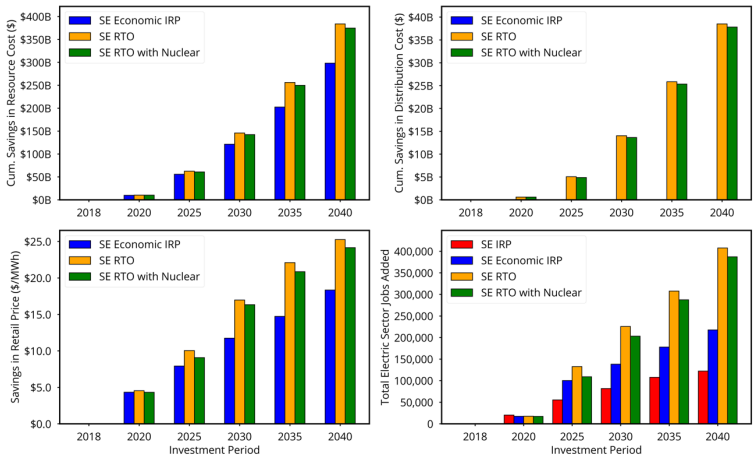

Figure 2.3: Comparison of difference in total resource cost (top left), distribution costs (top right), retail rates (bottom left) against the IRP values and total jobs added in each scenario compared to 2018 (bottom right).

The savings in total resource costs for the optimal capacity expansion scenarios translated to reduced retail rates for consumers. The "SE RTO" scenario showed the highest reduction in retail rates of $25.25/MWh compared to the "SE IRP" scenario, followed closely behind by the "SE RTO with Nuclear" scenario showing a reduction in retail rate of $24.14/MWh. The "SE Economic IRP" scenario showed a reduction in retail rate of $18.34/MWh.

In addition to the cost savings above, the optimal capacity expansion scenarios resulted in more job creation compared to the "SE IRP" scenario. By 2040, the "SE RTO" scenario added 407,631 jobs with "SE RTO with Nuclear" coming in close behind with 387,235 jobs. The "SE Economic IRP" scenario added 217,681 jobs while the "SE IRP" scenario added 122,133 jobs. The significantly higher job creation in the RTO scenarios is driven by the larger increases in VRE installations as well as transmission expansion.

Figure 2.4 shows the location of jobs created at state level. It is seen that Florida leads by a substantial margin in job creation. This is driven mainly by the large installations of NGCC, wind and solar (both utility scale and distribution scale) in Florida to meet its large demand.

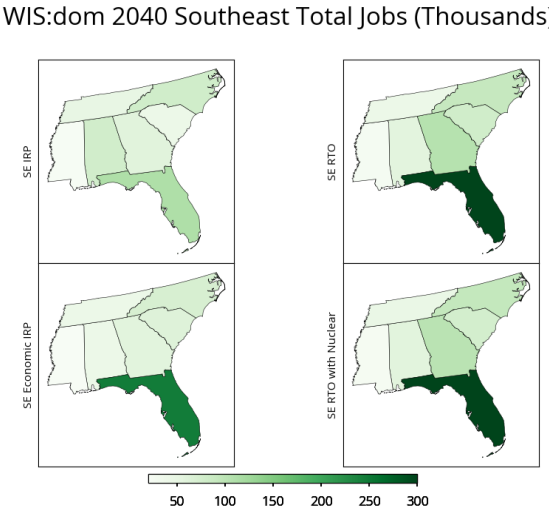

Figure 2.4: Total jobs (in Thousands) arising in the electricity industry by 2040 for all scenarios run. This total is across all generator technologies, transmission and distribution jobs.

2.4 Impact of Not Retiring Nuclear

To study the impact of the nuclear fleet not retiring, the "SE RTO with Nuclear" scenario modeled optimal capacity expansion with the exception of not allowing nuclear to retire. An important outcome of this scenario is that not allowing nuclear to retire affects natural gas installations the most. By 2040, in the "SE RTO with Nuclear" scenario, 5 GW less of natural gas is installed, while there is about 3 GW less of distributed PV compared to the "SE RTO" scenario (see Figure 2.5). The reason for reduction in distributed PV in the "SE RTO with Nuclear" scenario is that the model needs to build more transmission to effectively use the nuclear fleet. As a result, the model uses utility scale generation more and less distributed resources to meet demand. It is also observed that the "SE RTO with Nuclear" scenario uses 20% less DSM and installed slightly lower distribution scale storage compared to the "SE RTO" scenario.

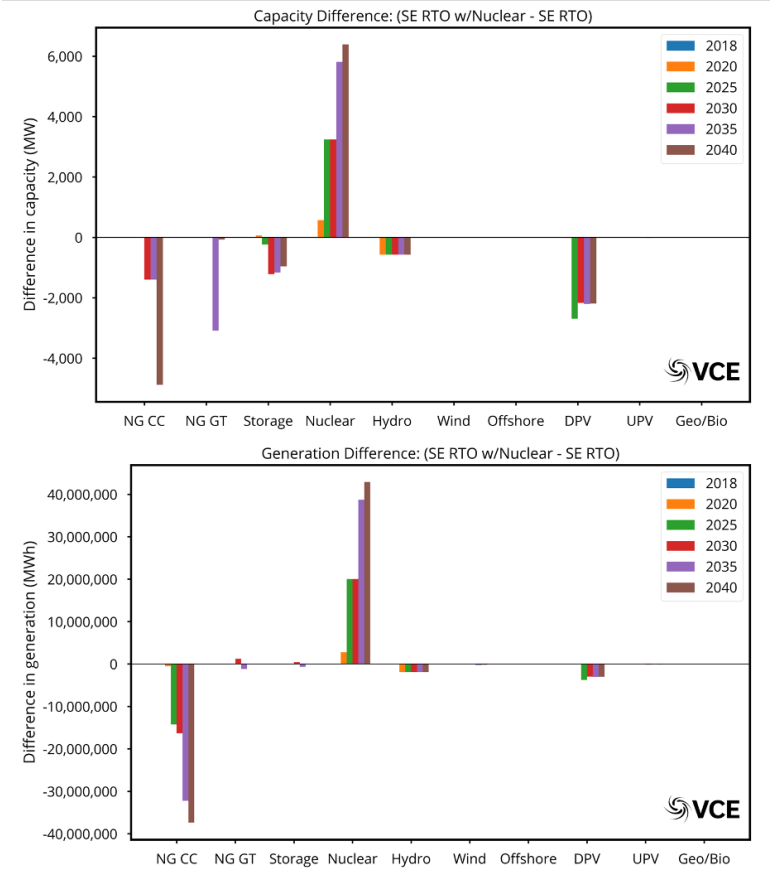

Figure 2.5: Difference in installed capacities and generation between the "SE RTO" and "SE RTO with Nuclear" scenarios

Comparing the difference in generation between the "SE RTO" and "SE RTO with Nuclear" scenario, it is observed that most of the generation lost to nuclear is by natural gas. As a result, there is a significant reduction in CO_2 emissions. Therefore, while the total system costs are slightly higher, the effect of not retiring nuclear results in additional savings of about 14 million tonnes of CO_2 per year by 2040, which results in a cost per tonne of CO_2 of $36 (see Figure 2.6). This additional cost in terms of retail rates paid by consumers is about 0.11 ¢ / kWh.

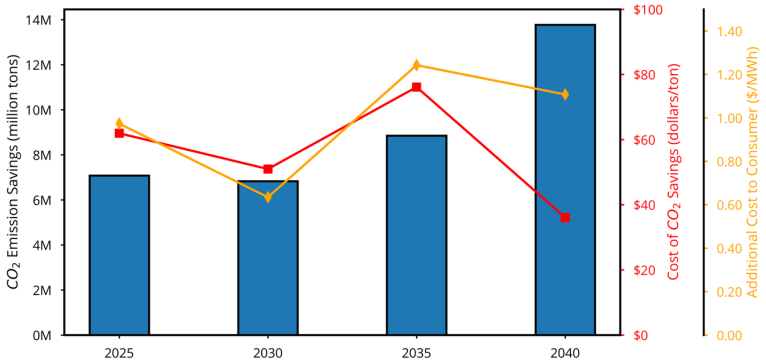

Figure 2.6: Impact of not retiring nuclear in terms of cost of saved CO_2 emissions and the additional cost of consumers.

2.5 Effect of VREs Across Wind & Solar Regimes

One of the fundamental constraints of the WIS:dom®-P model is that there is no loss of load at any time during the weather years evaluated. The model is required to satisfy load at every time step while satisfying the required PRM and have an additional 7% load following reserve. During any given weather year, there will be periods where the generation from both wind and solar is low simultaneously. These periods are defined as *high system stress* periods, where the sum of all Variable Renewable Energy (VRE) generation is low, thermal units are running high and load is high. These are times where thermal plants, including Peaker plants, are online to account for lack of generation from renewable sources.

Shown below are three regimes of interest from the 2040 model results for each scenario. Figure 2.7 shows the dispatch of wind and solar during a low wind period. Figure 2.8 shows the dispatch of wind and solar during a high wind regime. Figure 2.9 shows the dispatch of wind and solar for a period where both wind and solar were low. During this period, thermal generation and load were also high relative to wind and solar.

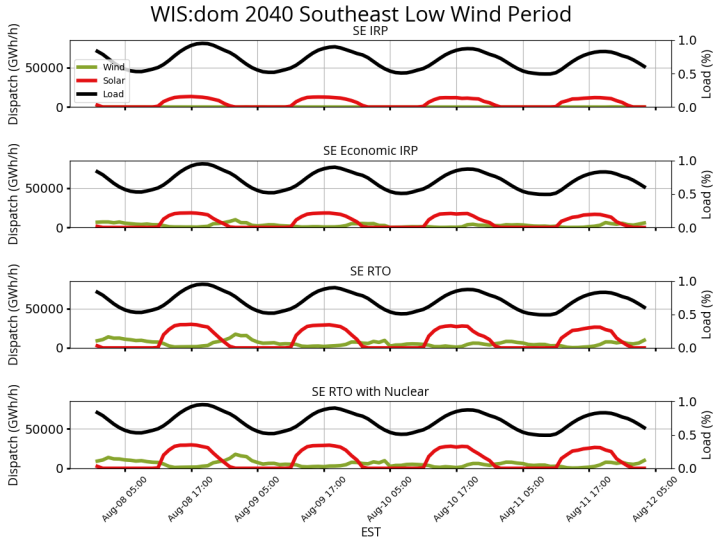

Figure 2.7: A summer period of low wind across the southeast. The wind and solar dispatches are shown (GWh/h) from the 2040 results from all scenarios run. The load (% of max load) is there for comparison as well. This can be directly compared to Figure 4.55 which shows the wind and solar resource capacity created by VCE® during this time.

Figure 2.7 shows the load alongside the wind and solar dispatch from all four scenarios for several days during a summer week in the 2040 investment period. The load is quite high during this time, as is typical during the summer months for the Southeast. The daily solar peaks are highly correlated with the daily peak load. The wind dispatch peaks in the nighttime hours after sunset. These wind peaks are relatively consistent, albeit, not very high during this period of low wind. Wind resource in the southeast does decrease in the summer months. Comparing the "SE IRP" scenario to the "SE RTO with Nuclear" scenario, it is shown how much more wind and solar generation was built out in the latter scenario. The solar and wind dispatch has a higher magnitude in the scenarios where the Southeast forms an RTO. Even in the "SE Economic IRP" scenario, where the Southeast is allowed to develop economically, wind and solar dispatch is much higher than that of the "SE IRP" scenario. Economically, this means there is value in wind and solar in the Southeast. Even during times where the wind resource is low, it is still utilized by the model for dispatch. For the scenarios that build out more wind and solar, the figure above shows that the wind and solar daily dispatch

shapes start to take on the typical patterns observed in the wind and solar resource capacities across the Southeast. This shows that the model is optimally deploying VRE generation to take advantage of the renewable resources available to the region.

Figure 2.8 shows the same as above except the wind capacity across the region is much higher for the week displayed. This week experienced a springtime weather pattern that brought consistently strong southerly winds across the Southeast. The "SE IRP" scenario is not able to capture or use any of the wind power during this period as the IRP builds almost no new wind. The other three scenarios, especially the two scenarios where the Southeast enters an RTO, show wind generation reaching as high as solar during this week. The anti-correlated nature of the wind and solar resource can be observed here as well. Solar peaks during the day and wind peaks in the evening hours. This week, in particular, had a larger scale weather event that kept wind resource higher even during the daytime hours. However, the nighttime peaking of the wind resource is still apparent in the wind dispatch. In the economic "SE Economic IRP" scenario, wind generators are still installed and dispatched.

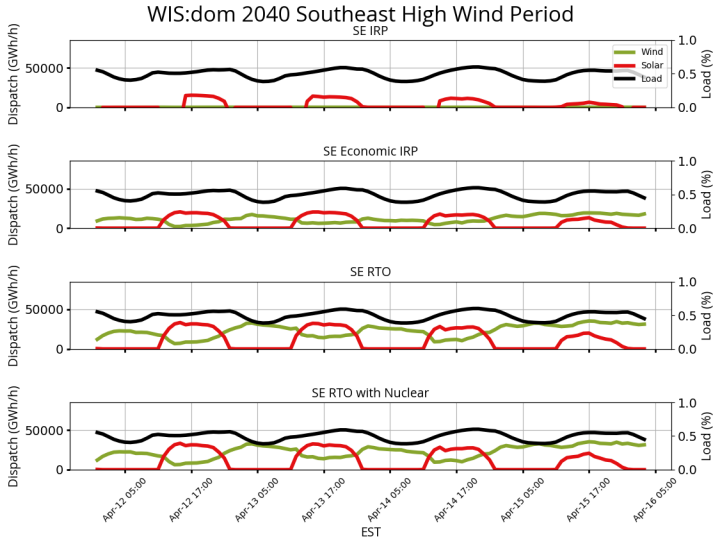

Figure 2.8: A spring period of high wind across the southeast. The wind and solar dispatches are shown (GWh/h) from the 2040 results from all scenarios run. The load (% of max load) is there for comparison as well. This can be directly compared to Figure 4.54 which shows the wind and solar resource capacity created by VCE® during this time.

Figures 2.7 and 2.8 can be compared directly to Figure 4.54 and 4.55 under the Section 4.4.4 (Southeast US Weather Analysis). That section breaks down typical diurnal load patterns observed across the Southeast as well as typical wind and solar diurnal patterns. The same high and low wind weeks are also looked at purely from the perspective of average wind and solar capacity factors over the southeast created by VCE®. It is observed that the shapes of the generation profiles from WIS:dom® installed capacities match the average capacity factor shapes. The matching of the shapes indicate how the model tries to reduce variability given constraints of siting and having to meet load. The creation of the wind and solar resource data is discussed in great detail in Section 4.4 (Renewable Generation Dataset).

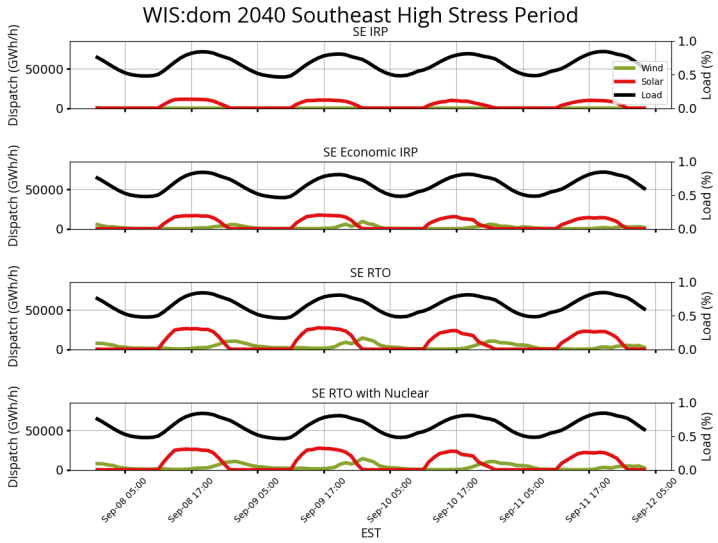

Figure 2.9: A late summer period of low wind, low solar and high load across the southeast. Not shown is the thermal generation, though that is also producing higher amounts during this period. The wind and solar dispatches are shown (GWh/h) from the 2040 results from all scenarios run. The load (% of max load) is there for comparison as well.

Figure 2.9 shows another period marked as *high system stress*. The wind and solar resources together were both lower during this time period as observed from the wind and solar dispatch. Solar daytime peaks do not reach as high as the other two weeks shown in Figure 2.7 and Figure 2.8. This was a late summer period where load was still high. Even during this period where wind and solar are not as high a resource, it was still observed that during this period, these resources were used to help fulfill the load during that time. Tying this to the dispatch of other technologies, Figure 2.10 shows the dispatch curves of all the technologies during this *high system stress* period where wind and solar were low, load was high and thermal unit generation was also high. Two scenarios are shown here. The first is the "SE IRP" scenario where little wind and some solar generation was installed by 2040. The second dispatch time series is the "SE RTO with Nuclear" scenario. It is observed that in the "SE IRP" scenario, the model has to dispatch almost entirely firm thermal generation to help meet peak demand during these high stress periods. However, as seen from the "SE RTO with Nuclear" dispatch, although wind and solar generation are lower, the model is able to pair them with storage and still meet the peak load. This example illustrates how VREs in combination with storage can meet load during difficult periods of low VRE generation.

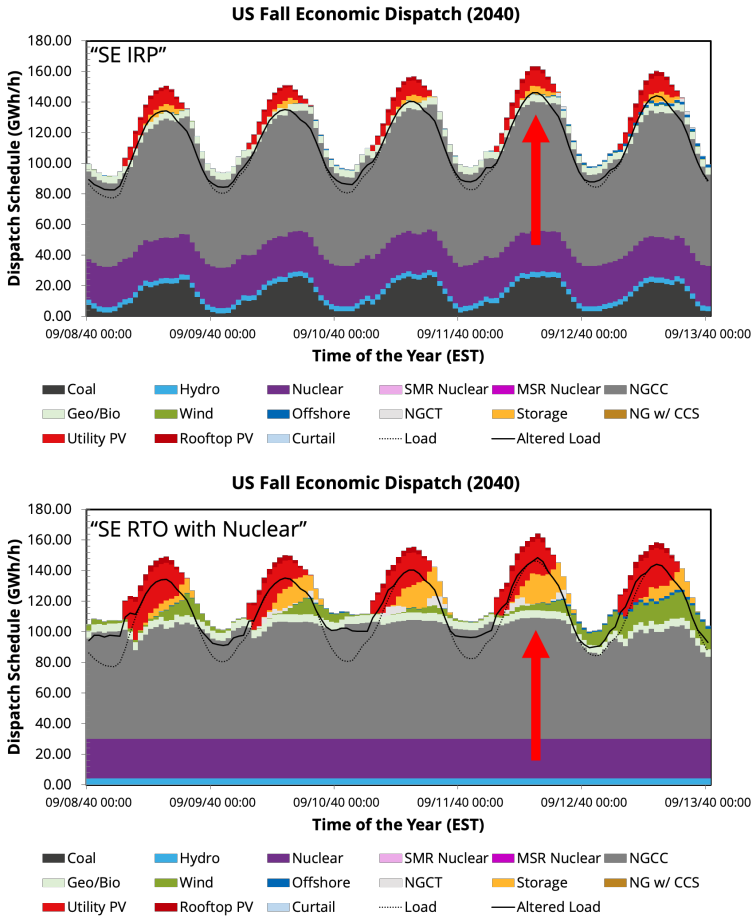

Figure 2.10: The 2040 dispatch curves for all technologies during the *high system stress* week in late summer. Two scenarios are shown: "SE IRP" and "SE RTO with Nuclear". Even though VRE generation during this week is low, the comparison of the dispatch curves show that the load peaks are filled with VRE generation instead of natural gas combustion turbines.

2.6 Meeting Winter & Summer Demand Peaks

The southeast region is seen to have a winter peaking demand profile with a bimodal shape over the day driven by heating demand. Wind generation in the southeast is well positioned to meet winter demand cheaply and reliably working with storage. Figure 2.11 shows average winter wind, solar and storage generation as fraction of load in the southeast region. As seen from Figure 2.11, WIS:dom® installed capacities weighted wind capacity factors are well correlated with the winter load profile. Wind generation paired with storage can thus help meet winter peak loads.

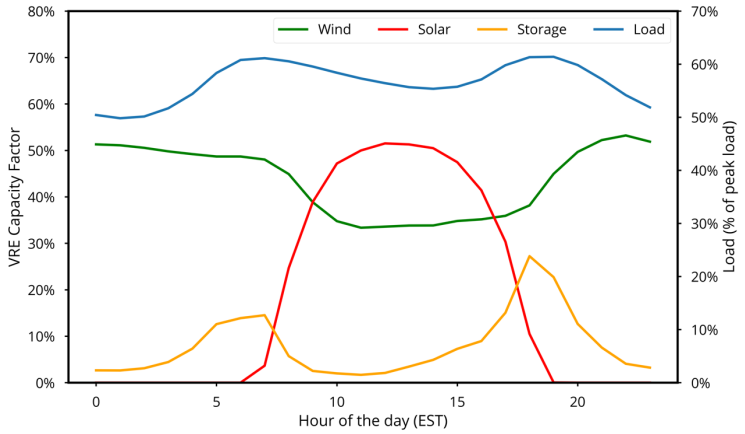

Figure 2.11: Winter averaged wind, solar and storage generation as percentage of load and winter averaged load as percentage of peak load.

It is observed that the "SE IRP" scenario does not take advantage of the above behavior of wind. Figure 2.12 shows that based on the siting and installed capacities of wind in the "SE IRP" scenario, it is seen that it is unable to contribute at all during periods of high load during the winter. Instead NGCT is deployed to meet peak loads.

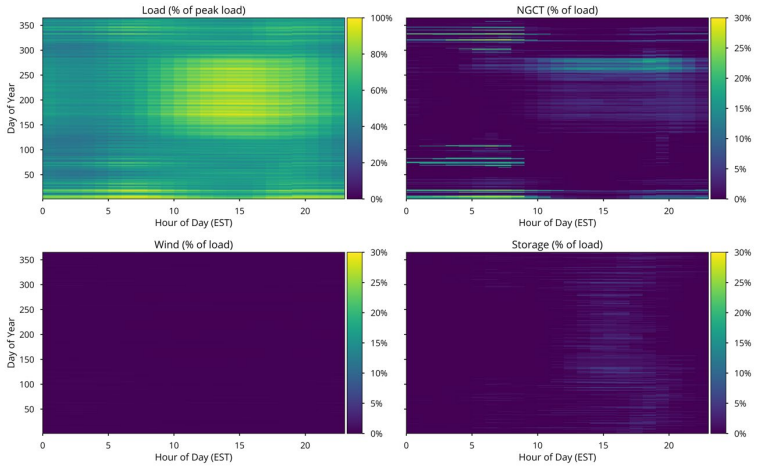

Figure 2.12: Generation from NGCT, wind and storage in the "SE IRP" scenario in year 2040.

However, in the "SE RTO" scenario (Figure 2.13), where WIS:dom® takes advantage of the patterns in wind capacity factors, wind is sited in appropriate locations with the right capacities to create the required generation profile that (in combination with storage) is used to meet winter loads. It is observed from Figure

2.13 that due to appropriate use of wind generation, NGCT is almost never used, resulting in reduced costs and emissions.

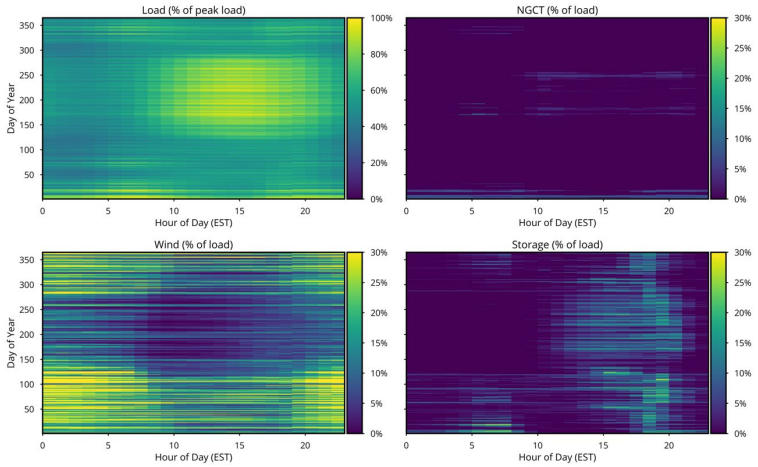

Figure 2.13: Generation from NGCT, wind and storage as percentage of load in the "SE RTO" scenario in year 2040.

During the summer, demand in the southeast is characterized by an afternoon peak around 2:00PM EST. As a result, in terms of VRE generation, solar is best positioned to meet summer loads. It is observed from Figure 2.14 that solar generation leads demand by several hours. Hence, storage (along with wind) comes into play in the late afternoon by providing generation as solar is ramping down.

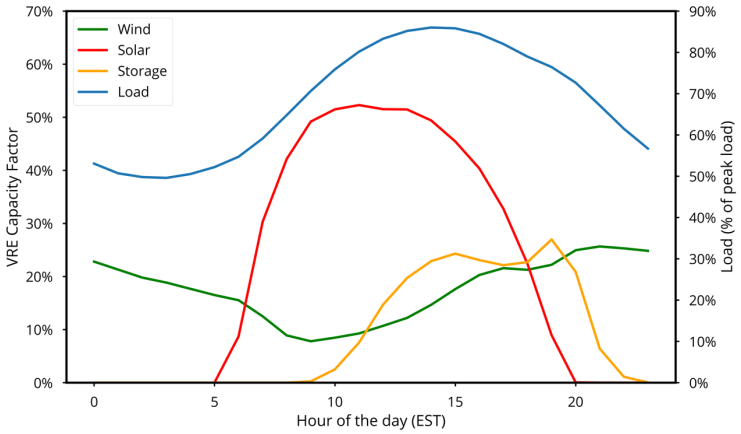

Figure 2.14: Summer averaged wind, solar and storage generation as percentage of load and summer averaged load as percentage of peak load

A consequence of the distinct difference in load shapes during summer and winter in the southeast, the behavior of storage changes to respond effectively to the different load shapes (see Figure 2.15). As seen from Figure 2.11, storage generation is deployed (along with wind) to meet the morning and evening peak in winter. In order to be ready to meet that demand, storage charges during the middle of the day (using part of solar generation) and during the nighttime periods (using wind generation) when demand is low. During summer, an almost opposite behavior is observed, where storage charges during the night (using wind generation) and early parts of the day (using portions of wind and solar generation) to be ready to meet the peak in demand that occurs just as solar is starting to ramp down.

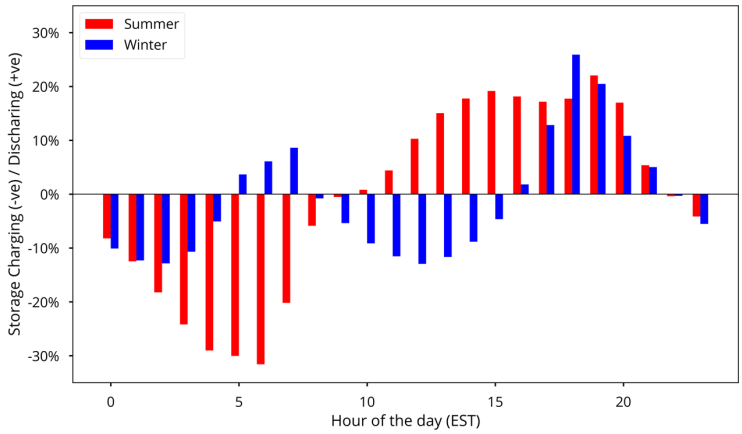

Figure 2.15: Diurnal charge/discharge behavior of storage during the summer and winter periods in the "SE RTO" scenario in year 2040.

Utility-scale storage and distribution-scale storage show unique charge and discharge behavior during the winter and summer seasons (see Figure 2.16). During the summer when the peak load occurs around 2:00PM EST, it is observed that both utility-scale and distribution-scale storage come into play. While both storage scales are helping meet demand, the model has chosen to install storage at distribution scale to ensure that the peak demand seen by the utility-scale generators is lower and reduces the costs associated with distribution network upgrades. Similar reasoning applies to meeting peak loads during the winter.

When it comes to charging, distributed-scale storage again shows interesting trends. During the summer it is observed that distribution-scale storage begins to charge only after demand has reached its minimum value over the diurnal period. While in winter, the model charges distribution scale storage at night and utility-scale storage during the day. By charging the distribution scale storage at night, the model ensures that the peak load at the distribution points is kept low, while during the day when demand is higher, it only charges utility-scale storage. This charging behavior not only helps to reduce/postpone distribution system upgrades, but also creates a flatter demand profile for the utility-scale generation to match.

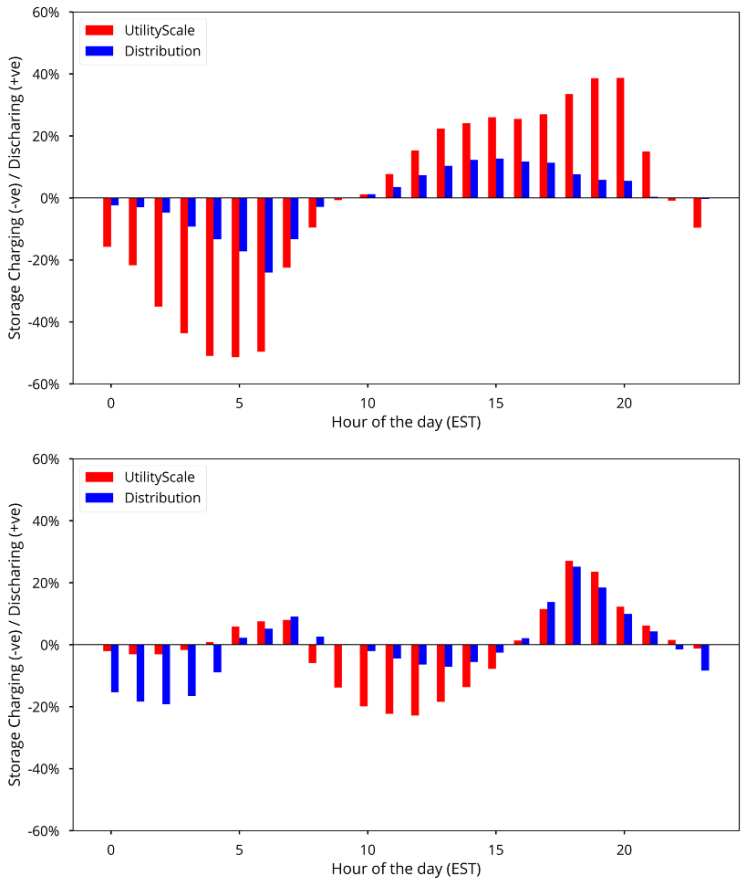

Figure 2.16: Diurnal charge/discharge behavior of utility scale and distribution scale storage in summer (top) and winter (bottom) in the "SE RTO" scenario in year 2040.

The impact of DER on load seen by the utility-scale generation can be visualized by looking at the load duration curves of the original load and the DER modified load from the "SE RTO" scenario for year 2040 (shown in Figure 2.17). It is observed that DER generation reduces the peak load by 27,347 MW (a 11.8% reduction), while increasing the minimum load by 18,158 MW. Thus, DERs flatten the demand seen by utility-scale generation that not only reduces the need to have utility-scale generation for the few time periods of peak load, but also defers costs associated with distribution network upgrades and utilizes equipment and infrastructure more appropriately.

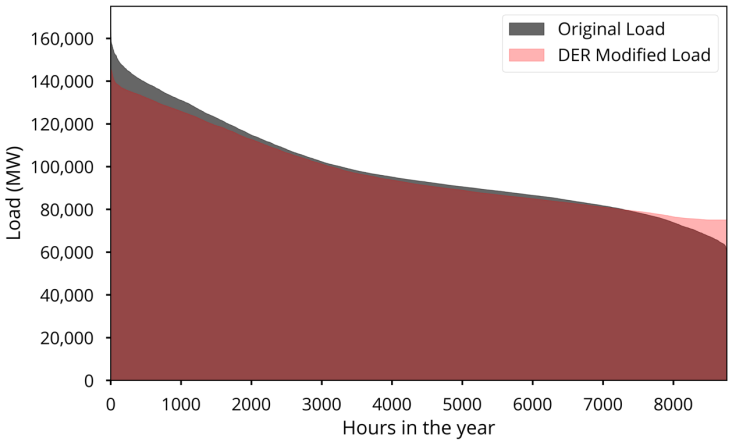

Figure 2.17: Duration curves of the original load and the DER modified load in "SE RTO" scenario for year 2040.

2.7 VRE capacity value

The fraction of a generator's nameplate capacity that can be counted towards resource adequacy metrics is known as capacity value of that generator. Ensuring resource adequacy is an important aspect of energy system planning and hence needs to be incorporated into any capacity expansion modeling. Capacity values for conventional generators are defined by the reliability metrics or the equivalent forced outage rate. Defining capacity values for variable renewable energy sources such as wind and solar is more difficult.

There are several methods to estimate capacity value of VRE generators, which use reliability-based metrics to calculate capacity value, such as: Equivalent Conventional Power (ECP), Effective Load Carrying Capacity (ELCC) and Equivalent Firm Capacity (EFC). The most commonly used metric is the ELCC, which estimates the equivalent "firm" capacity that will create the same loss of load probability as the VRE generator under consideration.

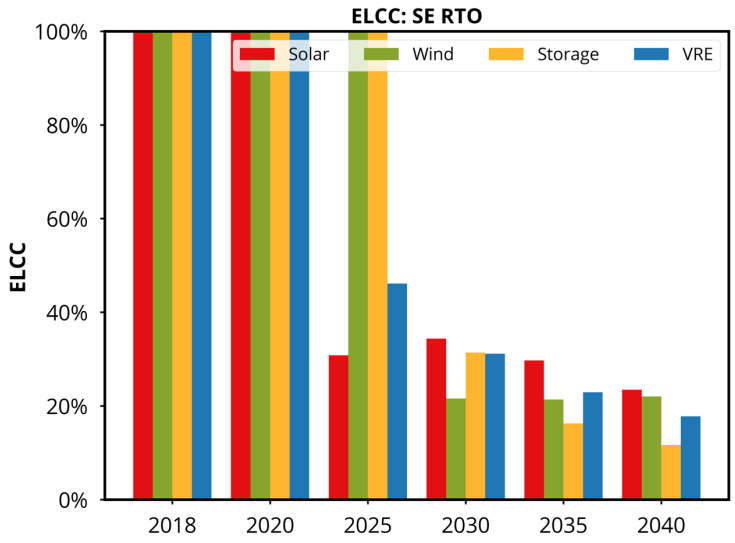

Figure 2.19: Equivalent load carrying capacity calculated for wind, solar, storage and all the VREs combined for the "SE RTO" scenario in each of the investment periods for the "SE RTO" scenario.

The ELCC is calculated for each investment period in the "SE RTO" scenario and shown in Figure 2.19. It is seen that up to 2020, the ELCC of the VRE technologies is 100%. The reason for this is that the installed capacities of VRE are still low and hence every optimally sited MW of the VRE generation helps reduce stress on the system. By 2025, ELCC of solar drops sharply to just above 30% driven by the fact that the solar generation peak is not exactly aligned with the daily load peak. As there is not much spatial variability in solar generation in the southeast, after a certain point, each additional MW of solar capacity contributes less to meeting the load. Wind and storage ELCC values begin to drop from 2030 onwards along with solar as those technologies get saturated as well.

While ELCC attempts to model the resource adequacy of a VRE generator in terms of "firm" capacity, it does not take into account the contributions from the generator during periods of peak demand. Another method to determine capacity value is by evaluating the contribution from that generator during the most difficult load periods. The duration curve method estimates capacity value as the reduction in highest peak net load hours relative to the highest load peak. The net load for a generator is calculated by subtracting the generation that went to meeting load from that generator from the full load. The average difference

between the highest load peak hours and highest net load hours as a fraction of the installed capacity is designated as the capacity value for that generator.

Figure 2.20 shows the capacity values for wind, solar, storage and all VREs combined using the duration curve method for the highest 50 load hours. It is observed that all VRE generators start with much lower capacity value compared to the ELCC method. The capacity value for solar starts at 31.5% and gradually reduces to 7% by 2040 as that resource saturates and each additional MW contributes less in terms of meeting peak demand (due to mismatch between solar generation profile and demand profile as discussed earlier). Wind on the other hand is seen to oscillate between a capacity value of 25% and 33% and eventually reaching 24% by 2040. The reason wind does not drop similar to solar is due to its role in meeting the winter peaking loads in the southeast as discussed in the previous sections.

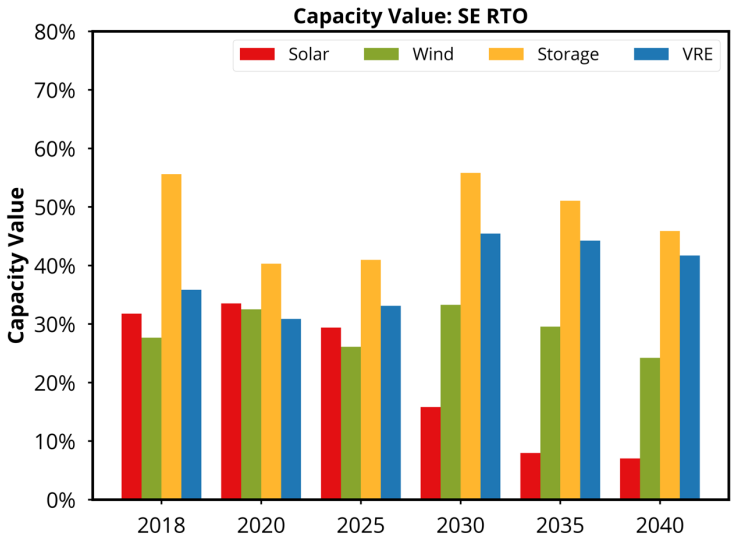

Figure 2.20: Capacity values of wind, solar and storage as well as their combined capacity value.

Finally, the capacity value of storage is seen to oscillate between 55% in 2018 to 55% in 2030 and falling down to 45% by 2040. Using the duration curve metric, storage capacity value remains high and even increases as it is deployed particularly during the most difficult periods in combination with wind or solar to meet peak demand. The ELCC metric does not capture this important role of storage in meeting load during difficult periods and gives it a much lower capacity value of 11% in 2040.

However, the duration curve metric to estimate capacity value is not perfect either. The choice of the number of peak load hours used can have a significant impact on the capacity value especially in regions where the load shape has strong seasonal peaks such as in the southeast. For example, if the highest 10 peak load hours were used to calculate capacity value using the duration curve method, solar gets less than 10% capacity value throughout, while wind gets a capacity value of about 80% in the initial investment periods. The reason for this is that when only the top 10 peak load hours are used, the periods selected are all in winter where wind is much more correlated with load. Selecting the top 50 hours ensures an even mix of winter and summer peaks to get an average estimate of capacity value for the various VRE technologies.

In addition to limitations of estimating capacity value discussed above, it may not be appropriate to use a single capacity value estimate for the full year given the different generation characteristics of wind and solar. Figure 2.21 shows the average monthly capacity values calculated for wind, solar and storage by

averaging the fraction of the daily peak load met by the VRE technology in each month of the year. It is seen that wind has higher capacity values in winter, while solar has higher capacity values in summer (complementing each other quite well). Storage is seen to have about a constant capacity value of 5%. Therefore, while this method brings out the seasonal behavior of the technologies and overcomes the issues of using a constant capacity value for the full year, it underplays the importance of storage in meeting load during difficult periods as demonstrated by the duration curve method.

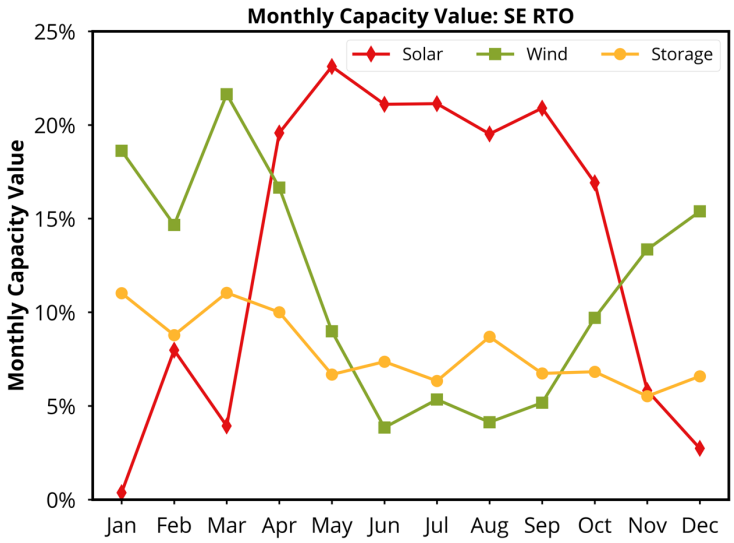

Figure 2.21: Seasonal change in capacity values of wind, solar and storage in the "SE RTO" scenario in year 2040.

From the above discussion, it is clear that the capacity value metrics for VREs should incorporate three important features of the technology:

(1) Should help during periods of peak demand,
(2) incorporate seasonal behavior of the resource and
(3) reduce loss of load probability.

Given the challenges in prescribing capacity values for VRE generators, WIS:dom® incorporates capacity values calculation endogenously to the capacity expansion and optimal dispatch. Therefore, for each siting decision that WIS:dom® makes for VREs, the capacity values of that installed capacity is incorporated into the PRM calculation using Eq. (3.14.1). The main advantage of using this method to evaluate capacity value is that it incorporates the features of all three capacity value estimation methods discussed above (help during periods of most difficult load, incorporate seasonal behavior of technologies and reduce loss of load probability). These features can be demonstrated by taking an example of the siting decisions made in 2040 for the "SE RTO" scenario shown in Figure 2.22.

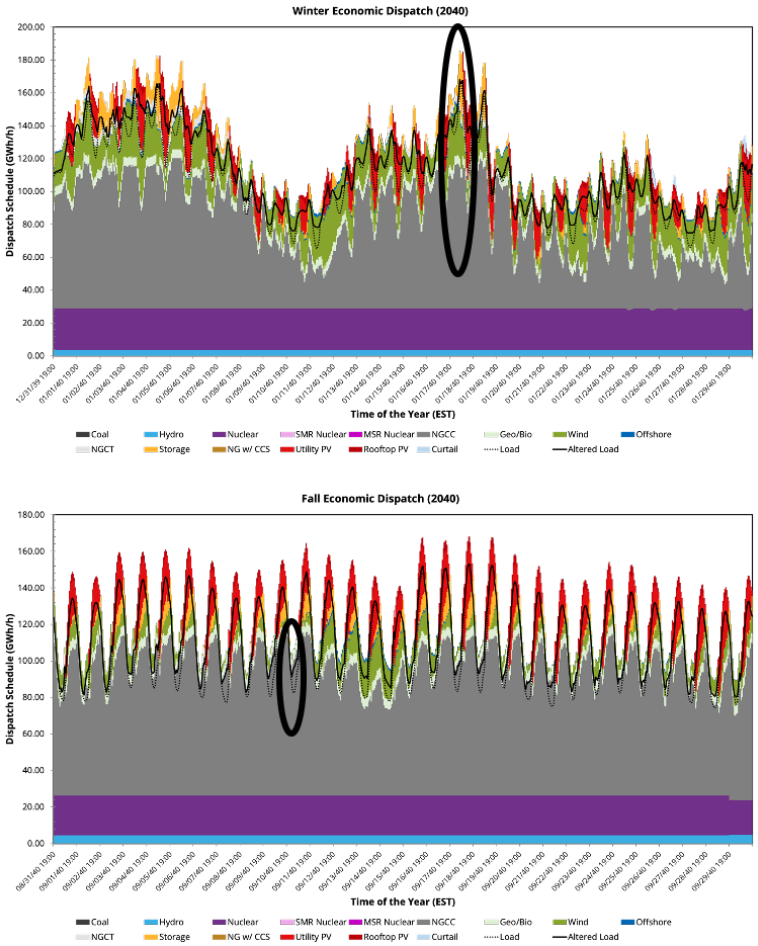

Figure 2.22: Economic dispatch from WIS:dom® for winter 2040 (top) and fall 2040 (bottom). The black oval in top plot shows period of most difficult load before siting VREs and black oval on the bottom plot shows the most difficult load period after optimal VRE siting.

The most difficult load period for the model in 2040, before any VREs are sited, is during winter (January 17th) at the morning load peak. It is seen from Figure 2.22 that during this period the siting decisions made by WIS:dom® ensure there is significant production from renewables. As a result of the optimal siting, it is found that the most difficult period is shifted to a nighttime period in Fall (September 10th). During this period, the system is at a lower stress levels as load is low and conventional generation is not deployed at full capacity. It is important to note that during this period generation from renewables is at its lowest thus ensuring that this period maintains reliability irrespective of actual weather conditions. Therefore, by incorporating the capacity value endogenously into the capacity expansion all three features that contribute to capacity value are captured simultaneously.

Another advantage of using this method to incorporate capacity value calculation endogenously is that the model is able to weigh, with each siting decision, the importance of added (or reduced) capacity value of that resource against ability to meet load at the lowest possible cost. It also ensures that the PRM is calculated accurately as the capacity value updates through the optimization process based on siting decisions. Finally, this method allows the model to inform its siting decisions based on meeting PRM limits and capacity value payments (if any), versus meeting load at lowest possible cost.

2.8 Transmission

As described in Section 3.5, WIS:dom® starts from a base-layer of transmission down to the 69 kV sub-station and this is reduced to the required resolution for the modeling purposes. For the current modeling, inter-state transmission was modeled at state-level resolution and within each state transmission is modeled at county-level to connect resources to the state node. For the "SE IRP" and "SE Economic IRP" scenarios, transmission was assumed to be fixed to 2018 levels with wheeling charges for inter-state power flow. For the "SE RTO" and "SE RTO with Nuclear" scenarios, transmission was allowed to expand and wheeling charges were dropped after setting up an RTO in 2025.

The model begins with an initial transmission topology at the appropriate resolution and an initial estimate of the transmission capacity using the Surge Impedance Method (SIL). The transmission capacities are then updated in the initialization by performing optimal dispatch using existing capacities in the initialization year (2018 in this case), weather during that year (informs VRE generation, heat-rates, transmission line ratings, transmission losses, heating and cooling loads), demand and available information on generation from EIA923. Based on these factors, the model adjusts the transmission capacities to ensure load is met assuming economic dispatch. Figure 2.23 shows the maximum import and export flows for each state as determined by WIS:dom® for 2018.

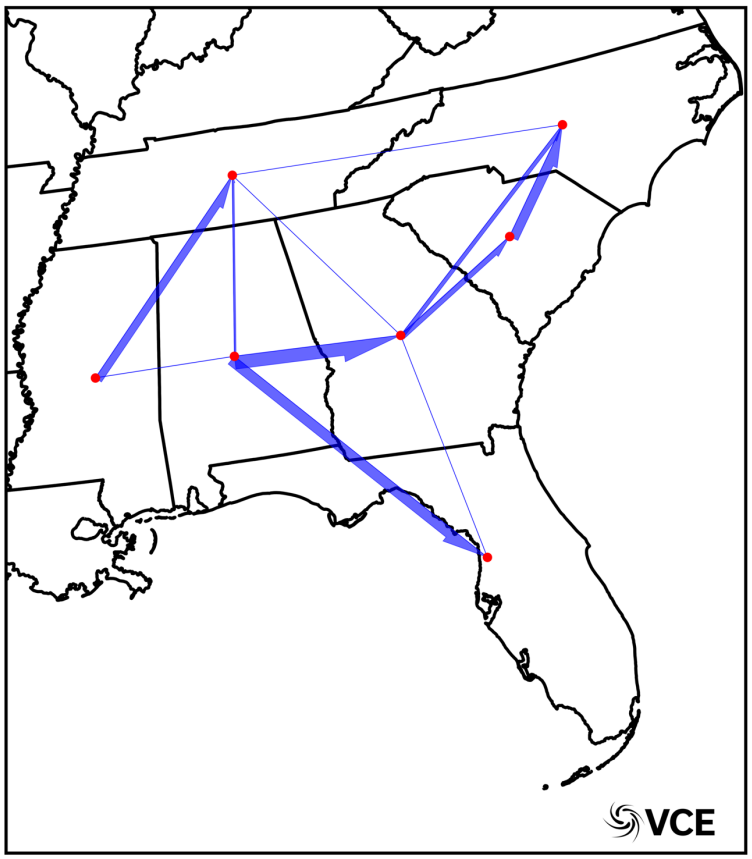

Figure 2.23: Initial maximum import and export capacities for each state in the southeast in 2018.

In the two scenarios that allowed transmission expansion, "SE RTO" and "SE RTO with Nuclear", the model installed about 10,000 MW of transmission capacity (see Figure 2.24). The "SE RTO with Nuclear" has a

slightly lower rate transmission buildout (since it has more firm nuclear generation and thus does not need to build transmission to optimize VRE use), but catches up to the "SE RTO" scenario buildout by 2040.

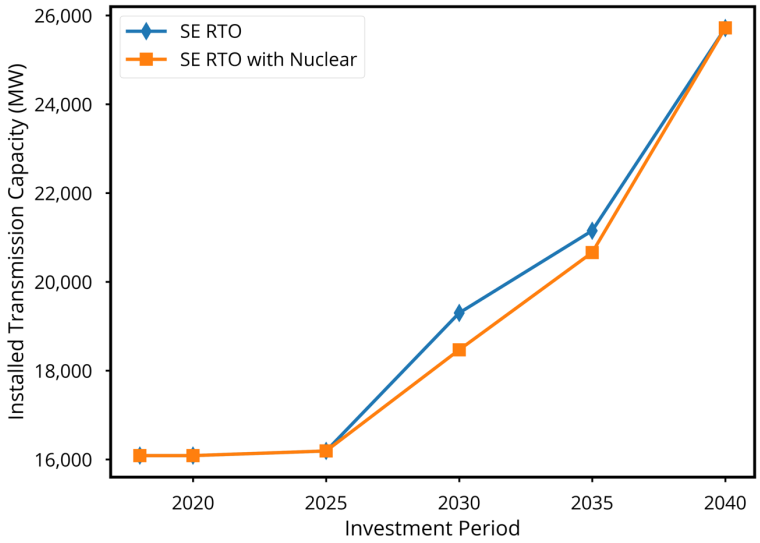

Figure 2.24: Installed transmission capacities for the southeast region in the "SE RTO" and "SE RTO with Nuclear" scenarios.

The maximum imports and exports from each state in the southeast in for the "SE RTO" and "SE RTO with Nuclear" scenarios in year 2040 are shown in Figure 2.25. It is observed that while the two scenarios take significantly different trajectories in terms of generation mix and utility versus distributed resource buildout, they end up having similar transmission buildouts. This indicates that transmission is a necessary ingredient in ensuring a cheap and reliable energy system.

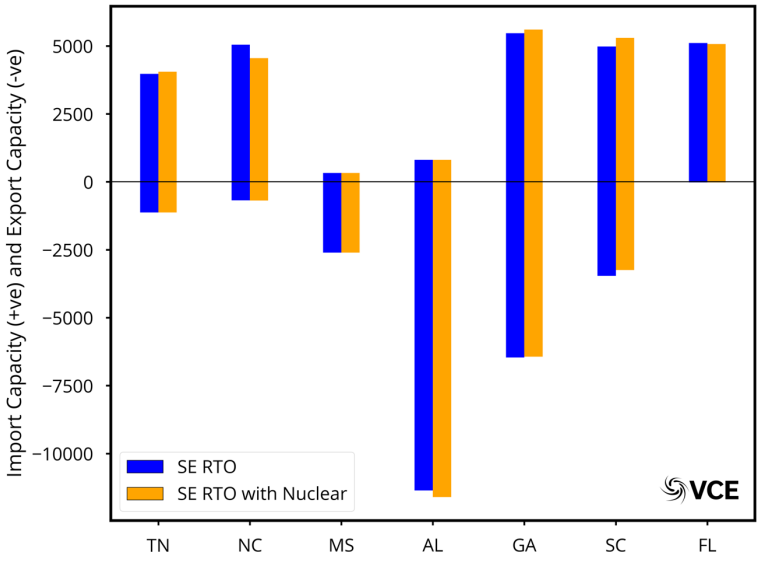

Figure 2.25: Max imports and exports by state for the "SE RTO" and "SE RTO with Nuclear" scenario in 2040.

Transmission is also seen to play a complimentary role in firming up VRE generation. Figure 2.26 shows the diurnal trend in winter and summer utilization rate of transmission along with wind, solar and storage capacity factors for Florida in the "SE RTO" scenario. Transmission is seen to have a clear diurnal trend in winter and summer where it has a high utilization rate during nighttime and lower utilization rate during

the daytime. The reason for this is that during the daytime when temperatures are higher, the transmission lines are prone to heating up faster which reduce their rating as well as increase losses. More importantly, during the daytime, solar generation offsets the need to import power from across state lines thus meeting load locally.

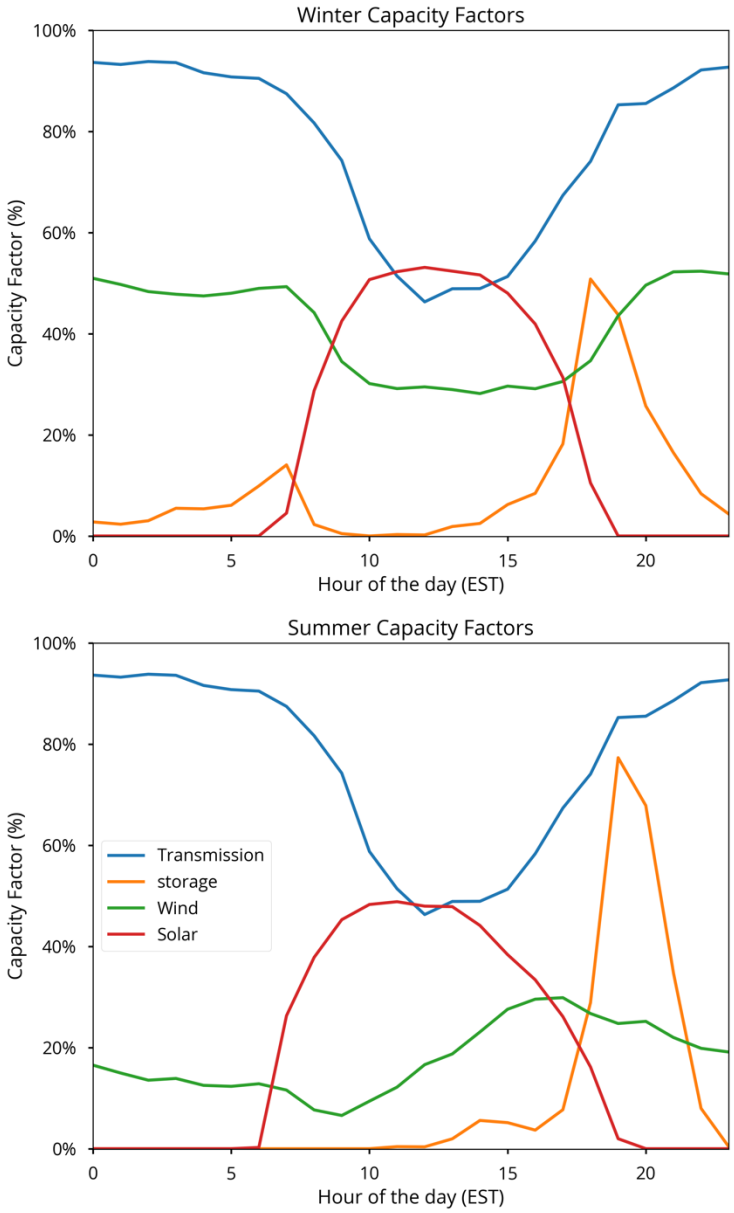

Figure 2.26: Diurnal winter (top) and summer (bottom) capacity factors of transmission (imports), wind, solar and storage in Florida in the "SE RTO" scenario.

Another reason for the higher utilization rates during the nighttime is that storage gets charged during the nighttime hours as shown in Figures 2.15 and 2.16. Transmission lines move excess power (due to lower nighttime loads) from across state lines to meet this load where needed.

2.9 Siting of WIS:dom® installed generation

Using the multi-year 3-km, 5-min weather dataset available over the contiguous United States, WIS:dom® is able to perform optimal siting of generators. Figure 2.27 shows the existing generators in 2018 and the optimal generator siting from the "SE RTO" scenario in 2040. Wind and solar generation are seen to be installed in the southern part of Florida where technical potential exists and is close to populations centers. North Carolina get the second largest wind installed capacity behind Florida, while more than 50% of all solar installed is seen to be installed in Florida.

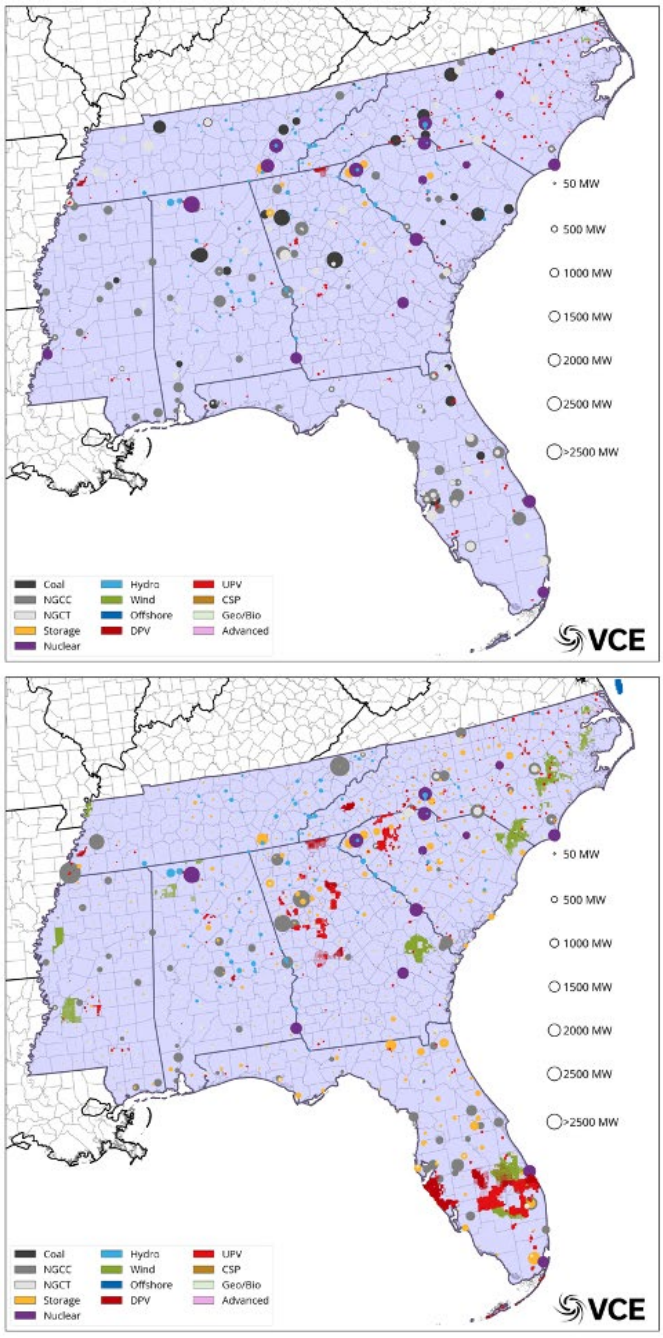

Figure 2.27: Existing generator siting in 2018 (top) and the optimal generator siting from "SE RTO" scenario in 2040 (bottom).

2.10 Impact of buildout constraints

To ensure reasonable results from capacity expansion planning, realistic constraints need to be imposed on the model in terms of capacity turnover allowed to occur per year. The capacity turnover limits depend on several factors, such as existing supply chains that can sustain a particular buildout rate for a technology, available skilled workforce that can be called upon, disruption in host communities from retirements which leads to job losses, lost tax revenues and other losses in the economy downstream of the power generator. In addition to the buildout limits, time lags are incorporated in installations for newer technologies.

For the southeast modeling, WIS:dom®-P was given capacity buildout and retirements rates for each technology as well as a limit on total capacity turnover rate specific to the southeast region. The installation rates allowed for each technology for the southeast modeling is shown in Figure 2.28. For the first investment period (2020) after the initialization, installation rate allowed is smaller given that there is less time to make any changes from the installation/retirement trajectory already in place. After 2020, allowed installation rates increase and grow at rate of 5% per year.

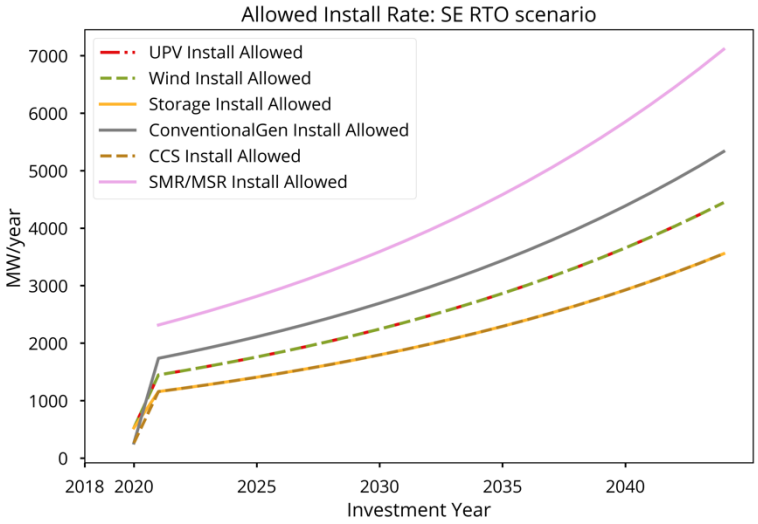

Figure 2.28: Installation rate allowed for technologies in WIS:dom®-P

In addition to the allowed installation rate, several technologies have a time-lag between planning and actual installation to replicate real-world dynamics. Utility-scale wind and solar PV have a one-year lag between planning and installation, storage has 6-month lag, SMR and MSR has 2.5-year lag and NG with CCS has a two-year lag. The limits on install rate and the time lag before they come online are important to restrain the model from making drastic changes to the capacity mix. Figure 2.29 shows the installation limits on wind and solar put in place for the southeast run and the actual WIS:dom®-P install rates. As seen from Figure 2.29, WIS:dom®-P attempts to install as much capacity as it can when it comes to renewables due to their lower cost in providing energy.

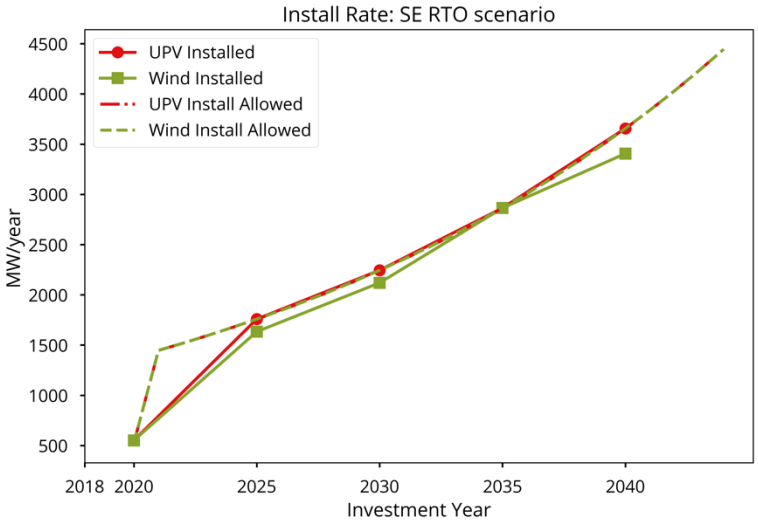

Figure 2.29: Installation rate allowed in the "SE RTO" scenario versus actual installation rate by WIS:dom®-P.

In addition to the limits on each technology, WIS:dom®-P has a limit on total capacity turnover that can occur per year. Starting year 2020, the total additional capacity that can be installed in the southeast is 3,500 MW / year and total capacity that can be retired is 2,900 MW / year. These rates also grow at 5% per year. The limits on total capacity additions and retirements mimic the real-world inertia to changing the composition of the grid and the adaptations that are necessary to run the grid reliably as newer technologies come online and the generation mix changes. The values are referenced against capital investments made historically within the US and other countries using the metric of kW / year / million $GDP; which normalizes all investments to a standard form.

2.11 Pollutants & GHG Emissions

The primary goal of the present study was to determine economic options for the southeastern United States to meet its electricity needs. However, it is also found that the economic benefits in the scenarios are accompanied with reduction in pollutants and greenhouse gas emissions. Figure 2.30 shows the cumulative reductions in major emission species observed in the scenarios compared against the "SE IRP" scenario.

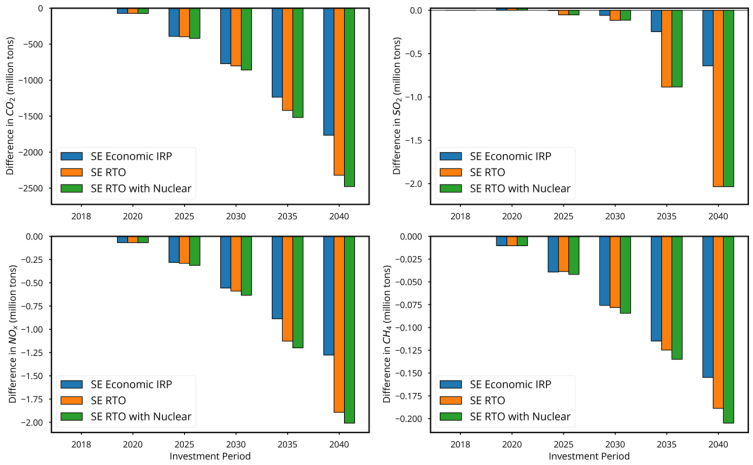

Figure 2.30: Cumulative reductions in pollutants and emissions in the scenarios modeled versus the "SE IRP" scenario.

The "SE RTO" scenario resulted in savings of 2,320 million metric tonnes of CO_2 (a 46% decrease) compared to the "SE IRP" scenario where emission increased by 16% (compared with 2018 levels) due to over build of fossil fuel generation. The emission reductions in the "SE RTO" scenario come from more efficient operation of grid assets, more renewables being installed due to their lower cost compared to conventional thermal generators and more transmission being built to allow efficient exchange of energy between the states. In the "SE RTO" scenario, all coal gets retired by 2040, which almost completely eliminates SO_2 emissions (as well as PM_{10} and $PM_{2.5}$) from the energy sector while contributing to big reductions in all other species of pollutants.

It is observed from Figure 2.30 that the impact of setting up an RTO has substantial benefits in term of emission savings. These emission reductions come with cost reductions, rather than cost increases. The emission savings in almost all species of pollutants are higher by 30% or more in the "SE RTO" scenario compared with the "SE Economic IRP" scenario. This further highlights the efficiencies achieved in a coordinated capacity expansion along with co-optimized transmission and distribution planning over the southeast region versus purely economic capacity expansion in individual states.

The "SE RTO with Nuclear" scenario resulted in higher emission savings compared with the "SE RTO" scenario. The effect of not retiring nuclear generation is cumulative CO_2 savings of an additional 156.76 million metric tonnes of CO_2 by 2040 compared with the "SE RTO" scenario (at an additional cumulative total system cost of $9 billion). As described in Section 2.4, this results in additional cost to consumers of approximately 0.11 ¢ / kWh. The "SE RTO with Nuclear" scenario still results in savings of $374.67 billion compared to the "SE IRP" scenario.

3. WIS:dom®-P Model Formulation

3.1 Overview

WIS:dom®-P is a ***fully combined*** capacity expansion and production cost model.

- ***Capacity expansion includes:***

  - ✓ Continental-scale (globally capable) & spatially-determined;
  - ✓ Co-optimization of transmission, generation, storage and distributed resources;
  - ✓ Myopically perform investment from 2020 through 2050 (in five-year windows);
  - ✓ Transmission resolved at each 69-kV substation;
  - ✓ Generation siting resolved at 3-km spatial resolution;
  - ✓ Existing policies, restrictions and incentives;
  - ✓ Detailed land-use screening for siting of technologies;
  - ✓ Future cost projections for technologies and fuels;
  - ✓ Detail accounting for retirement of generation assets;
  - ✓ Includes climate change data from CMIP-5 for possible future drivers of infrastructure stress;

- ***Production cost includes:***

  - ✓ Unit commitment;
  - ✓ Start-up & shutdown profiles of generators;
  - ✓ Ramp constraints, minimum up and minimum down times;
  - ✓ Transmission power flow, dynamic line ratings and line losses;
  - ✓ Planning reserve margins and operating reserves, with detailed VRE accounting;
  - ✓ Distribution planning & hybrid optimization of the grid edge;
  - ✓ Weather forecasting and physics of weather engines for resources and demands;
  - ✓ 5-minutely temporal granularity for a minimum of one calendar year (up to seven);
  - ✓ Zero loss of load at any time or location;
  - ✓ Detailed energy storage subroutines for arbitrage & reliability asset configurations;
  - ✓ Demand flexibility modeling based on granular weather drivers;
  - ✓ Novel technology inclusion (SMR, MSR, EGS, CCS, DAC, H_2, NH_3, CH_4, P2X);
  - ✓ Existing generator and transmission asset characteristics such as heat rates, power factor, variable costs, fixed costs, capital costs, ramp rate constraints, minimum up and down time, undepreciated value, fuel supply chain, and fuel costs.

3.2 Geographic Scope

The WIS:dom®-P optimization model was designed to be able to cover numerous different geographic regions. The version used for the present study was reduced down from the contiguous United States to only include the South East of the United States. In particular it comprises Alabama, Florida, Georgia, Mississippi, North Carolina, South Carolina and Tennessee. Figure 3.1 displays the existing generators across the study region.

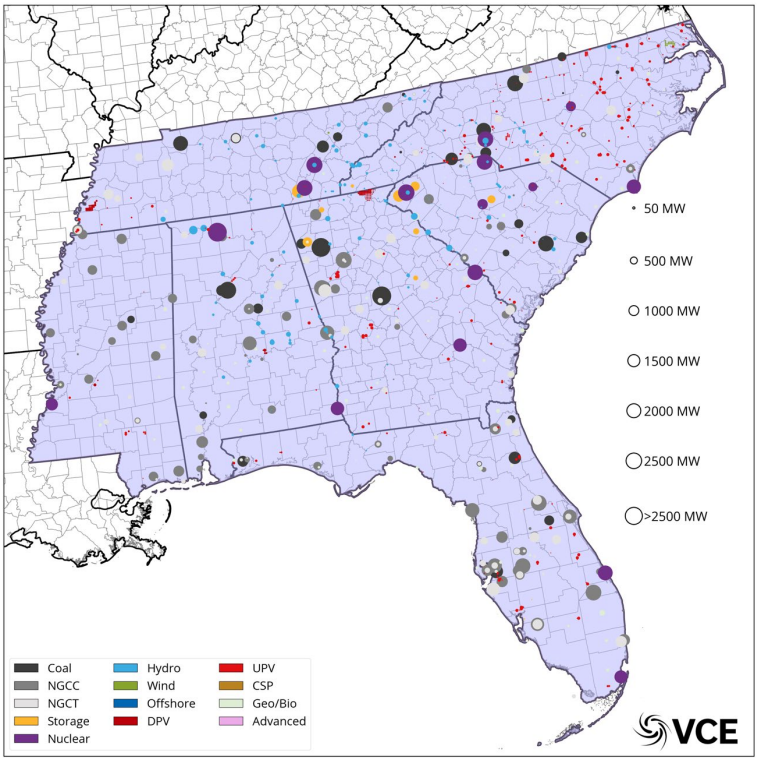

Figure 3.1: The geographic scope of the present study with the 2018 generator siting displayed.

The model had access to 3-km, 5-minutely generation profile data for the entire geographic footprint for multiple calendar years. Screening was performed to determine accurate resource technical potential for siting new generation (as discussed in Section 4).

3.3 Objective Function

The WIS:dom®-P optimization model is typically run in linear programming mode. This means that the equations and constraints are all described as linear (and convex) relaxation formulations. There are mixed integer and non-linear formulations available within WIS:dom®-P; however, accuracy is not enhanced in an appreciable manner for capacity expansion studies considering the additional computational burden.

The objective function is to minimize the total system cost for a given construct of constraints and sectoral coupling. The total system cost includes: amortized generator capital expenditures, fuel costs, start-up and shutdown costs, amortized transmission capital expenditures, amortized storage capital expenditures, variable operation and maintenance (O&M) expenditures, fixed O&M expenditures, amortized natural gas transport expenditures, transmission wheeling charges, transmission access charges, interconnection expenditures, demand-side management and demand response expenditures, distribution costs and access charges, curtailment charges, reserve costs, retirement costs, and international trading costs.

Equation (3.1) is the mathematical formulation of the objective function:

$$\Gamma = \min \sum_{\mathcal{L}} \left\{ \begin{array}{c} \sum_{\mathcal{T}} \left\{ \mathcal{C}^{\mathcal{G}}_{\mathcal{T}\mathcal{L}} \cdot x_{\mathcal{T}\mathcal{L}} + \hbar \cdot \sum_{t} [(\mathcal{V}^{\mathcal{G}}_{\mathcal{T}\mathcal{L}t} + (\mathcal{F}^{\mathcal{G}}_{\mathcal{T}\mathcal{L}t} + \mathcal{V}^{c}_{\mathcal{L}} \cdot \mathfrak{F}_{\mathcal{T}\mathcal{L}}) \cdot \mathcal{H}^{\mathcal{G}}_{\mathcal{T}\mathcal{L}t}) \cdot \mathcal{p}_{\mathcal{T}\mathcal{L}t} + \Delta \cdot (\mathcal{V}^{\mathcal{O}}_{\mathcal{T}\mathcal{L}t} \cdot \phi_{\mathcal{T}\mathcal{L}t})] \right\} + \hbar \cdot \sum_{t} (\mathcal{V}^{\mathcal{J}}_{\mathcal{L}t} \cdot \mathcal{J}_{\mathcal{L}t}) \\ + \sum_{\eta} \left[\sum_{\alpha} (\mathcal{C}^{\mathcal{S}}_{\alpha\eta\mathcal{L}} \cdot \mathcal{y}_{\alpha\eta\mathcal{L}}) + \hbar \cdot \sum_{t} (\mathcal{V}^{\mathcal{S}}_{\eta\mathcal{L}t} \cdot \mathfrak{D}_{\eta\mathcal{L}t}) \right] + \sum_{\mathfrak{B}} \left\{ \begin{array}{c} \sum_{\hat{\mathcal{L}}} \left[\frac{\mathcal{C}^{tr}_{\mathfrak{B}\mathcal{L}\hat{\mathcal{L}}} \cdot \mathcal{R}^{tr}_{\mathfrak{B}\mathcal{L}\hat{\mathcal{L}}} \cdot \mathcal{Q}^{tr}_{\mathfrak{B}\mathcal{L}\hat{\mathcal{L}}} \cdot z^{tr}_{\mathfrak{B}\mathcal{L}\hat{\mathcal{L}}}}{2} + \hbar \cdot \sum_{t} (\mathcal{V}^{w}_{\mathfrak{B}\mathcal{L}\hat{\mathcal{L}}t} \cdot \mathfrak{f}_{\mathfrak{B}\mathcal{L}\hat{\mathcal{L}}t}) \right] \\ + \sum_{\beta} (\mathcal{C}^{\mathcal{N}}_{\mathfrak{B}\mathcal{L}\beta} \cdot n_{\mathfrak{B}\mathcal{L}\beta}) + \hbar \cdot \sum_{t} (\mathcal{V}^{\mathcal{N}}_{\mathfrak{B}\mathcal{L}t} \cdot u_{\mathfrak{B}\mathcal{L}t}) \\ + \Delta \cdot \Delta^{\mathfrak{B}} \cdot (\mathcal{V}^{\mathcal{O}}_{\mathfrak{B}\mathcal{L}t} \cdot \phi_{\mathfrak{B}\mathcal{L}t}) \end{array} \right\} \\ + \hbar \cdot \sum_{\mathfrak{D}} \sum_{t} (\mathcal{V}^{\mathfrak{D}}_{\mathfrak{D}\mathcal{L}t} \cdot r^{-}_{\mathfrak{D}\mathcal{L}t}) + \sum_{t} (\hbar \cdot \mathcal{V}^{\mathcal{H}}_{\mathcal{L}t} \cdot \mathcal{W}_{\mathcal{L}t} + \mathcal{V}^{\mathcal{R}}_{\mathcal{L}t} \cdot q_{\mathcal{L}t}) + \Theta \cdot \left(\sum_{\mathcal{T}} (\mathcal{C}^{\mathcal{G}\sigma}_{\mathcal{T}\mathcal{L}} \cdot x^{\sigma}_{\mathcal{T}\mathcal{L}} + \mathcal{C}^{\mathcal{G}r}_{\mathcal{T}\mathcal{L}} \cdot x^{r}_{\mathcal{T}\mathcal{L}}) + \Re_{\mathcal{L}} \right) \\ + \Lambda \cdot \left\{ \mathcal{C}^{dp}_{\mathcal{L}} \cdot [\mathcal{E}^{p}_{\mathcal{L}} + \lambda_a \cdot (\mathcal{E}^{\mathfrak{k}}_{\mathcal{L}} + \mathcal{E}^{m}_{\mathcal{L}})] + \hbar \cdot \mathcal{C}^{de}_{\mathcal{L}} \cdot \sum_{t} (\mathcal{E}_{\mathcal{L}t} - \lambda_b \cdot \mathcal{J}_{\mathcal{L}t}) \right\} \end{array} \right\} \tag{3.1}$$

The objective function, Eq. (3.1), contains the following sets:

$\mathcal{T}$ the set of technologies considered as generation;
η the set of storage technologies;
$\mathcal{L}$ the set of spatial location that the model resolves;
t the set time steps considered by the model for production cost;
$\mathfrak{B}$ the set of technologies that require flows / transmission corridors;
α the set of component parts to storage (power and energy);
β the set of component parts to coupled fuel production sectors (production and storage);
$\mathfrak{D}$ the set of demand-side flexibility resources;
$\hat{\mathcal{L}}$ the dummy set of spatial locations that the model resolves.

The objective function, Eq. (3.1), contains the following (user-defined) parameters:

$\mathcal{C}^{\mathcal{G}}_{\mathcal{T}\mathcal{L}}$ is the amortized capital and fixed costs for generation technologies;
$\mathcal{C}^{\mathcal{G}\sigma}_{\mathcal{T}\mathcal{L}}$ is the adjustment to the amortized capital and fixed costs for "old" generation technologies;
$\mathcal{C}^{\mathcal{G}r}_{\mathcal{T}\mathcal{L}}$ is the amortized remaining balance cost to retire "old" generation technologies;
$\mathcal{C}^{\mathcal{S}}_{\alpha\eta\mathcal{L}}$ is the amortized capital and fixed costs for storage technologies;

$\mathcal{C}^{tr}_{\mathfrak{B}\mathcal{L}\hat{\mathcal{L}}}$ *is the amortized capital and fixed costs for transmission technologies;*
$\mathcal{C}^{\mathcal{N}}_{\mathfrak{B}\mathcal{L}\beta}$ *is the amortized capital and fixed costs for fuel production technologies;*
$\mathcal{C}^{dp}_{\mathcal{L}}$ *and* $\mathcal{C}^{de}_{\mathcal{L}}$ *are the amortized capital and fixed costs for distribution infrastructure;*
$\mathfrak{R}_{\mathcal{L}}$ *is the retirement payments still being paid for "early" shuttered generation technologies;*
$\mathcal{V}^{\mathcal{G}}_{\mathcal{T}\mathcal{L}t}$ *is the variable cost per unit of electricity for generation technologies;*
$\mathcal{V}^{\mathcal{O}}_{\mathcal{T}\mathcal{L}t}$ *is the start-up cost per unit of capacity for generation technologies;*
$\mathcal{V}^{\mathcal{O}}_{\mathfrak{B}\mathcal{L}t}$ *is the start-up cost per unit of capacity for novel fuel (chemical) technologies;*
$\mathcal{V}^{\mathcal{J}}_{\mathcal{L}t}$ *is the trade price per unit of electricity for imports and exports;*
$\mathcal{V}^{c}_{\mathcal{L}}$ *is the carbon tax per unit of carbon for fossil fuel consumption;*
$\mathcal{V}^{\mathcal{S}}_{\eta\mathcal{L}t}$ *is the variable cost per unit of electricity for storage technologies;*
$\mathcal{V}^{w}_{\mathfrak{B}\mathcal{L}\hat{\mathcal{L}}t}$ *is the wheeling charge cost per unit of electricity for transmission technologies;*
$\mathcal{V}^{\mathcal{N}}_{\mathfrak{B}\mathcal{L}t}$ *is the variable cost per unit of electricity consumed for fuel production technologies;*
$\mathcal{V}^{\mathfrak{D}}_{\mathfrak{D}\mathcal{L}t}$ *is the variable cost per unit of electricity shifted by demand-side flexibility resources;*
$\mathcal{V}^{\mathcal{K}}_{\mathcal{L}t}$ *is the variable cost per unit of electricity curtailed;*
$\mathcal{V}^{\mathcal{R}}_{\mathcal{L}t}$ *is the variable cost per unit of electricity of rapid-response reserves available;*
$\mathcal{F}^{\mathcal{G}}_{\mathcal{T}\mathcal{L}t}$ *is the fuel cost per unit of primary energy for generation technologies;*
$\mathcal{H}^{\mathcal{G}}_{\mathcal{T}\mathcal{L}t}$ *is the weather-dependent heat rate value for generation technologies;*
$\mathfrak{F}_{\mathcal{T}\mathcal{L}}$ *is the carbon content per unit of primary energy for generation technologies;*
$\mathcal{R}^{tr}_{\mathfrak{B}\mathcal{L}\hat{\mathcal{L}}}$ *is the pathway distance matrix of the transmission technologies;*
$\mathcal{Q}^{tr}_{\mathfrak{B}\mathcal{L}\hat{\mathcal{L}}}$ *is the cost allocation matrix of the transmission technologies;*
$\hbar$ *is the adjustment for temporal resolution (5-minutely would mean* $\hbar = {}^{1}/_{12}$*),*
Δ *and* $\Delta^{\mathfrak{B}}$ *are the unit commitment activation indicators (binary);*
Θ *is the retirement tracking activation indicator (binary);*
Λ, λ_a *and* λ_b *are the DER subroutine adjustment factors (all are typically set to unity).*

The objective function, Eq. (3.1), contains the following (endogenous) variables:

$x_{\mathcal{T}\mathcal{L}} = \sum_{\mathfrak{L}\in\mathcal{L}}(x_{\mathcal{T}\mathfrak{L}})$ *is the installed capacity of generation technologies;*
$x^{o}_{\mathcal{T}\mathcal{L}} = \sum_{\mathfrak{L}\in\mathcal{L}}(x^{o}_{\mathcal{T}\mathfrak{L}})$ *is the "old" installed capacity of generation technologies;*
$x^{r}_{\mathcal{T}\mathcal{L}} = \sum_{\mathfrak{L}\in\mathcal{L}}(x^{r}_{\mathcal{T}\mathfrak{L}})$ *is the retired "old" installed capacity of generation technologies;*
$\mathcal{y}_{\alpha\eta\mathcal{L}} = \sum_{\mathfrak{L}\in\mathcal{L}}(\mathcal{y}_{\alpha\eta\mathfrak{L}})$ *is the installed capacity of storage technologies;*
$z^{tr}_{\mathfrak{B}\mathcal{L}\hat{\mathcal{L}}}$ *is the installed capacity of transmission technologies;*
$n_{\mathfrak{B}\mathcal{L}\beta} = \sum_{\mathfrak{L}\in\mathcal{L}}(n_{\mathfrak{B}\mathfrak{L}\beta})$ *is the installed capacity of fuel production facilities;*
$\mathcal{p}_{\mathcal{T}\mathcal{L}t} = \sum_{\mathfrak{L}\in\mathcal{L}}(\mathcal{p}_{\mathcal{T}\mathfrak{L}t})$ *is the generation output from generation technologies;*
$\mathfrak{D}_{\eta\mathcal{L}t} = \sum_{\mathfrak{L}\in\mathcal{L}}(\mathfrak{D}_{\eta\mathfrak{L}t})$ *is the discharge from storage technologies;*
$\mathcal{W}_{\mathcal{L}t} = \sum_{\mathfrak{L}\in\mathcal{L}}(\mathcal{W}_{\mathfrak{L}t})$ *is the electricity that is curtailed;*
$\mathfrak{f}_{\mathfrak{B}\mathcal{L}\hat{\mathcal{L}}t}$ *is the energy flow transmission matrix;*
$u_{\mathfrak{B}\mathcal{L}t} = \sum_{\mathfrak{L}\in\mathcal{L}}(u_{\mathfrak{B}\mathfrak{L}t})$ *is the electricity demand for fuel production from the fuel production facilities;*
$\mathcal{I}_{\mathcal{L}t}$ *is the electricity trade occurring;*
$q_{\mathcal{L}t} = \sum_{\mathfrak{L}\in\mathcal{L}}(q_{\mathfrak{L}t})$ *is the rapid-response reserves available;*
$r^{-}_{\mathfrak{D}\mathcal{L}t} = \sum_{\mathfrak{L}\in\mathcal{L}}(r^{-}_{\mathfrak{D}\mathfrak{L}t})$ *is the demand-down-shifted by the demand-side flexibility resources;*
$\phi_{\mathcal{T}\mathfrak{L}t} = \sum_{\mathfrak{L}\in\mathcal{L}}(\phi_{\mathcal{T}\mathfrak{L}t})$ *is the generation capacity being started;*
$\phi_{\mathfrak{B}\mathcal{L}t} = \sum_{\mathfrak{L}\in\mathcal{L}}(\phi_{\mathfrak{B}\mathfrak{L}t})$ *is the capacity of the novel fuel (chemical) facility being started;*
$\mathcal{E}_{\mathcal{L}t} = \sum_{\mathfrak{L}\in\mathcal{L}}(\mathcal{E}_{\mathfrak{L}t})$ *is the electricity demand;*
$\mathcal{J}_{\mathcal{L}t} = \sum_{\mathfrak{L}\in\mathcal{L}}(\mathcal{J}_{\mathfrak{L}t})$ *is the distribution-level generation;*
$\mathcal{E}^{\mathcal{p}}_{\mathcal{L}}$ *and* $\mathcal{E}^{\mathcal{p}}_{\mathcal{L}}$ *are the peak consumption and injection of power for the distribution level;*
$\mathcal{E}^{m}_{\mathcal{L}}$ *is the minimum input electricity demand, which is included as a correction term.*

Since Eq. (3.1) is linear, the subsets of spatial locations, $\mathcal{L}$, that are not electrically connected will solve as independent systems. Further, the equation can be sub-divided by the user (through identifying tuples) to include only specific regions and the resulting solution can be stitched back together. The generalized formulation of Eq. (3.1) allows the spatial granularity to be reconfigured for any domain of interest without altering the mathematics; however, the inputs will need adjusting to respect the aggregation or averaging of parameters. The amortized capital and fixed costs include the "spur" transmission line costs to connect sub-scale asset locations ($\mathfrak{L}$) to the nearest modeled locations ($\mathcal{L}$).

Equation (3.2) is the mathematical formulation of the amortization and fixed cost for assets:

$$\mathcal{C}_{\varepsilon\delta}^{\mathrm{X}} = \left(\widehat{\mathcal{C}_{\varepsilon\delta}^{\mathrm{X}}} + \widehat{\mathcal{C}_{\varepsilon\delta}^{tr}}\right) \cdot \frac{\mathcal{DR}_{\varepsilon\delta} \cdot (1 + \mathcal{DR}_{\varepsilon\delta})^{\mathrm{T}_{\varepsilon\delta}}}{(1 + \mathcal{DR}_{\varepsilon\delta})^{\mathrm{T}_{\varepsilon\delta}} - 1} + \mathfrak{O}_{\varepsilon\delta}^{\mathrm{X}} \tag{3.2}$$

In Eq. (3.2) the (user-defined) parameters are:

$\widehat{\mathcal{C}_{\varepsilon\delta}^{X}}$ is the capital cost per unit capacity for each asset;
$\widehat{\mathcal{C}_{\varepsilon\delta}^{tr}}$ is the capital cost per unit capacity of "spur" transmission for each asset;
$\mathcal{DR}_{\varepsilon\delta}$ is the weighted cost of capital (WACC) for each asset;
$T_{\varepsilon\delta}$ is the expected book-life for each asset;
$\mathfrak{O}_{\varepsilon\delta}^{X}$ is the fixed operation and maintenance cost for each asset.

For the present study, Eq. (3.1) was solved for each individual Balancing Authority Area (BAA) over the South East United States for the "Business As Usual" and "Non RTO" scenarios. For the RTO scenarios, Eq (3.1) was solved for the entire South East United States as a single BAA from 2025 (when the RTO is assumed to have formed). Further, in the RTO scenario, the wheeling charges were removed from 2025 onwards ($\mathcal{V}_{\mathfrak{B}L\hat{L}t}^{w} = 0 \; \forall \; \mathfrak{B}, \mathcal{L}, \hat{\mathcal{L}}, t$). No carbon tax was applied for any of the scenarios ($\mathcal{V}_{\mathcal{L}}^{c} = 0 \; \forall \; \mathcal{L}$). No novel technologies or synthetic fuel production were assumed for any of the scenarios ($\beta = \{\quad\}$ and $\mathfrak{B} = \{transmission\}$). Full unit commitment was turned off ($\Delta = 0$ and $\Delta^{\mathfrak{B}} = 0$), retirement tracking was turned off ($\Theta = 0$), while the DER subroutine was turned on ($\Lambda = \lambda_a = \lambda_b = 1$). There was assumed to be no electricity trade from the South East domain to the rest of the world ($\mathcal{I}_{\mathcal{L}t} = 0 \; \forall \; \mathcal{L}, t$). The storage technologies were resolved as distribution- and utility- scale ($\eta = \{Utility\ Storage, Distr.Storage\}$). There was no cost to curtailing variable renewable generation ($\mathcal{V}_{\mathcal{L}t}^{\mathcal{K}} = 0 \; \forall \; \mathcal{L}, t$). The remaining inputs and assumptions pertaining to costs for the objective function are described in Section 4.

3.4 Robust Supply and Demand Balance

A unique feature of WIS:dom®-P is the ability to co-optimize for capacity expansion of generation, storage, transmission, and demand-side resources while simultaneously simulating the production costs of those assets. The production cost is simulated over the entire grid at 3-km, 5-minute granularity for a minimum of a calendar year for each investment period. Typically, seven calendar years are also simulated after a pathway solution is found. Future simulations will also include 175 years of 50-km, hourly data to determine the robustness of solutions. The dominant constraint in the production cost component of WIS:dom®-P is the supply and demand balance equation set. This equation set ensures that generation, power flow, storage, distributed resources, and load are in constant equilibrium with each other, without fail, throughout the electricity system simulated. The supply and demand balance equation set includes: power production from generators, transmission power flow, the transmission dynamic line ratings and losses due to weather, the unforced outages of generators, the weather-driven (wind, solar, and hydro) resource potential, charge/discharge cycles of storage and demand flexibility, changes in demand requirements throughout the entire simulation period, the electricity consumption for fuel production, curtailment of generation, electricity trade, and distribution generation. The supply and demand balance equation set directly (and indirectly) connect with numerous other equation sets (described later); that together ultimately act in concert to increase the value of the objective function.

Equation (3.3) is the mathematical formulation of the supply and demand balance equation set:

$$\sum_{\mathfrak{L}\in\mathcal{L}}\left\{\begin{array}{l}(1-\ell^{\delta}_{\mathfrak{L}t})\cdot\left[\sum_{\mathcal{T}}(p_{\mathcal{T}\mathfrak{L}t})-\mathcal{W}_{\mathfrak{L}t}+\sum_{\eta}\left(\mathfrak{D}_{\eta\mathfrak{L}t}-\mathfrak{C}_{\eta\mathfrak{L}t}\right)\right]\\ -(1+\ell^{\delta}_{\mathfrak{L}t})\cdot\left(\mathcal{E}_{\mathfrak{L}t}+r^{+}_{\mathfrak{D}\mathfrak{L}t}-r^{-}_{\mathfrak{D}\mathfrak{L}t}+\sum_{\mathfrak{B}}u_{\mathfrak{B}\mathfrak{L}t}\right)\end{array}\right\}+\mathcal{I}_{\mathcal{L}t}+\left(\widehat{f^{tr}_{\mathcal{L}t}}-\widehat{f^{\ell}_{\mathcal{L}t}}\right)=0\quad\forall\,\mathcal{L},t \tag{3.3}$$

The supply and demand equation set, Eq. (3.3), contains some of the sets from Eq. (3.1), and in addition contains the set:

> $\mathfrak{L}$ *the set of all sub-scale locations for each set element of* $\mathcal{L}$.

The supply and demand equation set, Eq. (3.3), contains only one (exogenous) parameter:

> $\ell^{\delta}_{\mathfrak{L}t}$ *the estimated "spur" line losses for each sub-scale location, determined in pre-processing to incorporate the weather driven changes to losses.*

The supply and demand equation set, Eq. (3.3), contains some of the variables from Eq (3.1), and in addition contains the following (endogenous) variables:

> $\mathfrak{C}_{\eta\mathcal{L}t}=\sum_{\mathfrak{L}\in\mathcal{L}}\mathfrak{C}_{\eta\mathfrak{L}t}$ *is the charging of the storage technologies;*
> $r^{+}_{\mathfrak{D}\mathcal{L}t}=\sum_{\mathfrak{L}\in\mathcal{L}}r^{+}_{\mathfrak{D}\mathfrak{L}t}$ *is the demand-up-shifted by the demand-side flexibility resources;*
> $\widehat{f^{tr}_{\mathcal{L}t}}$ *is the net electrical transmission flux;*
> $\widehat{f^{\ell}_{\mathcal{L}t}}$ *is the sum of all the electrical transmission line losses.*

Equation (3.3) is a generalized formulation, and if there are no sub-scale locations (nodal version) the "spur" line losses disappear. The "spur" line losses are used to parameterize distribution- and utility-scale

generation and demands as well as represent power transmission that is not explicitly resolved. The transmission flux and line losses ($\widehat{\not{p}_{\mathcal{L}t}^{tr}}$ and $\widehat{\not{p}_{\mathcal{L}t}^{\ell}}$) are described in the transmission equation sets. The two terms are decomposed to ensure Kirchhoff current and voltage laws are obeyed and for computational expedience.

For the purposes of modeling, the variable for curtailed electricity ($\mathcal{W}_{\mathcal{L}t}$) must be constrained. The constraint stops the model being allowed to curtail electricity when variable generation ($\sum_{\mathcal{T}\in VRE}(\not{p}_{\mathcal{T}\mathcal{L}t})$) is not available (i.e. ensures that curtailing thermal generation does not happen). The main purpose of constraining curtailment is to strengthen the enforcement of ramp constraints on generators (described later), particularly down ramping. The constraint is represented mathematically in Eq. (3.4):

$$\sum_{\mathcal{T}\in VRE}(\not{p}_{\mathcal{T}\mathcal{L}t}) - \mathcal{W}_{\mathcal{L}t} \geq 0 \quad \forall\, \mathcal{L}, t \tag{3.4}$$

For the present study, the set of locations ($\mathcal{L}$) is the BAAs in the South East and the set of sub-scale locations ($\mathfrak{L}$) is the county and 3-km resource sites. There is not electricity trading outside the domain of the South East ($\mathcal{I}_{\mathcal{L}t} = 0\ \forall\, \mathcal{L}, t$). There is no synthetic fuel production ($\sum_{\mathfrak{B}} \mathcal{u}_{\mathfrak{B}\mathcal{L}t} = 0\ \forall\, \mathfrak{B}, \mathcal{L}, t$). The demand ($\mathcal{E}_{\mathcal{L}t}$) and demand-side flexibility resources ($r^{+}_{\mathfrak{D}\mathcal{L}t}, r^{-}_{\mathfrak{D}\mathcal{L}t}$) are populated with data from the Integrated Resource Plans (IRP) for each of the constituent States. However, the profiles of the demand and demand-side flexibility resources are weather-aligned for the purposes of the modeling.

3.5 Transmission & Flows

Another important feature of WIS:dom®-P is that it resolves the transmission topology and power flow for the electricity system being modeled. Moreover, the model can expand the transmission explicitly and economically as a co-optimization with other assets. The modeling of the transmission from a capacity expansion perspective must assess the amount of power that can flow along the transmission lines, the losses it may encounter (a function of distance, voltage and weather) to satisfy the balance of demands everywhere. From the production cost perspective, the transmission must obey the two fundamental Kirchhoff laws (current and voltage) at all times and at all locations.

The transmission can be reduced in complexity and the sub-scale locations can be modeled implicitly within WIS:dom®-P. This enables the model to rescale for computational efficiency and be run iteratively using the larger geographic scope (and coarser transmission representation) as boundary conditions for the smaller geographic scope (with finer transmission representation).

The construction of new transmission lines can happen in two ways: the model augments an existing right-of-way (ROW) as well as expanding the substations if required, or the model builds a completely new transmission line and connects two existing substations (and augments them if necessary). The costs are different for performing the two different approaches.

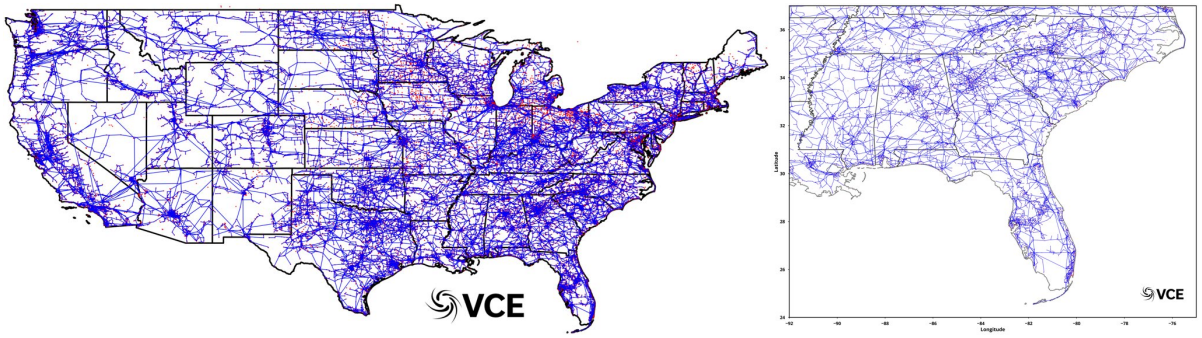

Figure 3.2: The full existing transmission topology for WIS:dom®-P across the contiguous (left) and Southeast (right) USA.

Figure 3.2 displays the fullest transmission representation that WIS:dom®-P can have for the contiguous United States and the South East. The data represented is every transmission line and substation down to 69-kV. Below 69-kV, the 3-km data includes implicit transmission for generation and loads. Figure 3.3 displays the same data, but in the reduced form of county-level (left) and state-level (right). Figure 3.3 displays two example reduced form topologies. Other reduced form setups can be created, such as Regional Transmission Operators (RTOs), utilities, BAA, or some other regional framework. The purpose of the reduced form topology is to enable computation of large geographic areas while maintaining resource fidelity and use the resulting solutions as boundary conditions for more granular representations.

For the special case of a High-voltage Direct Current (HVDC) transmission network (or overlay), the model adds an element to the set $\mathfrak{B}$ with (typically) nodes in every state with potential lines connecting each state to its adjoining neighbors. This is in addition to the existing High-voltage Alternating Current (HVAC) transmission system. The HVDC is tied to the HVAC system via inverter and rectifier stations at the HVDC nodes. The HVDC transmission lines and stations must be paid for by the model and are co-optimized with the HVAC system and all the other grid assets.

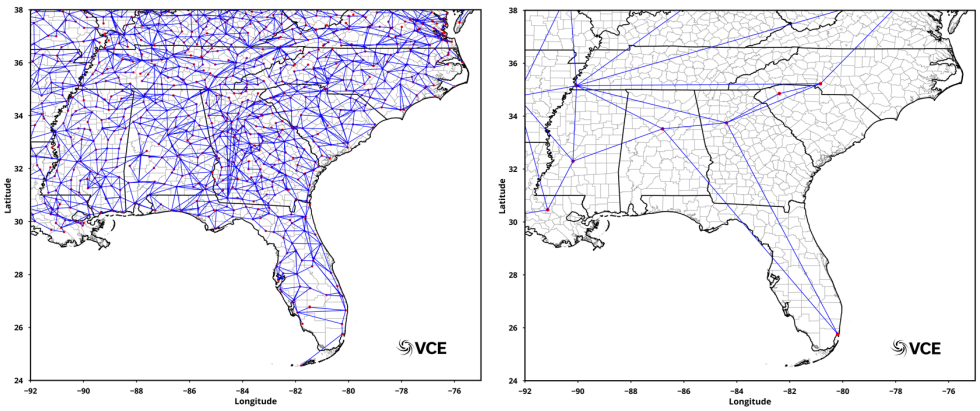

Figure 3.3: The reduced form transmission topology representation in WIS:dom®-P for county-level (left) and state-level (right).

WIS:dom®-P does not only model the electricity transmission lines. The model also accounts for natural gas system (pipelines and storage). Further, the model can build a hydrogen economy, an infrastructure for synthetic ammonia production and an infrastructure for carbon capture and sequestration or utilization (for synthetic fuels). Mathematically, these can be modeled in a very similar way to electricity transmission. The limitation being that the representation will not account for gas pressures along the pipelines explicitly, only the flow between points, amounts held in storage, and conservation of mass. Further simulations can be carried out with gas pressures being computed. A leakage rate can be computed (and is included), but the standard inputs assume zero leakage in the transmission and storage of fuels.

For the production (or capture) of fuels and chemicals (e.g. H_2, NH_3, CO_2, CH_4) additional modeling is required for the capacity build out and electricity (and possible other fuel or chemical) consumption. These can all be reduced down to a single set of equations defined over the set $\mathfrak{B}$. These extra equations for products are described in a subsection 3.12.

Equation (3.5) is the mathematical description of the transmission (and flow) capacity constraint:

$$\mathfrak{DCR}_{\mathfrak{B}L\hat{L}t} \cdot z^{tr}_{\mathfrak{B}L\hat{L}} - \sum_{\hat{L}} (\mathfrak{f}_{\mathfrak{B}L\hat{L}t} + \mathfrak{f}_{\mathfrak{B}\hat{L}Lt}) \geq 0 \quad \forall\, \mathfrak{B}, L, \hat{L}, t \tag{3.5}$$

Equation (3.5) only has one new parameter:

$\mathfrak{DCR}_{\mathfrak{B}L\hat{L}t}$ *the dynamic capacity rating of the lines or pipes.*

Equation (3.5) ensures that the capacity of the transmission (or flow) is sufficient to accommodate the movement within that arc. The dynamic capacity rating embeds the weather data into the capacity, such that changes are automatically detected by WIS:dom®-P. For some transmission, the dynamic capacity rating is unity (e.g. underground HVDC transmission lines). The summation in the constraint encodes the fact that if capacity is expanded in one direction, it can be utilized in the other direction. This links directly to the objective function [Eq. (3.1)] and explains the ½ multiplier, since the summation results in a double counting within the capacity matrix. Equation (3.5) can be simplified by removing the $\mathfrak{f}_{\mathfrak{B}\hat{L}Lt}$ term from the summation, which results in a computational speed up. The trade-off is that (particularly for electric transmission) the lines are not able to move power in both directions; resulting in higher costs and lower benefits to geographic diversity of resources.

Equation (3.5) only constrains the flows to be within capacities. There are three more fundamental constraints for transmission and flows. They represent the delivery of the product (electricity, fuel or chemical) at each location at each time step (without fail), conservation of current (or mass), and losses (electric or leakage). Equation (3.6.1) defines the delivery of the product and Eq (3.6.2) defines the conservation of current (or mass):

$$\widehat{\mathbb{f}}^{\mathfrak{B}}_{\mathcal{L}t} - \sum_{\hat{\mathcal{L}}} (\mathbb{f}_{\mathfrak{B}\hat{\mathcal{L}}\mathcal{L}t} - \mathbb{f}_{\mathfrak{B}\mathcal{L}\hat{\mathcal{L}}t}) = 0 \quad \forall\, \mathfrak{B}, \mathcal{L}, t \tag{3.6.1}$$

$$\sum_{\mathcal{L}} \widehat{\mathbb{f}}^{\mathfrak{B}}_{\mathcal{L}t} = 0 \quad \forall\, \mathfrak{B}, t \tag{3.6.2}$$

Equation (3.6.1) ensures delivery of products to each node at each time step. Implicitly, it also obeys conservation of current (or mass); but to ensure it always does (reducing the impact of solver tolerance), Eq. (3.6.2) is used so that the sum of all nodes at each time step is zero. Essentially, Eq. (3.6.1) is tracking the flows in and out of the nodes using the flow matrices (Kirchhoff's current law for electric transmission). In Eq. (3.3) the flows are transmission line flows and the nodes represented are denoted $\widehat{\mathbb{f}}^{tr}_{\mathcal{L}t}$.

The final constraint is to define the losses when flows are occurring. Typically, WIS:dom®-P assumes leakage is zero, but electrical losses existing in transmission lines. The mathematical description of the flow losses is given by Eq. (3.7):

$$\widehat{\mathbb{f}}^{\mathfrak{B}\ell}_{\mathcal{L}t} - \sum_{\hat{\mathcal{L}}} \left[\left(1 - \ell^{\mathfrak{B}\ell}_{\mathfrak{B}\hat{\mathcal{L}}\mathcal{L}t}\right) \cdot \mathbb{f}_{\mathfrak{B}\hat{\mathcal{L}}\mathcal{L}t} \right] = 0 \quad \forall\, \mathfrak{B}, \mathcal{L}, t \tag{3.7}$$

Equation (3.7) contains a new parameter:

> $\ell^{\mathfrak{B}\ell}_{\mathfrak{B}\hat{\mathcal{L}}\mathcal{L}t}$ *is the flow losses for each time step along each arc for each of the flow assets. For example, in Eq. (3.3) it is represented as* $\widehat{\mathbb{f}}^{\ell}_{\mathcal{L}t}$ *because (typically) WIS:dom®-P assumes the others to be zero.*

Equation (3.7) allows WIS:dom®-P to compute the losses that occur within all flow parameters, but in particular completes the electric transmission equations by ensuring Kirchhoff's voltage law is adhered to. If leakage is required for product flows, this would be modeled in these equation sets by defining the values for $\ell^{\mathfrak{B}\ell}_{\mathfrak{B}\hat{\mathcal{L}}\mathcal{L}t}$. The values do not necessarily change with time, but they do for transmission power flow because of the weather influencing the conditions around the lines.

For the present study, the bulk transmission was reduced down to "state-level" and each county was modeled for resources and demands for connecting transmission. The siting was considered at 3-km and these were connected to counties via spur line transmission.

3.6 Electric Storage

Electric storage is crucial for future pathways of the electric grid. As a technology it performs in a completely different way to all conventional generation; because it is not generation. The electric storage must consume electricity from the grid before it can release it onto the grid. If no losses are assumed, it will balance consumption and supply (with charge remaining in storage). However, in reality there are conversion inefficiencies when charging and discharging; there are self-discharge rates; depth-of-discharge constraints; and weather-dependent operational characteristics.

Within WIS:dom®-P there is a distinction between utility-scale and distributed-scale electric storage ($\eta = \{Utility\ Storage, Distr.Storage\}$) and they are modeled separately; however, the mathematical operational defining behaviors are within the same set of equations. The distributed-storage will act in concert with the other DER equations resulting in a change to the grid-edge performance.

Equation (3.3) only interacts with storage via the term $\sum_{\mathfrak{L}\in\mathcal{L}}\left[(1-\ell^{s}_{\mathfrak{L}t})\cdot\sum_{\eta}\left(\mathfrak{D}_{\eta\mathfrak{L}t}-\mathfrak{C}_{\eta\mathfrak{L}t}\right)\right]$, which models the discharge and charging of the storage fleet and accounting for transmission losses. More equations are required to constrain how the electric storage operates. Equation (3.8) defines the power capacity of each electric storage facility:

$$\Lambda_{\eta}\cdot\left\{\sum_{\mathfrak{L}\in\mathcal{L}}\left[\mathcal{Y}_{\alpha\eta\mathfrak{L}}-\left(1-\ell^{ts}_{\eta\mathfrak{L}t}\right)\cdot\mathfrak{C}_{\eta\mathfrak{L}t}-\mathfrak{D}_{\eta\mathfrak{L}t}\right]\right\}\geq 0\quad\forall\,\eta,\mathcal{L},t,\alpha=\{power\}$$

(3.8)

In Eq. (3.8) there is two new parameters:

> $\ell^{ts}_{\eta\mathfrak{L}t}$ *is the electric losses encountered when charging storage; these can include AC to DC conversion losses, parasitic load for cooling/heating, or inefficiencies in converting electricity into chemical bonds;*
> Λ_{η} *is the adjustment factor for the DER subroutine.*

Equation (3.8) simply states that the power capacity ($\alpha=\{power\}$) of each storage facility must exceed the peak charge or discharge rate. The equation ensures that the WIS:dom®-P model correctly tracks where the binding constraint comes from (either charging or discharging) and (via the objective function) accounts for the costs associated with the need for larger inverters to facilitate the power requirements of charging *or* discharging at higher rates. As with previous equations, the weather-dependency appears in the loss ($\ell^{ts}_{\eta\mathfrak{L}t}$) term, as more cooling (heating) may be required at higher (lower) temperatures. The distribution-scale electric storage can be activated and deactivated by the parameter Λ_{η}, which is related to the DER subroutine adjustment factors.

Electric storage must hold energy to be worthwhile, and to model this in an efficient manner WIS:dom®-P utilized a set of three related equations, namely Eqs (3.9.1) – (3.9.4):

$$\Lambda_{\eta}\cdot\left\{\sum_{\mathfrak{L}\in\mathcal{L}}\left[\mathcal{Y}_{\alpha\eta\mathfrak{L}}-\mathfrak{E}_{\eta\mathfrak{L}t}\right]\right\}\geq 0\quad\forall\,\eta,\mathcal{L},t,\alpha=\{energy\}$$

(3.9.1)

$$\mathcal{A}_{\eta} \cdot \Lambda_{\eta} \cdot \left\{ \sum_{\mathfrak{L} \in \mathcal{L}} \left[\mathcal{Y}_{\alpha' \eta \mathfrak{L}} \cdot \mathfrak{H}_{\eta \mathfrak{L}} - \mathcal{Y}_{\alpha'' \eta \mathfrak{L}} \right] \right\} \geq 0 \quad \forall\, \eta, \mathcal{L}, t, \alpha' = \{power\}, \alpha'' = \{energy\} \tag{3.9.2}$$

$$\Lambda_{\eta} \cdot \left\{ \sum_{\mathfrak{L} \in \mathcal{L}} \left\{ \mathfrak{E}_{\eta \mathfrak{L} t} - \left[\hbar \cdot \left(1 - \ell_{\eta \mathfrak{L} t}^{ts}\right) \cdot \mathfrak{C}_{\eta \mathfrak{L} t} - \hbar \cdot \left(1 + \ell_{\eta \mathfrak{L} t}^{fs}\right) \cdot \mathfrak{D}_{\eta \mathfrak{L} t} + \left(1 - \ell_{\eta \mathfrak{L} t}^{is}\right) \cdot \mathfrak{C}_{\eta \mathfrak{L} (t-1)} \right] \right\} \right\} = 0 \quad \forall\, \eta, \mathcal{L}, t \tag{3.9.3}$$

$$\Lambda_{\eta} \cdot \left\{ \sum_{\mathfrak{L} \in \mathcal{L}} \left\{ \mathfrak{E}_{\eta \mathfrak{L} t} - \left(1 - dod_{\eta \mathfrak{L}}\right) \cdot \mathcal{Y}_{\alpha \eta \mathfrak{L}} \right\} \right\} \geq 0 \quad \forall\, \eta, \mathcal{L}, t, \alpha = \{energy\} \tag{3.9.4}$$

The Eqs (3.9.1) – (3.9.4) contains five new (exogenous) parameters:

> *$\mathcal{A}_{\eta}$ an activation parameter, if the user wishes to enforce a specific number of hours of storage to be modeled;*
> *$\mathfrak{H}_{\eta \mathfrak{L}}$ the number of hours of storage allowed for specific sites;*
> *$\ell_{\eta \mathfrak{L} t}^{fs}$ the electric losses encountered when discharging storage; these can include DC to AC conversion losses, parasitic load for cooling/heating, or inefficiencies in converting chemical bonds into electricity;*
> *$\ell_{\eta \mathfrak{L} t}^{is}$ the electric losses encountered due to self-discharge; these can include parasitic load for cooling/heating or leakage of chemical bonds breaking down;*
> *$dod_{\eta \mathfrak{L}}$ is the depth of discharge allowed for each of the storage facilities.*

Equations (3.9.1) – (3.9.4) contain a single new (endogenous) variable:

> *$\mathfrak{E}_{\eta \mathcal{L} t} = \sum_{\mathfrak{L} \in \mathcal{L}} \mathfrak{E}_{\eta \mathfrak{L} t}$ is the energy stored in each storage facility at each time step.*

Equation (3.9.1) dictates that the model must install enough electric storage capacity (in terms of energy) that exceeds the amount ever stored. This equation is directly linked to the objective function through the cost of electricity storage, enabling WIS:dom®-P to determine the trade-off between power and energy in a storage facility along with the grid requirements of that storage facility. Equation (3.9.2) is an optional constraint that requires WIS:dom®-P to install storage in "blocks" of multiples of hours of storage (e.g. 4-hour duration storage); meaning that if one of the variables changes the other must change in lock-step with the ratio multiplier. In general, WIS:dom®-P is run with this deactivated, and this allows the model to inform the user of the best trade-off between power and energy requirements of storage facilities.

Equation (3.9.3) is the most important one of the storage subroutines as it tracks the amount of energy remaining in each storage facility for each time step. The equation highlights the importance of chronological, high-temporal granularity modeling, since the model needs to know what power and energy can be drawn upon at each site any given moment and this is dependent on the previous time periods via $\mathfrak{C}_{\eta \mathfrak{L} (t-1)}$. Equation (3.9.3) takes into account losses in charging, discharging and self-discharge, rather than simple round-trip efficiency. This enables WIS:dom®-P to embed weather details for different behavior patterns without altering the core code.

Finally, Eq. (3.9.4) informs WIS:dom®-P of any limitation in the amount the storage can be discharged to. This allows for the possibility of emergency reserve modeling, but also for general depth-of-discharge analysis.

For the present study Eqs (3.8) – (3.9.4) are used fully for modeling storage facilities in the South East USA. The self-discharge rate is assumed to be 1% per month, the conversion losses to and from storage are assumed to be 7% before weather-dependency, the number of hours of storage are only applied to distribution-scale storage (applied at 4-hours), and the depth-of-discharge is assumed to be 100%.

Interestingly, as storage is accommodated in the modeling, the shape of the entire system adapts. The storage facilities are not there to reduce emissions or support renewables; rather they appear to support the system and gain profitability. The consequence of their appearance is typically reduced emissions because it can make use of low-cost electricity from VREs; however, it is more correlated with clean electricity, but even that is a weak correlation. The best metric appears to be ***system strain***; when the electricity system has surplus capacity and generation, the storage will charge (and this generally marries with lower prices) and when there is a shortage of capacity and generation, the storage will discharge. Of course, these are relative terms, since the model can detect impending *system strain* and charge beforehand accordingly. Moreover, at low levels (<25%) of *system strain* (majority of the time), the storage behaves in the familiar diurnal charge-discharge cycling (in arbitrage mode). In moderate levels (25% - 50%) of *system strain*, the storage starts becoming more careful it its cycling with deeper charging cycles and longer duration discharge at lower power. Finally, in high levels (>50%) of *system strain* the storage discharges and acts as peaking generation, but very rarely charges. Note that utility-scale storage will charge more frequently at moderate levels of system strain to generate better revenues, while distribution-scale storage will charge more frequently at low levels of system strain to help avoid peak demand charges (more discussion on this in subsection 3.9).

Figure 3.4 shows an example of storage performance vs the *system strain* metric (defined as average thermal generation utilization multiplied by average missing VRE generation utilization multiplied by load factor):

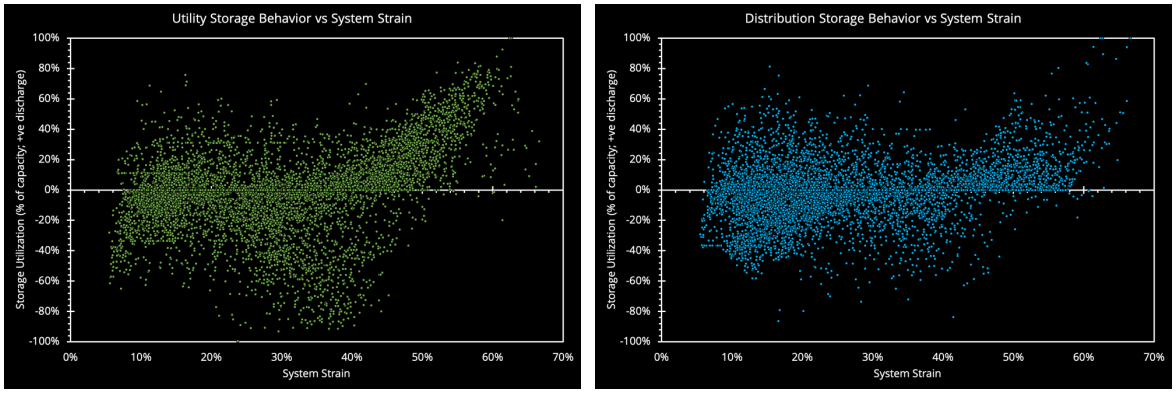

Figure 3.4: An example of storage discharge (positive) and charge (negative) behavior with *system strain* (higher values are more binding *system strain*). Left panel is utility-scale storage and right panel is distribution-scale storage.

3.7 Generator Production Constraints

The system of generators that the WIS:dom®-P model can choose from must always perform within operating parameters. For the optimization to understand these, constraints must be imposed. The following equation sets will force WIS:dom®-P to obey maximum production, minimum production, maximum up and down times, and ramping conditions. These equations are generalized to include the WIS:dom®-P description of unit commitment, which can be activated and deactivated by the user.

The first equation set, Eq. (3.10), is to ensure that each power plant does not exceed its maximum production. This will take into account the capacity of the generator, the probability of availability, refueling schedule (nuclear), river flow (hydroelectric), water availability, and the power factor:

$$\sum_{\mathfrak{L}\in\mathcal{L}}\{\mathcal{P}^{max}_{\mathcal{T}\mathfrak{L}t}\cdot[(1-\Delta)\cdot x_{\mathcal{T}\mathfrak{L}}+\Delta\cdot\xi_{\mathcal{T}\mathfrak{L}t}]-\mathcal{p}_{\mathcal{T}\mathfrak{L}t}\}\geq 0\quad\forall\,\mathcal{T},\mathcal{L},t \tag{3.10}$$

Equation (3.10) includes a new (exogenous) parameter:

> $\mathcal{P}^{max}_{\mathcal{T}\mathcal{L}t}$ *is the percentage of the installed capacity that is available for generating electricity for each time step.*

Equation (3.10) also introduces a new (endogenous) variables:

> $\xi_{\mathcal{T}\mathcal{L}t}$ *is the unit commitment variable for the amount of capacity that is committed at the current time step. Note that if unit commitment is deactivated, this variable is irrelevant.*

The only role of Eq. (3.10) is to guarantee that the production of electricity at each generation power plant does not exceed its installed capacity and any limitations on its capacity at each time step (from refueling, water availability, power factor, river flow, temperature of water). Note that the parameter $\mathcal{P}^{max}_{\mathcal{T}\mathcal{L}t}$ includes all the limitations, and as such the WIS:dom®-P model within the optimization does not change the limitations placed on the generators; however, in between the optimizations (investment periods) the algorithm updates the limitations based upon the changing generation mix. Equation (3.10) applies to all generation technologies. There is no need to have storage perform unit commitment (there are no startup costs); however, it is possible to expand all equations to include it if necessary.

The second equation set, Eq (3.11), ensures that the power plants operate above the minimum output level. There is no equivalent equation set for storage because it is assumed that there is no minimum operating floor. The equation set changes form when unit commitment is activated or deactivated:

$$\sum_{\mathfrak{L}\in\mathcal{L}}\left\{\Delta\cdot\left(\mathcal{p}_{\mathcal{T}\mathfrak{L}t}-\mathcal{P}^{min}_{\mathcal{T}\mathfrak{L}t}\cdot\xi_{\mathcal{T}\mathfrak{L}t}\right)+(1-\Delta)\cdot\left(\sum_{t}\frac{\mathcal{h}\cdot\mathcal{p}_{\mathcal{T}\mathfrak{L}t}}{8760}-\overline{\mathcal{P}^{min}_{\mathcal{T}\mathfrak{L}t}}\cdot x_{\mathcal{T}\mathfrak{L}}\right)\right\}\geq 0\quad\forall\,\mathcal{T},\mathcal{L},t \tag{3.11}$$

Equation (3.11) introduces two new (exogenous) parameters:

> $\mathcal{P}^{min}_{\mathcal{T}\mathfrak{L}t}$ *the minimum allowed generation at each time step based upon operating parameters;*
> $\overline{\mathcal{P}^{min}_{\mathcal{T}\mathfrak{L}t}}$ *the average minimum allowed generation over the entire optimization horizon.*

Due to the linear nature of this formulation within WIS:dom®-P, when unit commitment is deactivated the minimum generation constraint becomes an average capacity factor constraint for that generator across the year. When unit commitment is activated, the constraint becomes a time-dependent function for the generators.

The final equation set controls how WIS:dom®-P can change the output of the generators based on previous timesteps (known as ramping). It is well understood that some generators might be able to ramp up (increase generation) at a different rate than they can ramp down (decrease generation). Thus, WIS:dom®-P contains a pair of equations, one for up ramp and one for down ramp.

For the up ramp, we have:

$$\sum_{\mathcal{Q}\in\mathcal{L}} \begin{Bmatrix} \Delta \cdot \left[\mathcal{UR}_{\mathcal{TQ}t} \cdot (\xi_{\mathcal{TQ}t} - \phi_{\mathcal{TQ}t}) + \mathcal{P}^{min}_{\mathcal{TQ}t} \cdot (\phi_{\mathcal{TQ}t} - \psi_{\mathcal{TQ}t})\right] + \\ (1-\Delta) \cdot \mathcal{UR}_{\mathcal{TQ}t} \cdot x_{\mathcal{TQ}} - \left(\mathcal{p}_{\mathcal{TQ}t} - \mathcal{p}_{\mathcal{TQ}(t-1)}\right) \end{Bmatrix} \geq 0 \quad \forall\, \mathcal{T}, \mathcal{L}, t \tag{3.12.1}$$

For the down ramp, we have:

$$\sum_{\mathcal{Q}\in\mathcal{L}} \begin{Bmatrix} \Delta \cdot \left[\mathcal{DR}_{\mathcal{TQ}t} \cdot (\xi_{\mathcal{TQ}t} - \phi_{\mathcal{TQ}t}) + \mathcal{P}^{min}_{\mathcal{TQ}t} \cdot (\psi_{\mathcal{TQ}t} - \phi_{\mathcal{TQ}t})\right] + \\ (1-\Delta) \cdot \mathcal{DR}_{\mathcal{TQ}t} \cdot x_{\mathcal{TQ}} + \left(\mathcal{p}_{\mathcal{TQ}t} - \mathcal{p}_{\mathcal{TQ}(t-1)}\right) \end{Bmatrix} \geq 0 \quad \forall\, \mathcal{T}, \mathcal{L}, t \tag{3.12.2}$$

Equations (3.12.1) and (3.12.2) introduce two new (exogenous) parameters:

> *$\mathcal{UR}_{\mathcal{TQ}t}$ the amount per time step that the generator can ramp up by as a percentage of the installed capacity;*
> *$\mathcal{DR}_{\mathcal{TQ}t}$ the amount per time step that the generator can ramp down by as a percentage of the installed capacity.*

Equations (3.12.1) and (3.12.2) also introduce two new (endogenous) variables:

> *$\phi_{\mathcal{TQ}t}$ the unit commitment variable for the generation capacity started in the current time step;*
> *$\psi_{\mathcal{TQ}t}$ the unit commitment variable for the generation capacity shutdown in the current time step.*

The purpose of Eqs (3.12.1) and (3.12.2) is to stop the generation technologies from over performing in terms of changing its generation. These equations only apply to generation that are constrained on timescales longer than the dispatch frequency of the model. These are typically thermal units, such as coal, natural gas combined cycle, natural gas combustion turbines, nuclear (traditional, SMR and MSR), hydroelectricity, geothermal/biomass, and natural gas with CCS.

The unit commitment generalization must account for the possibility of generation being started or shutdown at any given time step. This means that the ramping constraints must accommodate power plants starting up to above the minimum generation or shutting down from above the minimum generation. In WIS:dom®-P a simplifying assumption is used to assume that any power plants starting up or shutting down must be at the minimum generation level. This is to ensure that generators do not shut down and turn on to circumvent the ramping constraints. The assumption also ensures that the constraint remains convex for solver efficiency.

The final equation set controls the amount of time a generator must be running for before it can be shut down and the time a generator must be shut down before it can be brought back online again. These are known as the minimum up and down times, respectively. The equations are in the form of rolling summation windows.

The minimum up time is described by:

$$\Delta \cdot \sum_{\mathfrak{L} \in \mathcal{L}} \left\{ \xi_{\mathcal{T}\mathfrak{L}t} - \sum_{\hat{t}=t-t_{up}}^{t} \phi_{\mathcal{T}\mathfrak{L}\hat{t}} \right\} \geq 0 \quad \forall\, \mathcal{T}, \mathcal{L}, t \tag{3.13.1}$$

The minimum down time is described by:

$$\Delta \cdot \sum_{\mathfrak{L} \in \mathcal{L}} \left\{ x_{\mathcal{T}\mathfrak{L}} - \xi_{\mathcal{T}\mathfrak{L}t} - \sum_{\hat{t}=t-t_{dwn}}^{t} \psi_{\mathcal{T}\mathfrak{L}\hat{t}} \right\} \geq 0 \quad \forall\, \mathcal{T}, \mathcal{L}, t \tag{3.13.2}$$

Equations (3.13.1) and (3.13.2) are only invoked when unit commitment is activated. There are two new (exogenous) parameters in these equations:

t_{up} *the amount of time that generators must be online for;*
t_{dwn} *the amount of time that generators must be offline for.*

Equation (3.13.1) essentially sums the capacity that have been started in each technology category at each site in the preceding time steps and ensures that the capacity committed exceeds this; ensuring that generation started in the window remain generating until their minimum up time has expired. Equation (3.13.2) is also summing, but the shutdown capacity and tracks this versus the installed capacity minus the committed capacity. Thus, ensuring that generation capacity remains offline for the allotted amount of time. The minimum up and down time only typically applies to thermal generators. It should be noted that the unit commitment description in WIS:dom®-P assumes continuous capacity at each site (the standard linear relaxation).

The present study utilizes the equations from this subsection as described. The data to determine the minimum and maximum generation as well as the ramping constraints is input from existing generator characteristics (explained in Section 4) and for new generation the data comes from numerous sources, such as NREL, EIA, commercial documents, PUC filings and other publicly available datasets. VCE® put all this data together and include them in the standard inputs. Note that any of the inputs is transferrable and adjustable by the user, by changing the standard inputs; these are then read back into WIS:dom®-P and can be resolved.

3.8 Planning & Load-following Reserves

3.8.1 Planning Reserves

There are many different ways to compute the planning reserve margins (PRM). There are typically two distinctions for capacity of thermal (or dispatchable) generation: the unforced capacity (UCAP) and the installed capacity (ICAP). In short, the UCAP takes into account the probability of forced and unforced outages a generator will have in any given time period. For variable generation, storage and DERs, the definitions are less formalized. WIS:dom®-P includes several different versions of the PRM formulations that can be enforced as a constraint, or simply determined in post-processing. These are different to an Effective Load Carrying Capacity (ELCC) computation[1], that is solely a post-processing calculation in WIS:dom®-P; though it is embedded in the standard WIS:dom®-P PRM constraint, endogenously.

The standard WIS:dom®-P PRM constraint enforced written as:

$$\sum_{\mathcal{L}\in\mathcal{R}}\sum_{\mathfrak{L}\in\mathcal{L}}\left\{\begin{array}{l}\sum_{\mathcal{T}\in CONV}[\mathcal{UF}_{\mathcal{T}\mathfrak{L}}\cdot x_{\mathcal{T}\mathfrak{L}}]+\sum_{\mathcal{T}\in VRE}\mathcal{P}_{\mathcal{T}\mathfrak{L}t}\\+\sum_{\eta}\left(\mathfrak{D}_{\eta\mathfrak{L}t}-\mathfrak{C}_{\eta\mathfrak{L}t}\right)+r^{-}_{\mathfrak{D}\mathfrak{L}t}-r^{+}_{\mathfrak{D}\mathfrak{L}t}\end{array}\right\}\geq\sum_{\mathcal{L}\in\mathcal{R}}\sum_{\mathfrak{L}\in\mathcal{L}}[(1+\mathcal{PRM}_{\mathfrak{L}})\cdot\mathcal{E}_{\mathfrak{L}t}]\quad\forall\,\mathcal{R},t \tag{3.14.1}$$

The standard PRM constraint, Eq. (3.14.1), adds a new set:

> $\mathcal{R}$ *the set of all regions that the PRM will be applied over; an aggregation of locations* $\mathcal{L}$.

There are two new (exogenous) parameters introduced in Eq. (3.14.1):

> $\mathcal{UF}_{\mathcal{TL}}(=\sum_{\mathfrak{L}\in\mathcal{L}}\mathcal{UF}_{\mathcal{T}\mathfrak{L}})$ *is the unforced capacity weighting, which is unity minus the forced outage rate;*
> $\mathcal{PRM}_{\mathcal{L}}(=\sum_{\mathfrak{L}\in\mathcal{L}}\mathcal{PRM}_{\mathfrak{L}})$ *is the planning reserve margin (PRM) that is enforced.*

The Eq. (3.14.1) states that the UCAP of dispatchable generation plus the net dispatch of variable generation, storage and DERs must exceed the demand scaled for the PRM at each time step throughout the modeling period. The formulation automatically takes into account the availability of the VREs (and any low production periods), while trying to avoid them, and ensures that there is enough capacity to meet the required reserves. It contains contributions from the DERs and storage automatically in a similar manner. It further connects the demand and VREs that are driven (at some level) by the same weather patterns. The first consequence of this choice is that the most difficult time period to provide the PRM shifts as the model installs different generation; which will inform VRE siting decisions about correlations with other generation (and demand) already outputting onto the grid. A secondary consequence of Eq. (3.14.1) is that the net load peak (after removing variable generation, storage and DERs) becomes the binding time periods for the requirement on the conventional generation; and even this time period shifts with new generation installed. A third consequence of Eq. (3.14.1) is that storage and DSM have two-way contributions to the PRM computation and can add to the demand requirement when they are "charging". This ensure that the model understands that to be able to dispatch these generators it must have available energy; and it can only do that if they have consumed electricity at a previous timestep.

[1] ELCC is the amount of load increase that a new VRE generation source can provide (or carry) before the Loss of Load Expectation (LOLE) is exceeded divided by the installed capacity of the new VRE.

A slightly different formulation of Eq. (3.14.1) disaggregates the demand-side resources and utility-scale resources for utility planning purposes. Essentially, planning for demand-side shifts that are enclosed within the PRM requirements, rather than contributors to the generation to provide for the PRM. This formulation is set out in Eq. (3.14.2):

$$\sum_{\mathcal{L}\in\mathcal{R}}\sum_{\mathfrak{L}\in\mathcal{L}}\left\{\begin{array}{c}\sum_{\mathcal{T}\in CONV}[\mathcal{UF}_{\mathcal{T}\mathfrak{L}}\cdot x_{\mathcal{T}\mathfrak{L}}]\\ +\sum_{\mathcal{T}\in\{util\}VRE}\mathcal{P}_{\mathcal{T}\mathfrak{L}t}\\ +\mathfrak{D}_{\{util\}\mathfrak{L}t}-\mathfrak{C}_{\{util\}\mathfrak{L}t}\end{array}\right\}\geq\sum_{\mathcal{L}\in\mathcal{R}}\sum_{\mathfrak{L}\in\mathcal{L}}\left[(1+\mathcal{PRM}_{\mathfrak{L}})\cdot\left(\begin{array}{c}\mathcal{E}_{\mathfrak{L}t}+r^{+}_{\mathfrak{D}\mathfrak{L}t}-r^{-}_{\mathfrak{D}\mathfrak{L}t}\\ +\mathfrak{C}_{\{dist\}\mathfrak{L}t}-\mathfrak{D}_{\{dist\}\mathfrak{L}t}\\ -\mathcal{P}_{\{dist\ PV\}\mathfrak{L}t}\end{array}\right)\right]\quad\forall\,\mathcal{R},t \tag{3.14.2}$$

The disadvantage of Eq. (3.14.2) is that it over emphasizes reserve needs in some instances and underemphasizes them in others. For example, it would increase PRM needs for DSM charging, but decrease it for DSM discharging. Thus, it assumes it is always contained within the demand seen by the utility. The advantage is that Eq. (3.14.2) allows for the model to determine DER placement and dispatch strategically to reduce the burden on the utility-scale grid to provide excess capacity and transmission build-out to support such capacity. Note Eq. (3.14.2) is not the standard PRM constraint used in WIS:dom®-P; that is Eq. (3.14.1), but is included in the model to determine how it might change planning decisions.

For the present study, we used Eq. (3.14.1) to enforce the PRM constraint. Further, we enforce the PRM at state-level in the Southeast region and the PRM requirements are displayed in Table 3.1.

Table 3.1: The Planning Reserve Margin Requirement for each state in the Southeast United States.

State	PRM Requirement
Tennessee	15%
North Carolina	20%
Mississippi	19%
Alabama	17%
Georgia	16.25%
South Carolina	18%
Florida	12%

There are two other formulations that can be used in WIS:dom®-P for the PRM constrain (or evaluation); however, these both necessitate the de-coupling of load and generation from concurrent datasets. Both of the formulations are stricter than the previous ones because they depend on both longer-term records of data and minimum contributions from VREs. These formulations are typically used to evaluate the "tails of distributions" rather than constraints for the PRM; but can be activated as constraints. The formulations derive the VRE contributions from long-term data sets.

There are three VCE®-created datasets typically drawn from:

1. Seven-year record of 3-km, 5-minute wind and solar potential generation over the contiguous USA (2013 – 2019);
2. 11-year record of 13-km, hourly wind and solar potential generation over the North-American domain (2006 – 2016);
3. 175-year record of 30-km, hourly wind and solar potential generation over the globe (1840 – 2015);

These datasets are purposefully overlapping so that VCE® can adjust from the finest resolution to the coarsest resolution to try and remove biases as much as possible. All three datasets can be used simultaneously as well as individually. We will only write the mathematical notation assuming one dataset is used, but it is trivial to use all of them in the same formulation.

The first of the two temporally decoupled PRM formulation is designed to embed the longer-term records without eroding the tractability of the WIS:dom®-P to solve in a reasonable amount of time. To that end, the formulation takes the minimum production for each time step (5-minutely or hourly) over the whole temporal extent for one of the VRE technologies and finds the complementary generation from the other technologies. This will be repeated for all the VRE technologies. Thus, regardless of temporal extent, the number of equation sets is limited to the number of VRE technologies. Additionally, the user does not have to use the minimum value, one could choose any defined value (for example, P95, or P90, or P50) and the formulation is identical from a mathematical standpoint.

Equation (3.14.3) defines the planning reserve margin computation as:

$$\sum_{\mathcal{L}\in\mathcal{R}}\sum_{\mathfrak{L}\in\mathcal{L}}\left\{\mathcal{P}^{\mu}_{\mathcal{T}'\mathfrak{L}t}+\sum_{\mathcal{T}\in VRE\setminus\mathcal{T}'}\mathcal{P}^{\bar{\mu}}_{\mathcal{T}\mathfrak{L}t}\right\}+\epsilon_{\mathcal{R}}\geq\sum_{\mathcal{L}\in\mathcal{R}}\sum_{\mathfrak{L}\in\mathcal{L}}\mathcal{E}^{\mathfrak{R}}_{\mathfrak{L}t}\quad\forall\,\mathcal{R},t \tag{3.14.3}$$

where

$$\mathcal{E}^{\mathfrak{R}}_{\mathfrak{L}t}=(1+\mathcal{PRM}_{\mathfrak{L}})\cdot\mathcal{E}_{\mathfrak{L}t}-\textstyle\sum_{\mathcal{T}\in CONV}[\mathcal{UF}_{\mathcal{T}\mathfrak{L}}\cdot x_{\mathcal{T}\mathfrak{L}}]-\sum_{\eta}\left(\mathfrak{D}_{\eta\mathfrak{L}t}-\mathfrak{C}_{\eta\mathfrak{L}t}\right)-r^{-}_{\mathfrak{D}\mathfrak{L}t}+r^{+}_{\mathfrak{D}\mathfrak{L}t}\;\forall\,\mathfrak{L},t.$$

The formulation in Eq. (3.14.3) states that the chosen generation probability (μ) for the VRE technology ($\mathcal{T}'$) defines the time slice where the generation from VREs is summed for the particular time step (t). The summed generation must exceed the residual PRM adjusted load after accounting for conventional generation, storage, and DSM under the original weather year. Equation (3.14.3) will perform this procedure for all VRE technologies and for all time steps across the entire weather dataset. The $\epsilon_{\mathcal{R}}$ term allows for Eq. (3.14.3) to be adjusted as a "softer" constraint, where some residual amount of load is allowed to be lost. The term can be used to compute the metrics for cost of different reserve margins under various conditions. For the strongest constraint, one would set the term to zero ($\epsilon_{\mathcal{R}}=0$).

An illustration of how Eq. (3.14.3) would work (for the 175-year dataset) is as follows: Take the initial time step in the time series; That particular time step could be a minimum for wind production at that time step in year 80 (of the 175); The model takes all the other VRE generation from that year as the complements; The process would then move to the second time step, and repeat the procedure; but this time the minimum for wind could be year 12 (of the 175); Once the process is completed for wind, all the other VRE technologies have the same procedure performed.

The advantage of Eq. (3.14.3) is that it incorporates numerous years of weather data in a reduced form that is mathematically tractable. Some disadvantages persist. First, the minimum years (time step by time step) can jump around across the dataset. Secondly, the weather and demand are decoupled from each other. Finally, to understand the dynamics of conventional generation, storage and DSM, the original weather year time step data are used, which could underestimate their performance. Overall, however, it does provide a

robust evaluation of the VRE contribution to planning reserve margins over a wide range of possible conditions.

A final version of the PRM constraint or formulation is an even more conservative version of Eq. (3.14.3), where the minimum of each VRE technology over all the years for each time step is summed to meet the residual PRM adjusted load values. This is the strictest, and least physical, definition for the PRM, but would guarantee, if VREs are picked that they would not negatively impact reserves over the given dataset horizon. The disadvantage is that the constraint can be overly binding on selection of VREs, since the anti-correlation between resources is completely removed. With the $\epsilon_{\mathcal{R}}$ term, however, it becomes a useful metric to determine how robust a solution is under extreme non-correlated conditions. It also provides insight into the value of the weather-driven patterns within the VRE generation mix. The definition of this particular formulation of the PRM equation set is given in Eq. (3.14.4):

$$\sum_{\mathcal{L}\in\mathcal{R}}\sum_{\mathfrak{L}\in\mathcal{L}}\left(\sum_{\mathcal{T}\in VRE} p^{\mu}_{\mathcal{T}\mathfrak{L}t}\right)+\epsilon_{\mathcal{R}} \geq \sum_{\mathcal{L}\in\mathcal{R}}\sum_{\mathfrak{L}\in\mathcal{L}} \mathcal{E}^{\Re}_{\mathfrak{L}t} \quad \forall\, \mathcal{R}, t \tag{3.14.4}$$

where

$$\mathcal{E}^{\Re}_{\mathfrak{L}t} = (1+\mathcal{PRM}_{\mathfrak{L}})\cdot\mathcal{E}_{\mathfrak{L}t} - \textstyle\sum_{\mathcal{T}\in CONV}[\mathcal{UF}_{\mathcal{T}\mathfrak{L}}\cdot x_{\mathcal{T}\mathfrak{L}}] - \sum_{\eta}\left(\mathfrak{D}_{\eta\mathfrak{L}t}-\mathfrak{C}_{\eta\mathfrak{L}t}\right) - r^{-}_{\mathfrak{D}\mathfrak{L}t} + r^{+}_{\mathfrak{D}\mathfrak{L}t}\ \forall\, \mathfrak{L}, t.$$

3.8.2 Load Following Reserves

The load following reserve (LFR) constraints in WIS:dom®-P are a strict set of conditions that the model must meet over (user-prescribed) geographic regions for all time steps. The formulation adapts between unit-commitment enabled and disabled variants. The formulation in WIS:dom®-P does not explicitly compute the individual power plant contributions to the LFR, but rather, ensures that it is available for each and every time step and region, without fail. Further, if the up and down LFR values are different, the model can embed that requirement within the same formulation; but the modeling does "wrap" all of the LFR components (regulation, fast frequency response, spinning reserves, operating reserves, or other naming convention or types of reserves that are sub-temporal resolution) into a single variable.

Equation (3.15.1) describes the value that the LFR must exceed at all time steps. It should be noted that this LFR is endogenous in the WIS:dom®-P model and adapts as different components change.

$$\varrho_{\mathcal{S}t} \geq \mathcal{LFR}_{\mathcal{S}}\cdot\left\{\sum_{\mathcal{L}\in\mathcal{S}}\left[\mathcal{I}_{\mathcal{L}t}+\sum_{\mathfrak{L}\in\mathcal{L}}\left(\mathcal{E}_{\mathfrak{L}t}+r^{+}_{\mathfrak{D}\mathfrak{L}t}-r^{-}_{\mathfrak{D}\mathfrak{L}t}+\sum_{\eta}\left(\mathfrak{C}_{\eta\mathfrak{L}t}\right)-\mathfrak{D}_{\{dist\}\mathfrak{L}t}\right)\right]\right\} \quad \forall\, \mathcal{S}, t \tag{3.15.1}$$

Equation (3.15.1), the LFR constraint, adds a new set:

$\mathcal{S}$ the set of all regions that the LFR will be applied over; an aggregation of locations $\mathcal{L}$.

Equation (3.15.1) also introduces one new (exogenous) parameter:

$\mathcal{LFR}_{\mathcal{S}}$ the amount of Load Following Reserves (LFR) for region the elements of set $\mathcal{S}$; typically defined as a percentage.

Equation (3.15.1) introduces a single new (endogenous) variable:

$\varrho_{\mathcal{S}t}$ the load following reserves being held derived from the modeling.

Equation (3.15.1) can be duplicated for different up and down reserve requirements, if the contributions needed are different. This would lead to two endogenous variables, rather than a single one: $\varrho_{\mathcal{S}t}^{+}$ (up LFR) and $\varrho_{\mathcal{S}t}^{-}$ (down LFR). For the purposes of documentation, we only describe the mathematics for a reflective LFR constraint (same positive and negative components); but the WIS:dom®-P model can be provided with heterogenous components to the LFR without difficulty. For the present study, we set the LFR requirement to 7% for all regions and time steps ($\mathcal{LFR}_{\mathcal{S}} = 7\% \; \forall \; \mathcal{S}$).

The down LFR constraint is described mathematically in Eq. (3.15.2):

$$\sum_{\mathcal{L}\in\mathcal{S}}\sum_{\mathcal{Q}\in\mathcal{L}}\left[\sum_{\mathcal{T}}\left(\mathcal{p}_{\mathcal{T}\mathcal{Q}t}-\Delta\cdot\mathcal{P}_{\mathcal{T}\mathcal{Q}t}^{min}\cdot\xi_{\mathcal{T}\mathcal{Q}t}\right)+\mathfrak{D}_{\{util\}\mathcal{Q}t}-\mathcal{W}_{\mathcal{Q}t}\right]\geq\varrho_{\mathcal{S}t}\quad\forall\,\mathcal{S},t \tag{3.15.2}$$

Equation (3.15.2) is solved trivially when unit commitment is not activated, since production always exceeds demand in the WIS:dom®-P model. When unit commitment is activated, Eq. (3.15.2) is slightly harder to solve because of the minimum generation term. Equation (3.15.2) is simply stating that the generators must be able to turn down production enough to cover the load following reserves without dropping below the minimum allowable production of the generation fleet committed at each time step.

The up LFR constraint is described mathematically in Eq. (3.15.3):

$$\sum_{\mathcal{L}\in\mathcal{S}}\sum_{\mathcal{Q}\in\mathcal{L}}\left[\begin{array}{l}\sum_{\mathcal{T}\setminus VRE}\{\mathcal{P}_{\mathcal{T}\mathcal{Q}t}^{max}\cdot[(1-\Delta)\cdot x_{\mathcal{T}\mathcal{Q}}+\Delta\cdot\xi_{\mathcal{T}\mathcal{Q}t}]-\mathcal{p}_{\mathcal{T}\mathcal{Q}t}\}\\+\left(\mathcal{y}_{\{power\}\{util\}\mathcal{Q}}-\mathfrak{C}_{\{util\}\mathcal{Q}t}-\mathfrak{D}_{\{util\}\mathcal{Q}t}\right)+\mathcal{W}_{\mathcal{Q}t}\end{array}\right]\geq\varrho_{\mathcal{S}t}\quad\forall\,\mathcal{S},t \tag{3.15.3}$$

Equation (3.15.3) is more complicated than Eq. (3.15.2) because the ability to have up LFR is generally more difficult to achieve. The formulation of Eq. (3.15.3) states that the difference between the committed (or installed, if UC not activated) capacity and generation from non-VRE technologies and storage along with curtailed VRE generation must be greater than the required up LFR for each time step. What this represents is enough "head room" to increase production by the LFR at any instant to cover events that could occur on the electricity grid. Implicitly, Eq. (3.15.3) allows VREs to contribute to the up LFR only if there is excess (curtailed) production occurring.

It is also noted that utility-scale storage is included in Eq. (3.15.3), which must be treated with care because there must be energy stored to dispatch. WIS:dom®-P overcomes this issue by having a depth of discharge constraint, Eq. (3.9.4), that ensures some level of emergency energy is held at all times (if depth of discharge is elevated above manufacturer required levels). Further, Eq. (3.15.1), along with Eq. (3.15.3), contains charging for utility-scale storage, which WIS:dom®-P can adjust to help ensure LFR is provided for every

time step. Further, it guarantees that combinations of charging and discharging do not exceed the capacity available when considering LFR contributions.

3.9 Distribution Energy Resources (& Co-optimization)

3.9.1 DER Technologies

For modern grid planning purposes, it is essential to consider the distribution system and how it connects and interacts with the utility-scale grid. For WIS:dom®-P, it is not possible to model the entire utility-scale grid (down to 69-kV) and the entirety of the distribution system with all the lines, consumers and resources. To represent the distribution system, WIS:dom®-P employs a parameterization method whereby it assumes all loads on the distribution system at located at the 69-kV substation. The same logic is applied to distributed energy resources (DERs) and the distribution infrastructure. To do this, WIS:dom®-P ingests the 3-km resource data and aggregates the resource data to the nearest 69-kV bus. Thus, WIS:dom®-P considers the infrastructure, demand profiles, flexibility available, and generation potential for the distribution grid explicitly within the model; but does not explicitly disaggregate exact siting or distribution line build out. Rather, it implicitly includes the cost and losses for distribution based on the resource potential analysis.

The technologies available to WIS:dom®-P defined as Distribution Energy Resources (DERs) are:

1. *Residential rooftop solar PV;*
2. *Commercial rooftop solar PV;*
3. *Industrial rooftop solar PV;*
4. *Community solar PV;*
5. *Demand Side Management (DSM);*
6. *Demand Response (DR);*
7. *Distributed-scale battery storage (BTM & FTM Storage);*
8. *Energy Efficiency (EE).*

The distributed-scale battery storage has already been covered in Section 3.6. The solar PV acts in the same way as the utility-scale expect that transmission interconnection is only required at the 69-kV bus and the technologies (and tilt/azimuth) are dictated by the land-use, roof slopes, and other locational factors. That means there are less technology options available to WIS:dom®-P for distributed solar PV compared with utility-scale (see Section 4).

Demand Side Management (DSM), Demand Response (DR) and Energy Efficiency (EE) can all be modeled endogenously within WIS:dom®-P. For EE, there is also the option to provide exogenous reductions to the demand profiles and turn off the endogenous functionality. For both DSM and DR, the quantity of each can be prescribed, but the operation is always endogenous (except when deactivated or made not available).

For EE there is a normalized curve shape for each region that is exogenous that can be applied for a specific cost per unit of peak reduction ($/MW). The curve would apply to the demand profile within each region and reductions would be multiplicative of the cost. The model also requires an upper bound for the amount of EE that can be applied within each region. The cost of such additions have not been described in Eq. (3.1) because almost always these EE decisions are assumed within the load shape *a priori*, due to the fact that all modeling chooses EE up to the upper bound when available.

For completeness, we show the endogenous equations for EE with Eq. (3.16) if a user wishes it to be endogenous within their modeling.

$$\mathcal{E}_{\mathcal{L}t} = \widehat{\mathcal{E}_{\mathcal{L}t}} - r^{-}_{\{\mathcal{E}\mathcal{E}\}\mathcal{L}t}, \qquad r^{-}_{\{\mathcal{E}\mathcal{E}\}\mathcal{L}t} = \Upsilon_{\mathcal{L}} \cdot \mathcal{E}\mathcal{E}_{\mathcal{L}t}, \qquad \Upsilon_{\mathcal{L}} < \widehat{\Upsilon_{\mathcal{L}}}, \qquad \forall\, \mathcal{L}, t \tag{3.16}$$

In addition to Eq. (3.16) a member of the set $\mathfrak{D}$ would be activated for the EE technologies. This would then apply costs in term $\hbar \cdot \sum_{\mathfrak{D}} \sum_{t} \left(\mathcal{V}^{\mathfrak{D}}_{\mathfrak{D}\mathcal{L}t} \cdot r^{-}_{\mathfrak{D}\mathcal{L}t} \right)$ in Eq. (3.1), where $\mathcal{V}^{\{\mathcal{E}\mathcal{E}\}}_{\{\mathcal{E}\mathcal{E}\}\mathcal{L}t} = \frac{\mathcal{C}^{\mathcal{E}\mathcal{E}}_{\mathcal{L}}}{\sum_{t} \mathcal{E}\mathcal{E}_{\mathcal{L}t}}$, which converts the cost of the EE in terms of $\mathcal{C}^{\mathcal{E}\mathcal{E}}_{\mathcal{L}}$ (the capital cost of the EE applied) to a cost per unit of electricity reduced. Note that $\widehat{\mathcal{E}_{\mathcal{L}t}}$ is purely a re-labeling of $\mathcal{E}_{\mathcal{L}t}$ due to the introduction of EE.

Equation (3.16) introduces two new (exogenous) parameters:

$\mathcal{E}\mathcal{E}_{\mathcal{L}t}$ the normalized reductions for each region at each time step for each investment of EE;
$\widehat{\Upsilon_{\mathcal{L}}}$ the upper bound for the capacity of EE for each region.

Equation (3.16) introduces a single new (endogenous) variable:

$\Upsilon_{\mathcal{L}}$ the capacity of EE that is being deployed in each region.

Demand Response (DR) is mathematically very similar to the EE formulation with some important alterations. Demand Response programs can differ depending on the jurisdiction, but in general they follow the same two possible principles: (1) a utility (or grid control entity) pays for a capacity of DR that can be executed for a maximum set number of hours (or electricity) per year calendar year for no additional cost; (2) A DR provider agrees to participate in a program that is offered a price per time period to reduce demand, but does not need to agree to reduce demand. Type (2) of the DR program is covered in WIS:dom®-P as a DSM entity rather than a DR one, which will be described in the next page. For type (1), WIS:dom®-P includes constraints to model the DR program effectively:

$$r^{-}_{\{\mathcal{D}\mathcal{R}\}\mathcal{L}t} < \widehat{r^{-}_{\{\mathcal{D}\mathcal{R}\}\mathcal{L}t}} \cdot \Omega_{\mathcal{L}}, \qquad \Omega_{\mathcal{L}} < \widehat{\Omega_{\mathcal{L}}}, \qquad \forall\, \mathcal{L}, t \tag{3.17.1}$$

$$\sum_{t} r^{-}_{\{\mathcal{D}\mathcal{R}\}\mathcal{L}t} < \Omega_{\mathcal{L}} \cdot \mathfrak{H}_{\mathcal{L}} \quad \forall\, \mathcal{L}, t \tag{3.17.2}$$

Equations (3.17.1) and (3.17.2) ensure that DR is modeled as a resource that can be dispatched to reduce demand (through Eq.(3.3)).

Equations (3.17.1) and (3.17.2) introduce three new (exogenous) parameters:

$\widehat{\Omega_{\mathcal{L}}}$ the upper bound for the capacity of DR for each region;
$\widehat{r^{-}_{\{\mathcal{D}\mathcal{R}\}\mathcal{L}t}}$ is a restriction to when the DR can operate (fractional between zero and unity);
$\mathfrak{H}_{\mathcal{L}}$ the number of hours of capacity that DR can be operated in each region.

Equations (3.17.1) and (3.17.2) introduce a single new (endogenous) variable:

$\Omega_{\mathcal{L}}$ the capacity of DR that is being deployed in each region.

The endogenous variable $\Omega_{\mathcal{L}}$ can be supplied exogenously and fixed to a set capacity within WIS:dom®-P, if the user desires. Note that because $r^{-}_{\{\mathcal{DR}\}\mathcal{L}t}$ is endogenous, the cost application must be computed outside of the optimization (otherwise the model would be nonlinear). Therefore, $\mathcal{V}^{\{\mathcal{DR}\}}_{\{\mathcal{DR}\}\mathcal{L}t} = \frac{\mathcal{C}^{\mathcal{DR}}_{\mathcal{L}}}{\mathfrak{H}_{\mathcal{L}}}$, must be supplied to the model as an input.

The exogenous parameter $\widehat{r^{-}_{\{\mathcal{DR}\}\mathcal{L}t}}$ allows WIS:dom®-P to receive information about when DR can be operated. If it is unity for all time steps, then WIS:dom®-P can use the DR to any level (under the capacity) at any time, as long as the summation is below the value in Eq. (3.17.2). A drawback to setting the parameter to unity is that the model could utilize a small amount of DR for many time steps, something that is not representative of current program functionality; this would essentially mimic EE. More appropriately, setting the parameter $\widehat{r^{-}_{\{\mathcal{DR}\}\mathcal{L}t}}$ to varying values allows for a more representative description of possible seasonal or month programs; basically, providing a shape for the DR to be constrained by. Thus, giving the model more information to utilize the technology/asset appropriately.

Demand Side Management (DSM) is an important feature of the WIS:dom®-P model. A substantial effort has been made to represent possible demand flexibility using DSM for existing and electrified profiles using the weather dataset that VCE® has created for its modeling. The main difference (mathematically and operationally) between DSM and DR or EE is that the electricity that is not served in a specific time step must be provided for at some other time step; and this must happen within some pre-determined window of time. In other words, DSM is more of a hybrid between storage and DR. It is often referred to as "demand shifting". Equations (3.18.1) – (3.18.3) describe how WIS:dom®-P incorporates DSM within its algorithms.

$$\sum_{\hat{t}=t-\mathrm{T}_{\mathfrak{D}}}^{t} (r^{+}_{\mathfrak{D}\mathcal{L}t} - r^{-}_{\mathfrak{D}\mathcal{L}t}) \geq 0, \qquad \forall\, \mathfrak{D}\backslash\{\mathcal{DR},\mathcal{EE}\},\mathcal{L},t \tag{3.18.1}$$

$$\sum_{t} (r^{+}_{\mathfrak{D}\mathcal{L}t} - r^{-}_{\mathfrak{D}\mathcal{L}t}) = 0, \qquad \forall\, \mathfrak{D}\backslash\{\mathcal{DR},\mathcal{EE}\},\mathcal{L} \tag{3.18.2}$$

$$r^{+}_{\mathfrak{D}\mathcal{L}t} < \widehat{r^{+}_{\mathfrak{D}\mathcal{L}t}}, \qquad r^{-}_{\mathfrak{D}\mathcal{L}t} < \widehat{r^{-}_{\mathfrak{D}\mathcal{L}t}}, \qquad \forall\, \mathfrak{D}\backslash\{\mathcal{DR},\mathcal{EE}\},\mathcal{L},t \tag{3.18.3}$$

Equations (3.18.1) and (3.18.3) introduce three new (exogenous) parameters:

$\mathrm{T}_{\mathfrak{D}}$ *the number of time steps that the DSM asset can shift electricity by;*
$\widehat{r^{+}_{\mathfrak{D}\mathcal{L}t}}$ *the profile that dictates how much each DSM asset can increase consumption by;*
$\widehat{r^{-}_{\mathfrak{D}\mathcal{L}t}}$ *the profile that dictates how much each DSM asset can decrease consumption by.*

Equation (3.18.1) is a rolling window of time for each DSM asset that requires the increase in demand to always meet or exceed the decrease in demand. This ensures that the electricity is always replenished within the required timespan. The $\mathrm{T}_{\mathfrak{D}}$ is actually more detailed than appearances: it is dictated not only by user parameters, but is also refined using the weather datasets to compute heat losses and other factors for different DSM assets. For example, if there is extreme cold, the time to replenish space heating is significantly reduced compared with milder temperatures. The purpose of this factor is to not unrealistically

assume that loads are flexible in the same manner at all time steps; the model needs the description of difficult events to manage them.

The standard timespans used for the largest DSM assets are as follows (before weather adjustment):

a. $T_{conventional}$ *is four hours;*
b. $T_{space\ heating}$ *is four hours;*
c. $T_{water\ heating}$ *is six hours;*
d. $T_{transport}$ *is twenty-four hours.*

Equation (3.18.2) guarantees that WIS:dom®-P will always create a balanced DSM asset over the entire production cost analysis. Note that there are periodic boundaries between the initial and final time steps in the production cost component of the modeling for all temporal constraints.

Equation (3.18.3) provides WIS:dom®-P with data about how much of a DSM asset can be dispatched at each time step. Again, similar to $T_{\mathfrak{D}}$, the weather dataset and electric utilization are used to embed data for WIS:dom®-P to make decisions with. For example, if there is an extreme cold weather phenomenon and the location has heat pumps as the space heating technology, then the space heating may have zero ability to increase demand (over heat the building stock) and may only have a small ability to reduce demand (before the building stock becomes too cold). This additional information results in WIS:dom®-P being able to plan and navigate difficult conditions in a robust manner without relying on flexibility that might not be available. Further, it may also be able to use the DSM in concert with other DERs to mitigate possible difficult conditions in a sophisticated manner that other modeling might not be able to resolve.

For the present study, we incorporated the SE IRP collected data for EE and DR, which results in exogenous parameters for Eqs (3.16) – (3.17.2) that can be dispatched within the bounds set by the data. For Eqs (3.18.1) – (3.18.3), the weather data enforces the DSM and existing programs are used for the remaining gaps.

3.9.2 Distribution Co-optimization & Coordination

A unique feature of WIS:dom®-P is its ability to resolve the utility-scale electricity grid with detailed granularity over large spatial domains. This unique feature has been expanded to allow for the model to co-optimize and coordinate the utility-scale electricity grid with the distribution grid. The tractability of such a co-optimization requires parameterization of all the distribution-level grid topology and infrastructure. Therefore, WIS:dom®-P disaggregates the DER technologies, but aggregates the distribution lines and other infrastructure as an interface (or "grid edge") that electricity must pass across. The model does assign costs and can compute inferred capacities and distances from the solutions, but cannot (with current computation power) resolve explicitly all the infrastructure in a disaggregated manner.

The main components of deriving the utility-distribution (U-D) interface are:

a. *Utility-observed peak distribution demand;*
b. *Utility-observed peak distribution generation;*
c. *Utility-observed distribution electricity consumption.*

The definition of "Utility-observed" is the appearance of the metric at 69-kV transmission substation or above. Below the 69-kV, the model is implicitly solving with combinations of DERs, and what remains is exposed to the utility-scale grid at the substation. Figure 3.5 is a schematic of how WIS:dom®-P represents

the U-D interface and Fig. 3.6 displays an illustration of how the distribution co-optimization results in two distinct concerts playing out: DERs coordinating to reshape the demand exposed to the utility-scale (*load shifting to supply*) and utility-scale generation and transmission coordinating to serve the demand that appears at the 69-kV substation (*supply shifting to load*).

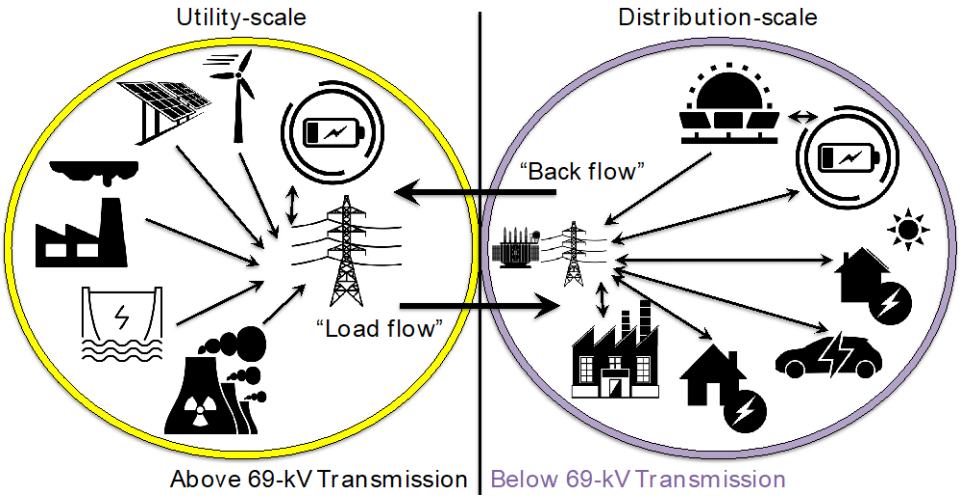

Figure 3.5: A schematic picture of the U-D interface within the WIS:dom®-P modeling platform.

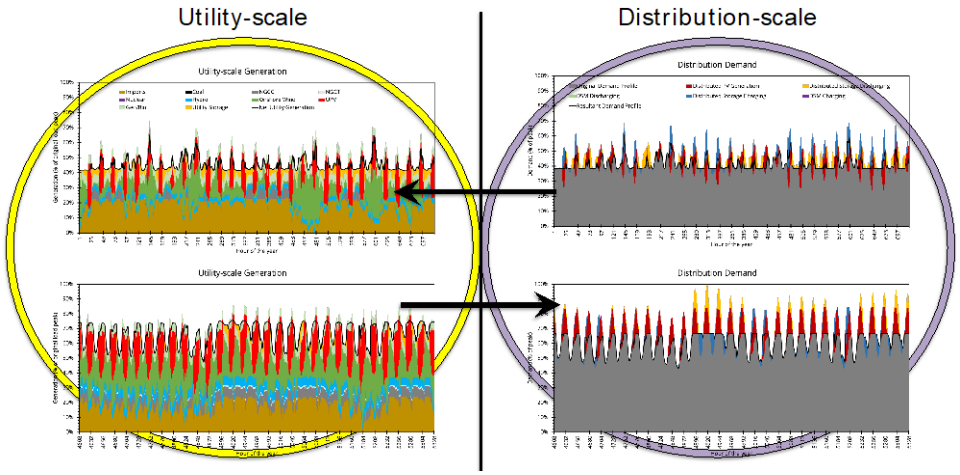

Figure 3.6: Example coordination at the distribution- and utility-scale within the WIS:dom®-P model.

To generate an interface for the modeling requires the parameterization of the three components enumerated above. The U-D interface is added as option in the WIS:dom®-P model that can be activated or deactivated easily by the user (using the binary parameter Λ). The equations that define the U-D interface directly link to Eq. (3.1) via the term

$$\Lambda \cdot \left\{ \mathcal{C}_{\mathcal{L}}^{dp} \cdot \left[\mathcal{E}_{\mathcal{L}}^{p} + \lambda_a \cdot \left(\mathcal{E}_{\mathcal{L}}^{b} + \mathcal{E}_{\mathcal{L}}^{m} \right) \right] + \hbar \cdot \mathcal{C}_{\mathcal{L}}^{de} \cdot \sum_{t} \left(\mathcal{E}_{\mathcal{L}t} - \lambda_b \cdot \mathcal{J}_{\mathcal{L}t} \right) \right\}.$$

This direct link provides more cost details to the objective function with respect to the distribution infrastructure requirements that results in changes in model logic to find the least-cost system. The U-D interface equations are relatively simple, but have direct influence on a substantial number of variables and

can result in a completely different solution space being accessible to WIS:dom®-P compared with the U-D interface equations being deactivated. There are exogenous parameters within the U-D interface equations [and the terms in Eq. (3.1)] that allow the users to adjust the sensitivity or tolerance to the U-D interface.

The U-D interface equations are written as:

$$\mathcal{E}_{\mathcal{L}}^{\mathcal{P}} - \mathcal{E}_{\mathcal{L}t} + \Lambda \cdot \sum_{\mathfrak{L} \in \mathcal{L}} \left[\mathcal{P}_{\{DPV\}\mathfrak{L}t} + \sum_{\mathfrak{D}} (r_{\mathfrak{D}\mathfrak{L}t}^{-} - r_{\mathfrak{D}\mathfrak{L}t}^{+}) + \left(\mathfrak{D}_{\{dist\}\mathfrak{L}t} - \mathfrak{C}_{\{dist\}\mathfrak{L}t} \right) \right] \geq 0, \qquad \forall\, \mathcal{L}, t \tag{3.19.1}$$

$$\mathcal{E}_{\mathcal{L}}^{\mathcal{P}} + \mathcal{E}_{\mathcal{L}t} + \Lambda \cdot \sum_{\mathfrak{L} \in \mathcal{L}} \left[\sum_{\mathfrak{D}} (r_{\mathfrak{D}\mathfrak{L}t}^{+} - r_{\mathfrak{D}\mathfrak{L}t}^{-}) + \left(\mathfrak{C}_{\{dist\}\mathfrak{L}t} - \mathfrak{D}_{\{dist\}\mathfrak{L}t} \right) - \mathcal{P}_{\{DPV\}\mathfrak{L}t} \right] \geq 0, \qquad \forall\, \mathcal{L}, t \tag{3.19.2}$$

$$\sum_{\mathfrak{L} \in \mathcal{L}} \left\{ \mathcal{J}_{\mathfrak{L}t} - \Lambda \cdot \left[\mathcal{P}_{\{DPV\}\mathfrak{L}t} + \sum_{\mathfrak{D}} (r_{\mathfrak{D}\mathfrak{L}t}^{-} - r_{\mathfrak{D}\mathfrak{L}t}^{+}) + \left(\mathfrak{D}_{\{dist\}\mathfrak{L}t} - \mathfrak{C}_{\{dist\}\mathfrak{L}t} \right) \right] \right\} = 0, \qquad \forall\, \mathcal{L}, t. \tag{3.19.3}$$

Equations (3.19.1) – (3.19.3) introduce no new sets, variables or parameters. Equation (3.19.1) defines the peak distribution electricity demand observed by the utility-scale grid. Equation (3.19.2) defines the peak back flow from the distribution grid to the utility-scale grid. Equation (3.19.3) defines the total distributed generation for each time step.

The Eqs (3.19.1) – (3.19.3) provide the values to the cost term in the objective function [Eq. (3.1)]. The exogenous parameters control the relative value of each of the terms. For Λ, there is only a binary option (activate or deactivate). For $\mathcal{C}_{\mathcal{L}}^{d\mathcal{P}}$ and $\mathcal{C}_{\mathcal{L}}^{de}$, we take values from the report "*Trends in Transmission, Distribution and Administration Costs for US Investor Owned Electric Utilities*[2]" by the University of Texas at Austin. These values are national averages, and VCE® apply a regionalization by State using internal datasets for locational cost multipliers. Finally, λ_a and λ_b influence the relative importance of the back flow and distributed generation on the co-optimization of the U-D interface. Typically, both are set to unity, but any value can be used. Perhaps the cost of back flow management at the distribution level is more expensive than peak demand flow.
With the different exogenous parameters, numerous different versions of co-optimization with the distribution level can be achieved:

1. $\Lambda = 0$, $\lambda_a = 0$, and $\lambda_b = 0$:
   No co-optimization with distribution-level infrastructure. Model does still co-optimize distribution-level generation, loads, demand flexibility and storage.

2. $\Lambda = 1$, $\lambda_a = 0$, and $\lambda_b = 0$:
   Co-optimization with distribution-level infrastructure, but when only accounting for load requirements and ignoring DER contribution to distribution-level infrastructure. Model does still co-optimize distribution-level generation, loads, demand flexibility and storage.

[2] https://energy.utexas.edu/sites/default/files/UTAustin_FCe_TDA_2016.pdf

3. $\Lambda = 1$, $\lambda_a > 0$, and $\lambda_b = 0$:
   Co-optimization with distribution-level infrastructure, while accounting for load requirements and peak back flow DER impacts to distribution-level infrastructure. Model does still co-optimize distribution-level generation, loads, demand flexibility and storage.

4. $\Lambda = 1$, $\lambda_a > 0$, and $\lambda_b > 0$ (typically $\lambda_a = \lambda_b = 1$):
   Full co-optimization with distribution-level infrastructure. Determines the benefits and costs associated with DER buildout on the distribution infrastructure. Model does still co-optimize distribution-level generation, loads, demand flexibility and storage.

5. $\Lambda = 1$, $\lambda_a \gg 0$, and $\lambda_b \gg 0$:
   The co-optimization heavily penalizes back flow onto the utility-scale grid and heavily subsidizes DER generation. This results in DER buildout that can cover the majority of distribution demands without pushing electricity to the utility-scale grid. Leads to micro-grid structures in the optimization. The distribution level can pull from the utility-scale grid for electricity, but will only do so for short periods of time due to the costs associated with it.

6. $\Lambda = 1$, $\lambda_a \gg 0$, and $\lambda_b \ll 0$:
   The co-optimization heavily penalizes back flow onto the utility-scale grid and heavily penalizes DER generation. This results in almost zero DER buildout and a tendency to only use the utility-scale grid. Leads to macro-grid utility structures in the optimization. The distribution level can generate electricity, but will not do so due to cost limitations.

For versions 5. and 6., care must be taken when reconstructing the solution to return costs to original values; since these are known as hybrid optimizations[3] and the objective function [Eq. (3.1)] no longer resembles true cost. For version 1. – 4., the costs in the objective functions remain true and there is no need to revert. For strict comparisons of solutions, the system costs metric will need to be identical in all cases regardless of the objective function form.

The current study used version 4. for all the RTO scenarios and version 1. for all the non-RTO scenarios.

[3] https://www.sciencedirect.com/science/article/abs/pii/S0142061514007765

3.10 Policy, Regulations & Mandates

There are many non-economic drivers transforming the electricity sector. Some are incentives, others are emission constraints, and others still are generation exceedances. WIS:dom®-P has been designed to model as many of these drivers as possible, while allowing new ones to be tested or enforced to determine impacts on the transformation of the energy system.

The summary list of policies, regulations and mandates that WIS:dom®-P includes is:

i. *Renewable Portfolio Standards (RPS);*
ii. *Solar, distributed, energy efficiency, and other carve outs;*
iii. *Energy storage mandates;*
iv. *Offshore wind mandates;*
v. *Clean energy (CE) mandates, targets, or goals;*
vi. *Greenhouse Gas (GHG) mandates, targets, or goals;*
vii. *Regional Greenhouse Gas Initiative (RGGI);*
viii. *Attainment zone criteria (NO_x, SO_x, $PM_{2.5}$, PM_{10}, CO, O_3);*
ix. *Investment Tax Credits (ITC);*
x. *Production Tax Credits (PTC).*

The summary list is not exhaustive and more can be added, or versions within the list can be augmented for a user's unique requirements. However, the list is the standard complement of policies, regulations and mandates that WIS:dom®-P always includes as a minimum.

From the list, *i.* – *v.* are all modeled in exactly the same manner, incorporating data from Section 4.3 (see Figs 4.21 – 4.26). The exact variables, parameters and configurations might differ, but the formulation is identical. The generic formulation is:

$$X - X_{goal} \geq 0. \tag{3.20}$$

Equation (3.20) simply states that the variable, X, must exceed the goal of that variable, X_{goal}. So, for example, for the RPS, it might be 30% of electricity must be provided by renewables. Therefore, X_{goal} would be 30% of electricity demand and X would be the generation from all eligible renewable resources.

From the list, *vi.* – *viii.* are all modeled in exactly the same manner, also including data from Section 4.3 (see Figs 4.21 – 4.26). The generic formulation is:

$$Y_{goal} - Y \geq 0. \tag{3.21}$$

Equation (3.21) simply states that the variable, Y, must remain below the goal of that variable, Y_{goal}. The formulation for RGGI is slightly more complex because of trading of carbon credits, but the most binding constraint is that of the form of Eq. (3.21). An example is the GHG mandate: If the mandate states that GHGs must be reduced by 20% from 2005 levels, WIS:dom®-P computes the allowed GHG emissions (Y_{goal}) and within the optimization the GHG emissions must remain below that value.

The final two from the list (*ix.* and *x.*) are applied to the costs with the objective function [Eq. (3.1)]. The ITC adjust the eligible technologies through Eq. (3.2) and parameter $\widehat{\mathcal{C}_{\varepsilon\delta}^{X}}$. It will convert the parameter to:

$$\widehat{\mathcal{C}_{\varepsilon\delta}^{X}} = \widehat{\mathcal{C}_{\varepsilon\delta}^{X}}' \cdot (1 - ITC_{\varepsilon\delta}).$$

(3.22)

The PTC adjusts the eligible technologies through their variable operating costs ($\mathcal{V}_{\mathcal{TL}t}^{\mathcal{G}}$) and is applied for the lifetime of the credit (typically 10 years). The conversion process is simply:

$$\mathcal{V}_{\mathcal{TL}t}^{\mathcal{G}} = \mathcal{V}_{\mathcal{TL}t}^{\mathcal{G}}{}' - PTC_{\mathcal{TL}}.$$

(3.23)

There are new (user-defined) policies, regulations and mandates that can be applied in a similar manner to Eqs (3.20) - (3.23) for carbon constraints, clean electricity, pollution control, renewable electricity exceedances, incentives, and taxes. There are also further formulations that are contained in the model that can mimic a *feebate* scheme or other more exotic policies. However, they are not typically included in the standard version of WIS:dom®-P.

For the present study, we included all the standard policies, regulation, and mandates for the Southeastern United States. We did not impose addition GHG constraints, carbon taxes, artificial build out requirements or anything else that was not already a stated goal or enacted as law (as of June 2019).

3.11 Capacity Change Constraints

With any energy system modeling there are assumptions and/or constraints placed around the amount of different resources that can be constructed over a specified time period. Indeed, WIS:dom®-P is no different in that manner; there are constraints (with assumptions embedded) that limit the capacity change for each technology, for all technologies combined, for each geographic region and for the entire geography being optimized over. The constraints relate to the supply chain of parts, the economic activity that can be diverted to producing energy, and the time to build the capacity (which is further imposed upon by regulations, permitting processes, and other non-economic drivers).

The metric of choice for WIS:dom®-P as standard is derived from the rate of change of capacity across the United States per million dollars of gross domestic product (kW / y / million $GDP)[4]. These units would be translated into real dollars for the initialization year (e.g. 2018). The data collected to derive the metric are for the previous two decades and the data is analyzed to compute the United States values and for each state or other geographic region. Figure 3.7 shows the change in capacity for each year from 1997 through 2016 along with the rate of change metric on the right-hand axis.

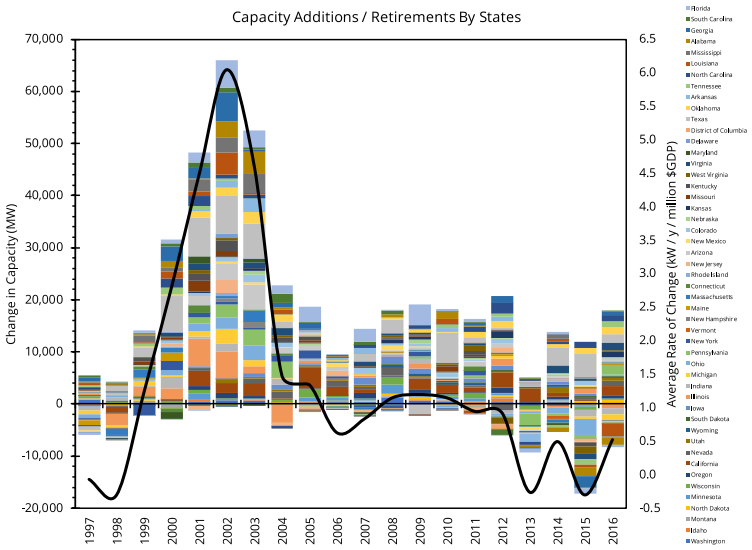

Figure 3.7: Net installed electricity capacity change by state for 1997 through 2016 (left-hand axis) and the average US rate of change of capacity (right-hand axis).

From the data represented in Fig. 3.7, it can be computed that the maximum rate of change over the previous two decades was 6.05 kW / y / million $GDP. The minimum was -0.3 and the mean was 1.45. The presented metric is used because in general electricity production requirements are linked to economic activity. Large increases in capacity needs will happen as older capacity must retire in a variety of states or sharp increase in demand are expected in the near future in many states simultaneously. For example, in 2002 there is a peak in capacity additions and approximately a decade later steep retirements begin. Another reason for using the metric is that as electrification occurs, the same analysis can apply to all energy infrastructure and capital spending can be diverted from other sectors to electricity increase supply chain opportunities to expand the build-out rate for electricity capacity and infrastructure.

[4] Clack et al., https://www.pnas.org/content/114/26/6722 (Figure S5)

The constraints within WIS:dom®-P around capacity changes are based upon the rate of change metric and, as standard, are tethered to the 1.45. For 2018 as the initialization year, this implies that (with $20.5 trillion GDP) the national net change in capacity can be 30,000 MW annually. Within the model, parameters can be adjusted to alter the rate of build-out or retirement of the capacity based upon this metric. For the standard model, we assume GDP growth of approximately 2.5% per annum.

The transmission capacity changes are linked to EIA data for investment in this infrastructure over the past two decades[5]. In the last decade there has been a dramatic increase in transmission investment, but the total cost is only 1% of the cost of electricity. Within WIS:dom®-P the investments in transmission must remain below a set threshold. Typically, this is 1.5% of the total system costs.

For storage, because the technology is much more nascent, the model assumes a fractional approach to available capacity build-out compared with mature technologies. Typically, the build-out is assumed to be 30% of a mature technology at the outset and increasing until 2030, at which point it is assumed to be a mature technology itself.

Finally, for novel technologies (e.g. Natural Gas with Carbon Capture and Sequestration, Small Modular Reactors, Molten Salt Reactors, Enhanced Geothermal Systems) are set to be 40% of a mature technology, but their installation dates are pushed into the future so that they cannot be installed before a set investment period.

For all technologies there is a build-out lag time for the capacity that can come online in each investment period. These lag times are user inputs, but the standards range between 6 months and 2.5 years. Longer lag times can be used, but that can be controlled by initial build dates.

The constraints on capacity and infrastructure, the build-out lag times, the first install date and growth of rate of change of build-out are all customization within WIS:dom®-P. The standard values are set to impose VCE® analysis to calibrate the model to current economic realisms and the potential for innovation to accelerate the changes that might occur.

The functionality of the capacity constraint is imposed via upper bounds on the endogenous capacity values as well as numerous equations within the optimization to limit the amount of capacity that can be constructed. Those equation take the form of Eq. (3.21) in that the combined capacity (over various geographies) must not exceed a specified value.

For the present study, it is assumed that the southeast can change capacity at a rate that is one-fifth the entire contiguous US. This means that it can build 3,500 MW of new capacity and retire 2,900 MW of older capacity per year (from 2020). It is assumed that the southeast will grow faster than the rest of the US and the model expands the rate by 5% per annum (compared with the 2.5% for the rest of the US). Transmission capacity expansion is limited some scenarios and allowed to be deployed more when an RTO is formed. Storage is limited to expanding by 1,000 MW per annum. More details on the present study specifics can be found in Section 2.10.

[5] https://www.eia.gov/todayinenergy/detail.php?id=34892

3.12 Novel Fuel (Chemical) Production & Capture

The production of fuels and chemicals (as well as the capture of carbon dioxide) using electricity and feedstocks is modeled in WIS:dom®-P in a compact form to reduce computational burden considering the complexity involved. The feed stocks are interlinking as required by the processes. The model also has the ability to purchase the chemicals and fuels from a competing local source (which has an associated price and assumed emission footprint).

The chemicals and fuels that are modeled explicitly (as standard) in WIS:dom®-P are:

1. *Hydrogen (H_2) through electrolysis;*

$$2n \cdot H_2O \rightarrow 2n \cdot H_2 + n \cdot O_2$$

2. *Methane (CH_4) through the Sabatier process;*

$$n \cdot CO_2 + 4n \cdot H_2 \rightarrow n \cdot CH_4 + 2n \cdot H_2O$$

3. *Ammonia (NH_3) through the Haber-Bosch process;*

$$n \cdot N_2 + 3n \cdot H_2 \rightarrow 2n \cdot NH_3$$

4. *Anhydrous Ammonium Nitrate (NH_4NO_3) through the Oswald (HNO_3) and Fertilizer processes;*

$$2n \cdot NH_3 + 4n \cdot O_2 + n \cdot H_2O \rightarrow 2n \cdot HNO_3 + 3n \cdot H_2O$$
$$2n \cdot HNO_3 + n \cdot NH_3 \rightarrow n \cdot NH_4NO_3$$

5. *Synthetic diesel and jet fuel (C_nH_{2n+2}) through the Fischer-Tropsch process;*

$$n \cdot H_2O + n \cdot CH_4 \rightarrow n \cdot CO + 3n \cdot H_2$$
$$(2n+1) \cdot H_2 + n \cdot CO \rightarrow C_nH_{2n+2} + n \cdot H_2O$$

6. *Synthetic gasoline (C_nH_m) through the Methanol Synthesis (CH_3OH), Dimethyl Ether Synthesis (CH_3OCH_3), and Gasoline Synthesis processes;*

$$n \cdot CO_2 + 3n \cdot H_2 \rightarrow n \cdot CH_3OH + n \cdot H_2O$$
$$2n \cdot CH_3OH \rightarrow n \cdot CH_3OCH_3 + n \cdot H_2O$$
$$n \cdot CH_3OH + 2n \cdot CH_3OCH_3 \rightarrow n \cdot C_2H_4 + n \cdot C_3H_6 + 3n \cdot H_2O$$
$$a \cdot C_2H_4 + b \cdot C_3H_6 \rightarrow x \cdot CH_5 + y \cdot C_nH_{2n}$$
$$v \cdot C_5 + w \cdot C_nH_{2n} \rightarrow \begin{Bmatrix} paraffins \\ Napthenes \\ Aromatics \end{Bmatrix} \rightarrow gasoline$$

7. *Capture, storage and utilization of Carbon Dioxide (CO_2).*

The list of seven novel fuel (chemical) production is not exhaustive, but it comprises the most fundamental set that can cover almost all energy requirements for the entire economy. The base of these sets is the production of hydrogen, which is assumed to be created from electrolysis (or locally produced outside of the model construct for a price and emission footprint). The WIS:dom®-P model does not solve the chemical formulae for the production of these fuels (chemicals); rather it computes the electricity inputs required per

unit of fuel (for heat, electricity, pumping and other demands) and calculates the required other fuel feedstocks per unit of fuel. Further, the model tracks where the fuel (chemical) flows between regions and how the fuel (chemical) is being stored. All the computations are endogenous to the model and have associated costs and losses.

The capture and utilization of carbon dioxide is treated slightly differently to the other novel fuels (chemicals) because there is CCS available in the model, and therefore there is additional computations required. Further, CO_2 is used in the synthesis of other fuels, but can also be directly captured; which must be sequestered (stored), to facilitate emission reductions from the atmosphere.

The fundamental equation set for the novel fuel and chemical production is given in Eq. (3.24). The equation set determines the amount of fuel (chemical) to produce for each time step, while considering transport of the fuel (chemical) to/from different regions and the injection or extraction of the fuel (chemical) from storage. WIS:dom®-P will optimize the production to reduce the cost of the fuel (chemical) while providing the necessary demand profiles of that fuel (chemical). For CO_2, there is an additional variable that relates the capture from electricity production with CCS.

$$\sum_{\mathfrak{L}\in\mathcal{L}}\left(\hbar\cdot\Omega_{\mathfrak{B}\mathfrak{L}}\cdot\mathcal{u}_{\mathfrak{B}\mathfrak{L}t}-\mathcal{E}_{\mathfrak{L}t}^{\mathfrak{B}}\right)+\widehat{\mathfrak{f}_{\mathcal{L}t}^{\mathfrak{B}}}+\widehat{\mathcal{s}\mathfrak{f}_{\mathcal{L}t}^{\mathfrak{B}}}+\mathcal{A}_{\mathfrak{B}}\cdot\mathcal{CCS}_{\mathcal{L}t}=0\quad\forall\,\mathfrak{B}\backslash\{\text{transmission}\},\mathcal{L},t \tag{3.24}$$

Equation (3.24) introduces two new (exogenous) parameters:

$\Omega_{\mathfrak{B}\mathfrak{L}}$ the conversion efficiency for the novel fuel (chemical) production;
$\mathcal{A}_{\mathfrak{B}}$ is the inclusion parameter for CO_2 from CCS electricity (zero for all except CO_2).

Equation (3.24) introduces three new (endogenous) variables:

$\mathcal{E}_{\mathfrak{L}t}^{\mathfrak{B}}$ the demand of the novel fuel (chemical) for each time step, see Eq. (3.25);
$\widehat{\mathcal{s}\mathfrak{f}_{\mathcal{L}t}^{\mathfrak{B}}}$ the storage flux of the novel fuel (chemical) for each time step, see Eqs (3.26.1) & (3.26.2);
$\mathcal{CCS}_{\mathcal{L}t}$ the carbon dioxide that is capture via electricity with CCS, see Eq. (3.31).

The demand of each novel fuel (chemical) is derived from an equation set in the model that links exogenous curves, external production, feed stock requirements for other fuels (chemicals), and synthetic fuel production for electricity generation. The equation set is:

$$\sum_{\mathfrak{L}\in\mathcal{L}}\left[\mathcal{E}_{\mathfrak{L}t}^{\mathfrak{B}}+\overline{\mathcal{E}_{\mathfrak{L}t}^{\mathfrak{B}}}-\widehat{\mathcal{E}_{\mathfrak{L}t}^{\mathfrak{B}}}-\sum_{\mathfrak{B}}\left(\mathfrak{Z}_{\mathfrak{B}\hat{\mathfrak{B}}\mathfrak{L}}\cdot\hbar\cdot\Omega_{\hat{\mathfrak{B}}\mathfrak{L}}\cdot\mathcal{u}_{\hat{\mathfrak{B}}\mathfrak{L}t}\right)\right]-\mathcal{A}_{n\mathscr{g}}\cdot\mathcal{NG}_{\mathfrak{B}\mathcal{L}t}-\mathcal{A}_{coal}\cdot\mathcal{COAL}_{\mathfrak{B}\mathcal{L}t}\geq 0\quad\forall\,\mathfrak{B}\backslash\{\text{transmission}\},\mathcal{L},t \tag{3.25}$$

Equation (3.25) introduces four new (exogenous) parameters:

$\widehat{\mathcal{E}_{\mathfrak{L}t}^{\mathfrak{B}}}$ the exogenous demand for the novel fuel (chemical) in set $\mathfrak{B}$;
$\mathfrak{Z}_{\mathfrak{B}\hat{\mathfrak{B}}\mathfrak{L}}$ the fraction of novel fuel (chemical) in set $\mathfrak{B}$, required another novel fuel (chemical) in set $\hat{\mathfrak{B}}$;
$\mathcal{A}_{n\mathscr{g}}$ an activation parameter for novel fuels that can replace natural gas for electricity production;
$\mathcal{A}_{coal}$ an activation parameter for novel fuels that can replace coal for electricity production.

Equation (3.25) introduces three new (endogenous) variables:

$\overline{\mathcal{E}^{\mathfrak{B}}_{\mathfrak{Q}t}}$ *the production of novel fuels (chemicals) outside of the model space;*
$\mathcal{NG}_{\mathfrak{BL}t}$ *the amount of natural gas displaced by the novel fuels (chemicals);*
$\mathcal{COAL}_{\mathfrak{BL}t}$ *the amount of coal displaced by the novel fuels (chemicals).*

Equation (3.25) states that the demand for a specific novel fuel (chemical) is the sum of the exogenously supplied demand, the production of the fuel (chemical) for other novel fuels (chemicals), the production of the fuel (chemical) to replace natural gas and coal for electricity production minus the specific novel fuel (chemical) produced outside of the model (with an associated cost and emission footprint). The activation parameters ($\mathcal{A}_{ng}$ and $\mathcal{A}_{coal}$) allow the user to switch on and off fossil fuel replacement or blending as a possible avenue for GHG emission reduction.

The parameter $\mathfrak{Z}_{\mathfrak{BB}\mathfrak{Q}}$ is important to convert quantities of each novel fuel (chemical) required to create another novel fuel (chemical). These are constrained by the chemistry of the novel fuels (chemicals). An example would be the quantities of H_2 and CO_2 to create CH_4. To produce 16.04 units of CH_4, there is a requirement to provide 8.06 units of H_2 and 44.01 units of CO_2[6,7] as feed stocks. Thus, we have:

$$\mathfrak{Z}_{\{\mathrm{H_2}\}\{\mathrm{CH_4}\}\mathfrak{Q}} = 0.50271 \text{ and } \mathfrak{Z}_{\{\mathrm{CO_2}\}\{\mathrm{CH_4}\}\mathfrak{Q}} = 2.74377.$$

The flow / transport variable ($\widehat{\mathscr{f}^{\mathfrak{B}}_{\mathcal{L}t}}$) in Eq. (3.24) is completely described by Eqs (3.5), (3.6.1), (3.6.2) and (3.7). We refer the reader back to those equations because they are computed in exactly the same way as transmission of electricity; with the exogenous parameters altered.

The storage flux variable ($\widehat{\mathscr{sf}^{\mathfrak{B}}_{\mathcal{L}t}}$) is calculated slightly differently to that of electricity storage. The WIS:dom®-P model assumes no leakage to or from storage for the novel fuels (chemicals). It is trivial, mathematically, to expand the equations to include leakage to and from storage (as is computed for electric storage[8]); however, the computation burden is substantial because there would be a doubling of the endogenous variables computing the flows in and out of storage. Due to the high temporal granularity, this leads to difficulties in solver performance. The novel fuel (chemical) storage equations are:

$$\left[\widehat{\mathfrak{E}}_{\mathfrak{BL}t} - \left(1 - \widehat{\ell^{ls}_{\mathfrak{BQ}t}}\right) \cdot \widehat{\mathfrak{E}}_{\mathfrak{BL}(t-1)}\right] + \widehat{\mathscr{sf}^{\mathfrak{B}}_{\mathcal{L}t}} = 0 \quad \forall\, \mathfrak{B}\backslash\{\text{transmission}\}, \mathcal{L}, t \tag{3.26.1}$$

$$n_{\mathfrak{BL}\{storage\}} - \widehat{\mathfrak{E}}_{\mathfrak{BL}t} \geq 0 \quad \forall\, \mathfrak{B}\backslash\{\text{transmission}\}, \mathcal{L}, t \tag{3.26.2}$$

Equations (3.26.1) and (3.26.2) introduce a single new (exogenous) parameter:

$\widehat{\ell^{ls}_{\mathfrak{BQ}t}}$ *the leakage rate for the novel fuel (chemical) while being stored.*

Equations (3.26.1) and (3.26.2) introduce a single new (endogenous) variable:

$\widehat{\mathfrak{E}}_{\mathfrak{BL}t}$ *the quantity of novel fuel (chemical) stored at each time step.*

[6] We can assume kg if computing under standard temperature and pressure.
[7] There would also be 36.03 units of H_2O produced.
[8] If full leakage is included, the novel fuel (chemical) storage equations would be mathematically identical to Eqs (3.9.1) and (3.9.3).

To close the equation sets for novel fuel (chemical) production, there needs to be constraints that describe the installed capacity of the facilities (in MW), the minimum production possible, the ramping capabilities of the production facilities, and the minimum up and down times of the facilities. These equations are closely related to Eqs (3.10), (3.11), (3.12.1), (3.12.2), (3.13.1), and (3.13.2). We write down the equations explicitly here due to the subtle differences that can be important. Not that if unit commitment is activated ($\Delta = 1$), and additional activation parameter ($\Delta^{\mathfrak{B}} = 1$) is required for novel fuels (chemicals) because (as standard) they are assumed to not be under unit-commitment even if the generation facilities are [see Eq. (3.1) for details on activation parameters].

The equations to complete the description of novel fuel (chemical) production are:

$$\sum_{\mathfrak{L}\in\mathcal{L}}\left\{\mathcal{P}^{max}_{\mathfrak{B}\mathfrak{L}t}\cdot\begin{bmatrix}\left(1-\Delta\cdot\Delta^{\mathfrak{B}}\right)\cdot n_{\mathfrak{B}\mathcal{L}\{cap\}}\\ +\Delta\cdot\Delta^{\mathfrak{B}}\cdot\xi_{\mathfrak{B}\mathfrak{L}t}\end{bmatrix}-u_{\mathfrak{B}\mathcal{L}t}\right\}\geq 0\quad\forall\,\mathfrak{B}\backslash\{\text{transmission}\},\mathcal{L},t \tag{3.27}$$

$$\sum_{\mathfrak{L}\in\mathcal{L}}\left\{\begin{matrix}\Delta\cdot\Delta^{\mathfrak{B}}\cdot\left(u_{\mathfrak{B}\mathcal{L}t}-\mathcal{P}^{min}_{\mathfrak{B}\mathfrak{L}t}\cdot\xi_{\mathfrak{B}\mathfrak{L}t}\right)+\\ \left(1-\Delta\cdot\Delta^{\mathfrak{B}}\right)\cdot\left(\sum_{t}\frac{\hbar\cdot u_{\mathfrak{B}\mathcal{L}t}}{8760}-\overline{\mathcal{P}^{min}_{\mathfrak{B}\mathfrak{L}t}}\cdot n_{\mathfrak{B}\mathcal{L}\{cap\}}\right)\end{matrix}\right\}\geq 0\quad\forall\,\mathfrak{B}\backslash\{\text{transmission}\},\mathcal{L},t \tag{3.28}$$

$$\sum_{\mathfrak{L}\in\mathcal{L}}\left\{\begin{matrix}\Delta\cdot\Delta^{\mathfrak{B}}\cdot\left[\mathcal{UR}_{\mathfrak{B}\mathfrak{L}t}\cdot\left(\xi_{\mathfrak{B}\mathfrak{L}t}-\phi_{\mathfrak{B}\mathfrak{L}t}\right)+\mathcal{P}^{min}_{\mathfrak{B}\mathfrak{L}t}\cdot\left(\phi_{\mathfrak{B}\mathfrak{L}t}-\psi_{\mathfrak{B}\mathfrak{L}t}\right)\right]\\ +\left(1-\Delta\cdot\Delta^{\mathfrak{B}}\right)\cdot\mathcal{UR}_{\mathfrak{B}\mathfrak{L}t}\cdot n_{\mathfrak{B}\mathcal{L}\{cap\}}\\ -\left(u_{\mathfrak{B}\mathcal{L}t}-u_{\mathfrak{B}\mathfrak{L}(t-1)}\right)\end{matrix}\right\}\geq 0\quad\forall\,\mathfrak{B}\backslash\{\text{transmission}\},\mathcal{L},t \tag{3.29.1}$$

$$\sum_{\mathfrak{L}\in\mathcal{L}}\left\{\begin{matrix}\Delta\cdot\Delta^{\mathfrak{B}}\cdot\left[\mathcal{DR}_{\mathfrak{B}\mathfrak{L}t}\cdot\left(\xi_{\mathfrak{B}\mathfrak{L}t}-\phi_{\mathfrak{B}\mathfrak{L}t}\right)+\mathcal{P}^{min}_{\mathfrak{B}\mathfrak{L}t}\cdot\left(\psi_{\mathfrak{B}\mathfrak{L}t}-\phi_{\mathfrak{B}\mathfrak{L}t}\right)\right]\\ +\left(1-\Delta\cdot\Delta^{\mathfrak{B}}\right)\cdot\mathcal{DR}_{\mathfrak{B}\mathfrak{L}t}\cdot n_{\mathfrak{B}\mathcal{L}\{cap\}}\\ +\left(u_{\mathfrak{B}\mathcal{L}t}-u_{\mathfrak{B}\mathfrak{L}(t-1)}\right)\end{matrix}\right\}\geq 0\quad\forall\,\mathfrak{B}\backslash\{\text{transmission}\},\mathcal{L},t \tag{3.29.2}$$

$$\Delta\cdot\Delta^{\mathfrak{B}}\cdot\sum_{\mathfrak{L}\in\mathcal{L}}\left\{\xi_{\mathfrak{B}\mathfrak{L}t}-\sum_{\hat{t}=t-t_{up}}^{t}\phi_{\mathfrak{B}\mathfrak{L}\hat{t}}\right\}\geq 0\quad\forall\,\mathfrak{B}\backslash\{\text{transmission}\},\mathcal{L},t \tag{3.30.1}$$

$$\Delta\cdot\Delta^{\mathfrak{B}}\cdot\sum_{\mathfrak{L}\in\mathcal{L}}\left\{n_{\mathfrak{B}\mathcal{L}\{cap\}}-\xi_{\mathfrak{B}\mathfrak{L}t}-\sum_{\hat{t}=t-t_{dwn}}^{t}\psi_{\mathfrak{B}\mathfrak{L}\hat{t}}\right\}\geq 0\quad\forall\,\mathfrak{B}\backslash\{\text{transmission}\},\mathcal{L},t \tag{3.30.2}$$

The Eqs (3.27) – (3.30.2) expand the unit commitment variables over the set $\mathfrak{B}\backslash\{\text{transmission}\}$, if the novel fuel (chemical) activation parameter, $\Delta^{\mathfrak{B}}$, is set to unity. For standard WIS:dom®-P uses it is most appropriate to set the novel fuel (activation) parameter to zero ($\Delta^{\mathfrak{B}} = 0$) because of data scarcity.

To complete the impact of novel fuel (chemical) production on the total energy system several more equation sets are required.

The first completes the cycle for CO_2 from CCS into the novel fuel (chemical) equations:

$$\mathcal{CCS}_{\mathcal{L}t} - \sum_{\mathcal{T}\in\mathcal{CCS}}\left[\hbar\cdot\mathcal{H}^{\mathcal{G}}_{\mathcal{T}\mathcal{L}t}\cdot\mathcal{p}_{\mathcal{T}\mathcal{L}t}\cdot\left(\mathfrak{P}_{\mathcal{T}\mathcal{L}t}-\mathfrak{P}_{\mathcal{T}'\mathcal{L}t}\right)\right] = 0 \;\; \forall\, \mathcal{L},t$$

(3.31)

Equation (3.31) introduces two new (exogenous) parameters:

$\mathfrak{P}_{\mathcal{T}\mathcal{L}t}$ *the carbon content release from a generation technology fuel without CCS;*
$\mathfrak{P}_{\mathcal{T}'\mathcal{L}t}$ *the carbon content release from a generation technology fuel with CCS.*

The second completes the cycle for the novel fuels (chemicals) to replace fossil fuels in combustion for electricity production; namely natural gas and coal for WIS:dom®-P, but can be extended to other fossil fuels. The links are provided by:

$$\sum_{\mathcal{T}\in\mathcal{NG}}\left(\hbar\cdot\mathcal{H}^{\mathcal{G}}_{\mathcal{T}\mathcal{L}t}\cdot\mathcal{p}_{\mathcal{T}\mathcal{L}t}\right)-\sum_{\mathfrak{B}}\left(\mathfrak{S}^{\mathcal{NG}}_{\mathfrak{B}}\cdot\mathcal{NG}_{\mathfrak{B}\mathcal{L}t}\right)\geq 0 \;\; \forall \;\; \mathcal{L},t$$

(3.32.1)

$$\sum_{\mathcal{T}\in\mathcal{COAL}}\left(\hbar\cdot\mathcal{H}^{\mathcal{G}}_{\mathcal{T}\mathcal{L}t}\cdot\mathcal{p}_{\mathcal{T}\mathcal{L}t}\right)-\sum_{\mathfrak{B}}\left(\mathfrak{S}^{\mathcal{COAL}}_{\mathfrak{B}}\cdot\mathcal{COAL}_{\mathfrak{B}\mathcal{L}t}\right)\geq 0 \;\; \forall \;\; \mathcal{L},t$$

(3.32.2)

Equations (3.32.1) and (3.32.2) introduce two new (exogenous) parameters:

$\mathfrak{S}^{\mathcal{NG}}_{\mathfrak{B}}$ *is the conversion of novel fuel (chemical) to natural gas million British Thermal Units (BTUs);*
$\mathfrak{S}^{\mathcal{COAL}}_{\mathfrak{B}}$ *is the conversion of novel fuel (chemical) to coal million BTUs.*

The purpose of Eqs (3.32.1) and (3.32.2) is to limit the creation of replacement novel fuels (chemicals) to the consumption of that fossil fuel. In the limit, all the fossil fuels could be replaced with the novel fuels (chemicals); however, it is noted that to produce these novel fuels (chemicals) there must be a source of energy (either directly in the model from electricity or external production).

With the inclusion of novel fuel (chemical) production that can possibly replace fossil fuels and the inclusion of direct air capture, the carbon dioxide constraints and calculations within WIS:dom®-P are updated. Since the mathematical equation for the pollution and emission tracker (or constraint) was not explicitly presented in Section 3.10, we show it in Eq. (3.33) along with the additional terms associated with the novel fuel (chemical) production. The pollution and emission tracking equation set is given by:

$$\mathfrak{M}_{\mathfrak{K}\mathcal{L}t}-\hbar\cdot\left[\begin{matrix}\sum_{\mathcal{T}}\left(\mathfrak{P}_{\mathfrak{K}\mathcal{T}\mathcal{L}t}\cdot\mathcal{H}^{\mathcal{G}}_{\mathcal{T}\mathcal{L}t}\cdot\mathcal{p}_{\mathcal{T}\mathcal{L}t}\right)\\ -\mathcal{A}_{\mathfrak{K}}\cdot\sum_{\mathfrak{B}}\left(\Omega_{\{\mathrm{CO_2}\}\mathcal{L}}\cdot\mathcal{u}_{\{\mathrm{CO_2}\}\mathcal{L}t}\right)\end{matrix}\right]+\left[\begin{matrix}\sum_{\mathfrak{B}}\left(\mathfrak{P}'_{\mathfrak{K}\{\mathcal{NG}\}\mathcal{L}t}\cdot\mathfrak{S}^{\mathcal{NG}}_{\mathfrak{B}}\cdot\mathcal{NG}_{\mathfrak{B}\mathcal{L}t}\right)+\\ \sum_{\mathfrak{B}}\left(\begin{matrix}\mathfrak{P}'_{\mathfrak{K}\{\mathcal{COAL}\}\mathcal{L}t}\cdot\mathfrak{S}^{\mathcal{COAL}}_{\mathfrak{B}}\cdot\mathcal{COAL}_{\mathfrak{B}\mathcal{L}t}\\ -\bar{\mathfrak{P}}_{\mathfrak{K}\mathfrak{B}\mathcal{L}t}\cdot\mathfrak{S}_{\mathfrak{B}}\cdot\overline{\mathcal{E}^{\mathfrak{B}}_{\mathcal{L}t}}\end{matrix}\right)\end{matrix}\right]=0 \quad \forall \;\; \mathfrak{K},\mathcal{L},t$$

(3.33)

Equation (3.33) introduces a single new set:

$\mathfrak{K}$ *the set of all pollutant species within WIS:dom®-P (e.g. CO_2, NO_x, SO_x, $PM_{2.5}$).*

Equation (3.33) introduces six new (exogenous) parameters:

$\mathfrak{P}_{\mathfrak{K}\mathcal{T}\mathcal{L}t}$ *the pollution content release from a generation technology fuel;*
$\mathcal{A}_{\mathfrak{K}}$ *the inclusion parameter for carbon dioxide (zero for all other pollutants);*
$\mathfrak{P}'_{\mathfrak{K}\{\mathcal{NG}\}\mathcal{L}t}$ *the reduction in pollutant due to novel fuel (chemical) replacement of natural gas;*
$\mathfrak{P}'_{\mathfrak{K}\{\mathcal{COAL}\}\mathcal{L}t}$ *the reduction in pollutant due to novel fuel (chemical) replacement of coal;*
$\widetilde{\mathfrak{P}}_{\mathfrak{K}\mathfrak{B}\mathcal{L}t}$ *the pollutants associated with externally produced novel fuel (chemical);*
$\mathfrak{S}_{\mathfrak{B}}$ *the conversion of novel fuel (chemical) to mmBTUs.*

Equations (3.33) introduces a single new (endogenous) variable:

$\mathfrak{M}_{\mathfrak{K}\mathcal{L}t}$ *the quantity of each pollutant for each region and each timestep.*

In simple terms, Eq. (3.33) describes how much of each pollutant species is emitted by combustion for electricity minus the captured CO_2 from the novel fuel equations, minus the reduction due to fossil fuel replacement by novel fuels (chemicals) plus the contribution (if any) from externally produced novel fuels (chemicals).

When WIS:dom®-P converts Eq. (3.33) into a constraint on any (or all) of the pollutants and emissions, it inserts $\mathfrak{M}_{\mathfrak{K}\mathcal{L}t}$ into Eq. (3.21) to replace Y.

The last change to the WIS:dom®-P model structure due to the inclusion of novel fuel (chemical) production is an additional set of terms to the objective function [Eq. (3.1)]. The additional terms add costs to the combustion of novel fuels (chemicals) to replace natural gas and coal. For example, there is additional costs to being able to combust hydrogen in the place of natural gas for electricity. This is modeled within WIS:dom®-P as additional variable costs. The purpose of the premium cost adder is to enable WIS:dom®-P to recognize the difference between replacing fossil natural gas with hydrogen and replacing fossil natural gas with synthetic natural gas. The latter has no additional variable costs, but is more expensive to produce; while the former is cheaper to produce; but requires additional spending to convert infrastructure.

The additional terms are:

$$\sum_{\mathfrak{B}}\sum_{\mathcal{L}}\sum_{t}\left(\widehat{\mathcal{V}^{\mathcal{NG}}_{\mathfrak{B}\mathcal{L}t}}\cdot\mathfrak{S}^{\mathcal{NG}}_{\mathfrak{B}}\cdot\mathcal{NG}_{\mathfrak{B}\mathcal{L}t}+\widehat{\mathcal{V}^{\mathcal{COAL}}_{\mathfrak{B}\mathcal{L}t}}\cdot\mathfrak{S}^{\mathcal{COAL}}_{\mathfrak{B}}\cdot\mathcal{COAL}_{\mathfrak{B}\mathcal{L}t}\right) \tag{3.34}$$

Equation (3.34) introduces two new (exogenous) parameters:

$\widehat{\mathcal{V}^{\mathcal{NG}}_{\mathfrak{B}\mathcal{L}t}}$ *the premium cost adder for each mmBTU of natural gas replaced with novel fuel (chemical);*
$\widehat{\mathcal{V}^{\mathcal{COAL}}_{\mathfrak{B}\mathcal{L}t}}$ *the premium cost adder for each mmBTU of coal replaced with novel fuel (chemical).*

The complete set of equations for the description of novel fuel and chemical production are contained in Eqs (3.24) – (3.34). The most difficult part to accurately address is the input assumptions for the exogenous parameters. Many of the technologies for producing novel fuels (chemicals) are new and untested at scale, while others may exist, but in very different forms to those envisioned in the modeling. Therefore, there care must be taken to prescribe the input parameters. The parameters are all adjustable by the user.

For the present study, we did not include any novel technologies.

3.13 Unit Commitment

To account for unit commitment more equations are required (in addition to the augmentation of earlier equations). The fundamental equations define the startups, committed and shutdowns for all generation (novel fuel production) assets. The purpose of unit commitment is to allow WIS:dom®-P to prioritize assets that are already committed to the grid; but to also embed the cost (and limitations) for running different assets. The unit commitment of generation assets is described by:

$$\Delta \cdot \sum_{\mathfrak{L} \in \mathcal{L}} \left(\xi_{\mathcal{T}\mathfrak{L}t} - \xi_{\mathcal{T}\mathfrak{L}(t-1)} + \psi_{\mathcal{T}\mathfrak{L}t} - \phi_{\mathcal{T}\mathfrak{L}t} \right) = 0 \quad \forall \ \mathcal{T}, \mathcal{L}, t \tag{3.35}$$

All of the terms in Eq. (3.35) have been presented before. The terms in Eq. (3.35) allow WIS:dom®-P to decide what generation assets to commit (ξ) in the current time step, which must equal the generation started (ϕ) and shutdown (ψ) in the present time step plus the committed generation from the previous time step. Every time a generation asset is started, there is a cost that appears in the objective function [Eq. (3.1)]. Note that if unit commitment is not activated ($\Delta = 0$), Eq. (3.35) is automatically solved and the terms inside are irrelevant to the optimization. There is an analogous equation for novel fuel production, as shown in Eq. (3.36):

$$\Delta \cdot \Delta^{\mathfrak{B}} \cdot \sum_{\mathfrak{L} \in \mathcal{L}} \left(\xi_{\mathfrak{B}\mathfrak{L}t} - \xi_{\mathfrak{B}\mathfrak{L}(t-1)} + \psi_{\mathfrak{B}\mathfrak{L}t} - \phi_{\mathfrak{B}\mathfrak{L}t} \right) = 0 \quad \forall \ \mathfrak{B} \backslash \{transmission\}, \mathcal{L}, t \tag{3.36}$$

Since WIS:dom®-P simultaneously solves capacity expansion and production cost, there are constraint equations on the committed, startup and shutdown variables. These are required because the capacities can change within the optimization; if production cost only is simulated, the constraints collapse to upper bounds on the variables. Equations (3.37.1) – (3.37.3) are the constraints for the generation asset variables and Eqs (3.38.1) – (3.38.3) are the constraints for the novel fuel production assets.

$$\Delta \cdot \left(x_{\mathcal{T}\mathcal{L}} - \sum_{\mathfrak{L} \in \mathcal{L}} \xi_{\mathcal{T}\mathfrak{L}t} \right) \geq 0 \quad \forall \ \mathcal{T}, \mathcal{L}, t \tag{3.37.1}$$

$$\Delta \cdot \left(x_{\mathcal{T}\mathcal{L}} - \sum_{\mathfrak{L} \in \mathcal{L}} \phi_{\mathcal{T}\mathfrak{L}t} \right) \geq 0 \quad \forall \ \mathcal{T}, \mathcal{L}, t \tag{3.37.2}$$

$$\Delta \cdot \left(x_{\mathcal{T}\mathcal{L}} - \sum_{\mathfrak{L} \in \mathcal{L}} \psi_{\mathcal{T}\mathfrak{L}t} \right) \geq 0 \quad \forall \ \mathcal{T}, \mathcal{L}, t \tag{3.37.3}$$

$$\Delta \cdot \Delta^{\mathfrak{B}} \cdot \left(n_{\mathfrak{B}\mathcal{L}\{cap\}} - \sum_{\mathfrak{L} \in \mathcal{L}} \xi_{\mathfrak{B}\mathfrak{L}t} \right) \geq 0 \quad \forall \ \mathfrak{B} \backslash \{transmission\}, \mathcal{L}, t$$

(3.38.1)

$$\Delta \cdot \Delta^{\mathfrak{B}} \cdot \left(n_{\mathfrak{B}\mathcal{L}\{cap\}} - \sum_{\mathfrak{L} \in \mathcal{L}} \phi_{\mathfrak{B}\mathfrak{L}t} \right) \geq 0 \quad \forall \ \mathfrak{B} \backslash \{transmission\}, \mathcal{L}, t$$

(3.38.2)

$$\Delta \cdot \Delta^{\mathfrak{B}} \cdot \left(n_{\mathfrak{B}\mathcal{L}\{cap\}} - \sum_{\mathfrak{L} \in \mathcal{L}} \psi_{\mathfrak{B}\mathfrak{L}t} \right) \geq 0 \quad \forall \ \mathfrak{B} \backslash \{transmission\}, \mathcal{L}, t$$

(3.38.3)

The present study does not have unit commitment activated, nor does it allow for novel fuel (chemical) production ($\Delta = \Delta^{\mathfrak{B}} = 0$).

3.13.1 Adjusted Heat Rates

When unit commitment is activated, the WIS:dom®-P model has an additional upgrade on the heat rate computations for thermal power plants. A new equation set is activated and the objective function is updated with a replacement term for variable costs. We did not write the replacement term in Eq. (3.1) due to space on the page, but we will document the changes here. Within WIS:dom®-P, when unit commitment is activated, so too is the heat rate expansion functionality. To not include the heat rate expansion requires removing the activation term.

In Eq. (3.1) the variable and fuel costs for thermal generators are contained in the term

$$\hbar \cdot \sum_{t} \left[\left(\mathcal{V}^{\mathcal{G}}_{\mathcal{T}\mathcal{L}t} + \left(\mathcal{F}^{\mathcal{G}}_{\mathcal{T}\mathcal{L}t} + \mathcal{V}^{c}_{\mathcal{L}} \cdot \mathfrak{F}_{\mathcal{T}\mathcal{L}} \right) \cdot \mathcal{H}^{\mathcal{G}}_{\mathcal{T}\mathcal{L}t} \right) \cdot \mathcal{p}_{\mathcal{T}\mathcal{L}t} \right],$$

which is replaced with

$$\hbar \cdot \sum_{t} \left\{ \begin{array}{c} \sum_{\mathcal{T} \in UC} \left[\widehat{\mathcal{V}^{\mathcal{G}}_{\mathcal{T}\mathcal{L}t}} \right] + \\ \sum_{\mathcal{T} \in non\ UC} \left[\left(\mathcal{V}^{\mathcal{G}}_{\mathcal{T}\mathcal{L}t} + \left(\mathcal{F}^{\mathcal{G}}_{\mathcal{T}\mathcal{L}t} + \mathcal{V}^{c}_{\mathcal{L}} \cdot \mathfrak{F}_{\mathcal{T}\mathcal{L}} \right) \cdot \mathcal{H}^{\mathcal{G}}_{\mathcal{T}\mathcal{L}t} \right) \cdot \mathcal{p}_{\mathcal{T}\mathcal{L}t} \right] \end{array} \right\}$$

(3.39)

In simple terms, the non-unit commitment generators are not impacted by the heat rate upgraded computation; but it is required for them to be split out from the unit commitment generators. The unit commitment generators have their variable costs imposed by another equation set to define $\widehat{\mathcal{V}^{\mathcal{G}}_{\mathcal{T}\mathcal{L}t}}$. This equation set always exists within WIS:dom®-P, but collapses to not being required when unit commitment is not activated.

The equation set that defines the variable costs for unit commitment generators is given by:

$$\widehat{\mathcal{V}_{\mathcal{TL}t}^{\mathcal{G}}} - \left\{ \mathcal{V}_{\mathcal{TL}t}^{\mathcal{G}} \cdot \mathcal{P}_{\mathcal{TL}t} + \left[\begin{pmatrix} \mathcal{F}_{\mathcal{TL}t}^{\mathcal{G}} + \\ \mathcal{V}_{\mathcal{L}}^{c} \cdot \mathfrak{F}_{\mathcal{TL}} \end{pmatrix} \cdot \mathcal{H}_{\mathcal{TL}t}^{\mathcal{G}} \right] \cdot \left\{ (1 - \Delta) + \Delta \cdot \left[\begin{matrix} \left(\mathcal{H}_{\mathcal{TL}}^{min} - \mathcal{H}_{\mathcal{TL}}^{max}\right) \cdot \mathcal{P}_{\mathcal{TL}t} \\ + \mathcal{H}_{\mathcal{TL}}^{max} \cdot \xi_{\mathcal{TQ}t} \end{matrix} \right] \right\} \right\} \geq 0$$

(3.40)

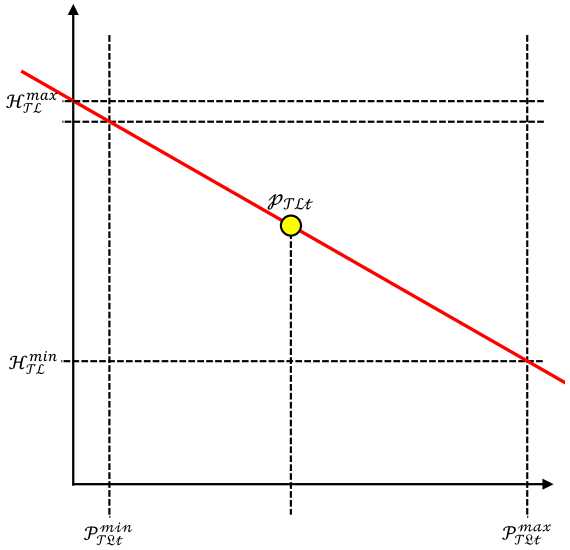

Figure 3.8: Illustration of the heat rate with generation multiplier. The higher the generation, the lower the heat rate.

Equation (3.40) introduces multipliers $\mathcal{H}_{\mathcal{TL}}^{min}$ and $\mathcal{H}_{\mathcal{TL}}^{max}$, which are illustrated in Fig. 3.8. The multipliers shift the temperature adjusted heat rate in correlation with the generation output of the power plants. The closer the generation output is to the committed capacity, the lower the heat rate. While the closer the generation output is to the minimum allowed generation the higher the heat rate. The multiplier $\mathcal{H}_{\mathcal{TL}}^{max}$ is the hypothetical value if there was no generation, whereas $\mathcal{H}_{\mathcal{TL}}^{min}$ is the multiplier when the generation is at its maximum allowed value.

The multipliers correct the average heat rate value that is used in WIS:dom®-P (which itself is already adjusted for the air temperature locally). It can be seen from the plot in Fig. 3.8 that the multipliers lie on a straight line. This is due to the model typically executed in linear programming mode. Other variations can be used if non-linear terms are required. These are more complicated and do not overly alter the results for capacity expansion.

3.14 Retirement Cost Calculations

For retirement cost calculations the WIS:dom®-P model must transfer information from a previous investment period to a future one. The WIS:dom®-P model is typically run in "*myopic mode*", which means that investment periods are solved sequentially (and chronologically). Information from previous investment periods impact future ones; but future ones do not impact previous ones. Performing the optimization in this manner ensures that decisions are made within each investment period without future changes in cost curves, performance and policy. In addition, it means that once a decision is made in a previous investment period, the model must take that into account (for example as sunk costs) and process how best to deal with the current investment period grid infrastructure and generation assets.

In performing the optimizations in a sequential manner in WIS:dom®-P facilitates scenario-based analysis investigating earlier price drops, faster or slower adoption of technologies, rapid retirements, and other time-dependent shifts in policy. A model that can see all future prices will be more optimal, but does not take into account decision making processes that occur in reality. WIS:dom®-P can be executed in "*seer mode*" that works backwards from a known end-state to the present computing the optimal pathway to reach that said end-state. In performing these optimizations, it has been found that decisions are "put off" until later (in general) and are more sensitivity to perturbations. One limitation of the "*seer mode*" is retirements of current (or future assets) because linking between time-periods in reverse is intractable (since the user does not know ahead of time what assets retire when). This is one of the reasons that WIS:dom®-P is almost always executed in "*myopic mode*".

To execute the model with explicit retirement cost calculations, the user must set $\Theta = 1$, which enables the retirement costs to be added into the objective function [Eq. (3.1)]. Without this activation, the model will assume that all assets have a zero cost to retire. When the retirement cost calculations are activated more equations and constraints are included in the optimization of each investment period. Critically, processing occurs between each investment period to exchange data from the previous investment period to the next. To represent the investment periods, we introduce a new (informal) set, $\mathbb{T}$. This notation will enable distinction between different (linked) investment periods and will allow us to describe computations between investment periods.

The term in the objective function [Eq. (3.1)] that embeds retirement costs is:

$$\Theta \cdot \left(\sum_{\mathcal{T}} \left(\mathcal{C}_{\mathcal{TL}}^{\mathcal{G}o} \cdot x_{\mathcal{TL}}^{o} + \mathcal{C}_{\mathcal{TL}}^{\mathcal{G}r} \cdot x_{\mathcal{TL}}^{r} \right) + \Re_{\mathcal{L}} \right).$$

There is actually only one endogenous variable in the term expressed above because the "old" generators and the "retired" generators are connected by:

$$\Theta \cdot \left(x_{\mathcal{TL}}^{o} + x_{\mathcal{TL}}^{r} - x_{\mathcal{TL}}^{(\mathbb{T}-1)} \right) = 0 \quad \forall\ \mathcal{T}, \mathcal{L}. \tag{3.41}$$

Thus, one can replace $x_{\mathcal{TL}}^{o}$ in the objective function using Eq. (3.41). All Eq. (3.41) states is that the "old" and "retired" capacity must sum to the total capacity that was present at the end of the previous investment period.

The additional equation set that adjusts the optimization within an investment period is:

$$\Theta \cdot \left[x_{\mathcal{TL}}^{(\mathbb{T})} - x_{\mathcal{TL}}^{\sigma}\left(= x_{\mathcal{TL}}^{(\mathbb{T}-1)} - x_{\mathcal{TL}}^{r}\right)\right] \geq 0 \quad \forall\ \mathcal{T}, \mathcal{L}.$$

(3.42)

Equation (3.42) states that the installed generation capacity in the current investment period must exceed or equal the remaining capacity from the previous investment period. Equations (3.41) and (3.42) combine to enforce that, in WIS:dom®-P, capacity that disappears must be retired and capacity that appears must be a new build (or augmentation at an existing site).

To ensure that the retirement cost calculations are valuable to the optimization, the exogenous parameters must be initialized and updated between each investment period. The exogenous parameters that are updated are $\mathcal{C}_{\mathcal{TL}}^{\mathcal{G}\sigma}$, $\mathcal{C}_{\mathcal{TL}}^{\mathcal{G}r}$, $\mathfrak{R}_{\mathcal{L}}$, $\mathcal{H}_{\mathcal{TLt}}^{\mathcal{G}}$, and $\mathbb{A}_{\mathcal{TL}}$. These parameters (with the exception of $\mathfrak{R}_{\mathcal{L}}$) are updated by "*blending*" the previous version with the new version through weighted averages (and based upon average age, $\mathbb{A}_{\mathcal{TL}}^{\mathcal{G}}$).

The first exogenous parameter computed is the average age of the generators:

$$\mathbb{A}_{\mathcal{TL}}^{(\mathbb{T})} = \begin{cases} \mathbb{A}_{\mathcal{TL}}^{(\mathbb{T})} & \forall\ \mathbb{T} = 1, \mathcal{T}, \mathcal{L} \\ \dfrac{\mathbb{L}^{(\mathbb{T}-1)} \cdot \left(x_{\mathcal{TL}}^{(\mathbb{T}-1)} - x_{\mathcal{TL}}^{\sigma(\mathbb{T}-1)}\right) + \left(\mathbb{A}_{\mathcal{TL}}^{(\mathbb{T}-1)} + \mathbb{L}^{(\mathbb{T}-1)}\right) \cdot x_{\mathcal{TL}}^{\sigma(\mathbb{T}-1)}}{x_{\mathcal{TL}}^{(\mathbb{T}-1)}} & \forall\ \mathbb{T} \geq 2, \mathcal{T}, \mathcal{L} \end{cases}$$

(3.43)

Equation (3.43) introduces a single new (exogenous) parameter:

$\mathbb{L}$ *is the number of years in the investment periods.*

The purpose of Eq. (3.43) is to provide the current investment period with the average age of the generator of each type at each location based upon the newly installed capacity in the previous investment period and the remaining older capacity from the previous investment period. For the initialization investment period ($\mathbb{T} = 1$) the ages of the generators are input data.

The second exogenous parameter calculated is the blended average heat rates:

$$\mathcal{H}_{\mathcal{TLt}}^{\mathcal{G}(\mathbb{T})} = \begin{cases} \mathcal{H}_{\mathcal{TLt}}^{\mathcal{G}(\mathbb{T})} & \forall\ \mathbb{T} = 1, \mathcal{T}, \mathcal{L}, t \\ \dfrac{\mathcal{H}_{\mathcal{TLt}}^{\mathcal{G}(new)} \cdot \left(x_{\mathcal{TL}}^{(\mathbb{T}-1)} - x_{\mathcal{TL}}^{\sigma(\mathbb{T}-1)}\right) + \mathcal{H}_{\mathcal{TLt}}^{\mathcal{G}(\mathbb{T}-1)} \cdot x_{\mathcal{TL}}^{\sigma(\mathbb{T}-1)}}{x_{\mathcal{TL}}^{(\mathbb{T}-1)}} & \forall\ \mathbb{T} \geq 2, \mathcal{T}, \mathcal{L}, t \end{cases}$$

(3.44)

Equation (3.44) provides the heat rate for the current investment period from the weighted average heat rates from the previous investment period. The more granular the geographic resolution, the closer Eq. (3.44) gets to an exact representation of each power plant. For the initialization investment period ($\mathbb{T} = 1$) the heat rates for the generators are input data.

The final three exogenous parameters relate to the adjustment to the amortized capital and fixed costs for keeping old capacity running ($\mathcal{C}_{\mathcal{TL}}^{\mathcal{G}\sigma}$), costs for retiring old capacity ($\mathcal{C}_{\mathcal{TL}}^{\mathcal{G}r}$), and the retirement costs remaining

to be cleared by rate payers, governments or utilities ($\mathfrak{R}_{\mathcal{L}}$). The amortized capital and fixed costs are computed by:

$$\mathcal{C}_{\mathcal{TL}}^{\mathcal{G}\sigma(\mathbb{T})} = \begin{cases} \mathcal{C}_{\mathcal{TL}}^{\mathcal{G}(input)} - \mathcal{C}_{\mathcal{TL}}^{\mathcal{G}(\mathbb{T})} & \forall\, \mathbb{T} \leq 2, \mathbb{A}_{\mathcal{TL}}^{(\mathbb{T})} < \mathbb{R}_{\mathcal{TL}}, \mathcal{T}, \mathcal{L} \\ \dfrac{\left(\mathcal{C}_{\mathcal{TL}}^{\mathcal{G}(\mathbb{T}-1)} - \mathcal{C}_{\mathcal{TL}}^{\mathcal{G}(\mathbb{T})}\right) \cdot \left(x_{\mathcal{TL}}^{(\mathbb{T}-1)} - x_{\mathcal{TL}}^{\sigma(\mathbb{T}-1)}\right) + \mathcal{C}_{\mathcal{TL}}^{\mathcal{G}\sigma(\mathbb{T}-1)} \cdot x_{\mathcal{TL}}^{\sigma(\mathbb{T}-1)}}{x_{\mathcal{TL}}^{(\mathbb{T}-1)}} & \forall\, \mathbb{T} > 2, \mathbb{A}_{\mathcal{TL}}^{(\mathbb{T})} < \mathbb{R}_{\mathcal{TL}}, \mathcal{T}, \mathcal{L} \\ \gamma_{\mathcal{TL}}^{\mathbb{A}} \cdot \mathcal{C}_{\mathcal{TL}}^{\mathcal{G}(\mathbb{T}=1)} - \mathcal{C}_{\mathcal{TL}}^{\mathcal{G}(\mathbb{T})} & \forall\, \mathbb{T} \geq 2, \mathbb{A}_{\mathcal{TL}}^{(\mathbb{T})} \geq \mathbb{R}_{\mathcal{TL}}, \mathcal{T}, \mathcal{L} \end{cases} \tag{3.45}$$

Equation (3.45) states that if the weighted average age of the generator is older than the retirement age for that type of generator ($\mathbb{R}_{\mathcal{TL}}$), the adjustment to the amortized capital and fixed costs is a percentage ($\gamma_{\mathcal{TL}}^{\mathbb{A}}$) of the initialization costs ($\mathcal{C}_{\mathcal{TL}}^{\mathcal{G}(\mathbb{T}=1)}$). The percentage is a function of how much older the generator is than the retirement age (a user defined value, which as standard is set to those shown in Fig. 3.9). It should be noted that the adjustment must take into account the fact that the old capacity is combined with the new capacity in the variable $x_{\mathcal{TL}}$.

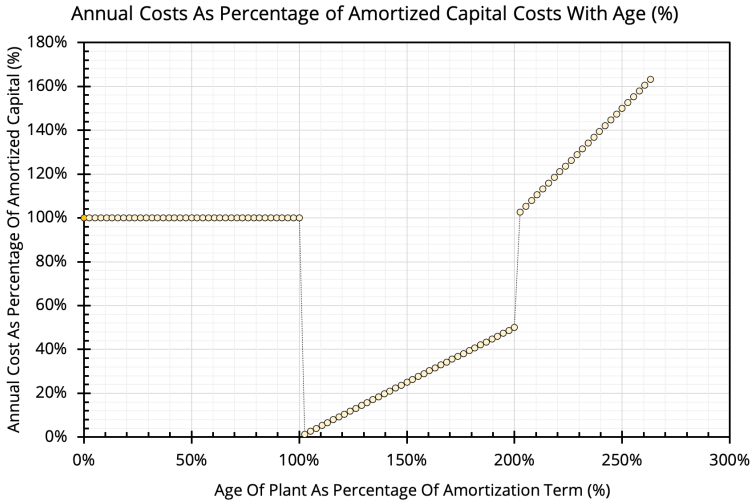

Figure 3.9: Illustration of the amortized cost for old capacity. When retirement age is reached, the cost falls to almost zero; but as it continues to age the costs increases due to repairs and maintenance requirements.

Equation (3.46) shows the calculation for the cost to retire the generators that is standard within WIS:dom®-P. There are many choices for how to compute these costs because there can be full repayment, losses for the owner, securitization, or some combination. Equation (3.46) would be altered through its multiplication parameter ($\mathbb{M}_{\mathcal{TL}}^{\mathcal{G}r}$) to accommodate the different (accelerated) retirement options or policies. These costs to retire are then passed through to Eq. (3.47), which tracks the remaining balances that must be continued to be repaid until they are cleared. The standard assumption in WIS:dom®-P is that the entity enclosing the location pays to the retirement. Again, these equations can be altered to investigate the possibility of socializing the costs or write-downs for the utilities or owners.

$$\mathcal{C}_{\mathcal{TL}}^{\mathcal{G}r(\mathbb{T})} = \begin{cases} 0 & \forall\, \mathbb{T} = 1, \mathbb{A}_{\mathcal{TL}}^{(\mathbb{T})} < \mathbb{R}_{\mathcal{TL}}, \mathcal{T}, \mathcal{L} \\ \mathbb{M}_{\mathcal{TL}}^{\mathcal{G}r} \cdot \left(\mathcal{C}_{\mathcal{TL}}^{\mathcal{G}(\mathbb{T})} + \mathcal{C}_{\mathcal{TL}}^{\mathcal{G}\sigma(\mathbb{T})}\right) \cdot \left(\mathbb{R}_{\mathcal{TL}} - \mathbb{A}_{\mathcal{TL}}^{(\mathbb{T})}\right) & \forall\, \mathbb{T} \geq 2, \mathbb{A}_{\mathcal{TL}}^{(\mathbb{T})} < \mathbb{R}_{\mathcal{TL}}, \mathcal{T}, \mathcal{L} \\ \delta_{\mathcal{TL}}^{\mathbb{A}} \cdot \mathcal{C}_{\mathcal{TL}}^{\mathcal{G}(\mathbb{T}=1)} & \forall\, \mathbb{T} \geq 2, \mathbb{A}_{\mathcal{TL}}^{(\mathbb{T})} \geq \mathbb{R}_{\mathcal{TL}}, \mathcal{T}, \mathcal{L} \end{cases}$$

(3.46)

$$\Re_{\mathcal{L}}^{(\mathbb{T})} = \begin{cases} 0 & \forall\, \mathbb{T} = 1, \mathcal{L} \\ \sum_{\mathcal{T}} \left\{ \sum_{n \geq 1}^{n \leq \mathbb{T}-1} \left[\mathcal{A}_{\mathcal{T}\mathcal{L}}^{(\mathbb{T}-n)} \cdot \mathcal{C}_{\mathcal{T}\mathcal{L}}^{\mathcal{G}r(\mathbb{T}-n)} \cdot \left(\mathbb{S}_{\mathcal{T}\mathcal{L}} - \sum_{m \leq n} \mathbb{L}^{(\mathbb{T}-m)} \right) \right] \right\} & \forall\, \mathbb{T} \geq 2, \mathcal{L} \end{cases}$$

(3.47)

The parameter $\mathcal{A}_{\mathcal{T}\mathcal{L}}^{(\mathbb{T}-n)}$ informs Eq. (3.47) of which terms to sum together and which to ignore. The parameter is defined by Eq. (3.48) below:

$$\mathcal{A}_{\mathcal{T}\mathcal{L}}^{(\mathbb{T}-n)} = \begin{cases} 0 \; if \sum_{m \leq n} \mathbb{L}^{(\mathbb{T}-m)} \geq \mathbb{S}_{\mathcal{T}\mathcal{L}} & \forall\, \mathbb{T} \geq 2, n \leq \mathbb{T}-1, \mathcal{T}, \mathcal{L} \\ 0 \; if \;\; \mathbb{A}_{\mathcal{T}\mathcal{L}}^{(\mathbb{T}-n)} \geq \mathbb{R}_{\mathcal{T}\mathcal{L}} & \forall\, \mathbb{T} \geq 2, n \leq \mathbb{T}-1, \mathcal{T}, \mathcal{L}. \\ 1 \;\; if \; \mathbb{A}_{\mathcal{T}\mathcal{L}}^{(\mathbb{T}-n)} < \mathbb{R}_{\mathcal{T}\mathcal{L}} \; and \sum_{m \leq n} \mathbb{L}^{(\mathbb{T}-m)} < \mathbb{S}_{\mathcal{T}\mathcal{L}} & \forall\, \mathbb{T} \geq 2, n \leq \mathbb{T}-1, \mathcal{T}, \mathcal{L} \end{cases}$$

(3.48)

Figure 3.10 illustrates the retirement costs as computed within WIS:dom®-P. It shows that, as standard, the total cost has to be repaid until the end of the amortization period and after that 7.5% must be paid for another 50% of the number of years, until finally the cost is zero to retire. All these values are adjustable by the user.

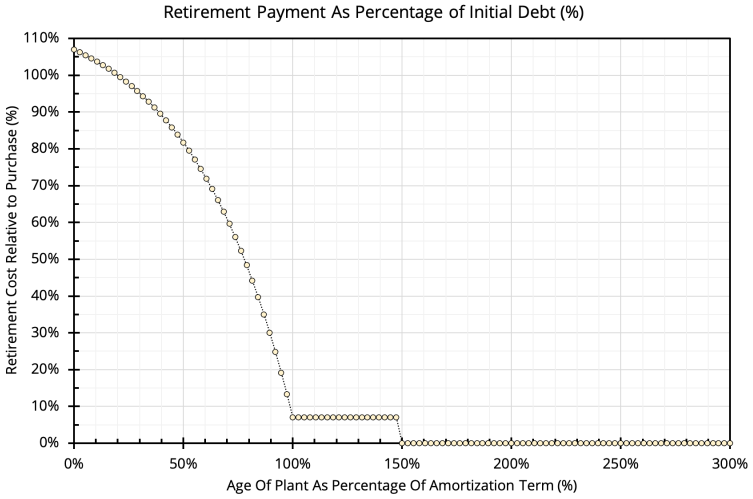

Figure 3.10: Illustration of the retirement payment required as a function of amortized lifetime. When retirement age is reached, the cost falls to 7.5%; but once it reaches 1.5x of its amortized lifetime the cost drops to zero.

Figure 3.11 displays how WIS:dom®-P also adjusts the heat rates (thermal) and efficiencies (non-thermal) of the power plants as they age and degrade. As with the other variables, this is performed using the weighted average age and the life time.

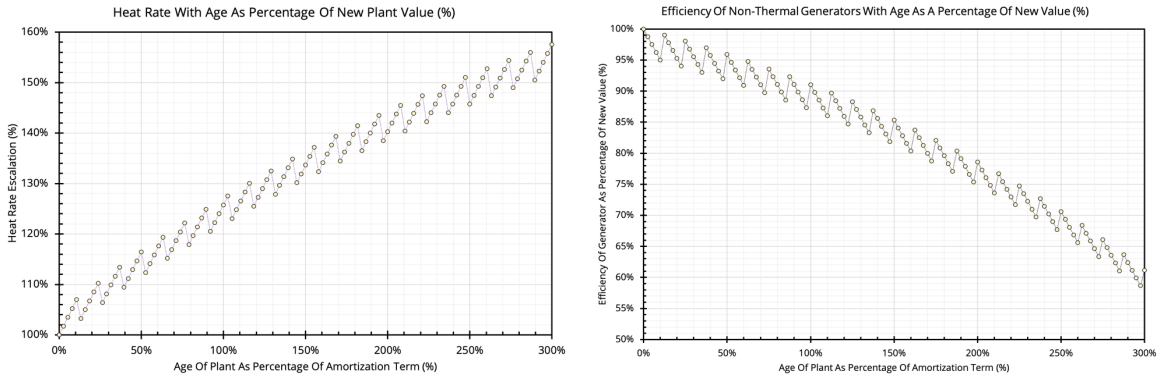

Figure 3.11: Illustration of the adjustments to the heat rates (left) and efficiencies (right) of the generators with age. There is a oscillatory behavior because it is assumed in WIS:dom®-P that there are retrofits periodically as part of the operating and maintenance costs.

It is clear from Eqs (3.42) – (3.48) that the weighted average computations result in information loss about specific power plants and exact ages. This is a construct of the method used to incorporate some age-related details while solving in a tractable amount of time over large geographic areas (at high spatial and temporal granularity). A version of WIS:dom®-P exists where the retirements are handled very differently and preserve more information about generator ages and characteristics; but over multiple states, as in the present study, the solve times are approximately an order of magnitude longer. From testing, the information lost results in minimal differences over most geographic footprints (of the order of 0.5% in terms of costs and similar for emissions). Of course, any inaccuracy is unwanted, but the authors feel that the tradeoff was advantageous to model retirements as described above.

4. VCE® Datasets & WIS:dom®-P Inputs

4.1 Generator Input Dataset

VCE® processed the Energy Information Administration annual data from 2018 to create the baseline input generator dataset for the United States. From this dataset, information for the Southeast states (Alabama, Georgia, Florida, Mississippi, North Carolina, South Carolina and Tennessee) was obtained. The Southeast has a large geographic extent and contains approximately 239,000 MW of generation capacity. WIS:dom® has the ability to solve over such scales at 5-minute resolution for several years chronologically.

The generator input datasets are based off of the publicly available EIA 860 and EIA 923 data. The 2018 data is what was available for this study. We go through several steps to align and aggregate technology types to the 3 km grid space to match with the NOAA HRRR weather data. In the process, we also analyze year-on-year changes. Across the US, general trends show coal capacities falling with natural gas combined cycle growing. Wind, solar and storage plants are on the rise as well. This continues even into the released December EIA 860M 2019 Monthly data.

The following outlines the process VCE® undergoes to prepare the generator input datasets:

1. Data is merged between the EIA 860 and EIA 923 data.
2. Initial quality control is applied to the data.
3. Align the location of the generators to the nearest 3 km HRRR cell. This can be more difficult for generators on state boundaries as well as land/water boundaries. As such, extra time is given to ensure that the mapped generators are correct.
4. Aggregation of the generator types in each 3 km grid cell. As an example, if two separate coal plants are in the same grid cell, the capacity is summed for coal in that grid cell.
5. Further spatial checks are performed to make sure the output aligns with the original data.
6. Final model input format produced. A county level average of all generator types is also created.

VCE® also works with the Catalyst Cooperative (https://catalyst.coop/), a company with the goal to help the energy research community by processing major publicly available sources into a format that is organized and stream-lined to use. This is helping our processes become quicker and eventually more frequent on this input dataset.

1	Coal
2	Natural Gas Combined Cycle
3	Natural Gas Combustion Turbine
4	Storage
5	Nuclear
6	Hydroelectric
7	Onshore Wind
8	Offshore Wind
9	Residential Solar
10	Utility-scale Solar
11	Concentrated Solar Power
12	Geothermal
13	Biomass
14	Other Natural Gas
15	Other Generation
16	Natural Gas - CCS
17	Pumped Hydro Storage
18	Small Modular Reactors
19	Molten Salts

Figure 4.1: The VCE® generator technology bins.

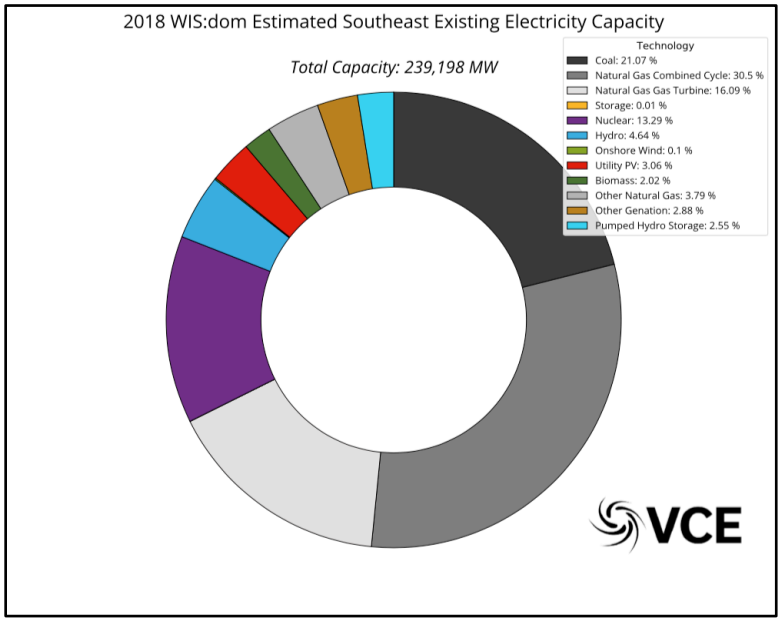

Figure 4.2: WIS:dom® estimated capacity for the Southeast States: Alabama, Georgia, Florida, Mississippi, North Carolina, South Carolina, Tennessee. The capacity is 239,198 MW.

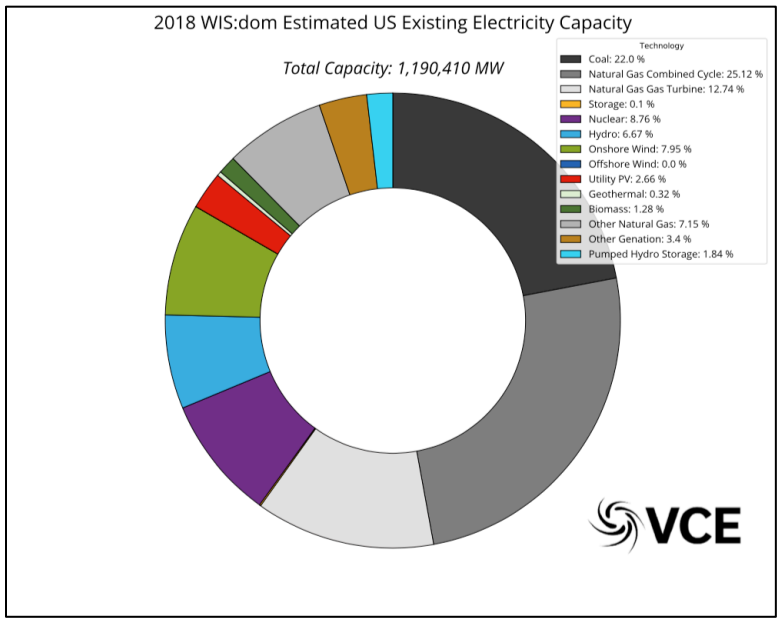

Figure 4.3: WIS:dom® estimated capacity share for the contiguous United States. The total capacity modeled is 1,190,410 MW.

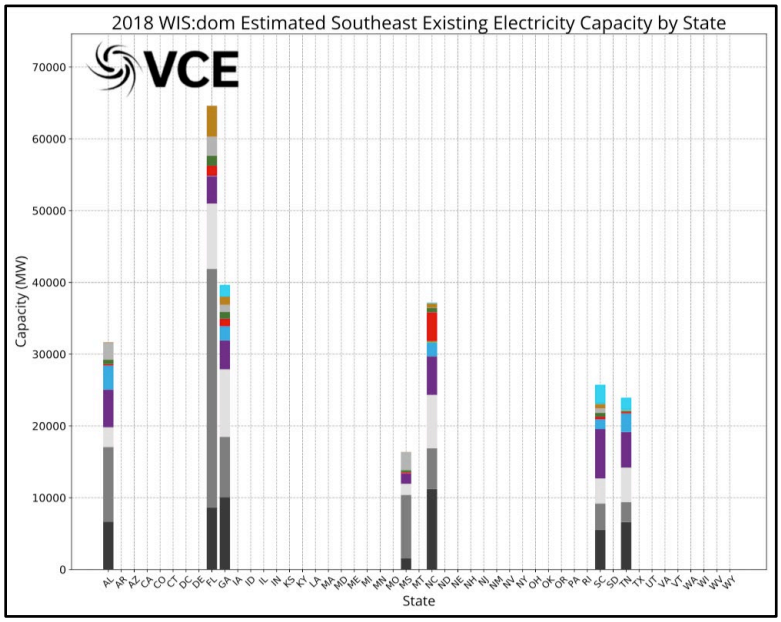

Figure 4.4: WIS:dom® Capacity for the states in the Southeast US.

Figure 4.5 shows the locations of installed generators across the US Southeast states modeled for this study. North Carolina has a large amount of smaller scale solar projects. Large nuclear, coal and natural gas plants make up the vast majority of the generator technologies in the Southeast. Hydroelectric plants can be seen along many of the rivers, most of it showing up in Alabama and Tennessee. Florida, by far, has the most installed capacity of all the Southeast states. It is predominantly natural gas units; though many other technologies can still also be observed in Florida as well. Nuclear capacities are evenly installed across all Southeast states. Apart from Mississippi, coal generator capacity is also evenly represented across the Southeast states.

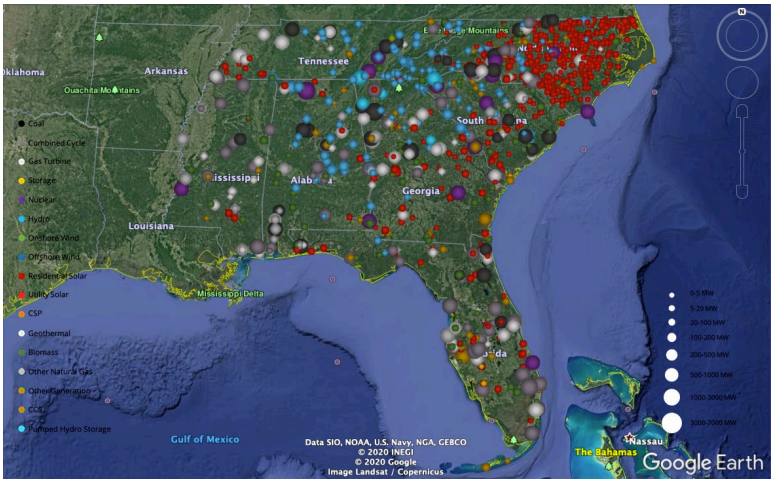

Figure 4.5: WIS:dom® estimated location of various technologies for the Southeast state.

4.2 Renewable Siting Potential Dataset

VCE® performs an extensive screening procedure to determine the siting potential of new generators across the contiguous US. This ensures that the WIS:dom® model has constraints on where it can build new generation. First, USGS land cover information is utilized as a base within each 3 km grid cell to determine what is there (Figure 4.6 top left panel).

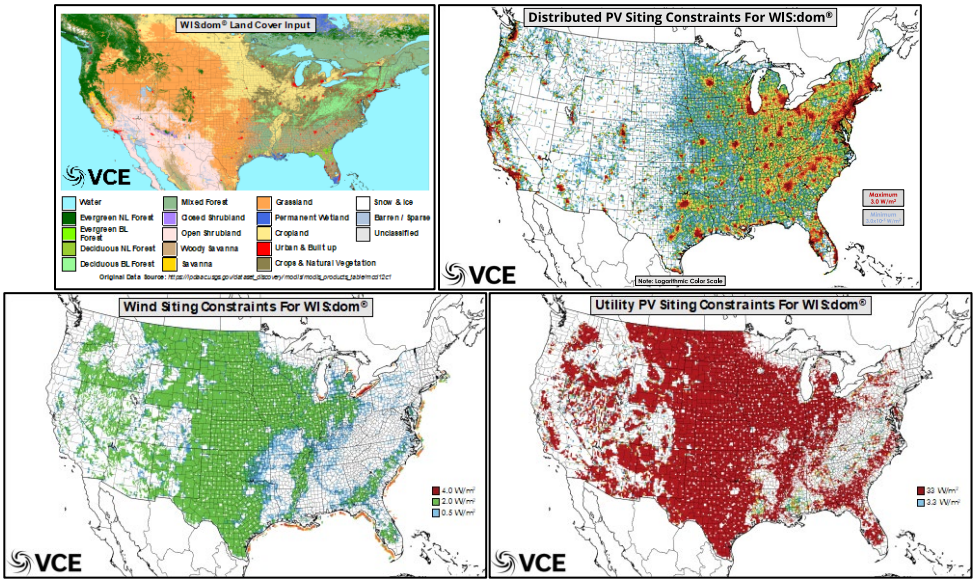

Figure 4.6: WIS:dom® land cover (top left), distributed solar PV siting bounds (top right), utility-scale wind bounds (bottom right) and utility-scale solar PV (bottom right).

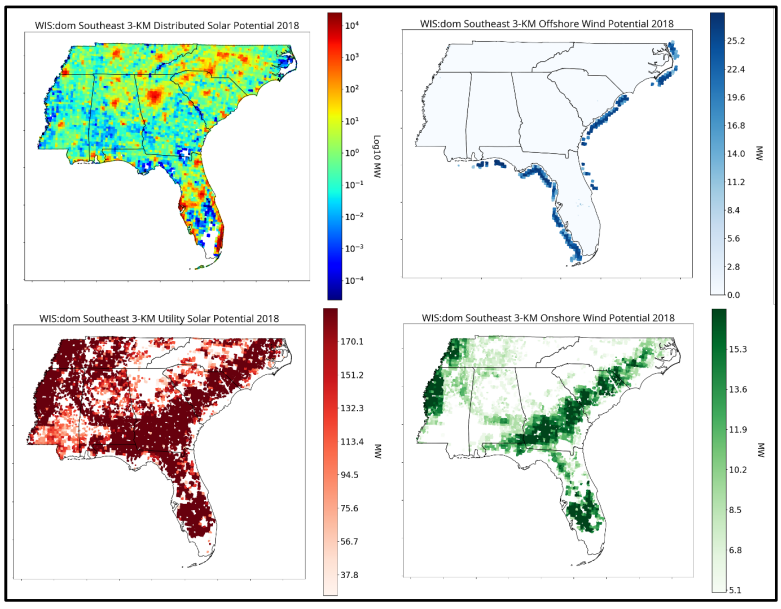

Figure 4.7: WIS:dom® Rooftop Potential (top left), Offshore Wind Potential (top right), Utility-scale Solar Potential (bottom right) and Onshore Wind Potential (bottom right) in MW. The Distributed Solar Potential is converted to a Logarithmic Base 10 scale due to the ranges of value for that parameter. This is a closer look at the Southeast states.

The first screening algorithm follows these steps:

1. Remove all sites that are not on appropriate land-use categories.
2. Remove all sites that have protected species.
3. Remove all protected lands; such as national parks, forests, etc.
4. Compute the slope, direction and soil type to determine its applicability to VRE installations.
5. Determine the land cost multipliers based on ownership type.
6. Remove military and other government regions that are prohibited.
7. Avoid radar zones and shipping lanes.
8. Avoid migration pathways of birds and other species.

The above, along with the knowledge of what is already built within a HRRR cell from the Generator Input data provides WIS:dom® with a view of where it can technically build certain generators as well as certain technologies. Figure 4.6 shows the siting constraints for wind, utility-scale solar PV and distributed solar PV.

For wind, utility-scale solar PV, distributed solar PV, and electric storage the available space use converted into capacity (MW & MWh) by assuming a density of the technologies. This is particularly important for wind and solar PV because of wake effects and shading effects, respectively. The maximum density of wind turbines within a model grid cell was restricted to no more than one per km^2 (< 4 MW / km^2). Solar PV was restricted to a maximum installed capacity of 33 MW per km^2. For storage, it is assumed for a 4-hour battery the density is 250 MW / km^2. For all thermal generation, the density assumed for new build is 500 MW / km^2. Thus, for a 3-km grid cell the resulting maximum capacities (in the CONUS) are:

- Wind – 36 MW;
- Utility Solar PV – 297 MW;
- Distributed solar PV – 68 MW;
- Storage (4-hr) – 2,250 MW or 9,000 MWh;
- Thermal generators – 4,500 MW.

These densities and values also ensure that WIS:dom® does not over build in a single grid cell because the combined space is constrained, as these numbers are maximums assuming only that technology exists.

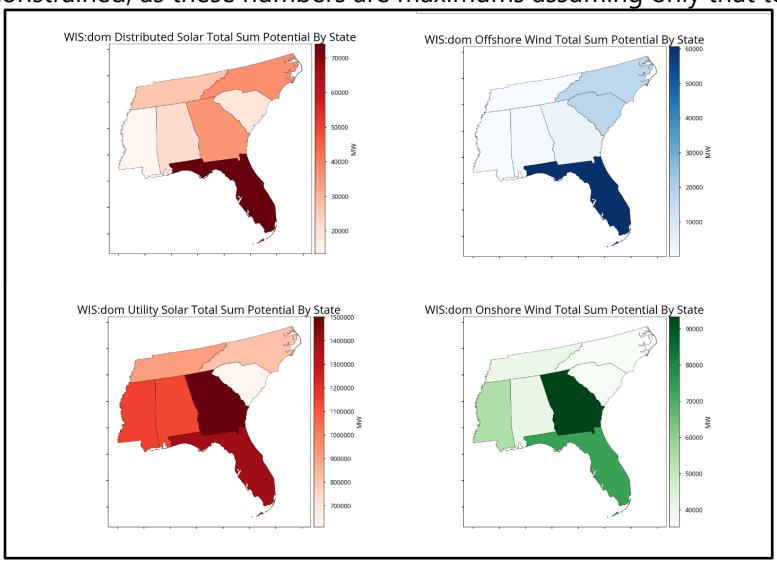

Figure 4.8: WIS:dom® Total Sum Potential by state for Rooftop (top left), Offshore Wind (top right), Utility-scale Solar (bottom right)

and Onshore Wind (bottom right) in MW.

The above figure shows that Florida has the largest potential for rooftop solar and offshore wind development when summing all the capability across the state. For utility scale solar and onshore wind, Georgia has the highest potential.

4.3 Standard Inputs

There is a standard suite of input data for the WIS:dom®-P model that sets the stage for several base assumptions about the energy grid and generator technologies. This includes:

- Generator cost data (capital, fixed, variable, fuel);
- Generator lifetime terms;
- Standard generator heat rates;
- Transmission/Substation costs;
- Legislature in the energy sector:
    - Renewable portfolio standards;
    - Clean energy mandates;
    - GHG emissions requirements;
    - Storage and offshore mandates);
    - PTC/ITC;
- Jobs for various technologies.

This is a list of the most commonly discussed standard inputs the model uses and are looked at in this document. The above list is not exclusive and much more information is ingested by WIS:dom®-P to narrow down characteristics of various generation technologies. The list of standard files is constantly growing as the industry evolves. Additional inputs can be easily incorporated into WIS:dom®-P.

The standard inputs remain constant throughout the scenarios modeled for the study unless specifically requested to change. However, the standard inputs are changing within each scenario throughout each investment period modeled. The overnight capital, fixed O&M and variable O&M costs for each generator technology are predominantly based upon the NREL ATB values. It is noted where this is not the case. The NREL values were chosen to be reputable values; are used by RTOs in their modeling; give high granularity and are updated frequently. The fuel costs come from the EIA Annual Energy Outlook data, another source that is reputable and regularly updated. VCE® provides fuel and capital costs multipliers by state to further tune the areal layout of these standard cost inputs. Other standard inputs are a combination of VCE® internal research and work with various partners in the industry.

These input assumptions are ingested into WIS:dom®-P to provide insight and bounds to the optimization selections for each investment period. It offers the model a picture of what cost options are available to optimize.

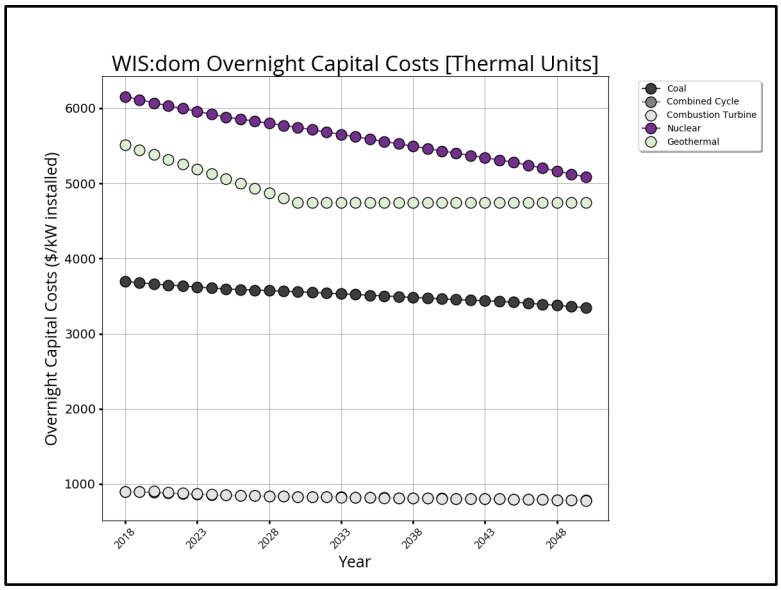

Figure 4.9: The overnight capital costs in real $/kW-installed for thermal power plants in WIS:dom® -P.

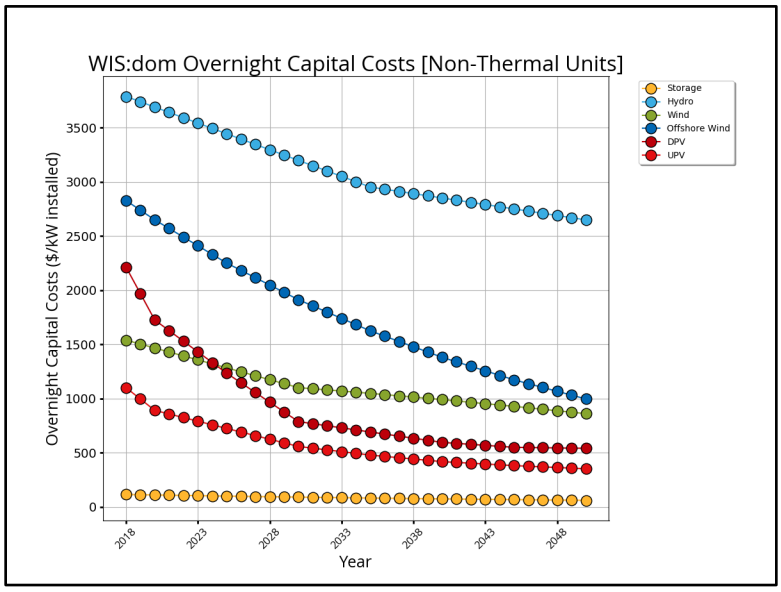

Figure 4.10: The overnight capital costs in real $/kW-installed for non-thermal power plants in WIS:dom® -P. All costs are from NREL ATB 2019, with the exception of storage costs, which were provided by Able Grid, Inc.

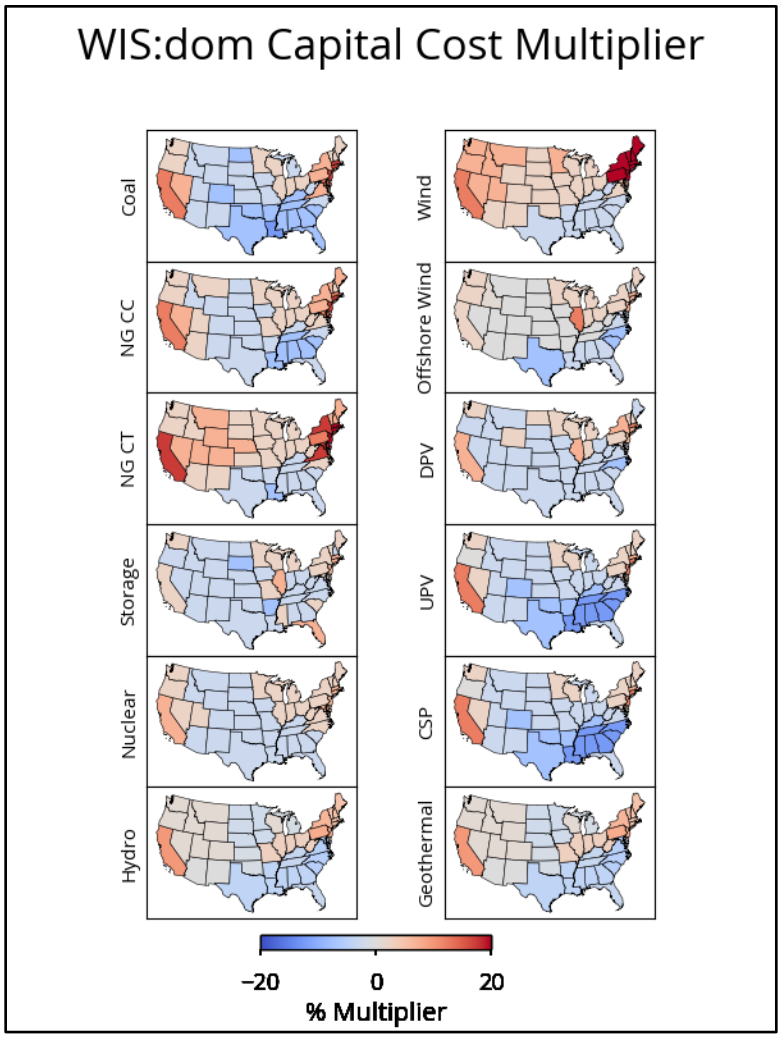

Figure 4.11: The WIS:dom® -P Capital Cost Multiplier is shown by state for each technology across the US. Shades of red show where the capital cost is scaled higher by a given percentage. Cool shades show where technology capital costs in the model are scaled down by a given percentage.

The previous figure shows that certain states and regions actually experience lower capital costs when building many technologies from the NREL ATB values. It is shown that Texas and, in general, the Southeast United States, have lower capital costs for all generator technologies. Storage capital cost is the one exception in the Southeast that is more expensive, though not for all southeast states. Certain technologies like Wind and Natural Gas Combustion Turbine technologies are more expensive in the Intermountain West. Wind is especially expensive in the northeast. In general, California and the New England states consistently show higher capital costs multipliers for all generator technologies.

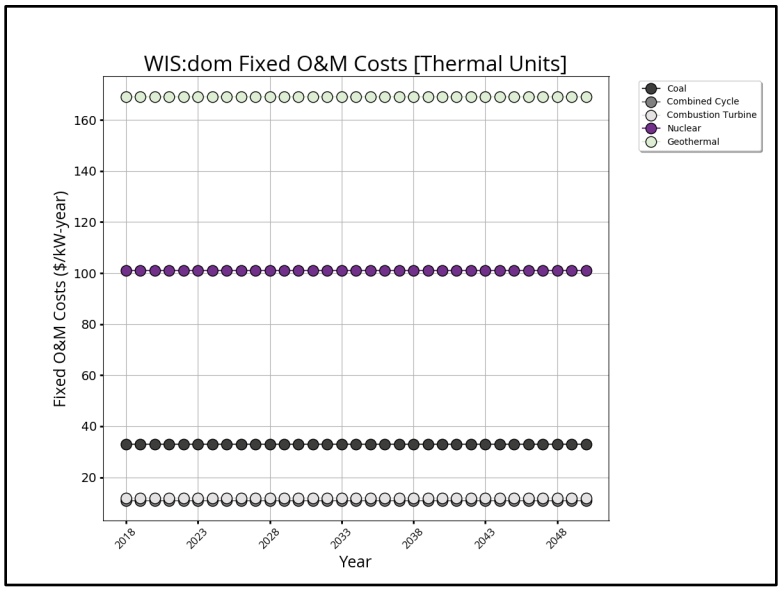

Figure 4.12: The fixed operations and maintenance (O&M) costs in real $/kW-yr for thermal power plants in WIS:dom® -P.

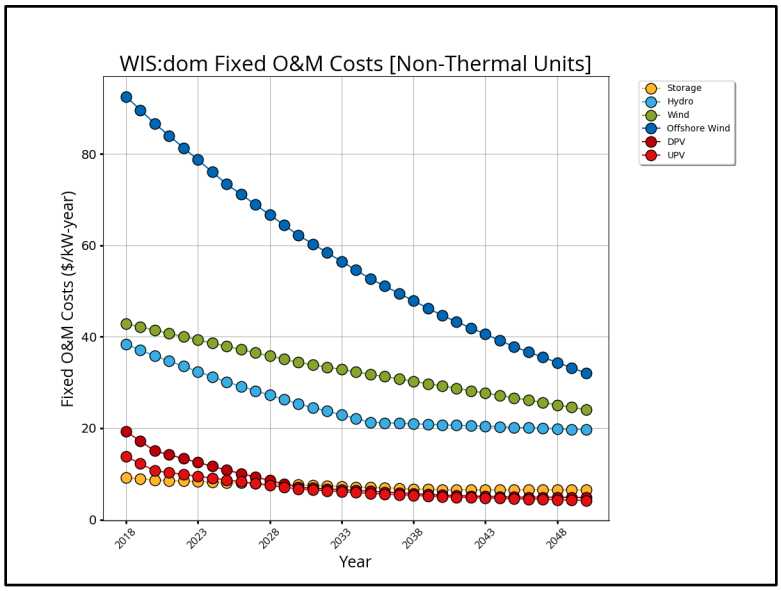

Figure 4.13: The fixed operations and maintenance (O&M) costs in real $/kW-yr for non-thermal power plants in WIS:dom® -P.

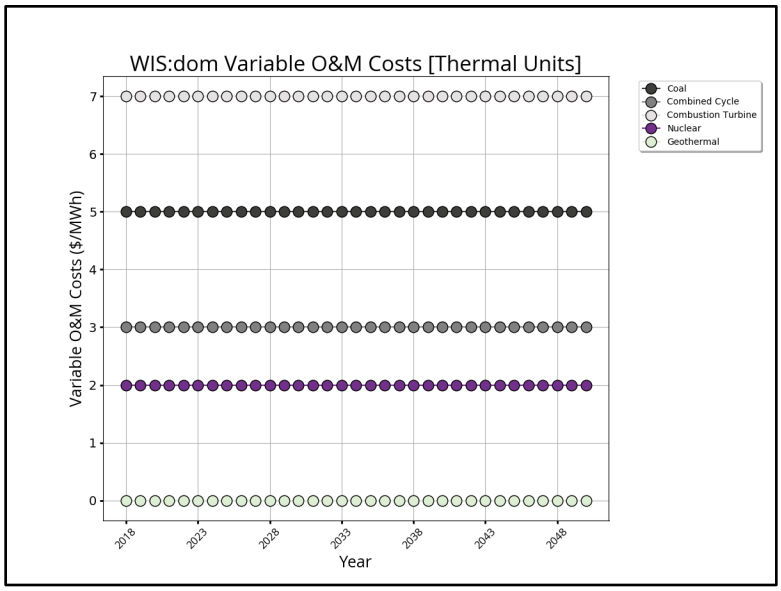

Figure 4.14: The non-fuel variable O&M costs for thermal generators in WIS:dom® -P in real $/MWh. The non-thermal units have zero variable O&M costs as those costs are combined into the fixed O&M costs.

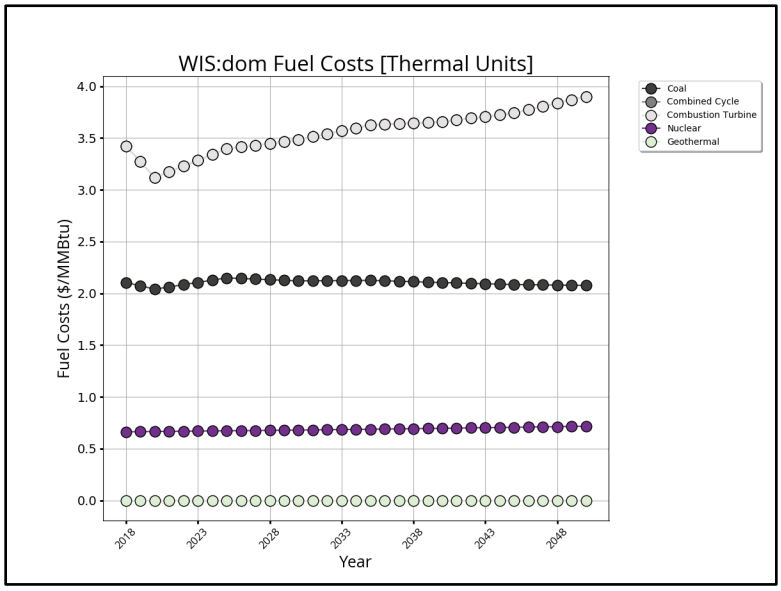

Figure 4.15: The fuel costs for thermal generators in WIS:dom® -P in real $/MMBtu.

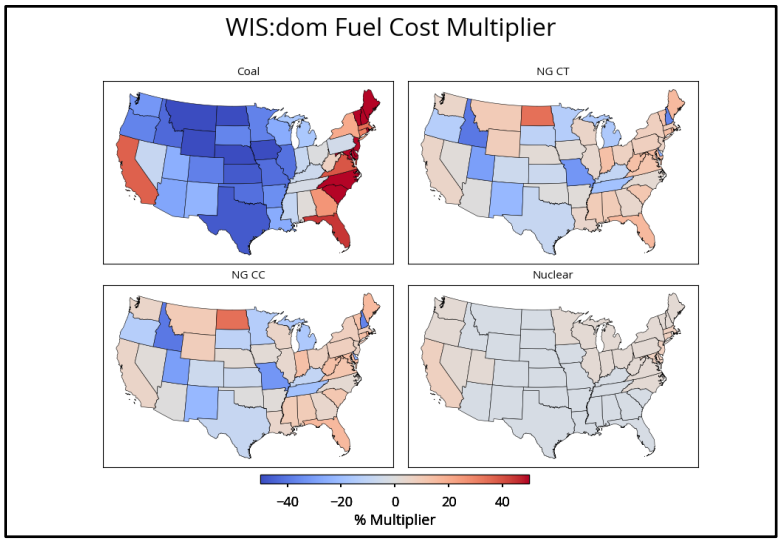

Figure 4.16: The WIS:dom® -P Fuel Cost Multiplier is shown by state for each technology across the US. The color scale shows a percentage multiplier applied to standard fuel costs. Shades of red show where the fuel cost is scaled higher by a given percentage. Cool shades show where technology fuel costs in the model are scaled down a given percentage. Renewable fuels are not shown here as those fuel costs are the same no matter where the technology is and those fuel costs are null.

The previous figure shows the spatial variations of fuel costs for thermal units (except geothermal since that cost is zero). California and the New England states show higher fuel costs for most of the technologies. New Hampshire is an exception for natural gas. Fuel costs for coal are much lower in the middle portion of the country. Natural Gas fuel costs are notably lower in Idaho, Utah, New Mexico, Missouri and New Hampshire. There is no fuel cost multiplier applied to renewable fuels (wind, solar, hydro) as those are the same everywhere across the US and they are fuels that have no cost.

Storage is one of the most discussed inputs. Storage can have highly variable cost input values depending on sources. It also is a heavy driver as to how the model handles renewables, transmission and future baseload. The following figure shows the difference between the 2019 NREL Low ATB costs for storage versus sources from Able Grid, Inc. VCE uses the latter in the modeling for storage.

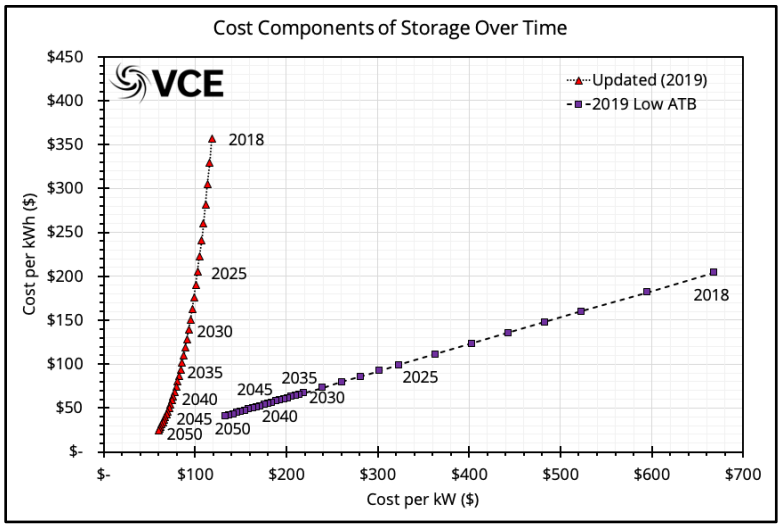

Figure 4.17: The Balance of System Capital Cost ($/kw) versus the Battery Pack Capital Cost ($/kWh). This is shown for the 2019 Low NREL ATB values in purple. The same information from Able Grid, Inc is show in red. The latter is used in the WIS:dom® -P model.

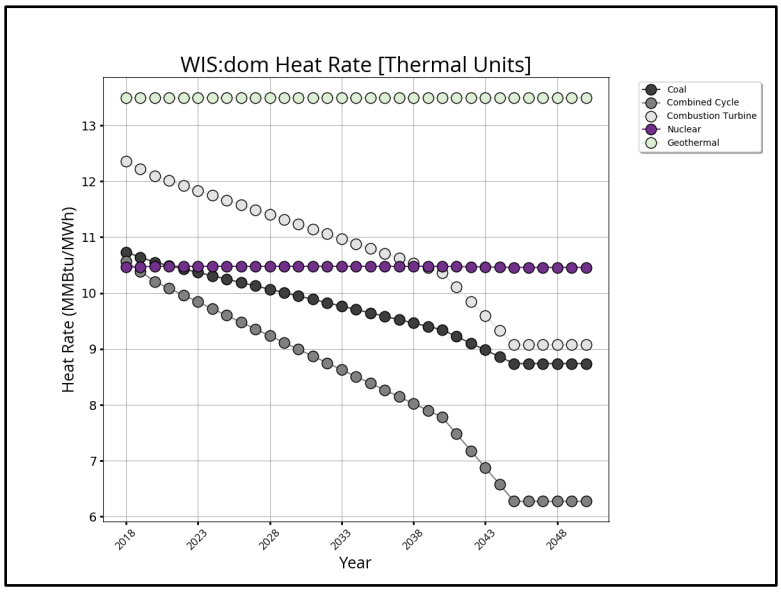

Figure 4.18: The generic heat rate for thermal generators in WIS:dom® -P in MMBtu/MWh of electricity generated. Explicit heat rates for currently installed generators come into the model through the Input Generator Datasets and the EIA 860/923 data.

We use the same discount rate for all generator technologies in the WIS:dom® -P model. This value is 0.0587 (%) which rolls into the cost equations within the model. The lifetime of the various technologies also impacts what/when the model optimally deploys generation as well as when it can retire units. The following figures shows the standard economic lifetimes for the various technologies used within WIS:dom® -P.

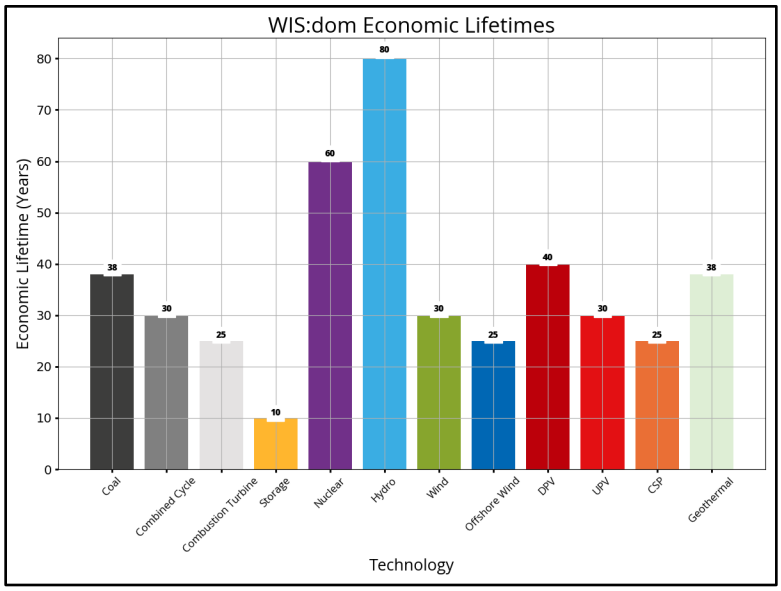

Figure 4.19: The economic lifetime for each generator type within WIS:dom® -P in years. The economic lifetime means the time that the debt must be cleared from the units.

Transmission plays a large part in the optimized decisions that the WIS:dom® -P model executes. The decision to build renewable technologies can be affected by the standard inputs around transmission aspects.

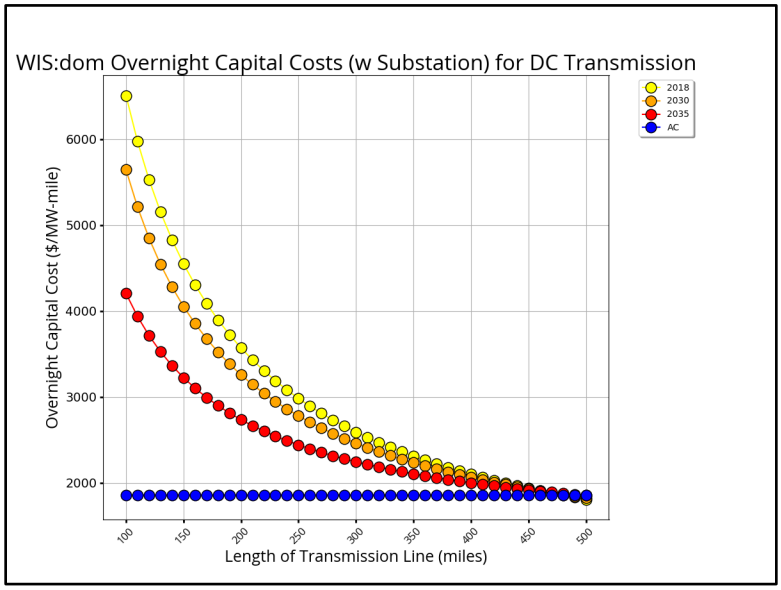

Figure 4.20: Shows the overnight capital cost of DC transmission in WIS:dom® -P in real $/MW-mile installed over various distances. Costs are shown for 2018, 2030 and 2050. The overnight capital cost of AC transmission (including substations) is also shown in blue. This is the same cost no matter the investment period.

The economic lifetime, or rather, length of amortization, of the transmission assets in the model are 60 years for all investment periods.

VCE® documents and researches the various state legislature and renewable energy goals by tracking Renewable Portfolio Standards, Clean Energy Mandates, Offshore Wind Mandates, Storage Mandates and GHG Emission Reduction Mandates. These are utilized to inform the WIS:dom®-P model of what is expected and what goals are set. This provides the bounds and definitions of what the model is required to build as it optimizes systems of the future. Over 30 states have a renewable portfolio standard in place. Just over 10 states currently have a clean energy mandate. The northeast has become increasingly aggressive in setting offshore wind energy targets. Storage mandates have started to show up in the recent years as well. The following figures lay out the legislative goals by 2050. The Production Tax Credit and the Investment Tax Credit for renewables is also discussed. This directly ties into the cost of renewables built in WIS:dom®-P.

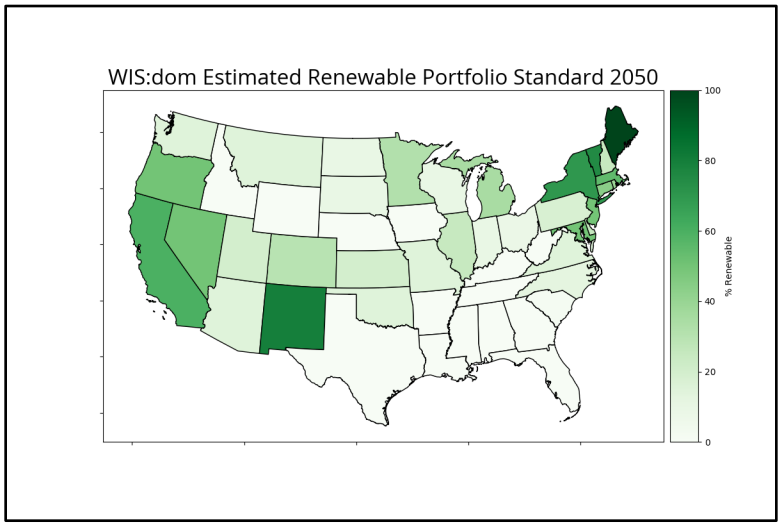

Figure 4.21: The Renewable Portfolio Standards percentage requirement of each state across the US.

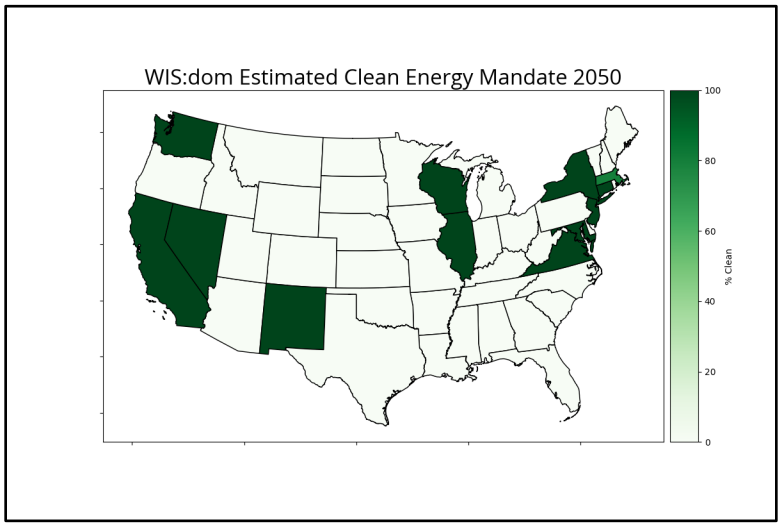

Figure 4.22: The Clean Energy Mandate percentage requirements of each state across the US.

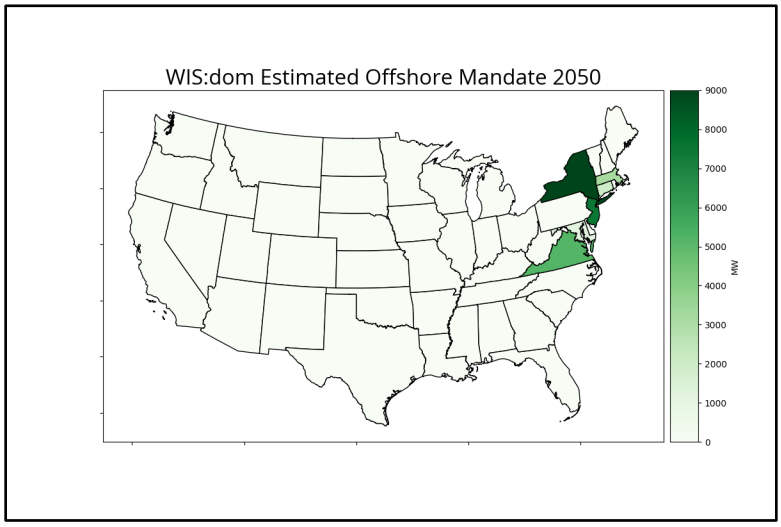

Figure 4.23: The Offshore Wind requirement in MW for each state across the US.

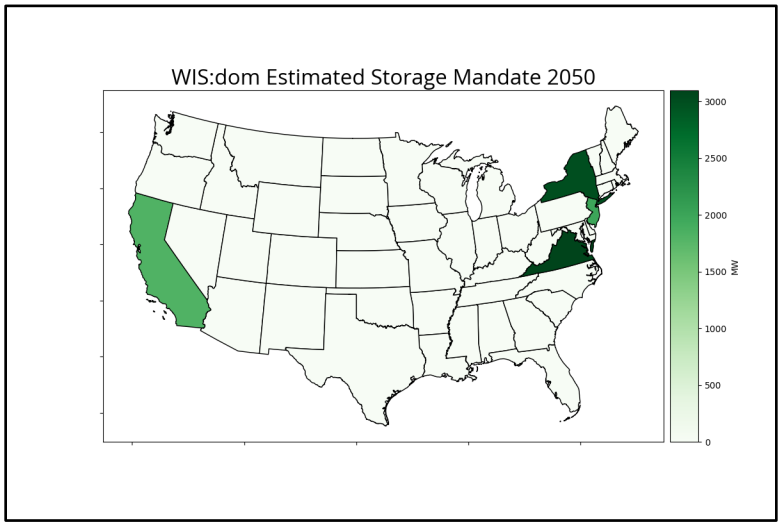

Figure 4.24: The Storage Mandates requirement in MW for each state across the US.

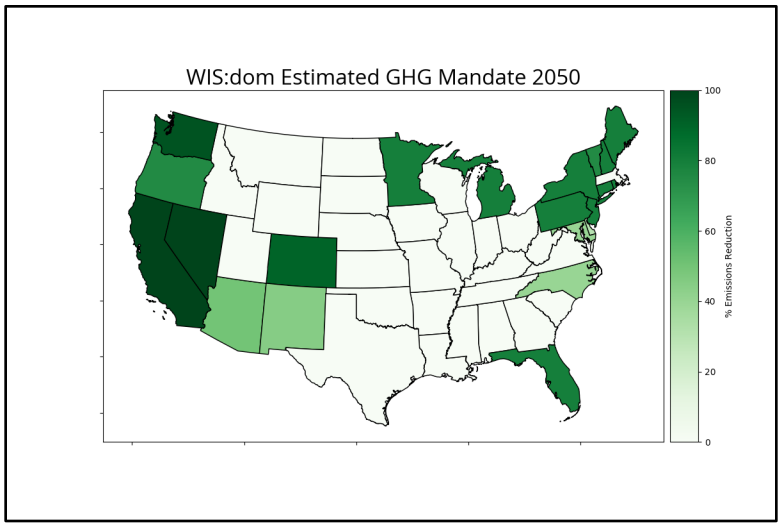

Figure 4.25: The GHG Emissions Reduction percentage requirement of each state across the US.

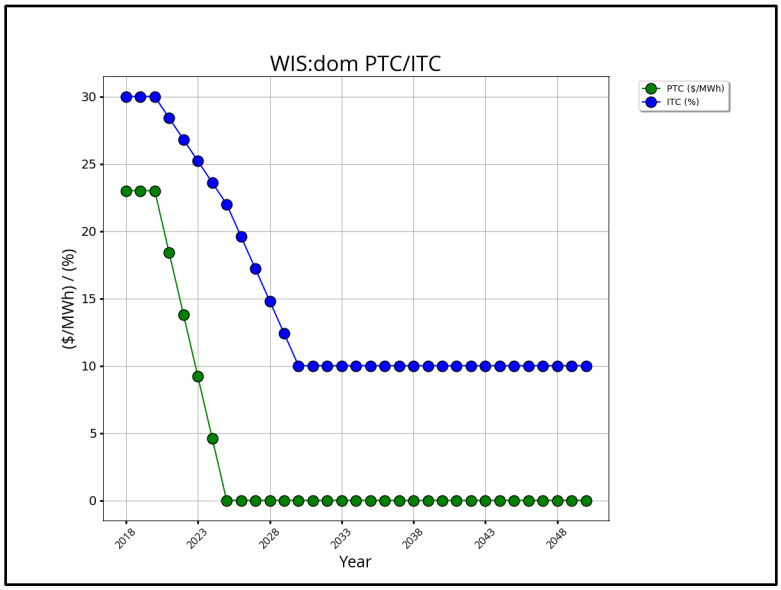

Figure 4.26: The Production Tax Credit subsidiary and the Investment Tax Credit. Note that for 2030 and beyond, the 10% ITC remaining is for utility scale projects only.

VCE® also performs work and analysis to represent job numbers that arise from various technologies and transmission across the US. These inputs set the stage for how many jobs become available depending on what is deployed during the various investment periods. This is an important metric for decision makers to know and understand as the energy industry evolves. VCE® uses a combination of sources to derive these numbers including IMPLAN, JEDI and US Energy Job reports.

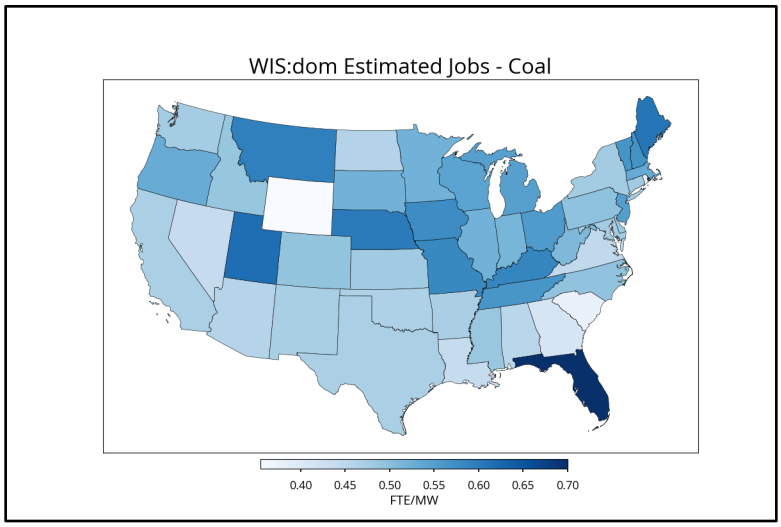

Figure 4.27: Employment per MW available from Coal.

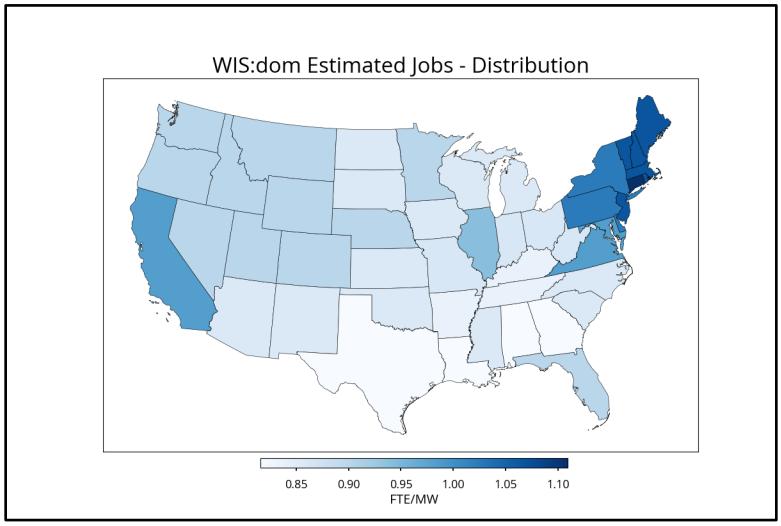

Figure 4.28: Employment per MW available from Distribution.

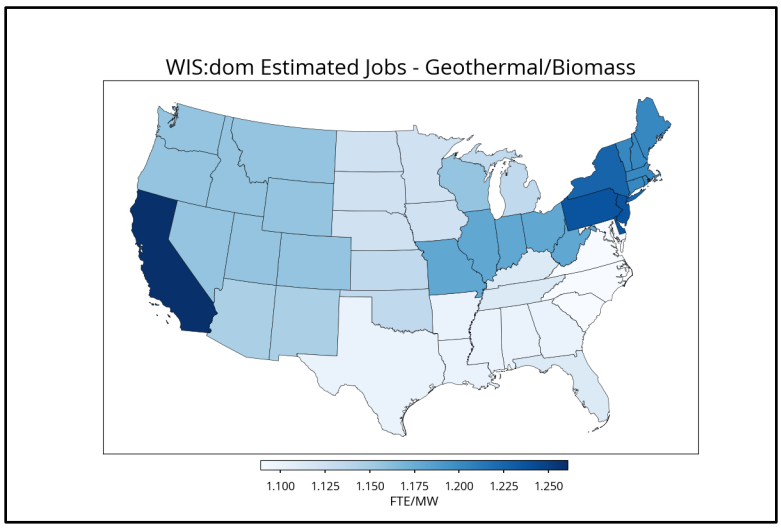

Figure 4.29: Employment per MW available from Geothermal and Biomass.

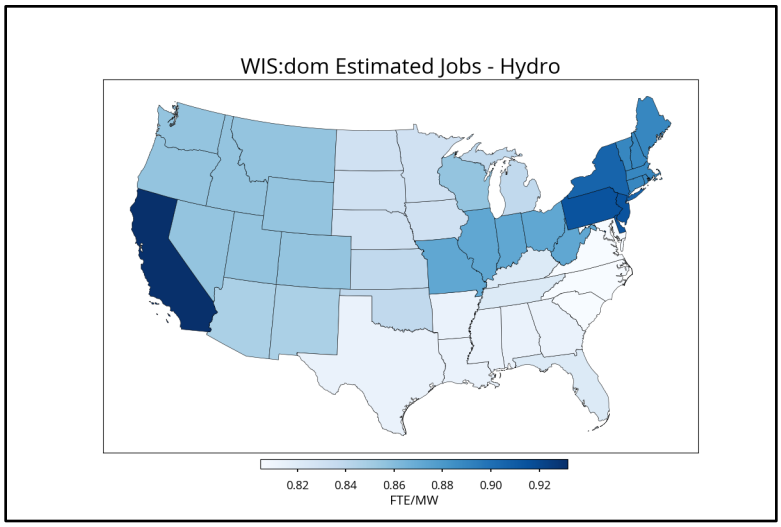

Figure 4.30: Employment per MW available from Hydro.

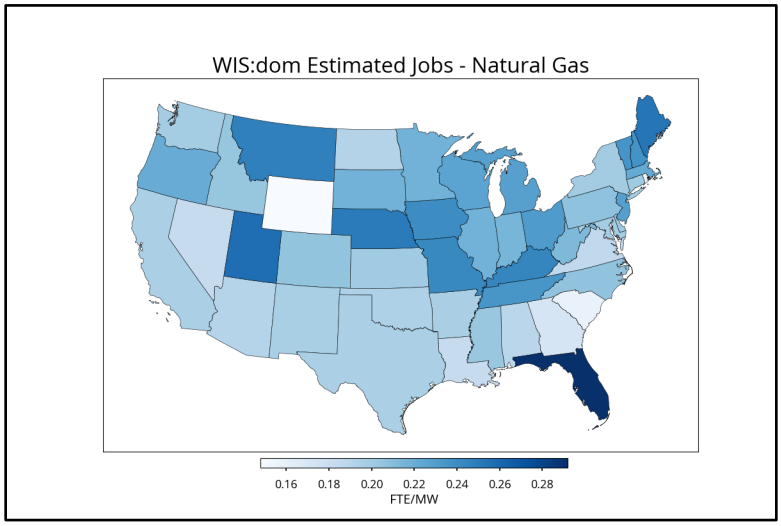

Figure 4.31: Employment per MW available from Natural Gas.

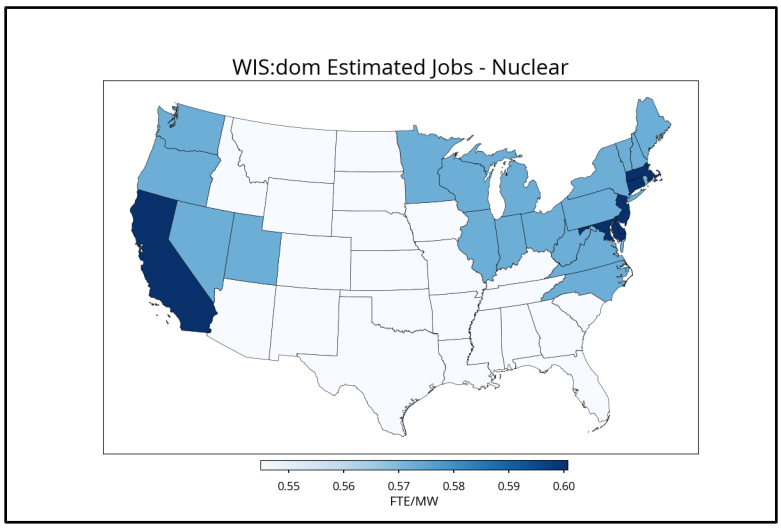

Figure 4.32: Employment per MW available from Nuclear.

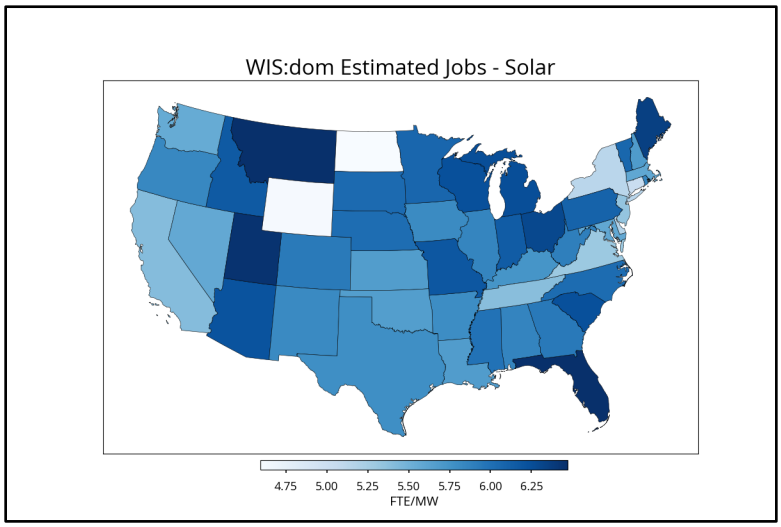

Figure 4.33: Employment per MW available from Solar.

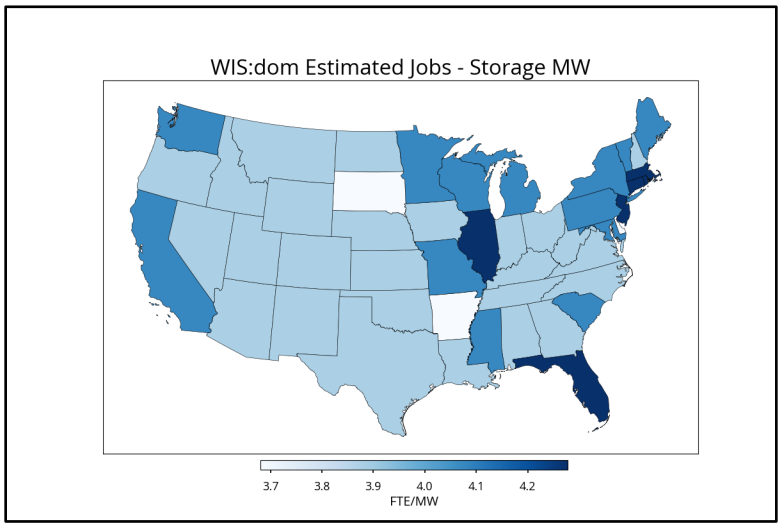

Figure 4.34: Employment per MW available from Storage MW.

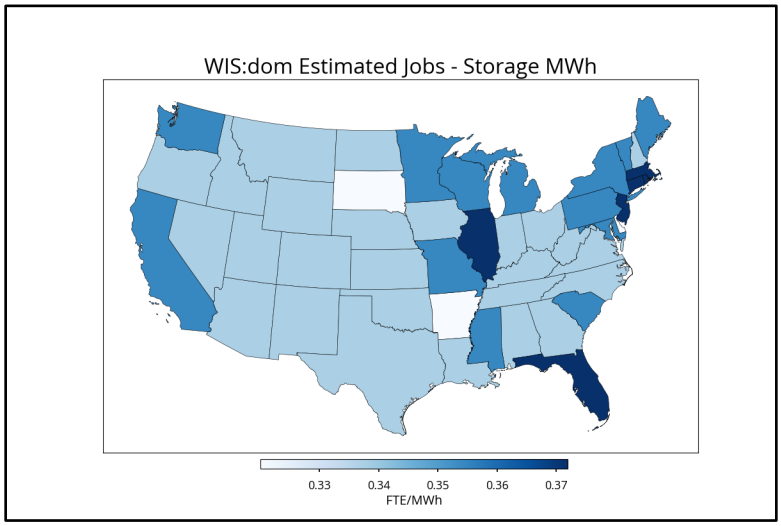

Figure 4.35: Employment per MWh available from Storage.

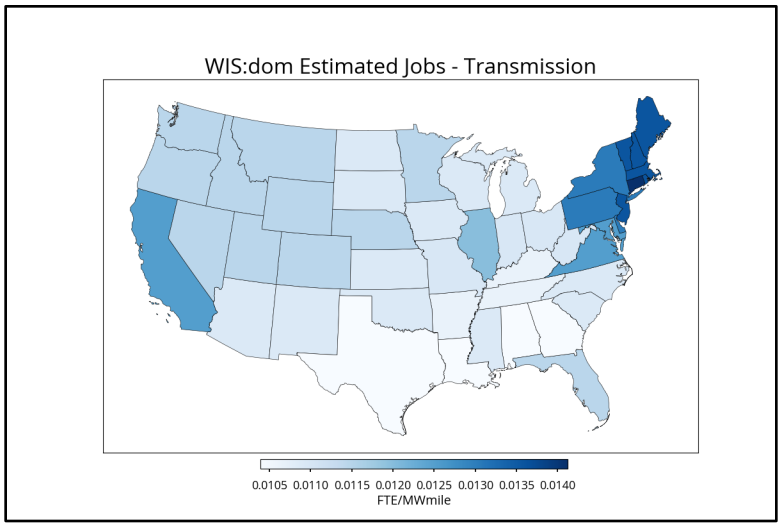

Figure 4.36: Employment per MW available from Transmission.

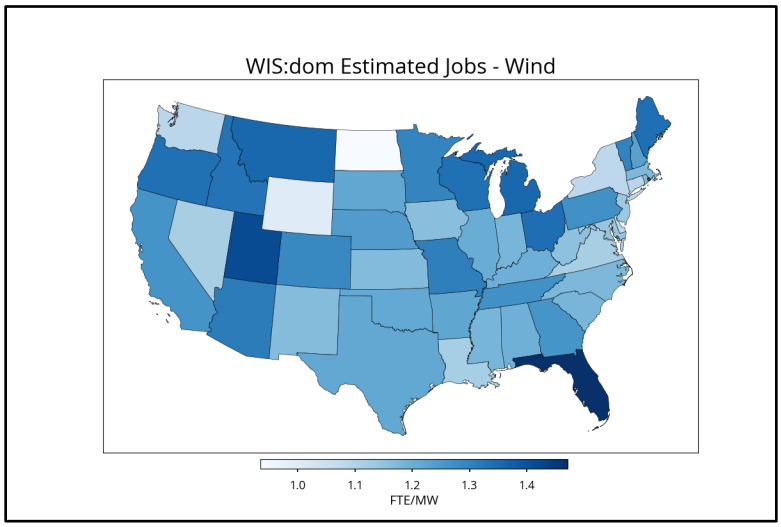

Figure 4.37: Employment per MW available from Wind.

4.4 Renewable Generation Dataset

Weather is an integral component to modeling generation from variable renewable energy sources (such as wind and solar), the efficiency of conventional generators, the transmission ampacity and electric losses, and the electric demand profiles (specifically traditional demands, electric space heating, electric water heating and electric vehicle charging).

The raw weather data is obtained from the National Oceanic and Atmospheric Administration (NOAA) High Resolution Rapid Refresh (HRRR) weather forecast model, which is a specially configured version of Advanced Research WRF (ARW) model. The HRRR is run every hour over a 3-km horizontal resolution that covers the continental United States as well as portions of Canada and Mexico. Since its inception, HRRR has undergone rapid and continuous improvement to its physical parameterization schemes, many of which have specifically targeted improved forecasts for the renewable energy sector. Through collaborative research efforts between the Department of Energy (DOE) and NOAA, projects such as the Solar Forecast Improvement Project [1], the Wind Forecast Improvement Projects I and II [2], [3] were conducted to improve forecasts of meteorological quantities important for wind and solar energy.

4.4.1 Wind power dataset method

The amount of wind power captured by a wind turbine is proportional to the cube of the wind speed directed into the wind turbine, parallel to the rotor. As wind turbines have grown taller and the rotor swept area has increased, different portions of the wind turbine rotor are exposed to (significantly) different conditions of wind speed, temperature, air density and precipitation. Therefore, it is critical to capture these impacts of varying meteorological conditions with height on wind power production in modeling. VCE® incorporates these profiles of meteorological conditions using the rotor equivalent formulations [4], [5]. The VCE® wind power model is described in the present section.

The VCE® wind power dataset is created using the HRRR weather forecast outputs. VCE® stores the HRRR outputs for forecast hours 0 (also known as initialization), 2, 6, and 12. The forecast hour 2 output has been found to be the most accurate, and thus is used for the wind power calculations[9]. The following variables are used to create the VCE® wind power dataset:

- *Horizontal components of wind (u, v)*
- *Pressure (P)*
- *Temperature (T)*
- *Specific humidity (spH)*
- *Geopotential height (GPT)*
- *Cloud-water mixing ratio (cwr)*
- *Rain-water mixing ratio (rwr)*
- *Wind gust at lowest level (WG)*

The HRRR variables are output on three different vertical coordinates: Pressure coordinates, Terrain following sigma coordinates, a Hybrid vertical coordinates. The hybrid vertical coordinate mitigates the small-scale noise found near steep terrain, while having better vertical resolution than the pressure coordinates. Figure 4.38 shows an example horizontal transect through complex terrain. It can be seen that the vertical velocity fields are much more realistic in magnitude and less noisy in the hybrid coordinate.

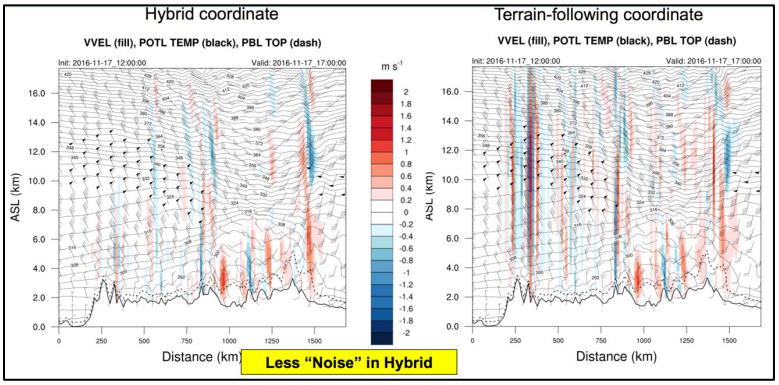

Figure 4.38: Reduction in noise in the hybrid coordinate (left) compared to the terrain following coordinate (right).

The HRRR model outputs do not include density and needs to be calculated. Density is calculated using a modified formulation of the ideal gas law

[9] During periods where forecast hour 2 is missing, the corresponding forecast hour 0 is used and for periods where forecast hour 0 is also missing, the corresponding forecast hour 6 is utilized.

$$\rho = \frac{P_o^{0.2854} P^{(1-0.2854)}}{RT_v} \quad (1)$$

where R is the specific gas constant (287.058 $Jkg^{-1}K^{-1}$ for dry air) and T_v is the virtual potential temperature, which is calculated using the formula

$$T_v = \frac{T}{\left(P/P_o\right)^{\kappa}}\left(1 + 0.61spH - (cwr + rwr)\right) \quad (2)$$

Here P_o is the standard pressure which is 10^5 Pa and κ is the Poisson constant given by

$$\kappa = 0.2854 * (1 - 0.24 * spH) \quad (3)$$

The modified formulation is utilized to account for the buoyancy effects for the change in temperature and pressure with height above the ground. The buoyancy effect is captured by the virtual potential temperature calculated in Eq (2). The horizontal wind speed components (u,v), density, temperature and cloud-water mixing ratio are interpolated for heights 20 m above the ground to 300 m above the ground with 15 m vertical resolution. The HRRR wind gust outputs are used to compute a gust factor expressed as a fraction of the mean wind speed.

4.4.1.1 Rotor equivalent calculations

Wind turbine power generation potential is derived as the kinetic energy flux through the wind turbine rotor layer. This general relationship is shown in Equation (4)

$$P_w = \frac{1}{2} C_p \rho A U^3 \quad (4)$$

where C_p is the coefficient of power (ratio of actual power generated to available power in the wind), ρ is the air density, A is area of the wind turbine rotor and U is the horizontal wind velocity component along the horizontal axis of the wind turbine rotor. The vertical component of the velocity does not contribute appreciably to wind power production as modern wind turbines use aerodynamic lift for propulsion. In addition, any drag-component due to vertical velocity is assumed to cancel out over the rotor swept area. Equation (4) is valid as long as the density and velocity do not change within the rotor swept area of the wind turbine. However, modern wind turbine rotors can span vertical extents of 100 m or more and the variables that impact wind power production can change significantly within this vertical extent (Figure 4.39).

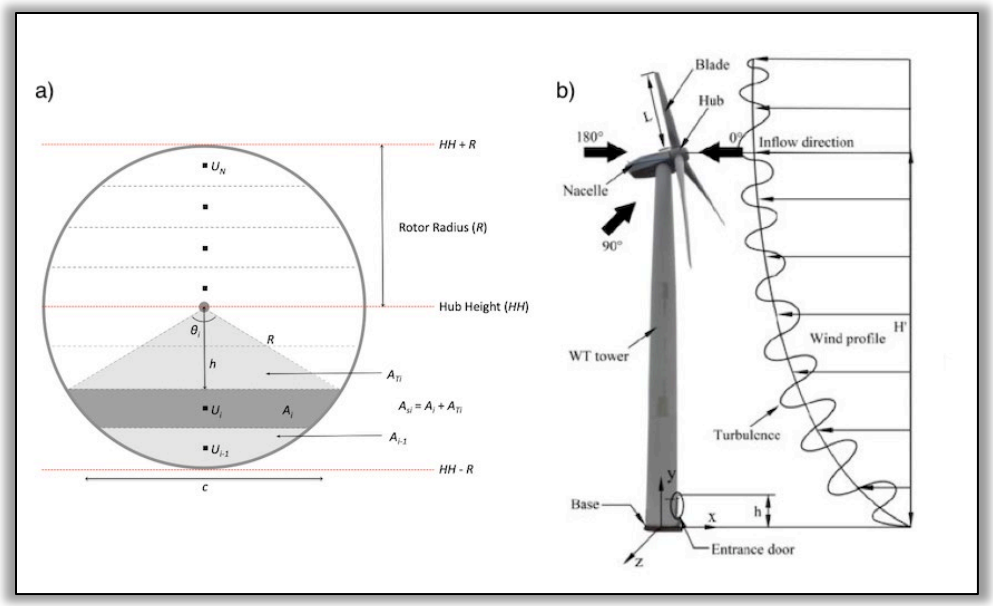

Figure 4.39: Schematic showing how the wind profile can change within the rotor layer and how the wind turbine rotor is divided to calculate the rotor equivalent variables.

The rotor equivalent formulation provides a more accurate estimate of wind power production by taking into account the vertical profile of the variables affecting wind power production. At its core, the rotor equivalent formulation allows calculation of the area weighted mean of the various meteorological variables across the wind turbine rotor. The rotor area is divided into sections with respect to height equal to the vertical resolution of the dataset (15m). Each of the variable values at a given height is area weighted by the portion of the wind turbine rotor it represents (equal to the vertical resolution) in order to estimate the equivalent effect of the vertical profile of that variable. Equations (5) and (6) show how the speed and density in Equation (4) can be replaced by their rotor equivalent counterparts.

$$U_{eq} = \frac{1}{A}\sum_i \frac{u_i u_H + v_i v_H}{U_H} A_i \tag{5}$$

$$\rho_{eq} = \frac{1}{A}\sum_i \rho_i A_i \tag{6}$$

In Equation (5), the effect of turbulence is neglected. The effect of turbulence can be included in the power calculations using Equation (7), as derived in [5]:

$$U_{eqT} = \frac{1}{A}\sum_i \frac{(u_i + u_i')(u_H + u_H') + (v_i + v_i')(v_H + v_H')}{[(u_H + u_H')^2 + (v_H + v_H')^2]^{1/2}} A_i \tag{7}$$

where $(.)'$ denotes tendency of that variable in a given time period (5-min in our case). Equation (7) shows that the effect of turbulence results in additional wind power being generated, which makes sense analytically as turbulence represents additional energy in the wind. However, actual wind turbine response to turbulence results in additional power generated at the lower end of the power curve (due to the additional energy). It also results in under-performance at the higher end of the power curve due to the positive velocity fluctuations being damped by the wind turbine control [6]. The effect of turbulence on power production due to wind turbine control can only be modelled through a full mechanical modeling of

the wind turbine as is done by the National Renewable Energy Laboratory (NREL) FAST software. In our analysis, this effect of turbulence is neglected as it is found to be much smaller compared to the effect of wind speed and direction shear [5].

The rotor equivalent formulation takes into account the change in density with respect to height as well as wind speed and direction shear on wind turbine power potential calculations. The rotor equivalent formulation is also applied to the temperature and moisture information as shown in Equations (8) and (9). The rotor equivalent temperature and moisture information is used to determine icing possibility within the wind turbine rotor.

$$T_{eq} = \frac{1}{A}\sum_{i} T_i A_i \tag{8}$$

$$cwr_{eq} = \frac{1}{A}\sum_{i} cwr_i A_i \tag{9}$$

The rotor equivalent quantities are then linearly interpolated to 5-min intervals for each of the HRRR grid cells. The linear interpolation also covers any possible periods of data outages. These 5-min rotor equivalent quantities are used in the power calculations. In order to calculate actual power generation from the theoretical available power in the wind a C_p curve is used. A C_p curve is the ratio of the actual electrical power generated for a given wind speed to the theoretical available power in the wind given by Equation (10)

$$C_p = \frac{P(u)}{P_{wind}(u)}. \tag{10}$$

As the wind moves passed the wind turbine blades, it transfers momentum to the turbine blades and produce electricity. This transfer of momentum from energy extraction results in the control volume of the wind passing through the turbine to expand downstream of the rotor to preserve continuity. Based on this, [7] calculated the theoretical maximum energy that can be extracted by a wind turbine. This theoretical maximum, called the Betz limit, is equal to 59.3% and is the maximum value a C_p can take.

The C_p curve varies for different types of wind turbines. The International Electrotechnical Commission (IEC) described four classes for wind turbines: Classes I, II, III and offshore. The shape of the C_p curve is defined not only by the physical limits on converting wind power to electricity, but also the control strategies employed by the wind turbine. For all onshore locations, the IEC-III curve is used and the offshore curve is used for all offshore locations.

To accurately calculate wind power generation, the following two components are important and depend on how the C_p curve is used:

- The impact of turbulence on power generation;
- Wind turbine response to changes in air density.

4.4.1.2 Effect of turbulence

As described earlier, turbulence has a complicated impact on the wind power generation. At wind speeds closer to the cut-in speed, the presence of turbulence increases power generated from the turbine, while at

wind speeds closer to the rated power, turbulence reduces the power output from a wind turbine [6]. The reason for this behavior is that near cut-in speed, the positive fluctuations due to turbulence are allowed to generate excess power, while the negative fluctuations do not have any effect as the turbine is not generating any power in that case. Near the rated speed, the positive fluctuations due to turbulence get damped out by the wind turbine control, while the negative fluctuations reduce power output, and hence the net effect is a reduction in power output from the turbine.

Modelling this effect analytically is difficult as seen from Equation (7), where presence of turbulence always results in increased power production. Therefore, instead of trying to model this effect analytically, it was decided to utilize the characteristics of the C_p curve to simulate the wind turbine control response. To do this, the HRRR model wind speed output needs to be perturbed in a manner that actual atmospheric turbulence would, as shown in Equation (11), known as the Reynold's decomposition.

$$U(t) = \bar{U}(t) + u'(t) \tag{11}$$

where, *U(t)* is the wind speed including effect of turbulence at given timestep, $\bar{U}(t)$ is the mean wind speed at a given timestep from the HRRR, and $u'(t)$ is the random turbulence perturbation at that timestep.

The perturbations that need to be added to the HRRR model wind speed are estimated using the wind gust HRRR model output. The HRRR model estimate of wind gust represents a sudden, brief increase in peak wind speed (lasting less than 20 seconds) expected at a given timestep. An estimate of the standard deviation of turbulence from this peak value is needed. Assuming that the turbulence distribution is symmetric (skewness of zero), which is reasonable for horizontal velocity turbulence, and that it follows a standard normal distribution, the standard deviation can be estimated using Equation (12):

$$\sigma_U = \frac{\left(U_{gust} - U_{eq}\right)}{4} \tag{12}$$

where, U_{gust} is the model outputted wind gust at a given timestep, U_{eq} is rotor equivalent wind speed from Equation (5), and σ_U is the standard deviation of wind speed due to turbulence.

The reasoning used in Equation (12) to calculate standard deviation is based on the following. Since the gust is the peak wind speed observed, it is assumed to be a value in the 99.9936th percentile which is four standard deviations from the mean. The standard deviation of wind speed due to turbulence calculated using Equation (12) is now used to calculate the random perturbation to the rotor equivalent wind speed at a given timestep using Equation (13):

$$U_{eqT}(t) = U_{eq} + rand(0, \sigma_U) \tag{13}$$

where, U_{eqT} is the rotor equivalent wind speed including the effect of turbulence. The rest of the calculations proceed as described earlier.

4.4.1.3 Wind turbine response to density fluctuations

Modern wind turbines have control responses to maximize wind generation in presence of changing air densities. This control response is usually active close to the rated wind speed, but can also extend to region 2 of the power curve. Figure 4.40 shows the turbine response in terms of the observed C_p values in response to changes in air density.

As seen in Figure 4.40 the C_p value is a function of both wind speed and density (top panel) and the changes in C_p values compared with the C_p value at standard density are highly non-linear (bottom panel). However, the change in C_p with respect to density at a given wind speed is linear. The slope and intercept of this linear behavior changes at every wind speed. Therefore, a model was constructed to predict the slope and intercept of the change in C_p at a given wind speed. This model allows predict of a "correction" to the C_p at standard density and given wind speed, which will produce the correct C_p value at that wind speed and density.

Figure 4.40 shows the comparison of the described model predicted C_p values against the actual manufacturer supplied C_p values. It is seen that the model is able to predict the changes to the C_p values at various densities and wind speeds accurately. The comparison of the C_p values at various densities to the C_p values at the standard density (1.225 kg/m^3) show that there can be differences of up 50% of the C_p value at a given wind speed. Hence it is very important to quantify the impact of density on the C_p values.

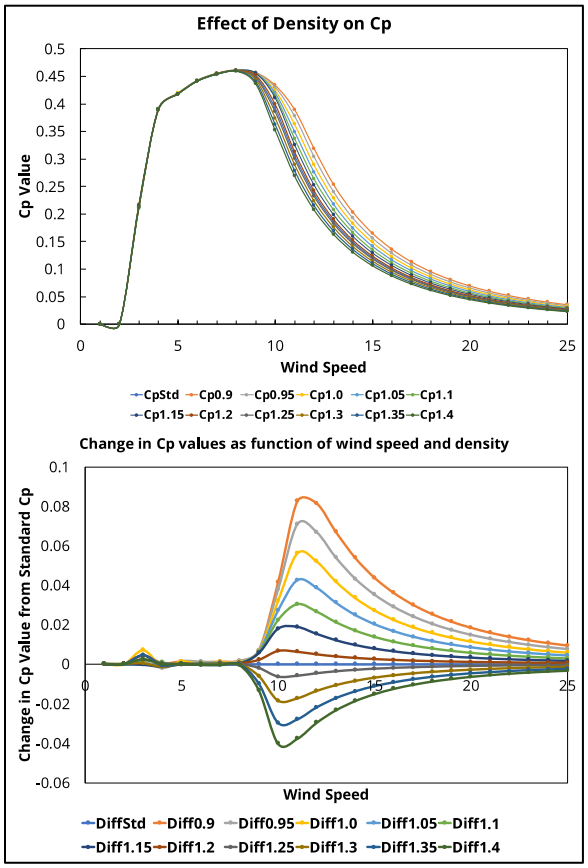

Figure 4.40: Impact of density on C_p values for a 2.3 MW Siemens wind turbine.

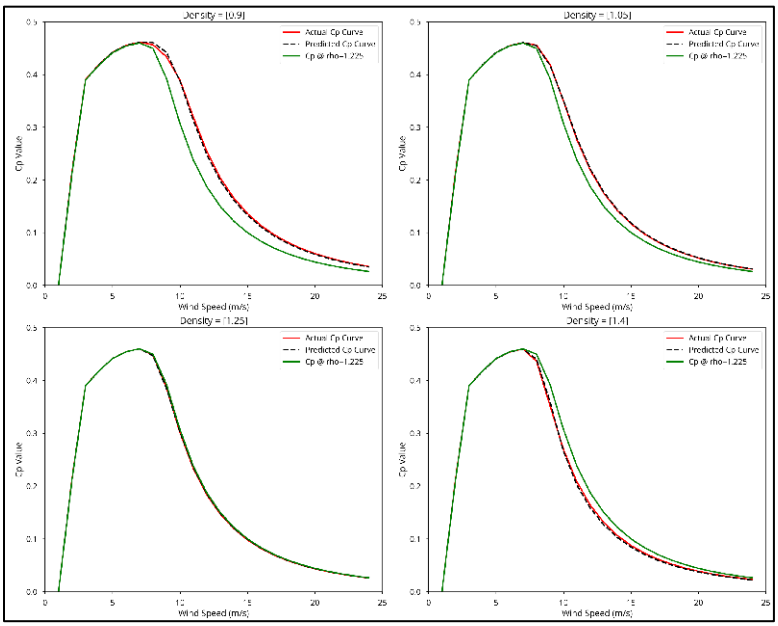

Figure 4.41: Comparison of model predicted C_p (black dashed line) values to the actual turbine C_p values (red solid line). The standard C_p value at density of 1.225 kg/m^3 is shown in solid green line.

The WIS:dom® model takes into account time periods where generation may not be possible due to extreme weather conditions. Normal operational temperatures for wind turbines are set to be between -25ºC and 45ºC. In addition, the potential for icing is also calculated. Icing is considered possible when temperatures are below -15ºC and cloud-water mixing ratio is greater than zero. The periods with potential for icing or temperatures outside of normal operating conditions are set to zero power output. It is important to identify periods such as the above where generation will be limited or zero as these are usually correlated with periods of high energy demand. WIS:dom® then has to ensure that the demand during these periods will be met in some other way.

The above power calculations are performed for each 3-km HRRR grid cell (~1.9 million grid cells) for all the years required to run WIS:dom®. The WIS:dom® model is run on the same grid as the HRRR, however, only a subset of the HRRR cells are made available for wind plant development. The potential for wind development in MW for each HRRR cell is made available to WIS:dom®, which is used in determining whether wind generation gets built or not. The available wind capacity potential provided to WIS:dom® is shown in Figure 4.41(d). When choosing to build wind generation, WIS:dom® can choose the most optimal hub-height wind turbine to build. As seen from Figure 4.41 (a) and 5(c), higher hub-heights give higher wind power capacity factors. However, there are additional costs associated with building taller towers and wind turbines capable to withstanding higher wind loading. WIS:dom® takes these costs into account and determines the optimal hub-height at a given location. The optimal height is determined by evaluating whether the increased cost due to the higher tower height is offset by increased revenue or demand met from additional power generation at the higher hub-height. In this analysis it is assumed that the same turbine rotor is installed on taller towers. An important impact of this assumption is that as the hub-heights increases, the wind power capacity factors also increase due to the higher average wind speeds at increased heights above the ground. However, beyond a certain hub-height, wind power capacity factors start to decrease. This decrease in power capacity factors is due to increased wind speeds at higher hub-heights, the wind turbines are in the cut-off portion of the power curve more often. Therefore, to take full advantage of the increased wind resource at higher heights will require a redesign of the turbine rotor to operate in the higher wind speed regime.

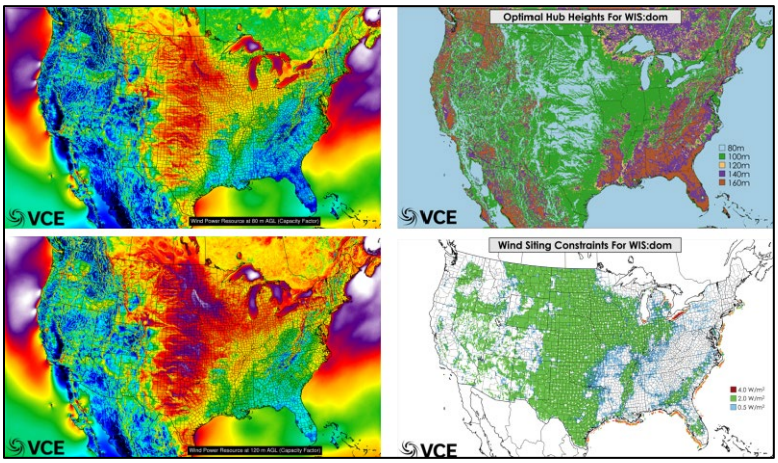

Figure 4.42: The wind power dataset. Mean wind power capacity factor at for 80-m hub-height using data from year 2014 (top left), optimal hub-height for the CONUS (top right), mean wind power capacity factor for 120 m hub-height using data from year 2014 (bottom left), and wind plant siting constraints for the CONUS (bottom right).

4.4.2 Solar power dataset method

Calculation of the solar PV power generation requires accurate forecasts of Global Horizontal Irradiance (GHI), Direct Normal Irradiance (DNI) and Diffuse Horizontal Irradiance (DHI). These variables are then input into a PV cell power modeling algorithm. The components of the solar irradiances are related to each other by:

$$GHI = DNI*cos(sza) + DHI \quad (14)$$

where *sza* is the solar zenith angle.

Numerical weather prediction models did not output forecasts of DNI and DHI until 2016. In addition, forecasts of DNI and DHI produced by the HRRR after 2016 have significant biases mainly due to improper representation of clouds. To obtain forecasts of DHI and DNI from HRRR model outputs for years before 2016 and correct for model biases for years after 2016, VCE® employs a linear multiple multivariate regression technique developed by [8]. The variables used to create the solar power data are the following:

- From the HRRR
  - ✓ *Downwelling shortwave (SW),*
  - ✓ *Downwelling longwave (LW),*
  - ✓ *10-m wind speed (Wind10m),*
  - ✓ *2-m temperature (T2m),*
  - ✓ *Direct normal irradiance (DNI) – 2016 onwards,*
  - ✓ *Diffuse horizontal irradiance (DHI) – 2016 onwards,*
- From GOES-east and GOES-west (for datasets before 2016 only)
  - ✓ *Visible band,*
  - ✓ *4μm band,*
  - ✓ *11μm band,*
  - ✓ *13μm band,*
  - ✓ *Water-vapor band,*
- Calculated
  - ✓ *Direct normal irradiance at the top of the atmosphere (DNI_0),*
  - ✓ *Solar zenith angle (sza),*
  - ✓ *Solar azimuth angle (azm),*
  - ✓ *Hour-angle (hrang),*
  - ✓ *Declination angle (dec).*

The satellite observations are not included starting in 2016, as these observations are already assimilated into the HRRR during data assimilation. To perform the regression, we get observations of GHI, DNI and DHI from fifteen ground-based radiation measurement sites (SURFRAD and SOLRAD) operated by the NOAA. The above variables are chosen as they are most likely to impact the amount of solar irradiance reaching the Earth's surface and its attenuation along the way. A significant portion of the effort in creating the solar power dataset is spent on getting the data ready for regression. First, the required HRRR variables are extracted from the HRRR output files at 1-hour resolution. These HRRR variables are then linearly interpolated to 5-min intervals. For data gaps of longer than 1-hour, persistence is assumed and they are filled in with data from the same hour on the previously available day. Linear interpolation is carried out only sub-hourly.

Satellite measurements from GOES-east and GOES-west are used, which allows a stereoscopic observation of the cloud field. Each of the GOES satellite observations cover the full CONUS with observations available at 15-min time interval. The GOES satellites make measurements in 5-channels listed above. The measurements are in bit count, which are converted to temperature (in Kelvin) using the formula [8]:

$$T = \frac{1}{2}(660 - B), \quad 0 \le B \le 176 \quad and$$
$$T = 418 - B, \quad 176 < B \le 255 \tag{15}$$

The spatial resolution of the satellite data is 1-km for the visible channel and 4.km for the remaining channels. Since the HRRR has a spatial resolution of 3-km, the satellite data are spatially interpolated on to the HRRR grid. This spatially interpolated satellite data is then linearly interpolated in time to 5-min intervals to match the interpolated HRRR output.

In addition to the variables obtained from the HRRR and satellite measurements, five additional variables are calculated. The calculation of solar irradiance at the top of the atmosphere needs to take into account the eccentricity of Earth's orbit. The average DNI_0 at the top of the atmosphere is 1360.8 W m^{-2} and is denoted by I_o. The equation for the actual irradiance hitting the top of the atmosphere is given by

$$DNI_0 = I_o \left(\frac{R_{avg}}{R}\right)^2 \tag{16}$$

where R_{avg} is the average Earth-Sun distance and R is the instantaneous Earth-Sun distance. The ratio of R_{avg} to R is given by the Fourier expansion in Equation (16) which is accurate to 0.0001 [9]

$$\left(\frac{R_{avg}}{R}\right)^2 \approx 1.000110 + 0.034221\cos(\delta) + 0.00128\sin(\delta) + 0.000719\cos(2\delta) + 0.000077\sin(2\delta) \tag{17}$$

where, the day angle $\delta = {}^{2\pi d}/_{365.242}$ radians and d is the day of the year.

The declination angle is also given as a Fourier expansion in Equation (18) which accurate to 0.0006 radians [9]

$$dec = 0.006918 - 0.399912\cos(\delta) + 0.070257\sin(\delta) - 0.006758\cos(2\delta) + 0.000907\sin(2\delta) - 0.002697\cos(3\delta) + 0.00148\sin(3\delta) \tag{18}$$

The hour angle, given by equation (19) is defined as the number of degrees the Sun moves across the sky compared to local Solar noon. The hour angle is zero at local Solar noon, positive in the afternoon and negative in the morning

$$hrang = 15 * (LST - 12), \tag{19}$$

where LST is the local solar time given by

$$LST = LT + \frac{TC}{60} \tag{20}$$

where LT is the local time and TC is the time correction factor that accounts for the variation in the local Solar time due to the range of longitudes within the same time zone, eccentricity of the Earth's orbit and

Earth's axial tilt (to calculate the last two, the equation of time given by Equation (23) is used). The time correction factor (*TC*) is calculated as

$$TC = 4 * (lon - LSTM) + EoT \tag{21}$$

where, *LSTM* is the local standard time meridian is the reference meridian used for a particular time zone and is calculated using the equation

$$LSTM = 15 * (LT - UTC) \tag{22}$$

and *EoT* is the equation of time, which is an empirically derived relationship that corrects for the eccentricity of the Earth's orbit and the Earth's axial tilt. The *EoT*, in radians, is given by a Fourier expansion that is accurate to 0.0025 radians or 35 seconds [9]

$$EoT = 0.000075 + 0.001868\cos(\delta) - 0.032077\sin(\delta) - 0.014615\cos(2\delta) - 0.040849\sin(2\delta). \tag{23}$$

Now the Solar zenith angle can be calculated using Equation (24)

$$\cos(sza) = \sin(lat)\sin(dec) + \cos(lat)\cos(dec)\cos(hrang) \tag{24}$$

where, the latitude (*lat*), declination angle (*dec*) and hour angle (*hrang*) are in radians.

Once all the quantities required for the regression are collected, the regression can be performed. The regression is performed separately for the GHI and DNI for computational efficiency and DHI is calculated using Equation (14) once the GHI and DNI are known. The regression is represented mathematically as [8]

$$Y_{n\times p} = X_{n\times(r+1)}\beta_{(r+1)\times p} + \varepsilon_{n\times p} \tag{25}$$

where, $Y_{n\times p}$ are the endogenous variables (here the ground-based measurements of GHI, DNI and DHI), $X_{n\times(r+1)}$ are the exogenous variables (here the variables from the NWP model, satellite measurements and calculated variables), $\beta_{(r+1)\times p}$ are the regression coefficients and $\varepsilon_{n\times p}$ are the measurement errors in the ground-based observations.

The ground-based observations of the irradiance components measured by the SURFRAD and SOLRAD sites are available at 1-min time resolution. These measurements are averaged to 5-min resolution, which reduces measurement noise and helps reduce the discrepancy between a point measurement from the SOLRAD/SURFRAD sites and the grid-cell average from the HRRR model. The errors in the SURFRAD/SOLRAD observations are modelled as

$$\varepsilon = 5 + 0.02 * (1 - \cos(sza)) + 0.01 * T2m + 0.005 * GHI. \tag{26}$$

The SURFRAD/SOLRAD measurements are known to have error bars of $\pm$5 W m^{-2} under ideal conditions. These errors get larger depending on various factors such as total irradiance, ambient temperature and solar zenith angle. The regression is performed using the advanced statistics package from IDL and analysis of variance (ANOVA) techniques are used to determine performance of the regression. The regression coefficients that give the best performance are applied to the HRRR data to get irradiance estimates over the whole contiguous United States. Once the irradiance components are calculated, the power production from a photovoltaic panel can be estimated.

4.4.2.1 Estimating power from solar photovoltaics

A photovoltaic (PV) cell converts solar radiation incident on its surface to electrical power. A PV cells utilizes both the direct (DNI) and diffuse (DHI) radiation to produce current and a voltage, which determine the power generated by the cell as shown in Figure 4.43 and is defined by Equation (27):

$$P_s = V * I. \tag{27}$$

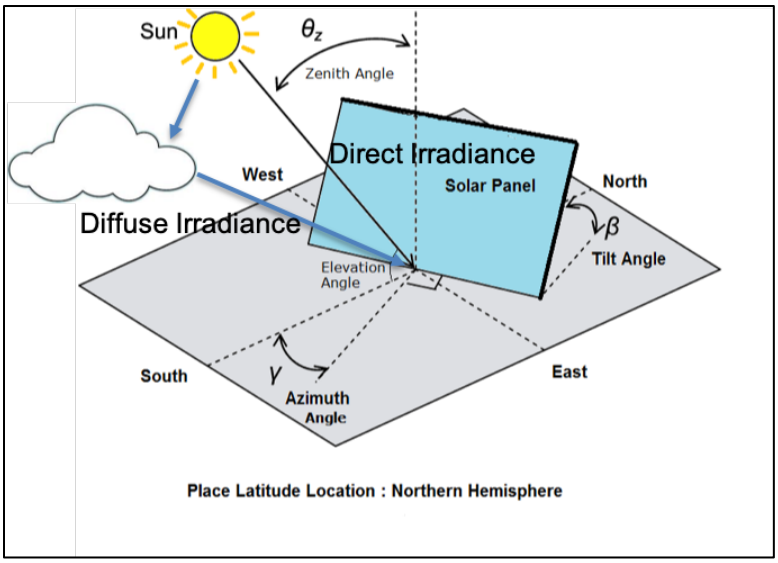

Figure 4.43: Schematic showing the direct and diffuse irradiance on a PV panel with respect to its tilt and azimuth orientation.

The power performance of a PV cell is a complex function of several environmental factors (such as ambient temperature, wind speed, incident irradiation) as well as the PV cell characteristics. These environmental factors interact non-linearly and make estimating the power output from a PV cell difficult. The power performance model used by VCE® is an empirically derived model developed by Sandia National Laboratory and described in [10]. To calculate the voltage and current induced in the PV cells, equations (11) to (20) from [10] are used. These equations attempt to model the non-linear response of a PV cell as an interaction of several factors each having well defined, experimentally derived relationships with the independent variables affecting PV cell performance.

To calculate the power produced from a PV cells requires being able to model the shape of the I-V curve of the PV panel accurately. The I-V curve of a PV cell shifts depending on the amount of incident radiation on the panel and ambient temperature. In order to replicate these effects accurately King et al. [10] model the voltage and current response separately using 3,300 measurements made over a range of clear and cloudy conditions, wide range of solar irradiance and module temperatures. The measured voltage values are first translated to a common temperature of 50ºC to remove effects of temperature. The translated measurements of voltage and associated irradiance are regressed using Equations (28) and (29) to find values of n, c_2 and c_3:

$$V_{oc} = V_{oco} + N_s \delta(T_c).\ln(E_e) + \beta_{Voc} E_e (T_c - T_o) \tag{28}$$

$$V_{mp} = V_{mp0} - c_2 N_s \delta T_c \ln(E_e) - c_3 N_s (\delta T_c \ln(E_e))^2 - \beta_{vmp} E_e (T_c - T_o) \tag{29}$$

where V_{oc} is the open-circuit voltage, V_{oco} is the open-circuit voltage constant, V_{mp} is the voltage at maximum power, V_{mp0} is the constant for voltage in I-V curve, $\delta(T_c) = n\,k\,(T_c + 273.15)/q$ is the thermal voltage per cell at temperature T_c, n, c_2, c_3 are constants for voltage formula, q is the elementary charge (1.60218e-19 coulomb), k is the Boltzmann's constant (1.38066e-23 J K^{-1}), N_s number of cells in series in a module's cell-string, T_o reference cell temperature, $T_c = GHI * e^{a+b*WS} + T_{2m}$ is the cell temperature inside the module, WS is the wind speed, T_{2m} is the 2-m temperature, and a, b are constants.

In a similar way, to determine the dependence of module current on incident irradiation, the current values are translated to a common temperature and regression coefficients, C_0, C_1, C_4, C_5, C_6, C_7, are determined using Equations (30), (31) and (32):

$$I_{mp} = I_{mpo}\{C_0 E_e + C_1 E_e^2\}\{1 + \alpha_{Imp}(T_c - T_o)\} \tag{30}$$

$$I_x = I_{xo}\{C_4 E_e + C_5 E_e^2\}\{1 + \alpha_{Isc}(T_c - T_o)\} \tag{31}$$

$$I_{xx} = I_{xxo}\{C_6 E_e + C_7 E_e^2\}\{1 + \alpha_{Imp}(T_c - T_o)\} \tag{32}$$

where, I_{mp} is the current at maximum power, I_{mp0} is the constant for current in I-V curve, I_x is the current at module V = 0.5 V_{oc}, I_{xx} is the current at module V = 0.5 $(V_{oc} + V_{mp})$, I_{x0} is the constant for current in I-V curve, I_{xx0} is the constant for current in I-V curve, α_{Imp} is the normalized temperature coefficient for I_{mp}, and α_{Isc} is the normalized temperature coefficient for I_{sc}, the short-circuit current.

In the above equations, E_e is the effective irradiance to which the PV cells in the module respond to and is given by

$$E_e = f_1 * SF * \left[\frac{E_b f_2 + f_d * DHI}{E_o}\right] \tag{33}$$

where, $E_b = DNI * \cos(AOI)$, which is the beam component of the solar irradiance incident on module surface, E_o is the reference solar irradiance (1000 W/m^2), f_1 is the relation between solar spectral variation and short circuit current given by $f_1 = a_0 + a_1 AM_a + a_2 AM_a^2 + a_3 AM_a^3 + a_4 AM_a^4$, where a_0, a_1, a_2, a_3, a_4 are constants and AM_a is the absolute air-mass (dimensionless), SF is the soiling factor, f_2 is the relation between optical influences and solar angle-of-incidence, $f_2 = b_0 + b_1 * AOI + b_2 * AOI^2 + b_3 * AOI^3 + b_4 * AOI^4$, where b_0, b_1, b_2, b_3, b_4 are constants, $AOI = \cos\beta\cos\theta_z - \sin\beta\sin\theta_z\cos\gamma$ is the angle of incidence, where β is tilt angle of the panel with respect to the ground, θ_z is solar zenith angle, γ is the azimuth angle with respect to the north-south, and f_d is the relative response to diffuse versus beam irradiance.

The empirical functions $f_1(AM_a)$ and $f_2(AM_a)$ quantify the effect of solar spectral variation and optical influences on short-circuit current. These functions are determined from laboratory testing and account for systematic effects that occur during clear sky periods. Absolute airmass provides a relative measure of the path length solar radiation has to travel at a given solar zenith angle compared to a solar position of directly overhead.

The performance of a PV panel also depends on the module temperature as seen in Equations (28)-(32). The thermal response of a PV cell can be modelled as

$$T_c = GHI * e^{a+b*WS} + T_{2m}. \tag{34}$$

The simple model for expected module temperature given by Equation (31) has been shown to have accuracy of ±5°C, which results in uncertainty in power output of less than 3%.

The constants in the power generation model are obtained from [11] and the NREL System Advisory Model (SAM) [12]. It is assumed that the individual panels are placed far enough apart so as not to create any shadowing effects. The above formulae are used to calculate solar power production for the following technologies:

- *Fixed PV panel for various tilt angles (0°, 15°, 30°, 45°, latitude tilt),*
- *One-axis tracking at latitude tilt,*
- *Two-axis tracking.*

Finally, the calculated power output is de-rated based on expected losses from wiring and soiling (4.5% loss), AC/DC conversion (3.3% loss) and presence of snow on the panels (assume no production if snow is present – for fixed panels at 0° and 15° elevation). WIS:dom® can update the magnitude of these losses to account for improved technology in the future or panel performance degradation with age.

The technologies for utility scale PV range from simplest and least cost (Fixed panels with 0-degree tilt) to most complex and highest cost (dual-axis panels). The fixed panels at 0-degree tilt will result in the lowest power capacity factors while the dual-axis panels will result in the highest as they track the sun across the sky to ensure maximum possible power production [see Figure 4.44-A (top-left and bottom-left panels, respectively)]. WIS:dom®-P can determine using the weather data if the added complexity of the PV technologies is worth the additional cost in terms of increased power production. As seen from Figure 4.44-A (top-right panel), Fixed panels at various elevation angles (with respect to the latitude of the geographic location) are the optimal choice for most of the CONUS with only the northern-most part of the country justified in using either single or dual axis tracking.

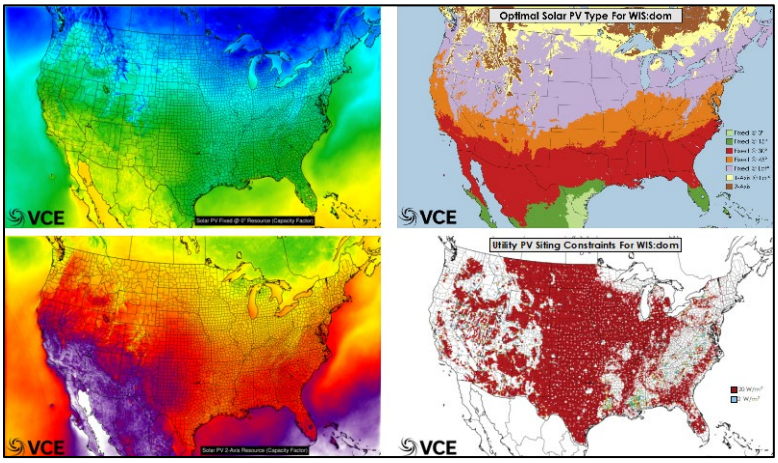

Figure 4.44-A. The solar power dataset. Mean solar PV capacity factor for fixed panel at 0° elevation for year 2014 (top left), mean solar PV capacity factor for a two-axis tracking PV panel for year 2014 (bottom left), optimal PV panel type for the CONUS (top right), and utility PV siting constraints for the CONUS (bottom right).

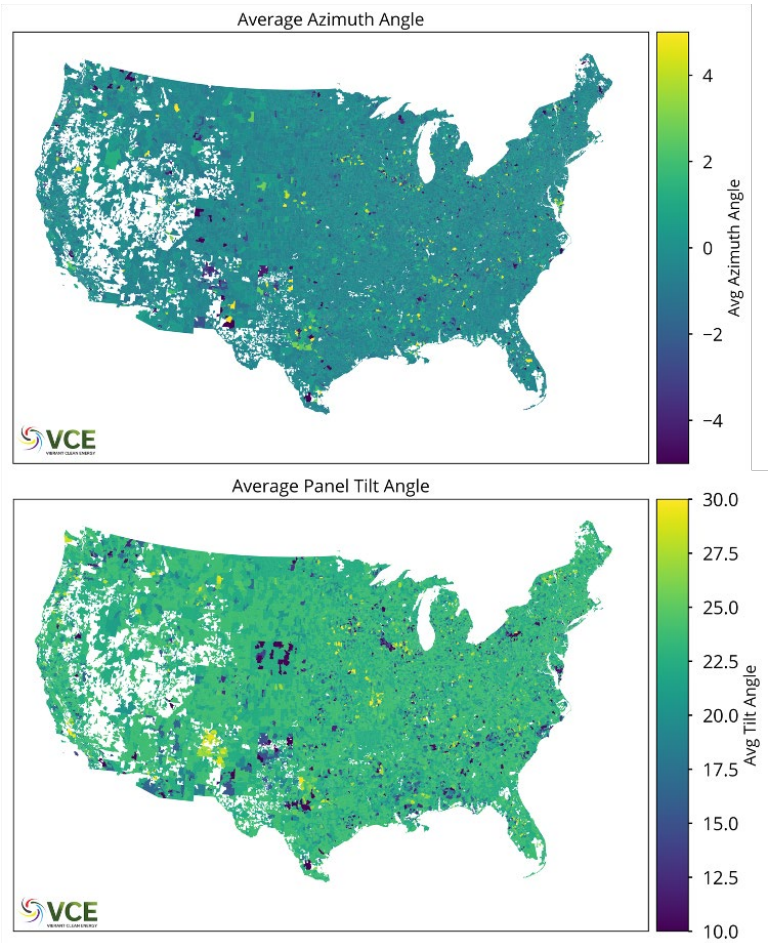

Figure 4.44-B: Average azimuth (top) and tilt (bottom) for each 3-km cell within the WIS:dom®-P model. Areas in white are locations with no available suitable rooftop area.

To accurately calculate expected power production from rooftop solar panels, the azimuth and tilts of suitable rooftop in each 3-km cell are needed. The most accurate dataset containing this information was compiled by the National Renewable Energy Laboratory (NREL) using Light Detection and Ranging (Lidar) measurements of rooftops over the CONUS[10]. Using the lidar measurements, the rooftop azimuth, tilt and rooftop area were calculated.

Shading of the rooftops was determined by running a shading simulation that calculated the number of hours of sunlight received by each square meter of the rooftop over four days: March 21, June 21, September 21, December 21 based on the geometry of the rooftop. Portions of the rooftop that were excessively shaded (more than 20% of the time) were marked as unsuitable. In addition, portions of the rooftop facing northwest through northeast (292.5° to 67.5° from north) were also considered unsuitable. Each rooftop plane with projected horizontal area smaller than 10 m^2 was also excluded.

The buildings in each zip-code were grouped into three categories: small (94% of buildings and 58% of the rooftop area), medium (5% of buildings and 18% of the rooftop area) and large (1% of buildings and 24% of rooftop area). For each of the building category, the tilts were grouped into 5 bins:

[10] Gagnon, Pieter; Margolis, Robert; Phillips, Caleb (2019): Rooftop Photovoltaic Technical Potential in the United States. National Renewable Energy Laboratory. https://data.nrel.gov/submissions/121

(1) flat (less than 9.5º in elevation);
(2) 15.8º (between 9.5º and 22.1º in elevation);
(3) 28.4º (between 22.1º and 34.8º in elevation);
(4) 41.1º (between 34.8º and 47.4º in elevation);
(5) 53.7º (between 47.4º and 60.0º in elevation).

The azimuths were also grouped into 5 bins:

(1) East (between 67.5º and 112.5º from north);
(2) Southeast (between 112.5º and 157.5º from north);
(3) South (between 157.5º and 202.5º from north);
(4) Southwest (between 202.5º and 247.5º from north);
(5) West (between 247.5º and 292.5º from north).

For each zip-code area, the rooftop area weighted azimuth and tilts are calculated. These values are then applied to each 3-km cell within the zip-code region. The resulting average rooftop azimuth and tilts for each 3-km cell are shown in Figure 4.44-B.

4.4.2.2 Estimating power from bi-facial solar photovoltaics

Bi-facial solar PV is included in the solar technologies modeled by VCE®, which are able to increase power production by using irradiance received on the backside of the panel. This increase in power comes at marginally higher cost compared to mono-facial PV panels allowing WIS:dom®-P to determine if the additional generation is worth the increased capital cost. VCE® computed the irradiance received by the backside of a solar panel using the equations from a method provided by NREL[11].

Power production from a bi-facial solar PV panel is calculated similar to a mono-facial panel as described in Section 4.4.2.1, with the radiation incident on the backside of the panel being added to the radiation incident on the front side of the panel. The frontside irradiance incident on the bi-facial solar PV panel is assumed to be the same as that received by a fixed solar panel with a latitude tilt. The total irradiance incident on the backside of a solar panel (E_{back}) can be calculated as:

$$E_{back} = \sum_{i=Latitude}^{180} CF_i * f_i \ * \ \rho * GRI \qquad \text{(BF-1)}$$

where, *GRI* is irradiance received by the ground, CF_i is the configuration factor for the i^{th} one-degree segment defined as:

$$CF_i = 0.5 * [\cos(\mathrm{i} - 1) - \cos(\mathrm{i})]$$

and f_i is the angle of incidence correction for the i^{th} one-degree segment calculated using the polynomial relationship:

$$f_i = b_0 + b_1 * AOI_i + b_2 * AOI_i^2 + b_3 * AOI_i^3 + b_4 * AOI_i^4$$

[11] B. Marion, S. MacAlpine, C. Deline, A. Asgharzadeh, F. Toor, D. Riley, J. Stein, C. Hansen, "A Practical Irradiance Model for Bifacial PV Modules," National Renewable Energy Laboratory, Presented at IEEE 44th Photovoltaic Specialists Conference, 2017.

where, AOI_i is the angle of incidence of the irradiance from the ground on the i^{th} one-degree segment on the back-side of the PV panel and b_0, b_1, b_2, b_3, b_4 are constants. The bi-facial solar PV panels are assumed to be deployed with a tilt equal to the latitude of their siting location. The field of view of the backside of the panel is divided into segments from the panel tilt angle to 180°. This limitation from a full 180-degree view is performed to exclude the portion of irradiance blocked by the solar panel itself. Finally, ρ is the Albedo defined as the ratio of the upward shortwave radiation from the surface versus the downward shortwave radiation

$$\rho = \frac{SW_{up}}{SW_{down}} \tag{BF-2}$$

where, SW_{up} is the shortwave radiation leaving the surface of the earth and SW_{down} is the shortwave radiation received at the surface of the Earth, both in W/m^2. The downward shortwave radiation will dominate, creating a ratio ranging between 0 and 1. A ratio of 0.5 means that 50% of the downward shortwave radiation is being reflected back up from the surface. For surfaces that are snowy, this ratio can easily be over 60%. In general, the albedo is lower in the summertime.

The irradiance received by the ground can be calculated using:

$$GRI_n = \alpha * (DNI + I_{cir}) + CF_{sky} * I_{sky} \tag{BF-3}$$

where, *GRI* is the ground irradiance, *n* denotes the n^{th} segment of the ground between solar panel array rows, α is the cosine of the solar zenith angle, I_{cir} is the circumsolar irradiance, I_{sky} is the Diffuse Horizontal Irradiance (DHI) and $CF_{sky} = 0.5 * (cos\theta_{s1} - cos\theta_{s2})$ is the configuration factor where θ_{s1} is the view angle of the sky blocked by a solar panel in the next row and θ_{s2} is the unblocked view angle of the sky. Since the array layout is unknown, no shading is assumed between PV panel rows. As a result, $\theta_{s1}\ is\ zero$ and θ_{s2} become 180 degrees which results in CF_{sky} to be a factor of 1.

As outputs from a numerical weather prediction model are used to calculate *DNI*, the circumsolar correction is unnecessary (*DNI* calculated from the HRRR is described in Section 4.4.2). In contrast, when using physical measurement devices that measure *DNI*, the circumsolar irradiance would have to be considered and added to the *DNI* separately[12]. As a result, Eq. (BF-3) reduces to:

$$GRI = \alpha * DNI + DHI \tag{BF-4}$$

From Eq. (BF-4), *GRI* is simply the Global Horizontal Irradiance (*GHI*) measured at the surface. This parameter is calculated as described in Section 4.4.2.

The irradiance on the back-side of the PV panel (E_{back}) calculated from Eq. (BF-1) is added to E_b [Eq. (33) in Section 4.4.2.1], which gives the total irradiation incident on a bi-facial solar PV panel. The solar power calculation procedure is exactly as described in Section 4.4.2.1 except the maximum power allowed from the bi-facial panel is limited to 125% of the solar PV panel nominal capacity.

[12] P. Blanc *et al.*, "Direct normal irradiance related definitions and applications: The circumsolar issue," *Sol. Energy*, vol. 110, pp. 561–577, 2014.

4.4.3 Temperature power dataset method

Temperature is an important variable in creating the load profiles datasets. Ambient temperatures affect heating (both space and water) and cooling demand, heat rates of conventional generators, transmission losses and ampacity as well as energy use by EVs. Temperature data is available from the HRRR at 3-km spatial resolution and 5-min temporal resolution.

The loads are evaluated at state-level and hourly time-resolution. Therefore, the temperature data needs to be aggregated to state-level, while preserving the spatial variability information present in the original higher resolution dataset. To do this, the temperature data is aggregated to state level by weighting each 3-km HRRR cell by the fraction of the state population in the cell. The population weighting ensures that locations of denser populations get greater weighting on temperatures and hence will have a stronger impact on the demand profile. A similar technique is used to create average temperatures at county level.

4.4.4 Southeast US Weather Analysis

Looking at the weather data specific to the states in the Southeast US can provide insight into what, where, and why certain renewable sources, in particular, are selected by the model. The states included in this analysis are Tennessee, North Carolina, South Carolina, Georgia, Alabama, Mississippi and Florida. The figure below demonstrates the average wind and solar capacity across all these southeast states by hour of the day. The wind is pulled from the 100-meter level. The solar technology is using a tilt set to the latitude. The load is also displayed for comparison. The series are shown for the average of the entire year and then the summer (June, July, August) and winter (January, February, March) seasons.

Unsurprisingly, the solar resource is both higher in peak and longer in duration during the summer, reaching over 50% capacity factors in those months. For wind, the reverse occurs where the resource drops during the summer and increases during the winter. The stronger jet stream and weather patterns in winter are apparent. Wind also exhibits a diurnal pattern where stronger resource is observed during the nighttime hours. This is a normal phenomenon for wind when the decoupling of the boundary layer near the surface at night allows for wind speeds to regularly increase due to less friction from the surface. Nighttime hours can see around 30% capacity from the wind resource on average for the whole year. It is easy to see the complementary temporal patterns in the wind and solar resource. The load in the southeast is much higher in the summer months than in the winter months. The shape of the load is highly correlated to the diurnal solar power patterns as well.

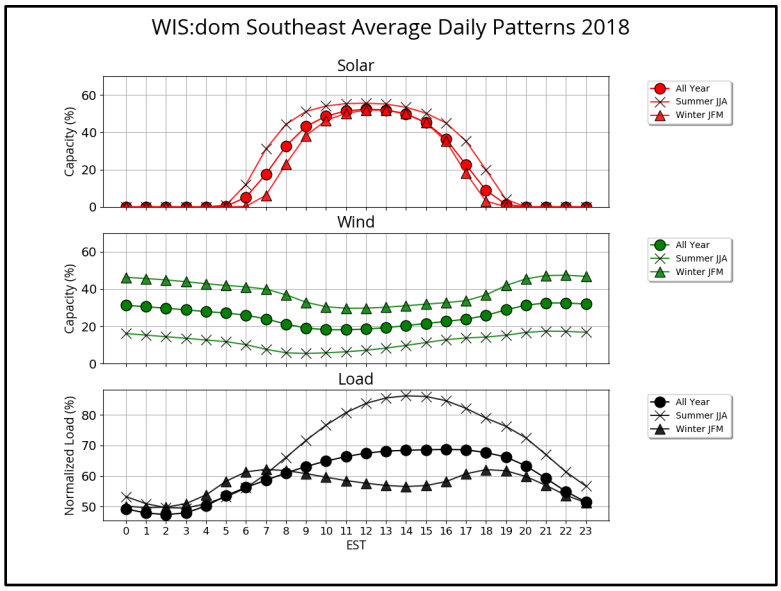

Figure 4.45: The average solar (red) and wind (green) resource shown for the Southeast US states alongside the corresponding load (black) by hour of the day (EST). The circles show the hourly averages for the entire 2018 year. The other two series look at the summer (JJA) and winter (JFM) months of 2018.

The following figure is similar to the previous image. The previous image shows how each parameter (solar, wind or load) changes against itself each season. The following figure looks at each season and overlaps the wind, solar and load data together for better comparison. Here it is easier to see how the solar resource peak compares to the load peak. In the yearly average, but especially in the summer months, the shapes of these two series align well. The peak of the solar tends to occur on average a few hours in advance of the diurnal peak load. In winter, the shape of the wind resource is highly correlated with the shape of the load, whereas solar peaks during the midday drop in load. This shows the viability of wind in the southeast alongside solar.

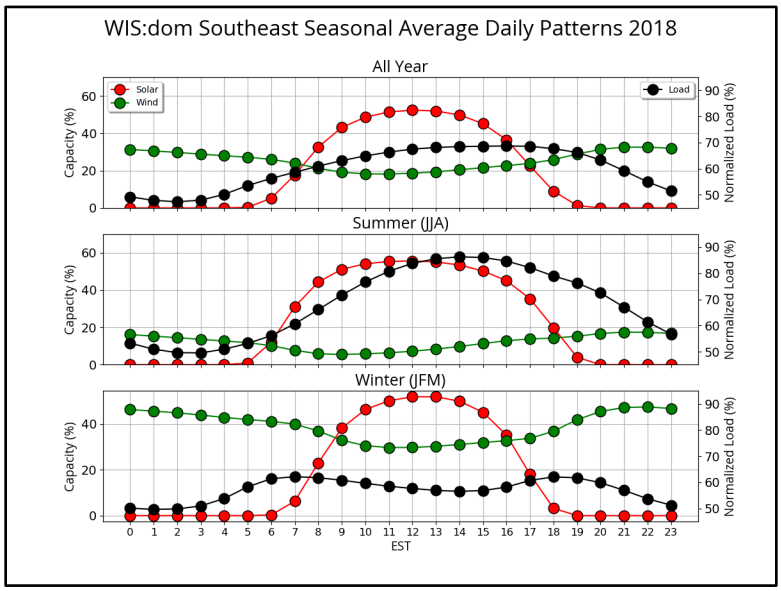

Figure 4.46: The average solar (red) and wind (green) resource shown for the Southeast US states alongside the corresponding load (black) by hour of the day (EST). This is shown in seasonal groupings now; the entire 2018 year, the summer (JJA) of 2018 and winter (JFM) of 2018.

VCE® investigated the wind and solar resources at different levels as well for analysis. The following figures shows the average annual wind and solar resources throughout the day for each of the Southeast states. For the 2018 weather year, it is shown that Florida experienced the highest amount of solar resource whereas Tennessee had the lowest. For wind, North Carolina shows on average the highest wind resource for 2018. This is followed by Tennessee and Mississippi. Florida shows the lowest wind resource on average, followed by Alabama and Georgia.

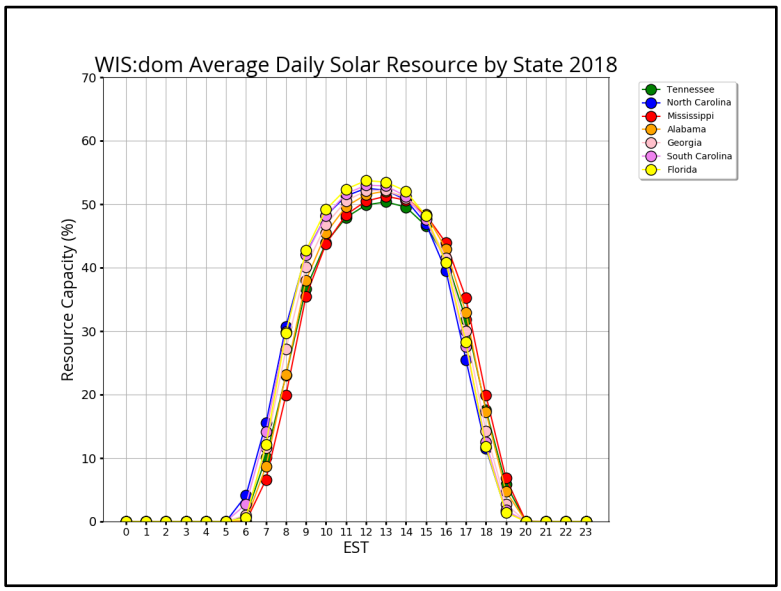

Figure 4.47: The 2018 average hourly solar resource capacity for each Southeast state.

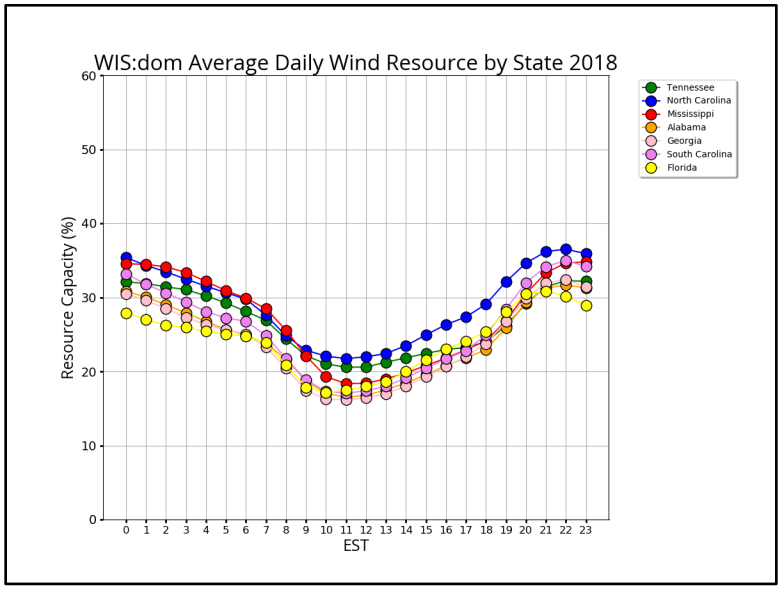

Figure 4.48: The 2018 average hourly wind resource capacity for each Southeast state.

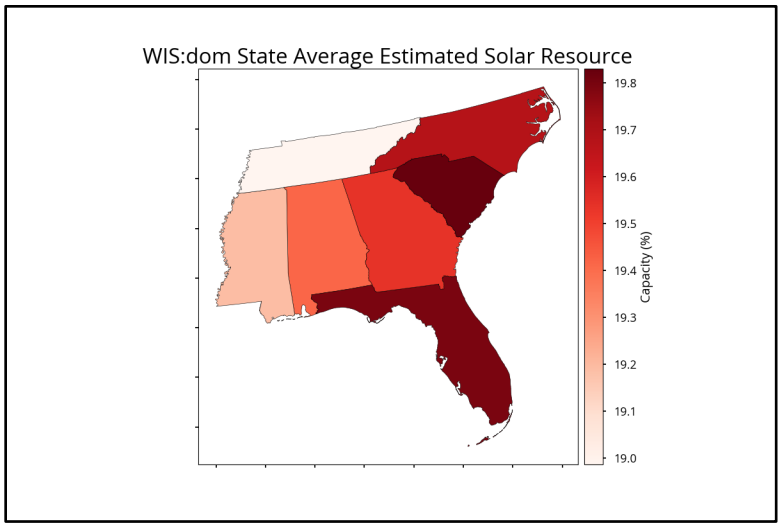

Figure 4.49: The average solar capacity (%) for 2018 by state in the Southeast US.

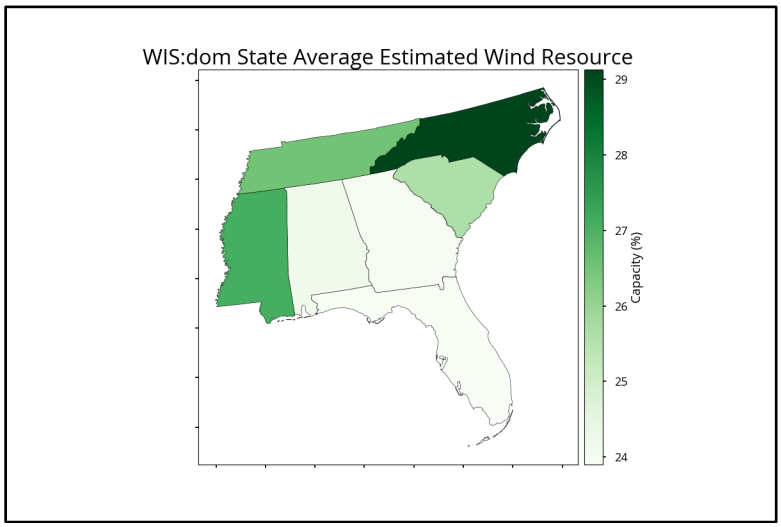

Figure 4.50: The average wind capacity (%) for 2018 by state in the Southeast US.

As described in great detail in earlier sections, VCE® utilizes the 3-km HRRR weather model as the base for the weather inputs. Below is a zoomed in look at the wind capacity resources at this granularity across the Southeast. The southern portion of the Appalachian mountain peaks and valleys creates areas of really low and high wind resources across North Carolina and Tennessee. Wind starts increasing along the western borders of both Tennessee and Mississippi, closer to the Mississippi River. Winds along the coast of North Carolina are high as well.

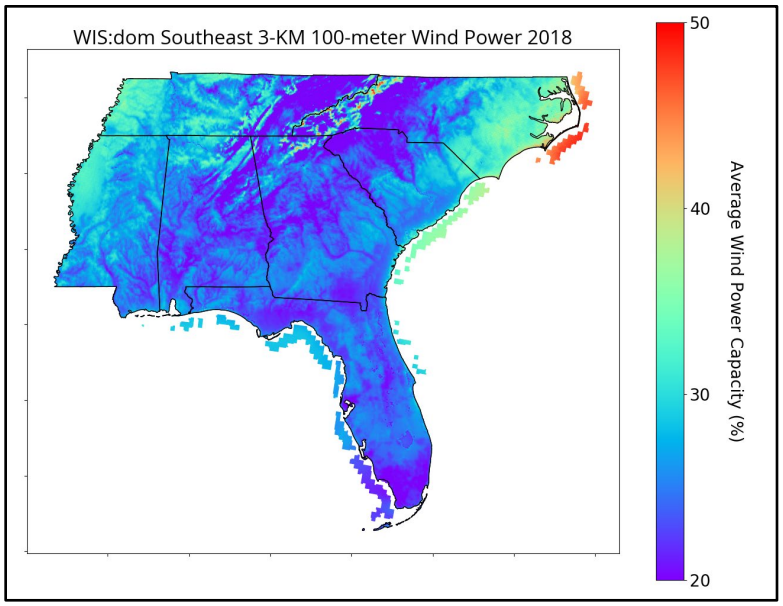

Figure 4.51: The 3-km 100-meter wind capacity resource across the Southeast US in 2018.

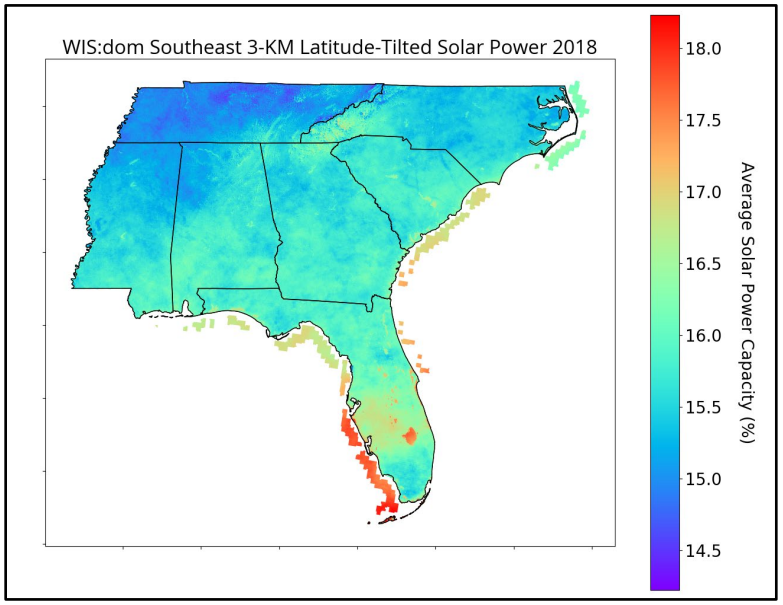

Figure 4.52: The 3-km latitude-tilted solar capacity resource across the Southeast US in 2018.

The following figures take a look at two time series during the year 2018 for the entire southeast. The first week is in April where a high wind event occurred. The latter week is in August where a very low wind period occurred. The solar and wind resource capacity factors are compared alongside the load. At this level, it is easy to observe the correlation of the solar resource with the daily load cycles. During the week in April, a very strong pressure gradient set up across the Southeast. Building low pressure over Kansas/Missouri, coupled with a strong offshore high pressure airmass brought consistently strong southerly winds across the region. This regime lasted for several days.

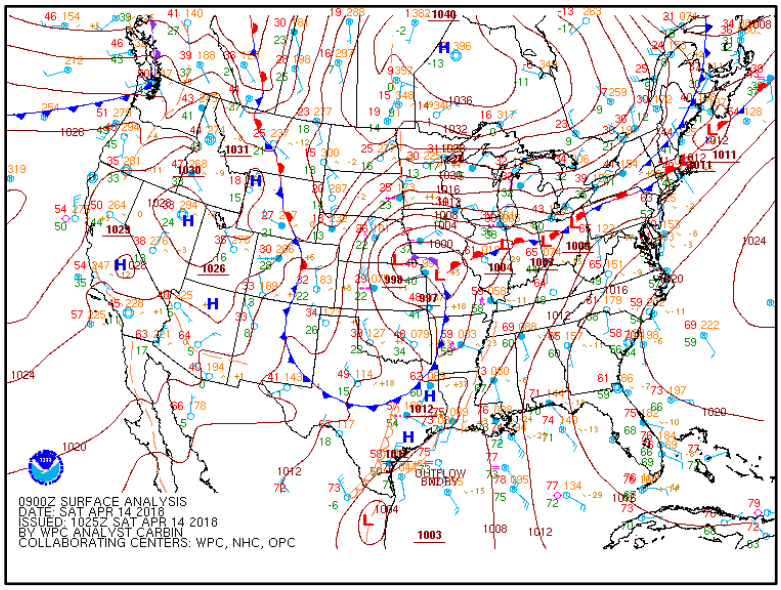

Figure 4.53: Surface Weather Analysis Plot from Saturday April 14th, 2018 at 09 UTC. This surface plot is provided from NOAA's Weather Prediction Center Archives (https://www.wpc.ncep.noaa.gov/archives/web_pages/sfc/sfc_archive.php).

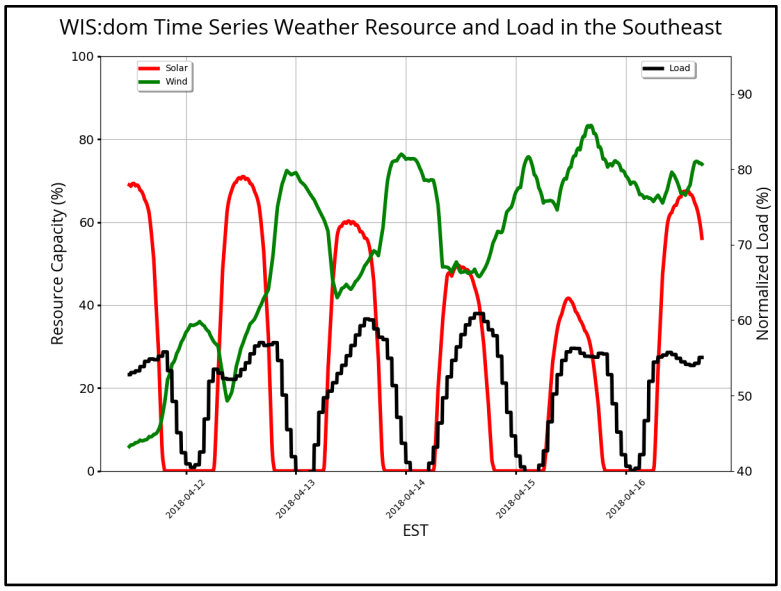

Figure 4.54: A time series of the average solar (red) and wind (green) resources across the Southeast in April 2018. The load (black) is also plotted. This was one of the highest wind periods from 2018.

The next figure shows an August week that had some of the lowest wind observed in 2018. The diurnal nighttime increase in wind speed is apparent. The wind resource is not too high during this period, but it consistently reaches between 10-20% capacity every night. This distinctly shows the anti-correlated nature of wind and solar.

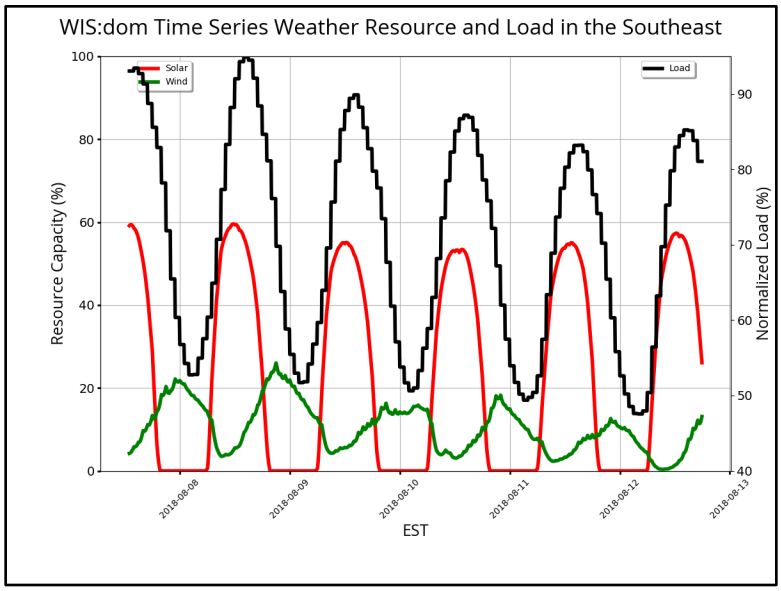

Figure 4.55: A time series of the average solar (red) and wind (green) resources across the Southeast in August 2018. The load (black) is also plotted. This was one of the lowest wind periods from 2018.

4.5 Electric Demand Dataset

The same methods outlined in the present section are applied to all counties and states across the contiguous USA. We provide example state profiles for descriptive purposes and provide a quantifiable example while explaining the concepts for creating the demand datasets.

4.5.1 Traditional demand profiles

State-level hourly loads were developed from FERC 714 data [13]. This database includes hourly load data from grid balancing authorities. Balancing authorities maintain appropriate operating conditions for the electric system by ensuring that a sufficient supply of electricity is available to serve expected demand, which includes managing transfers of electricity with other balancing authorities [14].

The balancing authorities in the database were assigned to states that they most represent and hourly profiles for each of the contiguous US states were developed for 2014 - 2018 by summing the hourly load data for each state. These profiles were then normalized by the annual energy consumption of each state for each year. The process is shown by Equation (35)

$$L_{j,h} = \sum_{i=1}^{n} BA_{i,j,h} \times \frac{L_{j,act}}{\sum_{h=1}^{8760} \sum_{i=1}^{n} BA_{i,j,h}}. \tag{35}$$

Here $L_{j,h}$ is the load for state j at hour h, $BA_{i,j,h}$ is the hourly output for each balance authority i (from the FERC 714 data) associated with state j at hour h (thus, the summation of which equals the calculated hourly load per state), and $L_{j,act}$ is the actual annual load for state j taken from EIA data. The double summation in the denominator of the fraction is simply the estimated annual state load for state j (from the FERC 714 data).

States that were not represented in the FERC database (for lack of a balancing authority or missing data) were assigned to have the same profile as a neighboring state, but were normalized by their own actual annual load.

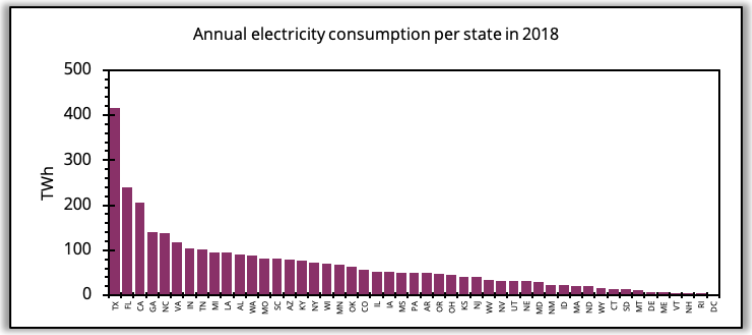

Figure 4.56: Total annual electricity consumption by state for year 2018 generated from FERC 714 data.

Finally, each county was assigned the share of its state load in proportion to its share of the total state population. While there will be differences in counties' load profiles based on their type of load, i.e. heavily industrialized counties will have different load patterns than mostly residential counties, these data simply do not exist in any currently-accessible form.

4.5.2 Space heating demand profiles

Space heating demand depends on local climate and variability in temperature over a year. It is assumed that the ideal indoor temperature (T_{ideal}) for the building stock is 22ºC. To calculate flexibility in space heating, it is assumed that the indoor temperature is allowed to drop to 20ºC.

The energy rate required to maintain the building stock at T_{ideal} given outside temperature of T_{out} is given by

$$\dot{Q} = H.A.(T_{ideal} - T_{out}) \tag{36}$$

where H is the heat transfer coefficient, and A is the cross-sectional area over which heat transfer occurs.

The value of the heat transfer coefficient varies as function of building material and insulation characteristics, and cross-section area (A) changes depending on size and shape of the buildings. However, assuming these values do not change over the course of the year, they do not need to be explicitly quantified if the fractional energy rate at a given time step is used. The fractional energy rate at a given time step is defined as

$$Q_{ideal}(t) = \frac{H.A.\dot{(}T_{ideal} - T_{out}(t))}{\sum_t H.A.(T_{ideal} - T_{out}(t))} \tag{37}$$

$$\Rightarrow Q_{ideal}(t) = \frac{T_{ideal} - T_{out}(t)}{\sum_t (T_{ideal} - T_{out}(t))}. \tag{38}$$

The negative values are set to zero (as no heating will be required when outside temperature is above the ideal indoor temperature) before normalizing. The fractional energy rate, when multiplied with the total space heating energy use in a year, gives the energy required for space heating for a given timestep in that year. Figure 4.57 shows fractional energy use profiles for Minnesota and California created for the year 2018.

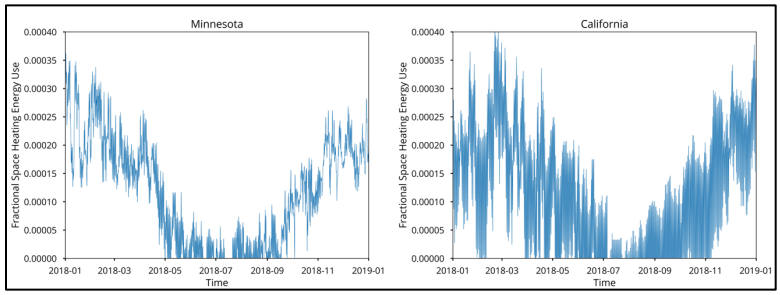

Figure 4.57: Average fraction energy used for space heating in Minnesota and California in 2018. It is observed that in Minnesota there is heating requirements throughout the year, whereas it goes to zero in California during the summer.

It can be seen in Figure 4.57 that Minnesota, which is a colder state, has heating requirement almost all year, while California has zero heating requirements for parts of the summer. It is important to note that although the fractional energy used per timestep in California may be larger in a given hour compared to Minnesota, the actual energy use might be much smaller as these fractional values get multiplied by the annual energy used for heating within that state.

4.5.3 Water heating demand profiles

Water heating is modelled in a similar manner to the space heating. It is assumed that the ideal water temperature to be maintained is 60°C. It is further assumed that the incoming water temperature is correlated to the outside air temperature. Given these assumptions, fractional energy use for water heating at a given timestep is calculated using Eq (38).

Figure 4.58 shows fraction water heating energy use in Minnesota and California. Unlike space heating energy use, it is observed that the profiles for the two states are very similar. The reason for this is that the temperature gradient required to be maintained is so large that the differences in climate is less important. It is, however, observed that energy use at the coldest time in winter is about double the energy use at the warmest time in summer.

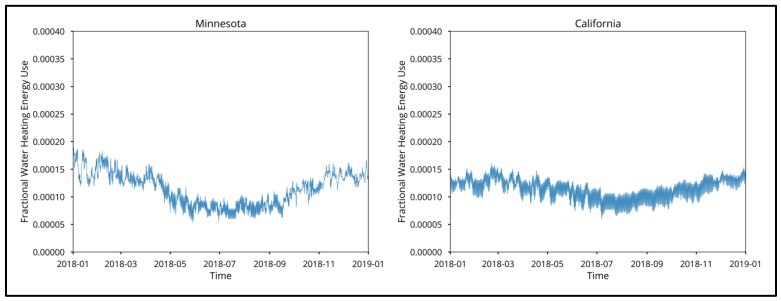

Figure 4.58: Average fractional energy used for water heating in Minnesota and California in 2018.

4.5.4 Space heating flexibility

To calculate flexibility in space heating load, it is assumed that the ideal indoor temperature can be allowed to drop to 20°C (T_{flex}) for short periods. Therefore, the fractional energy use at each time step assuming temperature is allowed to drop to T_{flex} is:

$$Q_{flex}(t) = \frac{T_{flex} - T_{out}(t)}{\sum_t \left(T_{flex} - T_{out}(t)\right)}. \tag{39}$$

The negative values are set to zero in a similar manner to the space heating calculation. From Equations (38) and (39), the flexibility at each time step can be defined as

$$flex(t) = 1 - \phi \frac{Q_{flex}(t)}{Q_{ideal}(t)}. \tag{40}$$

Here ϕ is a parameter to set the enforced strictness of flexibility. This parameter can be any value between 0 and 1. When $\phi = 1$ the flexibility is at its strictest (fully constrained by ambient outside temperature), while at $\phi = 0$ flexibility is fully available regardless of outside temperature.

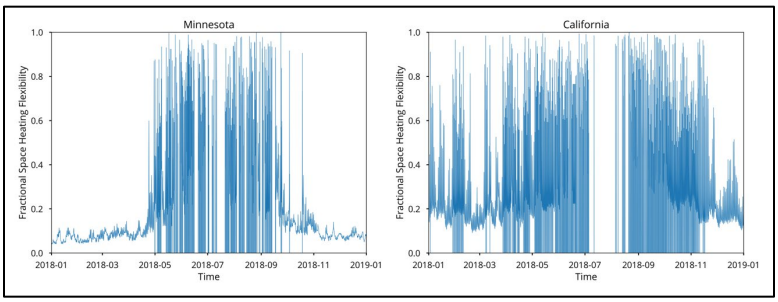

Figure 4.59: Space heating flexibility for Minnesota and California in 2018 for $\phi = 1$.

As seen in Figure 4.59, when space heating demand is very high (see Fig. 15) the availability of flexibility is limited in Minnesota during winter because the ambient air temperature is so low that the buildings would cool below the allowed threshold. For California, there is substantial flexibility in space heating for many timesteps during the winter, because the ambient temperatures tend to be much milder. It is also observed that flexibility goes to zero in California in summer. This is due to the fact that no space heating is required during those timesteps and hence there is zero flexibility for space heating load. In colder states, such a Minnesota, space heating needs are present for more time-periods over a year and, thus, there is flexibility associated with that space heating need.

4.5.5 Transportation demand profiles

Energy used by electric vehicles can be broadly divided into two components: Energy used for driving the vehicle and energy used for cabin heating/cooling. Both these components are dependent on weather and have trends that change over the course of a year. In addition, driving habits vary depending on the region and time of the year.

The energy consumed for cabin heating and cooling is given by a modified form of Equation (36) as

$$\dot{Q_{cabin}} = H.A.|(T_{ideal} - T_{out})|, \tag{41}$$

where T_{ideal} is the ideal cabin temperature assumed equal to 22°C and T_{out} is the outside temperature. The absolute value of temperature gradient is used because when outside temperature is too high, cabin cooling takes over from cabin heating, but the energy use is still proportional to the temperature gradient. The fractional energy use for cabin heating or cooling at each time step can now be calculated using an equation similar to (38):

$$Q_{cabin}(t) = \frac{|T_{ideal} - T_{out}(t)|}{\sum_t |(T_{ideal} - T_{out}(t))|}. \tag{42}$$

To calculate the energy used for driving, the driving behavior for each state in the contiguous United States (CONUS) is obtained from the Department of Transport, Office of Highway Policy Information for year 2018. The data is available as monthly averages for the year 2018. The curves are cubic interpolated to create data at each 5-min timestep. The fractional energy use for driving can then be calculated as

$$Q_{drive}(t) = \frac{D_s(t)}{\sum_t D_s(t)}, \tag{43}$$

where, $D_s(t)$ is the miles driven at each timestep.

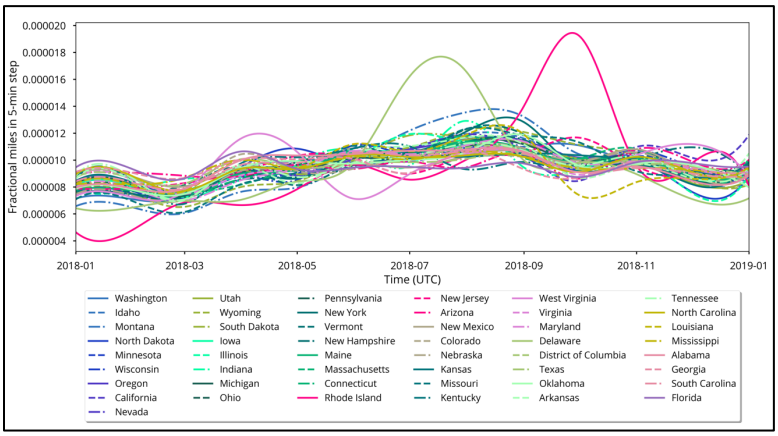

Figure 4.60: Fractional miles driven in a 5-min timestep for each state in the CONUS.

The total energy used by EVs is now a sum of Equations (42) and (43). Since the values are fractional energy use, a multiplier, α (equal to 10%), is applied to Q_{cabin}, which is then added to Q_{drive}. This is done because it is assumed that heating/cooling accounts for about 10% to the total energy used for EVs. Thus, the total fractional energy use is calculated as

$$Q_{total} = \frac{1}{(1+\alpha)}[Q_{drive} + \alpha Q_{cabin}]. \tag{44}$$

The efficiency of running EVs depends on ambient temperatures. The impacts of ambient temperature are (in addition to the cabin heating/cooling) battery internal resistance changes, tire pressure changes, and air density changes. Therefore, the actual energy used by an EV is obtained by multiplying the total energy use by the inverse of the energy efficiency (given by $\eta(t)$ – see Figure 4.61 left panel) due to the ambient temperature at that time step as shown in Equation (45).

$$Q_{actual}(t) = \frac{1}{\eta(t)}\frac{1}{(1+\alpha)}[Q_{drive} + \alpha Q_{cabin}]. \tag{45}$$

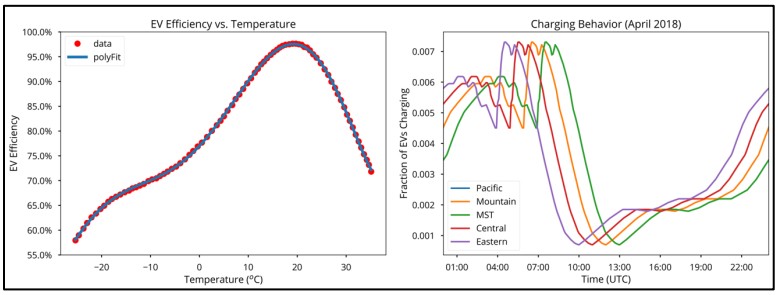

Figure 4.61: Relationship between EV efficiency and temperature (left) and EV charging behavior (right).

The way the EV energy use becomes a load on the grid is when the EV is plugged in to charge the battery. The charging behavior is obtained from a study of charging behavior performed by Idaho National Laboratory in 2013. In this study, a composite profile of all the states studied in the Idaho National Laboratory report at hourly resolution is used. The charging behavior is then adjusted for time-zone (see Figure 4.62) and normalized by the sum of the time series.

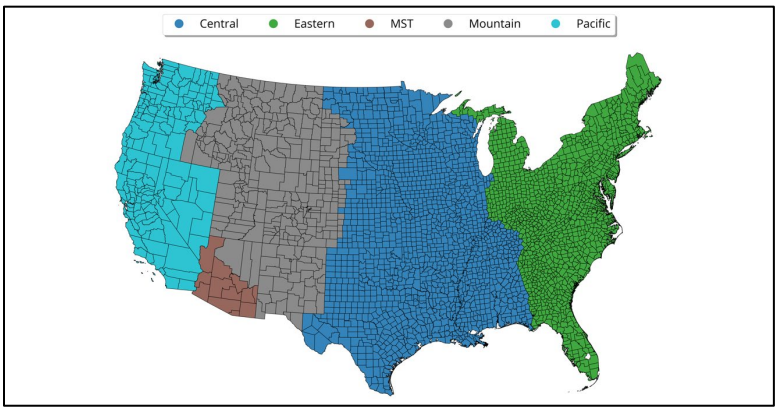

Figure 4.62: Time zones for counties in the CONUS used to localize charging behavior.

The fractional charging behavior is multiplied with the actual EV energy use profile to get the fractional energy demand by EVs at each time step

$$Q_{EV}(t) = C_f(t) * Q_{actual}(t), \tag{46}$$

where C_f is the fractional charging behavior at each time step.

Figure 4.63 shows fractional transportation electricity demand profiles in Minnesota and California. The shape of the electricity demand profile in Minnesota resembles the shape of the heating energy use. The reason for this is that the cold weather in Minnesota increases energy use for heating the cabin, while dealing with lower energy efficiency, which results in much higher electricity demand in winter than in summer. Whereas, the California transportation electricity demand profiles show much better correlation with the driving behavior. This points to the milder climate in California.

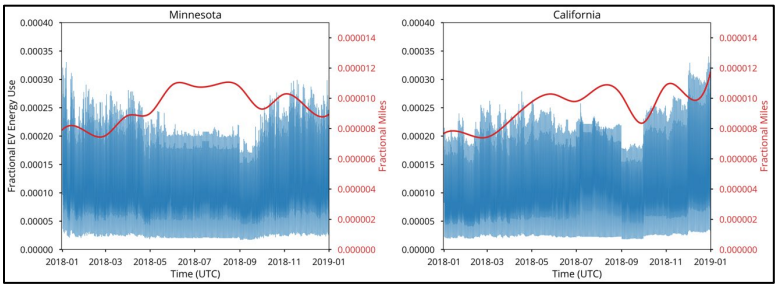

Figure 4.63: Fractional EV energy use for two states for 2018. The relative importance of efficiency and energy use as function of temperature compared to driving behavior is clearly seen.

4.6 Removing Space, Water Heating and Transport from Historical Electricity Use

WIS:dom® uses historical load data from FERC form 714 to create the basis for the demand curves as explained in Section 3.1. The historical data contains contributions from demand for space heating, water heating and EV energy use. To enable modeling demand from space heating, water heating and transport separately, they need to be removed from historical energy use numbers to avoid double counting the demand.

The total demand is given by:

$$D_{total}(t) = A_{conv}N_{conv}(t) + A_{(spHeat)}N_{spHeat}(t) + A_{wHeat}N_{wHeat}(t) + A_{EV}N_{EV}(t) \quad (47)$$

where, $D_{hist}(t)$ is the historical demand curve, A_{conv} is the annual conventional demand, $N_{conv}(t)$ is the normalized conventional demand curve at hourly resolution, A_{spHeat} is the annual space heating demand, $N_{spHeat}(t)$ is the normalized space heating demand curve at hourly resolution, A_{wHeat} is the annual water heating demand, $N_{wHeat}(t)$ is the normalized water heating demand curve at hourly resolution, A_{EV} is the annual demand for EV, and $N_{EV}(t)$ is the normalized EV demand curve at hourly resolution.

Since the FERC data does not split the demand out into categories, the historical demand obtained from FERC is given by:

$$D_{hist}(t) = \left(A_{conv} + A_{spHeat} + A_{wHeat} + A_{EV}\right) * N_{hist}(t) \quad (48)$$

where, $D_{hist}(t)$ is the historical demand curve from FERC form 714 and $N_{hist} = {}^{D_{hist}}/_{\sum_t D_{hist}(t)}$ is the normalized historical demand curve at hourly resolution.

The normalized historical demand curves for Minnesota and California are shown in Figure 4.64.

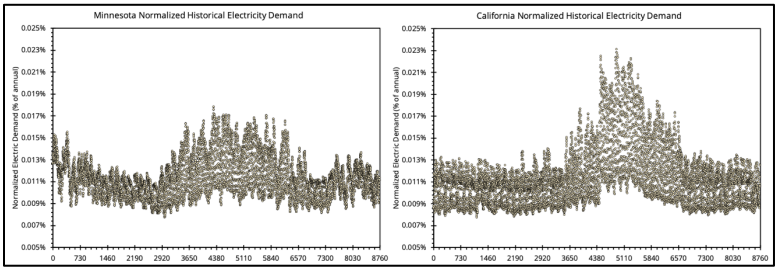

Figure 4.64: Normalized historical demand curves calculated from FERC form 714 for Minnesota (left) and California (right).

Since, the historical demand is equal to the total demand at model initialization, the adjusted normalized conventional demand, which removed contributions from space heating, water heating and transport can be calculated using Equations (47) and (48) by:

$$N_{conv}(t) = \frac{1}{A_{conv}}\left[\begin{matrix}\left(A_{conv} + A_{spHeat} + A_{wHeat} + A_{EV}\right) * N_{hist}(t) \\ -\left(A_{spHeat}N_{spHeat}(t) + A_{wHeat}N_{wHeat}(t) + A_{EV}N_{EV}(t)\right)\end{matrix}\right] \quad (49)$$

The adjusted normalized conventional demand curve calculated using Equation (49) is shown in Figure 4.65. It is observed that the winter periods show a smaller fraction as the space heating contributions are removed

and the summer portion of the curve show larger fractions as they make up a larger portion of the energy use.

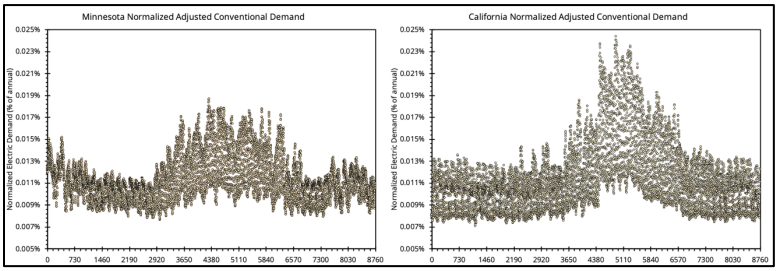

Figure 4.65: Adjusted normalized conventional demand curves after removing contributions from space heating, water heating and transport for Minnesota (left) and California (right).

4.7 Transmission Line Rating & Electric Losses Dataset

As ambient temperatures increase, transmission lines are less able to reject heat generated due to resistive heating of the transmission lines. As a result, a decision has to be made on whether to operate the transmission line at a higher temperature (which increases losses) while keeping the full rating or to de-rate the transmission capacity to prevent damage to the conductor or the surroundings due to the sag of the transmission line. WIS:dom® models the transmission lines assuming steady state energy balance, where heat gained due to resistive heating ($q_{current}$) and solar irradiance ($q_{solarIrr}$) equals heat lost due to convective heat transfer ($q_{convHeatTransfer}$) and radiative heat transfer ($q_{radiativeHeatTransfer}$) as

$$q_{current} + q_{solarIrr} = q_{convHeatTransfer} + q_{radiativeHeatTransfer}. \quad (50)$$

Resistive heating is given by

$$q_{current} = I^2 R(T_{cond}), \quad (51)$$

where, I is the current in the transmission line, and $R(T_{cond})$ is the resistance of the transmission line which itself is a function of conductor temperature (T_{cond}). The resistance of the conductor is related to the conductor temperature by

$$R(T_2) = R(T_1) * [1 + \alpha(T_2 - T_1)], \quad (52)$$

where, α is a constant with a value of 0.0039 and T_1 and T_2 are the initial and final temperatures of the conductor.

Heating due to solar irradiance is calculated assuming the conductor is a black body and can be calculated using

$$q_{solarIrr} = \delta * \pi D * a_s, \quad (53)$$

where, δ is the downward short-wave solar radiation in W/m^2, D is the diameter of the conductor, and a_s is the absorptivity of the conductor (assumed to be 0.9).

The convective heat transfer from the conductor to its surroundings is given by

$$q_{convHeatTransfer} = h * \pi D * (T_{cond} - T_{air}). \quad (54)$$

Here, h is the convective heat transfer coefficient given by

$$h = Nu * {}^{k}/_{D}, \quad (55)$$

where, Nu is the Nusselt number and k is the thermal conductivity of air in W/m-K.

The Nusselt number can be calculated using

$$Nu = 0.3 + \frac{a}{b}(1 + c)^{4/5}, \quad (56)$$

where, $a = 0.62 * Re^{1/2} * Pr^{1/3}$, $b = \left[1 + \left(\frac{0.4}{Pr}\right)^{2/3}\right]^{1/4}$, $c = \left(\frac{Re}{282{,}000}\right)^{5/8}$, $Re = V * {}^{D}/_{\nu}$ is the Reynold's number, *Pr* is the Prandtl's number, *V* is the wind speed, and ν is the dynamic viscosity.

The heat lost from the conductor due to radiative heat transfer is calculated using

$$q_{radiativeHeatTransfer} = \varepsilon * \sigma * \pi * D * (T_{cond}^4 - T_{air}^4), \tag{57}$$

where, ε is the emissivity of the conductor (assumed to be 0.7) and σ is the Stefan-Boltzman constant equal to 5.67E-8 W/m^2-K^4.

Using Equations (50) - (57), the allowable current to maintain a given conductor temperature (T_{cond}) is given by

$$I = \sqrt{\frac{\pi * h * D * (T_{cond} - T_{air}) + \pi * \varepsilon * \sigma * D * (T_{cond}^4 - T_{air}^4) - \delta * \pi * D * a_s}{R(T_{cond})}}. \tag{58}$$

The current method for computing the high-temporal (dynamic) transmission line rating assumes that each transmission line is already appropriately rated based on yearly average local weather conditions. It is then determined what the up- and down- rating should be applied to safely utilized the transmission line. Therefore, Equation (58) is used to calculate the maximum current that can be sent through a transmission line while maintaining an ideal conductor surface temperature of 75°C. Once the allowable current values are calculated, the current values are normalized by the average current value for the CONUS over the year, which gives the fractional dynamic line rating for each timestep over the year.

From the above method of determining the fractional dynamic transmission line rating, there will be periods (usually in winter) where the transmission rating will be greater than unity and periods (usually in summer) where it will be less than unity. A secondary step is now added to the method, where it is assumed that when the fractional dynamic transmission line rating is less than unity, the conductor temperature can increase up to 95°C in order to try and increase the fractional dynamic transmission line rating back to unity. The conductor temperature can be calculated using Equation (55) by iteratively increasing conductor temperature until a fractional dynamic transmission line rating of unity is achieved. If the conductor temperature reaches 95°C before the fractional dynamic line rating reaches unity, no further increase in temperature is allowed. Thus, some periods will have a fractional dynamic line rating that is less than unity since it is no longer safe to increase the fractional dynamic line rating.

An additional constraint imposed is that the temperature gradient between the conductor core and its surface is not allowed to exceed a safe value (IEEE recommended value is 10°C). The temperature gradient between the conductor surface and its core can be calculated using

$$T_{core} - T_s = \frac{I^2 R(T_{avg})}{4\pi k_{th}}, \tag{59}$$

where T_{core} is the conductor core temperature, T_s is the conductor surface temperature, k_{th} is the thermal conductivity of the conductor material, $R(T_{avg})$ is the conductor resistance at the average temperature of the surface and core.

Since the calculations performed here are relative, the safe temperature gradient is determined by using the average temperature gradient observed during periods of fractional dynamic line rating greater than unity. The line ratings are then re-calculated to ensure this temperature gradient is not exceeded.

The final conductor temperatures obtained from the above procedure are used to calculate the change in dynamic transmission line electric losses. The dynamic transmission line electric losses depend on the current passing through the conductor as well as its resistance. The resistance of the conductor is a function of temperature as given in Equation (52), while at higher conductor temperatures, the transmission line is de-rated to send lower current through the line. Therefore, the dynamic transmission electric losses is calculated using

$$Loss_{change} = \frac{I(t)^2 R(t)}{I_{avg}^2 R(75^o C)}, \tag{60}$$

where, *I(t)* is the current rating of the conductor at each timestep calculated from Equation (58), *R(t)* is the resistance at each timestep calculated using Equation (52), I_{avg} is the average current rating of the conductor, and *R(75°C)* is the resistance of the conductor at 75°C.

Equation (60) shows that the dynamic transmission line electric losses are proportional to the square of the current flowing through the conductor and directly proportional to the change in resistance, which increases linearly with conductor temperature. As a result, during colder periods, more current will be flowing through the transmission lines (due to the dynamic transmission line rating being greater than unity) and, hence, will have larger dynamic transmission line electric losses even though the resistance will be lower. Whereas, in hotter periods, the transmission line will be de-rated, so transmission line electric losses will be lower although the resistance of the conductor is higher. There will be variations to this behavior depending on the amount on derating/uprating and change in conductor temperature.

It is important to note that this method of determining fractional dynamic transmission line rating is designed to be relative and not absolute. The method assumes that transmission lines are already rated for the yearly average local weather conditions. Starting from that assumption, it is determined how much uprating/derating results from requiring that the transmission line is used to its maximum potential while ensuring safe operational conditions.

Figure 4.66 shows the fractional dynamic transmission line rating and dynamic transmission line electric losses for Minnesota and California. While California has lower fractional dynamic transmission line rating compared to Minnesota due to its warmer weather, it has less variability in transmission rating changes due to its lower inter-seasonal variability in temperature. For Minnesota, the dynamic transmission line electric losses show a similar pattern as the fractional dynamic transmission line rating because the losses are proportional to the square of the current passing through the conductor and hence the change in current dominate in the changes to the losses. It is further observed from Figure 4.66 (bottom panel) that change in losses in California are less correlated with changes in transmission rating. The is due to the smaller variability in transmission rating in California resulting in smaller changes to the current, which makes them on the same order as changes to the resistance of the conductor.

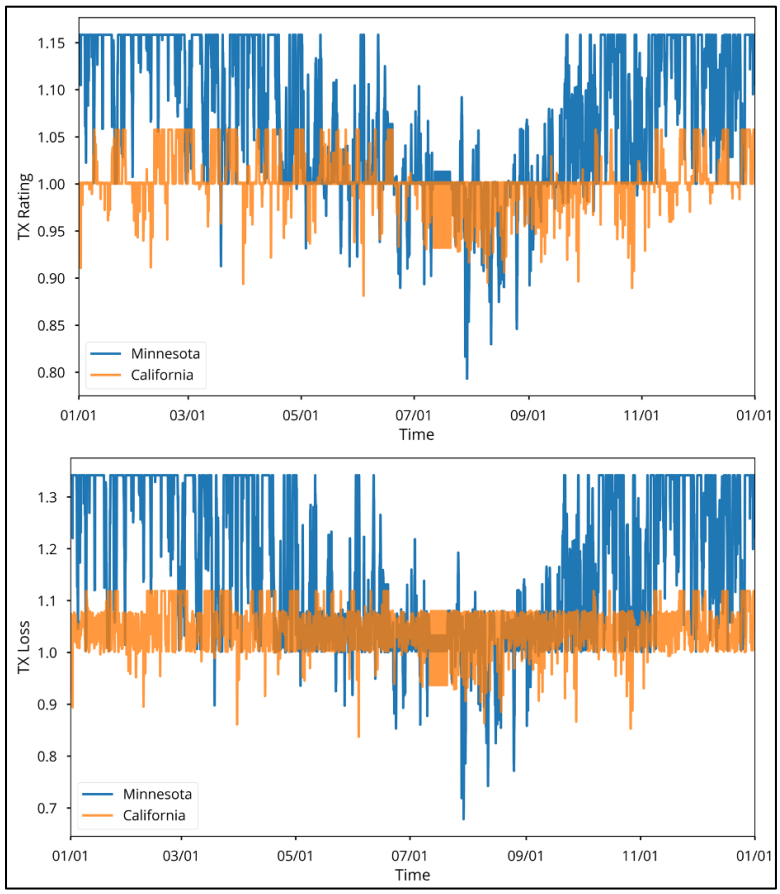

Figure 4.66: Fractional dynamic transmission line rating (top) and fractional dynamic transmission line electric losses (bottom) for Minnesota and California.

The fractional dynamic transmission line ratings and electric losses exhibit the expected patterns for the CONUS as seen in Figure 4.67. It is observed that warmer regions of the CONUS such as the south-east and the south-west have lower than average fractional dynamic transmission line ratings (and consequently, lower average fractional dynamic transmission line electric losses). Meanwhile the Midwest and central portions of the CONUS have higher than average fractional dynamic transmission line rating (and consequently higher average fractional dynamic transmission line electric losses).

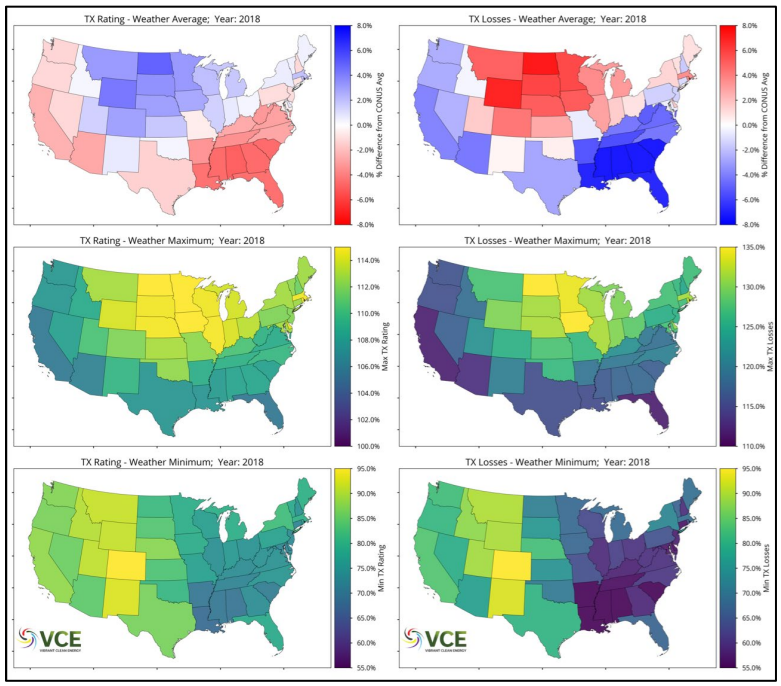

Figure 4.67: Average fractional dynamic transmission line rating (left) and electric losses (right) for the CONUS for weather year 2018. Top panels show deviation of line rating and electric losses from the CONUS average, middle panels show the maximum line rating and losses, and the bottom panels show the minimum line rating and losses.

Looking at the maximum line rating for the year (middle panel), it is observed that the higher than average line ratings in the Midwest are driven mostly by the higher maximum line ratings possible in those states (as these states also tend to have lower minimums). It is also observed that states with lower than average line ratings show a smaller spread between in their maximum and minimum values.

4.8 Climate Change Dataset

Anthropogenically driven climate change creates changes in mean meteorological parameters such as wind speed, solar irradiance reaching the surface, precipitation, temperature and so on. Changes in these meteorological parameters result in alterations in the performance of wind turbines, solar PV cells, conventional power plants (through heat rates and water availability) and transmission line ratings and losses on the generation side. On the demand side, the changes due to climate will result in shifts to the heating and cooling loads, available flexibility, and EV energy use.

WIS:dom® models the impact of climate change on both the demand side and generation side. The United Kingdom Meteorological (UK Met) climate model, HagGEM2-ES, results from CMIP5 are used to estimate the changes in various meteorological variables affecting energy generation and demand. WIS:dom® updates the impact of climate change on the meteorological variables at each investment period, which occurs every 5 years. As a result, effects of large-scale climate cycles, such as El Nino/La Nina, can create large variations depending the year chosen as investment period. To reduce the variability introduced through these large-scale climate cycles, the meteorological variables from the climate models are smoothed using a 5-year moving window. Figure 4.68 shows the change in surface temperature for two Representative Concentration Pathway (RCP) scenarios after applying the 5-year moving average. The impact of climate change on surface temperatures is clearly seen. In the RCP 4.5 scenario, it is observed that more temperature increases are seen in the winter months compared to the summer while in the RCP 8.5 scenario, higher temperature rises are observed in the summer and extends warmer weather to later parts of the year.

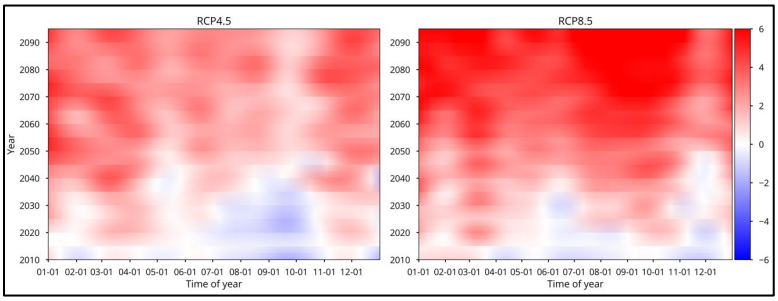

Figure 4.68: Change in average temperature over the CONUS over the course of a year out to 2100.

The following subsections describe how the climate change impacts each aspect of generation and demand within the WIS:dom® modeling framework.

4.8.1 Changes to wind energy production potential

The CMIP5 model data that VCE® has access to only provides monthly mean wind speed at 10 m. Therefore, the monthly mean 80 m wind speed is estimated using a power law assuming a power law coefficient of 1/7 (commonly found for neutral boundary layers). The monthly means can be used to create Weibull distributions of wind speed for that month. The Weibull distributions are created assuming a shape factor (k) of 2, which is commonly found to be the case, and by calculating the scale factor using

$$c = \frac{2 * v_m}{\sqrt{\pi}}, \tag{61}$$

where v_m is the monthly mean wind speed at 80 m.

Once the shape and scale factors are determined, the estimated wind energy production within that month can be determined using

$$P_{est} = 0.5 * \rho * A * C_p * \sum_{v=0}^{25} v^3 * f(v). \quad (62)$$

The estimated wind energy production is calculated for every year from 2010 to 2100. Now, the change in wind energy production with respect to the reference year (2018 in this case) can be calculated. The change in wind energy production is now estimated at monthly resolution from 2010 to 2100. The monthly change in wind energy production is cubic spline interpolated to hourly resolution, which is used to nudge the wind power capacity factors described in Section 2.

Changes in expected wind power over the CONUS show significant spatial variability in both the climate RCP scenarios as seen in Figure 4.70. In RCP 4.5, an increase in expected wind power is forecasted over the great plains and most of the western part of the CONUS. However, in RCP 8.5, larger increases in wind power are forecasted in smaller regions, such as the southeast and the southern great plains, while the northern and western parts of the CONUS show a reduction in expected wind power.

It is observed from Figures 4.69 and 4.70 that available wind power over the CONUS under both climate scenarios shows significant variability year over year with a generally positive trend. It is unclear whether this increase in wind power is observed due to higher wind speeds observed from increased storm and hurricane activity. The significant variability observed between each 5-year period shows the challenge that might face wind developers as there would be substantial uncertainty on the performance of the wind farms which would be difficult to plan for. In addition, locally suitable sites might become undevelopable.

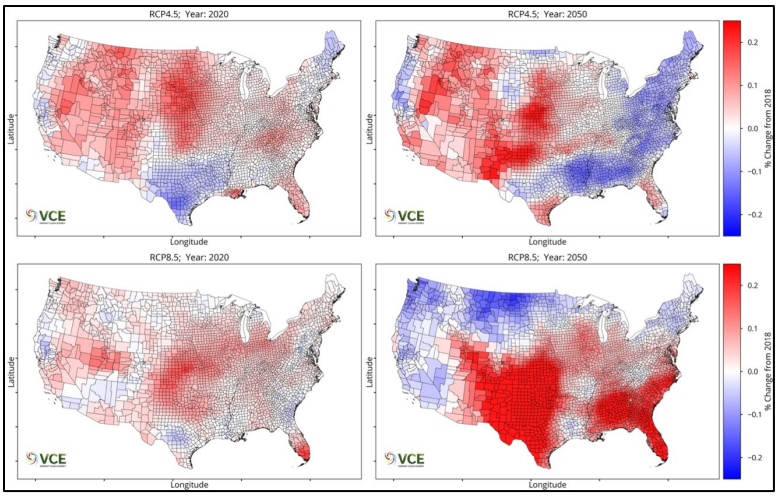

Figure 4.69: Change in wind power due to climate change in the RCP 4.5 scenario for 2020 (top left) and 2050 (top right) and in RCP 8.5 scenario for 2020 (bottom left) and 2050 (bottom right).

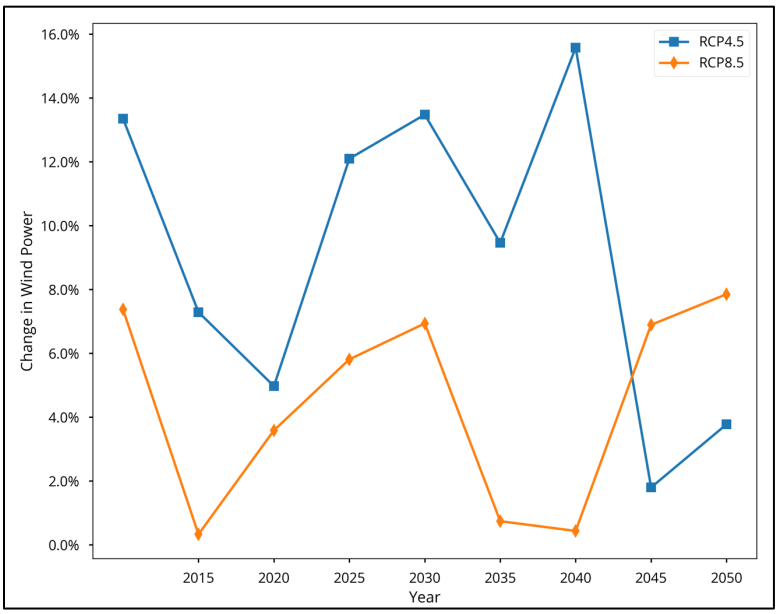

Figure 4.70: Average change in wind power potential over the CONUS under the RCP 4.5 and RCP 8.5 scenarios.

4.8.2 Changes to solar PV energy production potential

As anthropogenic climate change progresses, it is observed that solar irradiance reaching the surface increases marginally due to dryer weather conditions. This increase in solar irradiance reaching the surface should increase power generation from solar panels. However, the ambient temperatures also increase. This increase in ambient temperatures makes solar panels less efficient with about 1% drop in efficiency observed for every 1°C increase in temperature [12]. Both these effects are modelled by VCE® to account for the impact of climate change on solar power generation potential.

Figure 4.71 shows that in the RCP 4.5 scenario, there is increase in solar irradiance in both the southwest and the southeast, however these are accompanied by increases in temperature and as a result there is a net reduction in the expected solar power potential (Figure 4.72). In the RCP 8.5 scenario, solar irradiance increases in the southeast, and is accompanied by larger increases in temperature in those regions as well.

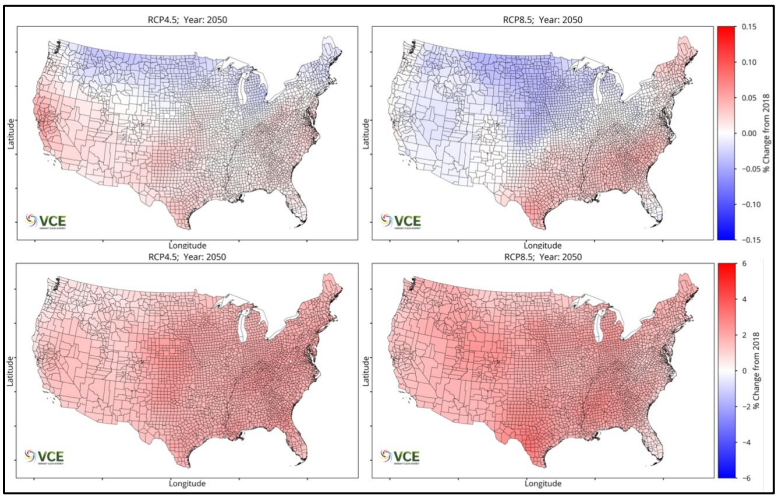

Figure 4.71: Change in solar irradiance reaching the surface in 2050 for climate scenario RCP 4.5 (top left) and RCP 8.5 (top right) compared to 2018 and change in 2-m temperature in 2050 in climate scenario RCP 4.5 (bottom left) and RCP 8.5 (bottom right).

It is observed that the combined effect of the change in solar irradiation and 2-m temperatures is to reduce the solar power generation by 2050 as displayed in Figure 4.72. The reduction in RCP 8.5 scenario is larger (about 2.5%) compared to the RCP 4.5 scenario (about 1.1%). The lower reductions in RCP 4.5 scenario is most probably due to the lower temperatures observed in that scenario, which enables higher solar PV cell efficiencies compared to those observed in the RCP 8.5 scenario.

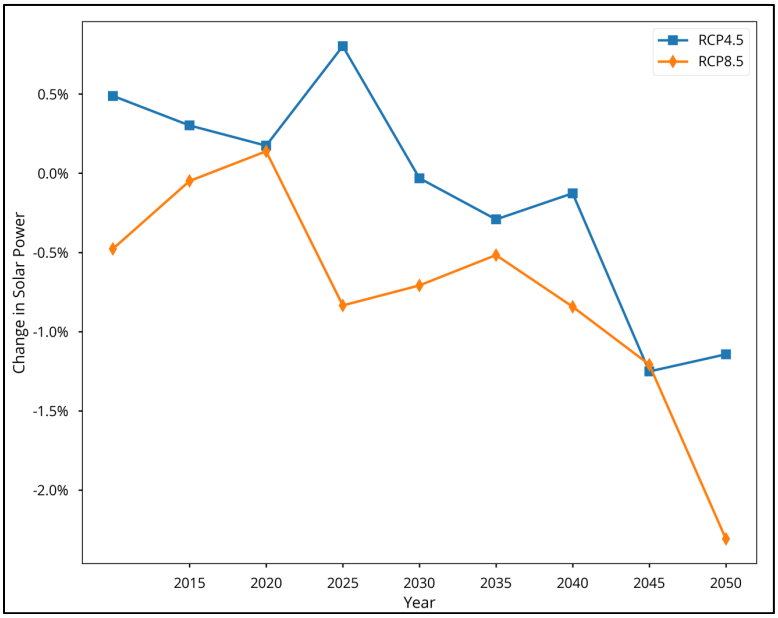

Figure 4.72: Change in solar power output based on changes in temperature and solar irradiance for the two climate scenarios.

4.8.3 Changes to thermal generator heat rates & water

Anthropogenic climate change impacts generation from thermal generators as well as weather-driven generators. Higher ambient temperatures result in less efficient operation of the thermal generators in form of higher heat rates. In addition, conventional generators are affected by access to water which depends on changes in precipitation observed in the two climate scenarios. As seen within Figure 4.73 (left panel), heat rates go up on an average by 2.8% in RCP 8.5, while in RCP 4.5 they go up by about 2.5%. The change in precipitation (Figure 4.73 right panel) is much more variable with year-on-year changes on the order of 20% in both climate scenarios. This indicates the additional uncertainty imposed on the operation of the thermal generators, which could lead to unplanned downtimes due to lack of access to water.

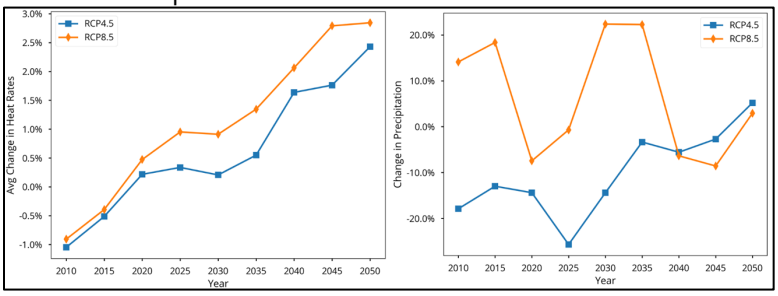

Figure 4.73: Average changes in heat rates (left) and precipitation (right) over the CONUS as a result of climate change for the two RCP scenarios.

An important aspect of the changes to the heat rates is the timing of their occurrence. During any given year, heat rates are their highest in summer due to the higher ambient temperatures. Figure 4.74 shows that the effect of climate change is to increase the summer peak heat rates even further. It is observed that in the RCP 4.5 scenario, heat rates are increased in winter and summer, while in the RCP 8.5 scenario, just the summer peak is seen to increase. This trend correlates to the temperature changes due to climate change (as shown in Figure 4.68), where the RCP4.5 scenario forecasts increased temperatures in winter and summer, while in RCP8.5 scenario, larger increases are seen in summer and extension of the summer period.

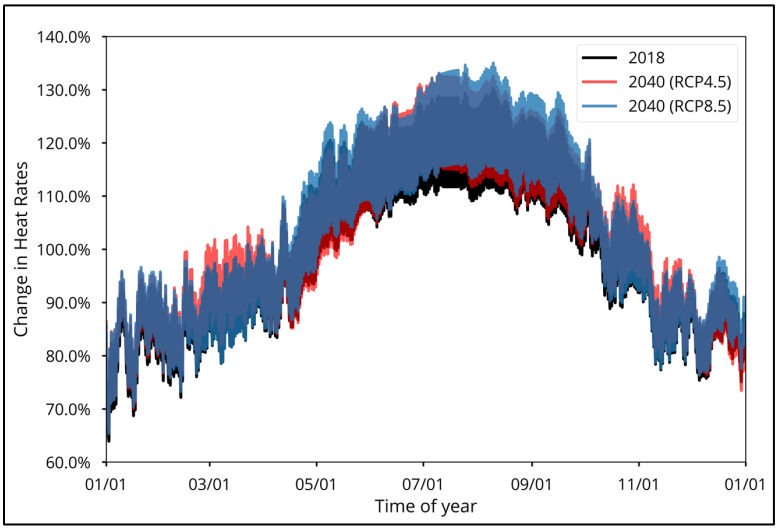

Figure 4.74: Change in heat rates, compared to the yearly averaged value, over the course of a year and impact of climate change in the two RCP scenarios.

4.8.4 Changes to line ratings & electric losses

As ambient temperatures increase due to climate change, the transmission lines will need to be de-rated to prevent excessive heating of the conductor. Some of this effect might be mitigated due to the increase in wind speed predicted by the climate models. The transmission line rating under climate stress is estimated using the climate data to calculate the allowable current in the conductors using Equation (55) and (56), however, it is normalized by the average current calculated for the CONUS using the 2018 weather data. The line ratings are then adjusted as before to ensure that the periods below a rating of unity are adjusted upward without exceeding safe operating maximum temperature of the conductor and the maximum allowable temperature gradient between the conductor core and the surface. The changes to the transmission electric losses are calculated by using the new conductor temperatures and current under influence of climate change stress and using Equation (57) to determine the new loss term.

As can be seen in Figure 4.75, there is a maximum reduction of about 1% in transmission line rating and approximately 2% reduction in transmission line losses averaged over a year in RCP 8.5 scenario, while there is about2% reduction in line rating and 3% reduction losses in RCP 4.5 scenario. The larger reduction observed in the RCP 4.5 scenario is mainly due to smaller increases in wind speeds forecasted in RCP 4.5 scenario, which have a larger adverse effect that the larger temperature increases forecasted in RCP 8.5 scenario.

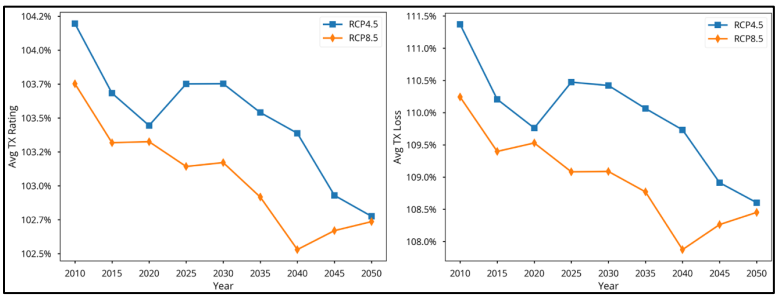

Figure 4.75: Change in transmission line rating (left) and losses (right) due to increase in ambient temperatures due to the effect of climate change.

Similar to heat rates, the change in transmission line rating and electric losses show seasonal trends. Figure 4.76 shows the change in CONUS average transmission line rating and electric losses over a year for weather year 2018 (black line), climate scenario RCP 4.5 (red line) and climate scenario RCP 8.5 (blue line). It is observed that RCP 4.5 shows higher line ratings and electric losses in the winter periods, which is mainly due to the RCP 4.5 scenario forecasting an increase in winter wind speeds compared to 2018. Meanwhile in RCP 8.5 scenario, the winter wind speeds are forecasted to decrease compared to 2018, which combined with the ambient temperature increase results in a significant reduction in line ratings (and consequently electric losses) in the winter. Both climate scenarios predict a decrease in the summer time transmission line rating and electric losses compared to 2018 values.

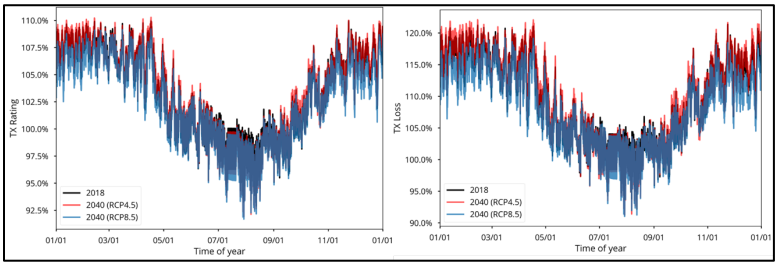

Figure 4.76: Change in transmission line ratings (left) and electric losses (right) compared with the 2018 yearly average value.

The change in transmission line rating and electric losses due to climate change are most sensitive to change in ambient temperatures and wind speeds. Figure 4.77 shows the changes in transmission line ratings (left panels) and electric losses (right panels) in RCP 4.5 (top panels) and RCP 8.5 (bottom panels) scenarios. It is observed in RCP 8.5 scenario that wind speeds decrease over the northern part of the CONUS and increase over the southern parts, while the temperatures are seen to increase more over the southern parts of the CONUS compared with the northern parts. As a result, the temperature increases in the southern parts of the CONUS are mitigated by the higher wind speeds and result in lower derating compared to the northern parts of the CONUS in RCP 8.5 scenario.

As explained previously, the transmission electric losses are more sensitive to the change in current rating of the conductors than change in resistance. This behavior is evident in the Midwest and a few north-western states. However, it is observed that the southeast and southwest states show an increase in losses although there is a reduction in the line rating. The reason for this is that they have a lower reduction in line rating (due to increased wind speeds) combined with a larger increase in ambient temperatures that lead to having higher electric losses.

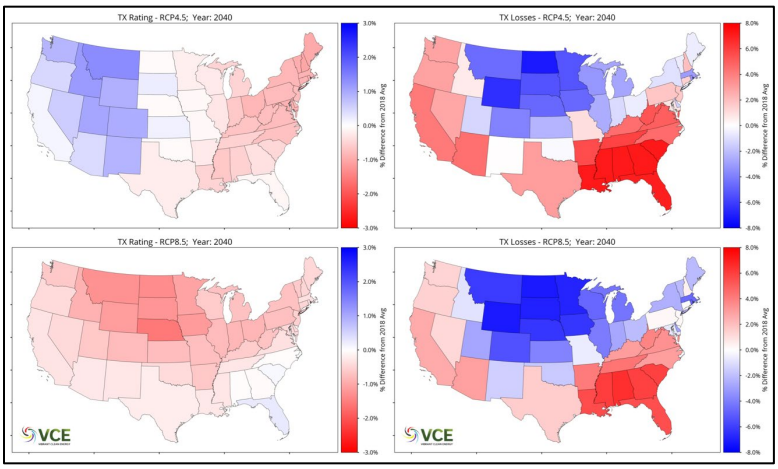

Figure 4.77: Impact of climate change on transmission line rating (left) and electric losses (right) for RCP 4.5 (top) and RCP 8.5 (bottom) scenarios.

4.8.5 Changes to space heating demand

As seen from Equation (38), increasing ambient temperatures (due to climate change) reduces the amount of energy required to maintain the ideal indoor temperature for the building stock. It is observed that the total reduction in energy required for space heating over the CONUS reduces by 8.2% for RCP 8.5 and by about 7.5% for RCP 4.5 (see Figure 4.78) due to the increase in ambient temperatures.

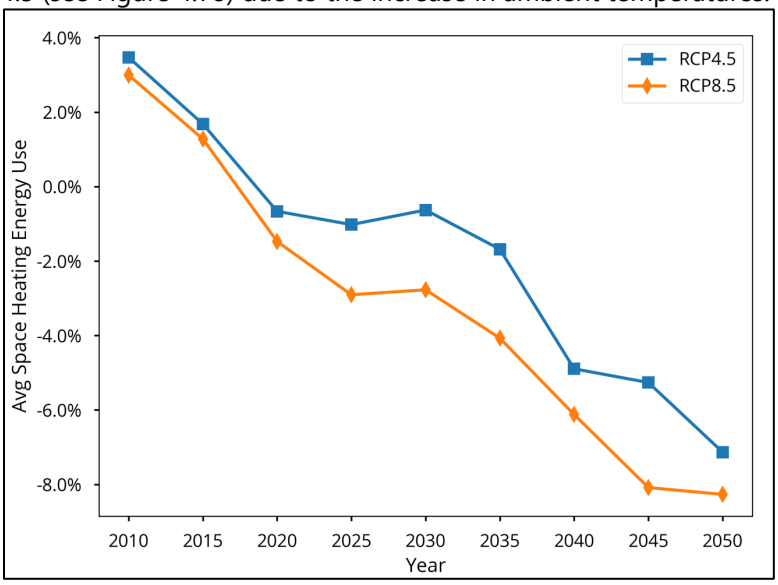

Figure 4.78: Change in space heating energy requirements over the CONUS in the two RCP scenarios.

In addition to the amount of reduction in the space heating load, it is important to know when the reduction is taking place. Figure 4.79 shows the average fractional space heating energy consumption for the CONUS in 2018 and in 2050 for the two RCP scenarios. It can be seen that in the RCP 4.5 scenario, there is a reduction in energy needed during the winter months as well as during the summer months. Whereas in the RCP 8.5 scenario, the reductions occur in the spring and summer season. As explained before, this trend is due to the differences in the timing of the temperature increases forecasted in the two RCP scenarios. The variability in the timing of the change in energy use can have important consequences on how WIS:dom® resource decisions are made.

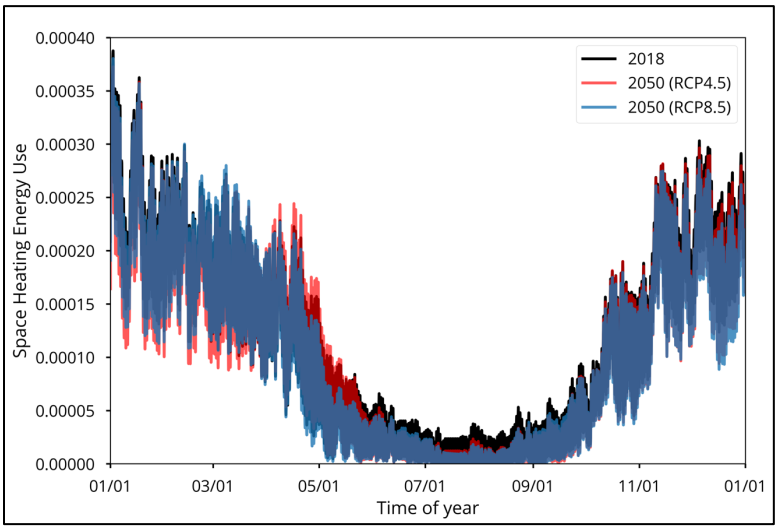

Figure 4.79: Fractional space heating energy use over the course of a year in the two RCP scenarios compared with 2018.

4.8.6 Changes to water heating demand

Impact on water heating is quite small due to the fact that the temperature gradient required to be maintained is large and hence smaller increases in ambient temperature due to climate change do not result in significant change to the energy requirements. The changes observed are similar to those observed for space heating (shown in Figure 4.80), where the RCP 4.5 scenario predicts lower energy usage during the winter and summer, while the RCP 8.5 scenario predicts lower energy usage in spring and summer.

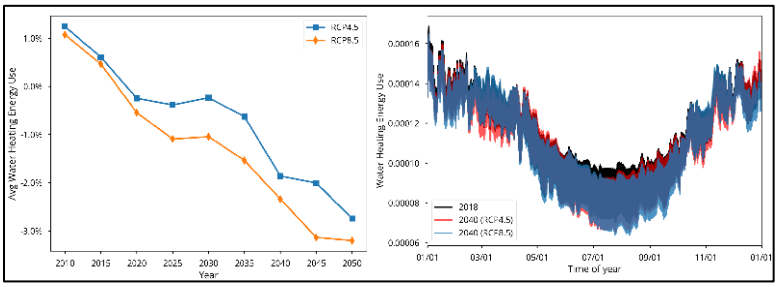

Figure 4.80: Change in fractional water heating energy use due to RCP change compared with 2018.

4.8.7 Changes to conventional & cooling demand

Energy use for space cooling is calculated in a similar manner to space heating energy use by assuming ideal indoor temperature as 22°C and using Equation (63) to calculate fraction energy use at each timestep

$$Q_{ideal}(t) = \frac{T_{out} - T_{ideal}(t)}{\sum_t \left(T_{out} - T_{ideal}(t)\right)}. \quad (63)$$

The fractional energy use is calculated at hourly time resolution for the whole US for each of the years for the two climate scenarios. Next, the change in cooling energy use for each timestep is calculated with respect to year 2018. Figure 4.81 shows the change in space cooling energy use for the CONUS in the two

climate scenarios. It is observed that there is about a 16% increase in energy use for cooling in RCP 8.5 and about 13% increase in RCP 4.5.

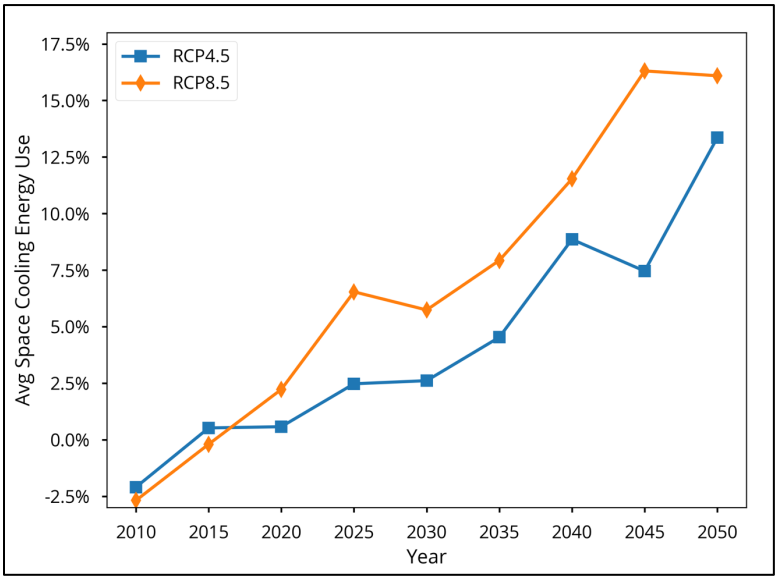

Figure 4.81: Change in space cooling energy use over the CONUS for the two RCP scenarios.

In addition to the magnitude of the increase, the timing of increase in energy use is important in determining how the demand profile changes. Figure 4.82 shows the change at each hourly timestep for all the years in the two climate scenarios. As it would be expected, the largest positive changes occur during the summer in both climate scenarios. It is observed that in RCP 8.5 scenario the increase in energy use occurs over larger portion of the year. While in the RCP 4.5 scenario, there is a reduction in space cooling energy use during spring and fall as the temperatures are forecasted to remain mild during those periods in the RCP4.5 scenario.

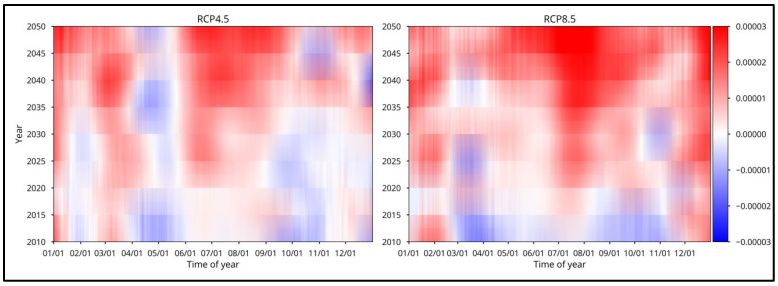

Figure 4.82: Fractional change in each hourly timestep in space cooling demand for the CONUS due to impact of climate change.

4.8.8 Changes to transportation demand

The transportation energy use has complicated interaction effects due to impact of climate change. The increasing temperatures reduce the need for heating in the winter while also increasing efficiency as milder winters improve battery performance. Whereas, in summer cooling needs increase thereby increasing energy use and, in addition, efficiency drops once the temperatures rise above the peak efficiency temperature (see Figure 4.84). Thus, climate change not only changes the magnitude of energy consumed by EVs over a year, but also changes the timing of the energy use.

Figure 4.83 shows that annual change in EV energy use initially decreases compared to 2018 value reaching a minimum in 2020. After 2020, EV energy use increases again until 2030 and after 2035 the trends in EV energy use for RCP 4.5 and RCP 8.5 diverge. RCP 4.5 shows a reduction in EV energy use while RCP 8.5 shows an increase. This upward and downward swings in energy use are due to the constructive and destructive interaction effects of change in heating/cooling needs and change in efficiency due to ambient temperatures.

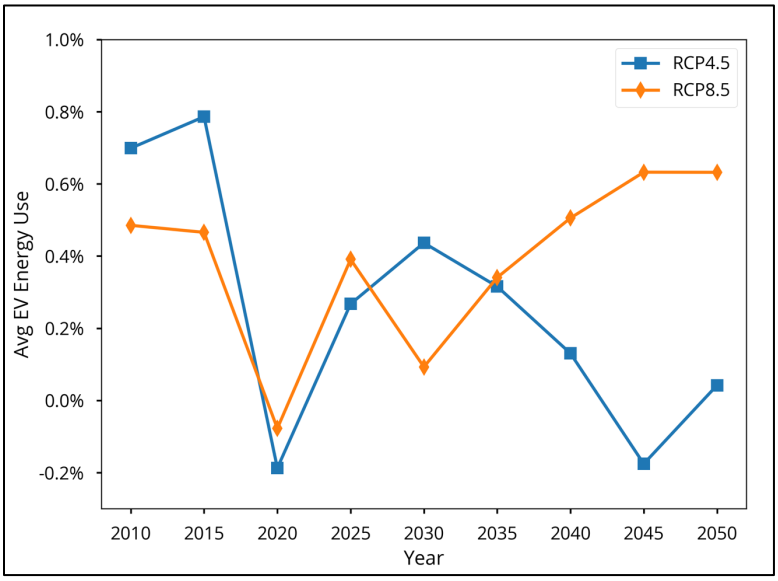

Figure 4.83: Change in EV energy use in the RCP 4.5 and RCP 8.5 scenarios compared with 2018.

To understand what is driving the increase and decrease in EV energy use better, the change in EV energy use for every hour in the year (averaged over the CONUS) is plotted from 2010 to 2050 in Figure 4.84. It is observed that the initial reduction in energy use seen from 2010 to 2020 is mainly due to the milder winters reducing energy use for cabin heating as well as improved efficiency due to better battery performance in the milder weather. However, after 2020, the increased cooling load in summer as well as efficiency dropping due to higher temperatures, negates the energy savings in the winter and net energy use increases again.

The diverging trends in RCP 4.5 and RCP 8.5 observed after 2035 are also evident in Figure 4.84. As discussed before, the RCP 4.5 scenario predicts milder winters and less hot summers compared to RCP 8.5 scenario. As a result, in the RCP 4.5 scenario the energy savings in winter catch back up to increased energy use in summer and net energy use drops. However, in RCP 8.5 scenario, while there is a decrease in winter energy use, the summer energy use increases substantially due to the much warmer temperatures leading to higher overall energy use by 2050.

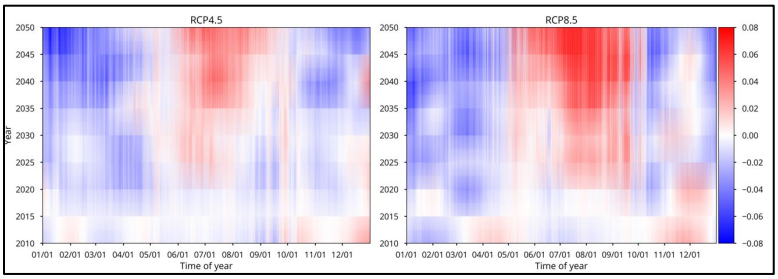

Figure 4.84: Change in average EV energy use over a year from 2010 to 2050 in the RCP 4.5 (left) and RCP 8.5 (right) scenarios.

It is also observed from Figure 4.84 that while the total energy change in Figure 4.83 are small, there is substantial changes in energy use observed at the hourly level. These changes are further magnified at the state level spatial resolution and hourly time resolution. Changes to EV energy use due to climate show expected patterns over the CONUS as seen in Figure 4.85. The warmer states in the southeast see an increase in EV energy use for both the RCP 4.5 and RCP 8.5 scenarios. In the northeast, there are interesting differences in the change to EV energy use in the two climate scenarios. It can be seen that in the RCP 4.5 scenario there is a small increase to EV energy use in the northwestern states, while in the RCP 8.5 scenarios, those states show a reduction in EV energy use. The reason for this is the milder spring weather forecasted in RCP 8.5 scenario, which not only reduces energy use for heating/cooling, but also increase battery efficiency resulting in energy savings.

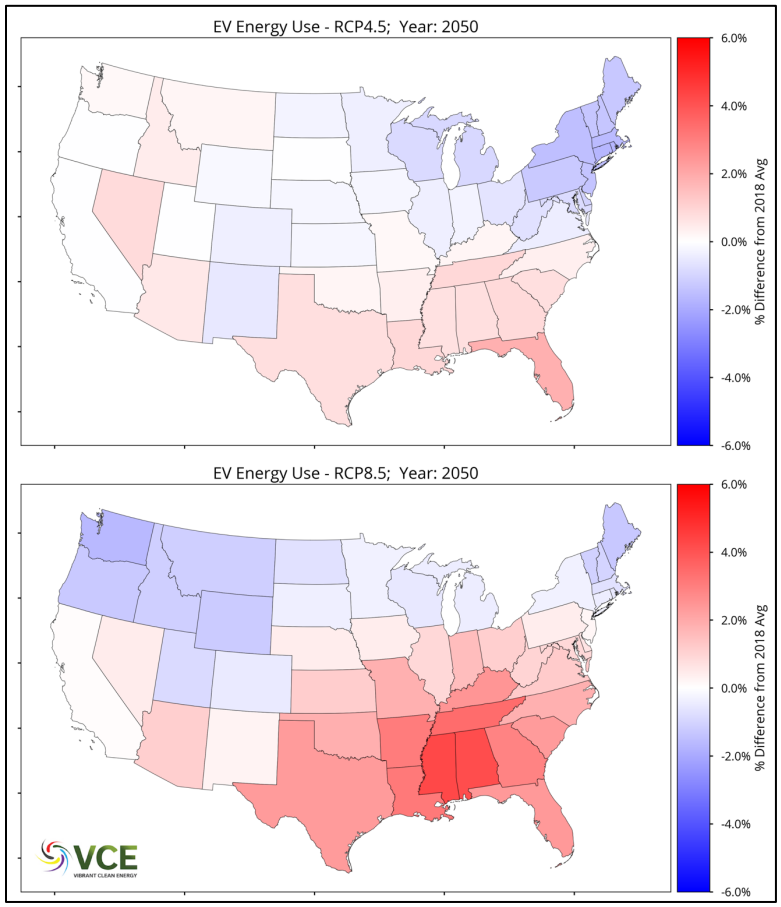

Figure 4.85: Change in EV energy use over the CONUS for the RCP 4.5 scenario (top) and the RCP 8.5 scenario (bottom).

4.9 Bibliography

[1] E. P. James, S. G. Benjamin, and M. Marquis, "A unified high-resolution wind and solar dataset from a rapidly updating numerical weather prediction model," *Renew. Energy*, vol. 102, pp. 390–405, 2017.

[2] J. Wilczak *et al.*, "The wind forecast improvement project (WFIP): A public-private partnership addressing wind energy forecast needs," *Bull. Am. Meteorol. Soc.*, vol. 96, no. 10, pp. 1699–1718, 2015.

[3] J. M. Wilczak *et al.*, "The second wind forecast improvement project (wfip2) observational field campaign," *Bull. Am. Meteorol. Soc.*, vol. 100, no. 9, 2019.

[4] C. T. M. Clack, A. Alexander, A. Choukulkar, and A. E. MacDonald, "Demonstrating the effect of vertical and directional shear for resource mapping of wind power," *Wind Energy*, vol. 19, no. 9, 2016.

[5] A. Choukulkar *et al.*, "A new formulation for rotor equivalent wind speed for wind resource assessment and wind power forecasting," *Wind Energy*, vol. 19, no. 8, 2016.

[6] S. Wharton and J. K. Lundquist, "Atmospheric stability affects wind turbine power collection," *Environ. Res. Lett.*, vol. 7, no. 1, 2012.

[7] A. Betz, "Das Maximum der theoretisch mo ̈glichen Ausnutzung des Windes durch Windmotoren," *Gesamte Turbinenwes.*, vol. 17, pp. 307–309, 1920.

[8] C. T. M. Clack, "Modeling solar irradiance and solar PV power output to create a resource assessment using linear multiple multivariate regression," *J. Appl. Meteorol. Climatol.*, vol. 56, no. 1, pp. 109–125, 2017.

[9] J. W. Spencer, "Fourier series representation of the position of the sun," 1971.

[10] D. L. King, J. a Kratochvil, and W. E. Boyson, "Photovoltaic array performance model," *Online*, vol. 8, no. December, pp. 1–19, 2004.

[11] W. De Soto, S. A. Klein, and W. A. Beckman, "Improvement and validation of a model for photovoltaic array performance," *Sol. Energy*, vol. 80, no. 1, pp. 78–88, 2006.

[12] P. Gilman, "SAM Photovoltaic Model Technical Reference SAM Photovoltaic Model Technical Reference," *Sol. Energy*, vol. 63, no. May, pp. 323–333, 2015.

[13] Federal Energy Regulatory Commission, "Form No. 714 - Annual Electric Balancing Authority Area and Planning Area Report," Washington, DC, 2019.

[14] US Energy Information Administration, "U.S. electric system is made up of interconnections and balancing authorities," *Today in Energy*, 2016. .